DISSERTATION

MRNA LOCALIZATION IN *CAENORHABDITIS ELEGANS* EMBRYOGENESIS

Submitted by

Dylan M. Parker

Department of Biochemistry and Molecular Biology

In partial fulfillment of the requirements

For the Degree of Doctor of Philosophy

Colorado State University

Fort Collins, Colorado

Summer 2021

Doctoral Committee:

Advisor: Erin Osborne Nishimura

Asa Ben-Hur
Tai Montgomery
Tim Stasevich
Tom Santangelo

ABSTRACT

MRNA LOCALIZATION IN *CAENORHABDITIS ELEGANS* EMBRYOGENESIS

From guiding cell specification to regulating protein output, post-transcriptional regulation of mRNA is essential for life. As a result, many mechanisms underlying post-transcriptional regulation are highly conserved across the kingdoms of life. As the spatial resolution of microscopy and sequencing assays has increased, mRNA localization has emerged as a prevalent form of post-transcriptional regulation directing various cellular processes. Perhaps most notably, our understanding of post-transcriptional mRNA regulation and cellular function as a whole has been revolutionized by the discovery that many well-studied mRNA foci, such as germ granules, P-bodies, and stress granules, do not follow the lock-and-key principle of stoichiometric complex formation, but are actually phase-separated, biomolecular condensates. Due to their liquid-like nature, biomolecular condensates can aggregate or disperse component transcripts and proteins with exquisite environmental and temporal sensitivity. As a result, biomolecular condensates can regulate myriad processes as varied as co-translationally organizing protein components for complex assembly (Budding yeast translation factor mRNA granules), reinforcing translation inhibition (Germ granules) or activation (Neuronal granules), and facilitating the organization of other organelles (Axonemal dynein foci/kl-bodies). While an influx of studies have provided insights into the function of well-studied and novel biomolecular condensates alike, much remains unknown. What factors govern assembly and disassembly of condensates? How do they interact with one another? Is condensation the cause or consequence of the functional regulation of any particular mRNA? To begin to answer these questions, this thesis defines *Caenorhabditis elegans* as a model organism for exploring mRNA localization, its mechanisms, and its functions with a focus on condensate transcripts. Thus, the discoveries made have contributed to the fields of post-transcriptional gene regulation, mRNA localization, and condensate biology by elucidating mechanisms of local-

ization, improving on methods of observing localization patterns, and establishing *C. elegans* as a tractable model for exploration of mRNA localization.

ACKNOWLEDGEMENTS

Throughout my time as a Ph.D. student, so many people have touched my life in immeasurable ways. I would like to thank as many of you as possible, but I am very sorry if I leave you out of these acknowledgments.

First, I would like to thank my advisor, Erin Osborne Nishimura. From the start of the lab, Erin has helped me grow both as a scientist and a human. I will always appreciate the mentorship you have provided and your flexibility in allowing me to explore the questions I was interested in, whether it be experiments or politics. The experiences I've had in your lab will stay with me for life.

I also want to thank all of the members of the Osborne Nishimura lab, past and present. Thank you, Marc Nishimura, for helping me develop as a scientist. Without your critical questions and scientific acumen, I would be a far worse scientist today, even if your questions were intimidating at some points! Thanks to Rob Williams for being bold enough to take the second graduate spot in our lab, even with me as your mentor! I don't know what the lab would have been without you, so thank you very much for sharing this crazy experience with me. It's been a blast. Thank you, David King, for all of the help with anything and everything tech, as well as making sure that I'm not just over here making up statistics. Our conversations about analysis have improved my research an incredible amount. Plus, the lab wouldn't be the same without Nealy breaks. Thanks also to all of my undergraduates: Sam Boyson, Annemarie Parker, and Camryn Daidone. It was great mentoring each one of you, and I'm thrilled to see what you will all accomplish. I'll still never forget the looks you all inevitably threw my way once you realized what you got yourselves into, but look how far you've come! Plus, it was nice to have you all on my team when I need someone to back me up and throw shade when the rest of the lab was getting sassy! I also want to appreciate the other undergrads, rotation students, and visiting scientists who have passed through the lab. In particular thanks to Izabella Mastrioni, Lauren Billow, Khalil Kacem, Nicolai Apenes, Paige Ostwald, Romario Romain, and Zaiab Al-Mazaydeh. You have all played a pivotal role in

my journey through grad school, and I will never forget you for it. Finally, to all of the new folks in the lab, Jessica Hill, Meghan Costello, and Naly Torres, I am so glad to have you all in the lab! You're wonderful people, and I'm going to be sad to miss out on the great times you will all have in our lab moving forward. Best of luck to all of you!

I would like to thank the C. elegans community at large for being such a warm and welcoming community. The collaborative nature of the people working with this model is genuinely incredible. It makes for a much more rewarding research experience. Sharing research, ideas, and experiences with people like Dustin Updike, Mike Boxem, Geraldine Seydoux, Chih-Yung Lee, Jim McGhee, David Greenstein, Caroline Spike, and Tatsuya Tsukamoto has shown me that research need not be a vicious experience, but one where all boats rise with the tide. Thank you all so much for fostering an environment that hasn't scared me away from pursuing research. Instead, I look forward to being your peer someday!

In particular, I would like to thank the Montgomery lab. Tai and Brooke Montgomery have been tremendous resources when we have questions about worms. Their willingness to share reagents made my thesis work possible. The Montgomery lab students have also been an absolute treat to befriend. I'll never forget the first meeting of the FayHeads and everything that followed, so thank you, Kristin Brown and Josh Svendsen. I still can't handle the night you showed up to a Halloween party as ghosts, and no one knew who you were for hours. That gets me every time I think about it. The same goes for you, Kailee. I still feel that your introduction of, "Hi, I may smell like embalming fluid," really set the stage for some of the ridiculous conversations we would have and the trouble we would all cause.

I would also like to specifically thank the rest of the Rocky Mountain Worm Group. Particular thanks go out to the Hoerndli lab. From learning how to make microneedles with Fred Hoerndli, running around the GAUSSI events with Dayton, and fantasizing about future ski trips with Rachel, you have all been so fun to work with. I'd also like to thank Christopher Link for having some of the most fun experimental ideas and spitballing about things others would brush off in an instant. Also, I'd like to thank Marko Melnick for all our adventures in CA and for introducing me to the

worst tattoo I've ever seen. And then there's David Fay. Where would I be today without the FayHeads?! All I can say to you is, I hope you see your mug someday.

A special thanks to Florian Mueller, too. Our collaboration was one of the most enjoyable and rewarding experiences of graduate school. I'm just hoping that someday I can make it out to France for a ski trip with you!

I have also had the pleasure of being inspired by so many people outside of CSU life. Thanks to my friends back home in Oregon (or wherever you wandered off to!) I will be missing many of you here. I want to dedicate a lot more thought to each of your dedications than I have the motivation for as I try to find jobs. Still, hopefully, I can tell you all how much I appreciate you next time I see you! Regardless, thank you, Tyler Giard, Ian Grensback, Mike Issertell, Kirsten Clark, Marty and Shauna Lowenthal (did she take your name? Sorry if you didn't Shauna,) Keith Repsher, Zach Goodman, Jensen Tittlefitz, Sara Cade, Joe Close, Jack Lively, Nick Propios, Justin James, James Cisneros, Alden Elias, Courtney Street. Thanks also to all those whose last names I forget, including most of my friends from my time at Hawaiian Time, so many more of my park-rat friends, and a bunch of friends from high school/college. I'm sorry if you were left out, but my life was shaped by each and every one of you. While the twenty minutes I'm spending on my thesis acknowledgments may miss you, I appreciate each of you.

This is not to leave out the extramural mentors in my life! I have had some truly amazing teachers throughout my life that deserve recognition. Thank you, Mark Nygard, Bruce Lawrence, Teresa Grube, and Lance Miller. You all managed to wrangle this little monster into some semblance of a functional human. I really appreciate how effectively each of you managed to learn who I was as an individual and help me grow into a better person.

One of the most essential thanks I have is for the entire Biochemistry and Molecular Biology department. I would never be the person I am today without all of you.

First, a shoutout to all of the office staff, past and present. You are way underappreciated for how much you hold all of our work together. Thanks to Tim David, Kristen DeQuasie, Neda

Amidon, Allison Baum, Staci Brazil-Engleman, Justine Barela for just keeping things running without making us worry about a second thought. It's much appreciated.

I'd also like to thank Brian Kalet, Laurie Stargell, Jennifer Nyborg for providing me with such a great environment during my TA assignments. I truly enjoyed working with you all to teach the next generation of aspiring scientists. I am also indebted to my rotation professors for providing me with a phenomenal skill set that allowed me to thrive in graduate school. I'm really just pulling things out of a hat here, but I'm going to highlight the single most impactful thing that each of you taught me. Steven Markus, thank you so incredibly much for teaching me that trying an experiment the same way twice and failing both times means it's time to change something. I can't imagine the hours you saved me with that advice. Eric Ross, thank you for teaching me that a well-organized project with standardized protocols and organized screening can significantly increase the chances of succeeding in experiments and actually finding something interesting. My rotation in your lab prepared me to help set up a brand new lab in ways that I think few others could have. Just quickly in the middle here, thank you, Olve Peersen, for getting our data storage and transfer set up. Watching you all figure that out again makes me appreciate your willingness to act as unpaid tech support in a way I never understood until now. That effort is understated and underappreciated, so thank you very much. I would also like to thank Cathy Radebaugh for letting me participate in some enjoyable outreach experiences. The Skyview days were some of the most rewarding days I've had in graduate school.

I would be remiss if I didn't also include the other graduate students in my thanks to the department. The other students/staff in the department made this experience so much more enjoyable. First, thanks to Charles (Squeegee) McDonald, Travis Sanders, Matt Saxton, Ryan Czarny, Wyatt Beyers, Julie Sun, Tatsuya Morisaki, Adam Koch, Ethan Ho, and Craig Marshall. I'd say more, but I'm pretty sure we're still going to keep up with each other regularly, so I'm not too worried about saying why each of you are some of my favorite people. I would also like to thank Lindsay Lammers, in particular, for inspiring much of my engagement throughout graduate school and providing sage advice. Thanks also to Kari Ecklund, Tyler Biebighauser, Amanda Broad, Hazheen

Shirneki, Andrew Lamb (you wet willy monster,) Kenneth Lyon, Sarah Bollinger, Sean Cascarina, Jenifer Shattuck, Melissa Ford, Julie Walker, Lexi Gehring. You have all guided my progress through graduate school, from watching me give pathetic practice presentations, inspiring me to develop wild hypotheses, and even helping get us kicked out of a few select venues...

This also includes the GAUSSI family, PIs and graduate students alike. Thank you, Carol Wilusz, Kate Sherill, Tom Chen, Adam Heck, Ariel Belk, Bridget Eklund, Heather Deel, Jessica Warren, Josue Rodrigues-Ramos, Julius Stuart, Luke Schwerdtfeger, Michael May, Mike Mangale, Reyes Murrieta, Sere Williams, Shannon Stiverson, Shaun Cross, and Zach Fox and all of the other GAUSSI folk for all of the training and friendship. There's definitely a special thanks for the ones who went on those 3am hikes at Pingree and made it back in time for seminars, though. You are the motivating maniacs I need in life.

Then there are my friends from my time in student government. Thanks to Mary Stromberger, Colleen Webb, Alyssa Melvin, Jeffery Ma, Savvanah Hobbs for making those such fruitful experiences.

Most importantly, though, is my cohort. I can guarantee I would not have made it out successfully without any one of you. I genuinely hope that we will be life-long friends because you were the most exceptional and motivating people to have spent this time with. The most profound appreciation goes out to Amand Koch, Charlotte Cialek, Robert Wimbish, Matthew Marzo, Colleen Watkins, Aaron Bilbao, and Phillip Gasser. Once again, I could go on for days about how you have all impacted me, but all I will say is this: Stay in touch.

I can't make it through acknowledgments without thanking my committee too. Thank you, Tim Stasevich, Tai Montgomery, Tom Santangelo, and Asa Ben-Hur. You have all made me a better scientist. Without any one of you, I would have fundamental gaps in my skills. Without Asa, I wouldn't hold a candle at programming; without Tim, I wouldn't know the answer to the question, "What is light?" Without Tai, I would have never learned the folly of fighting the worm cuticle (which has ultimately led to my methods publication); without Tom, I would have never learned

how to critically evaluate. And this is just the slightest description of what you've all taught me. Thanks to each of you for developing me into a rounded scientist.

I would also like to thank my lovely girlfriend, Lindsay Winkenbach. I still laugh every time I think of Andrea telling you that you will probably fall in love with someone in these very halls and having you scoff at the idea. Look at us now! The last couple of years of adventures we've had together have been truly remarkable, and I look forward to many more.

I would like to thank my family. Without the influence of my parents, Bob and Diane, and my sister, Kayla, I would have never made it to this point. You have all been an integral part of my life through the ups and downs of graduate school. I truly appreciate everything that you have done to make my life the incredible journey that it has been. I can't wait to see what fun adventures we all go on together.

Beyond just my immediate family, I want to give a shoutout to all my other phenomenal relatives. Thanks to the entire Pedone family; my grandparents, Janie and Montey, all of my aunts (particularly aunty Karen for your excellent illustrations), and the cousins, all for giving me the feistiness that I needed to fight through the challenges of graduate school. I'm so excited to see more of you all now that my parents are closer to you. Thanks also to the entire extended Parker family. Having a family network in Fort Collins through this crazy period of my life has been so helpful. Visiting Grandma Ruthanne, Grandpa Jay, Aunt Cath, and Aunt Beth for the occasional dinner and debate has been such a nice thing to look forward to over the years. Plus, the occasional visits from Parker, Quinn, Brooke, Craig, Bruce, Janice, Heather, Garth, and the rest of the gang have helped me stave off some insanity throughout the more challenging times.

Just a few last, quick thanks to some random friends from my time in graduate school who stand out: Steamboat Meghan, FASEB Severin, and our homie from Australia whom we tried to teach how to bike with limited success, Dr. Riley, and Moose, all of the cohorts exes whose names may not be spoken, and all of my ski and skate buddies from CO, and the wild roommates I had my first year (RIP alpha the beta), among many others.

There are so very many more people I would like to thank but don't have space for. I'm terribly sorry if I've left you out, but know that's not for lack of thought, but rather because this acknowledgment will almost certainly never be seen by you anyway, and I should be working on other things.

Finally, I would like to thank you, Yaw. I tried to say it in my defense but couldn't squeeze out the words; you were the most genuine person I have ever known. When I imagine what my very best self would look like, it pales in comparison to how kind, excited, courteous, and just generally lovely you were as a person. You will remain an inspiration to myself and so many others for the rest of our lives. I wish we could all tell you how much we all love you.

TABLE OF CONTENTS

Chapter 1

Introduction; It's just a Phase: Exploring the relationship between mRNA, biomolecular condensates, and translational control[1]

1.1 Introduction

1.1.1 mRNAs on the move

The spatial organization of cells has fascinated scientists since the advent of the microscope. Observations as early as the 1890s documented dyes concentrating within cytoplasmic aggregates of insect germ cells, structures now known as germ granules [1, 2]. Even as those structures remained mysterious, scientists found evidence of mRNA localization in embryogenesis, neurobiology, and yeast mating-type switching [3–6]. The mRNAs localized in those studies are now classic models of mRNA transport and localization.

In 1983, Jeffery et al. first documented mRNA localization in sea squirt embryos (*Styela plicatea*) when they reported β-actin mRNA concentrating within myoplasm (progenitor muscle tissue) [7]. Later, observation of chicken embryonic fibroblasts found β-actin mRNA polarization, this time to the leading edge of motile cells [8]. Subsequent studies found a conserved RNA sequence, or "zip code," in its 3'UTR sufficient to direct its localization and repress its translation when bound by the RNA binding protein (RBP) ZBP1 [9–11]. β-actin has since served as a foundational example of the relationship between mRNA localization and translational control.

Subsequent studies in various fields have highlighted a diversity of localized mRNA. In the mid-1980s, studies first in *Xenopus* and later *Drosophila* illustrated some maternally-deposited transcripts partition asymmetrically in oocytes to establish cell fate [3,4]. The maternally-inherited

[1] This chapter is a modified version of a manuscript under review

transcripts *bicoid, oskar, nanos,* and *gurken* in *Drosophila* were instrumental in determining how mRNA transport, tethering, and localized protection from degradation contribute to spatial patterning, ultimately directing cell fate specification and morphogenesis during embryonic development [12–14].

In neurobiology, the discovery of ribosomes in dendritic spines led researchers to search for distally localized RNAs [15]. Soon after, a transcript instrumental to synapse formation, *Map2* (*microtubule-associated protein 2*), was found sequestered in rat hippocampal dendrites [5]. Identifying localized neuronal transcripts demonstrated that mRNA localization could extend beyond just maternally-inherited transcripts in large egg cells. These discoveries suggested mRNA localization may be a more common feature of biology than previously imagined.

As RNA detection methods have improved, so have observations of mRNA localization in finer structures and within smaller cells. mRNA localization has been discovered in organisms as varied as bacteria, fungi, plants, and animals [16–19]. For instance, the *bglG-bglF* operon localizes to the cell membrane in *E. coli* [20], the *ASH1* RNA localizes to the daughter cell bud tip in yeast [6], genes essential for chloroplast function enrich at the chloroplast in *Arabidopsis thaliana* [21, 22], and characterization of region- and organelle-specific transcriptomes in humans is occurring rapidly [23–26]. In a noteworthy study, researchers surveyed the localization of 8000 transcripts by *in situ* hybridization within *Drosophila* embryos. They found that, depending on developmental stage, up to 90% were spatially restricted [27, 28]. By combining genomics assays with subcellular dissection, fractionation (subRNA-seq), or proximity labeling (APEX-seq), an expanding catalog of subcellular transcriptomes has exploded into view leading to discoveries of many localized mRNAs [23–26]. To organize the newfound knowledge, the RNALocate database has manually curated 190,000 RNAs with 44 subcellular localizations in 65 species (as of January 25, 2021) [29].

Together, these advances have shifted our understanding of RNA localization from a phenomenon exclusive to specialized cells to a common feature of cell biology. The widespread

nature of mRNA localization demonstrates the need to better understand mRNA localization, its mechanisms, and its functions.

1.1.2 Functions of mRNA localization

Why do mRNAs concentrate in different regions of the cell? The known functions of localization vary. In the cytoplasm, mRNA localization often correlates with translational control but with diverse relationships.

mRNA localization can direct translation to occur in an environment that fosters proper protein processing, folding, or assembly [30, 31]. Local translation, such as at a synapse, facilitates rapid protein synthesis in response to local stimuli [32]. Additionally, linking translation repression with mRNA localization reduces potentially adverse protein-protein interactions that impede function or cause damage [33]. Ensuring protein synthesis occurs in the appropriate location is also important during early embryonic development, where ectopic translation can disrupt cell fate [34, 35].

mRNA localization can also be associated with the environmental regulation of translation. In intestinal enterocytes, refeeding after starvation changes the polarization of many mRNAs and ribosomal protein-encoding RNAs to facilitate a positive feedback loop, thereby upregulating metabolism [36]. Further, the translation of some mRNAs at distinct subcellular locales aids in differentiating cellular proteomes. For instance, *ASH1* mRNA localization to the daughter-bud-tip in budding yeast results in bud-specific protein expression [6]. The ASH-1 encoded transcription factor then allows the daughter cell to express a unique proteome from its mother and ultimately determines its cell state.

mRNA localization can underlie cellular structure. Similar to long non-coding RNAs (lncRNAs) that can have structural roles in the cell, mRNAs too have been shown to act as scaffolds for organelle formation [37]. The structural role of RNA extends beyond simply acting as a scaffold as well. Emerging evidence suggests that localization of transcripts can form an "assembly line" type organization where assembly of specific proteins occurs in a spatially ordered manner. For instance, the spatial organization of transcripts important for dynein complex assembly are spatially

distinct but in close proximity [38, 39]. Disruption of this organization leads to malfunctioning dynein complexes [38–40].

Fascinatingly, one distinct form of mRNA localization can mediate diverse functions: the concentration of mRNA in biomolecular condensates. My thesis covers various aspects of mRNA localization, with a focus on mRNA concentration in biomolecular condensates, from recent findings in well-studied condensates to newly discovered condensates, and how concentration within condensates affects translation regulation and protein output.

In many instances, the functions and consequences of mRNA condensation are just beginning to be understood. It is tempting to hypothesize that RNA condensation always occurs for some purpose or promotes a given expression outcome. However, mRNA localization can also occur as the downstream result of regulatory processes such as translational repression, RNA interference, processing, or decay.

1.2 Biomolecular condensates can link translation repression and mRNA localization

1.2.1 RNAs can concentrate in biomolecular condensates

Many mRNA molecules concentrate within biomolecular condensates, membraneless organelles that phase separate from the surrounding substrate when weak, multivalent interactions of their components create liquid-liquid, liquid-gel, or liquid-crystalline partitioning [41–43]. Within condensates, specialized biological processes can occur. In recent years, many biological fields have been surprised to find examples of biomolecular condensates in their systems. However, it was the study of RNA biology that heralded this paradigm shift. Biomolecular condensates of the nucleus – the nucleolus, Cajal bodies, and paraspeckles – coordinate ribosome assembly, RNA processing, or still uncharacterized functions, respectively [44–47]. Those of the cytoplasm – P-bodies, stress granules, germ granules, and Balbiani bodies – are sites of mRNA metabolism,

sequestration, regulatory control, or serve to bring mRNAs, proteins, and organelles together, respectively [48–54].

The initial experiments that define phase-separated condensation are straightforward, typically involving characterization of their liquid-like properties, dissolution using solvents, and mixing with the exterior environment [42, 55]. However, the interpretation of these experiments takes careful consideration as other types of interactions can appear deceptively similar to phase separation [56]. Even once established, determining the functional roles a condensate plays is challenging due to the difficulty differentiating the effects of their physical disruption from the perturbation of their components. For this reason, biomolecular condensates of tractable model systems are of great utility.

1.2.2 P granules: a model condensate

The P granules of *Caenorhabditis elegans* were among the first membraneless organelles recognized as phase-separated condensates [57]. P granules, the nematode germ granules, concentrate through the progenitor germ lineage contributing to gamete production and fertility in adults [53, 58]. First observed through inadvertent cross-reactivity against a mouse secondary antibody, they were termed "P granules" for their progressive accumulation in the P (posterior) lineage culminating its development in the germline (Figure 1.1) [59]. Immediately after fertilization, P granules are free-floating and cytoplasmic but later amalgamate around the nucleus, where they extend the nuclear pore complex environment into the cytoplasm and branch into substructures hypothesized to contribute to RNA interference [59–62].

Because the function of P granules has been mysterious, researchers looked to their components for insight. The P granule proteome contains proteins associated with RNA binding, degradation, splicing, small RNA-mediated processing, and translational control [63–65]. Additionally, many P granule proteins form multivalent interactions characteristic of condensate formation [64, 66]. P granules notably appear to have at least two distinct phase behaviors: an internal liquid-like core characterized by the PGL and GLH proteins and an external, gel-like shell composed of the MEG

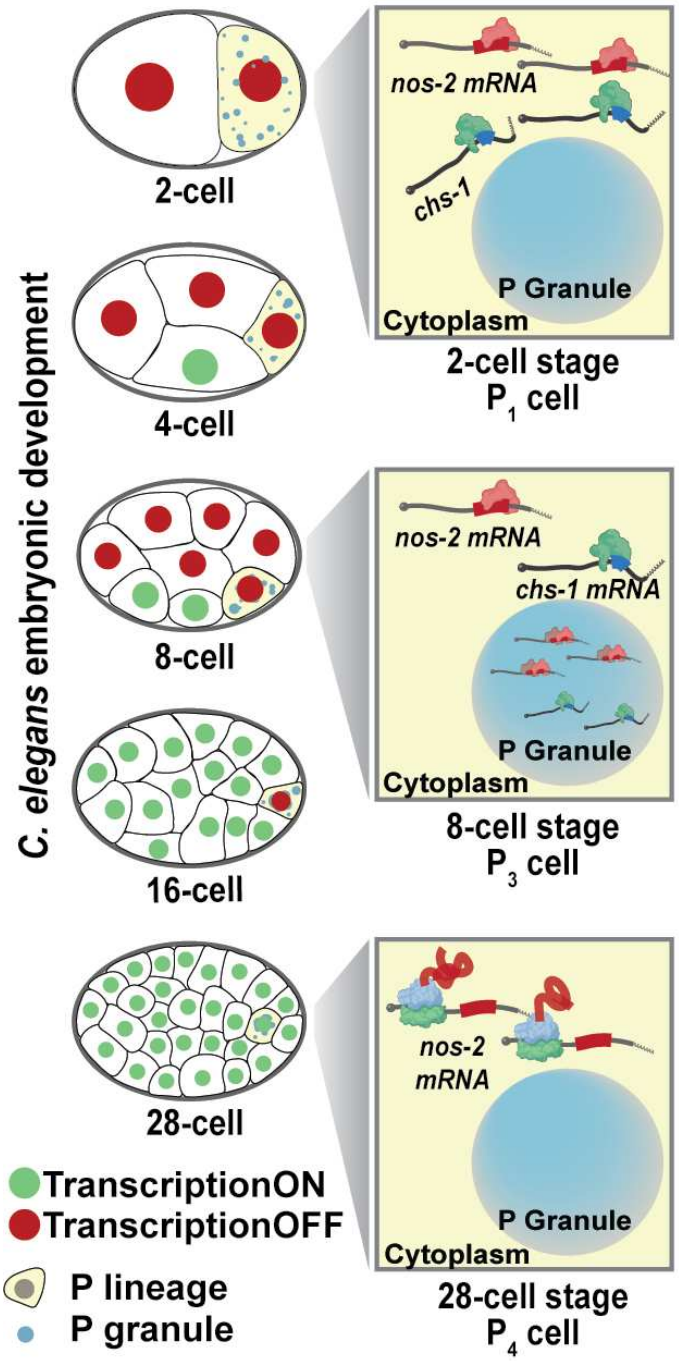

Figure 1.1: P granules accumulate RNA in the *C. elegans* germline. *C. elegans* P granules are germ granules that successively concentrate in the posterior P cells eventually giving rise to the germline. *nos-2* mRNA is found in the cytoplasm of 2-cell stage embryos in a translationally repressed state. From the 4-cell stage to the 28-cell stage, *nos-2* mRNA concentrates into P granules though many *nos-2* mRNA molecules also reside in the cytoplasm. *nos-2* mRNA in P cells is spared from the degradation seen in somatic cells accounting for its concentration down the P lineage. At the 28-cell stage, *nos-2* mRNA emerges from P granules and is translated. *chs-1* mRNA also accumulates in P granules in a manner similar to *nos-2* but is rapidly degraded.

proteins. The MEG-phase appears to allow P granules to form a Pickering emulsion, a solid-phase-stabilized emulsion, in the cytoplasm [65, 67, 68].

It was first appreciated that P granules contain specific mRNAs when hybridization experiments demonstrated P granule enrichment of polyA RNA and *C. elegans*-specific 5' sequences. They were also depleted of or unconcentrated for rRNA [69–71]. Initial efforts identified half a dozen mRNAs associated with P granules [71]. Of these, a homolog of *Drosophila nanos, nos-2*, has emerged as a model transcript illustrating how P granules may function to sequester mRNA for germline-specific expression [72–74].

Why is it useful during germline development to organize RNAs into these structures? In the P granule field, the major historical hypotheses have suggested mRNAs are brought to P granules for translational repression, small RNA mediated silencing, or to enrich transcripts in the P lineage prior to the onset of zygotic transcription.

1.2.3 The P granule transcriptome is comprised of translationally quiescent transcripts with distinct functional categories

The model transcript, *nos-2*, accumulates in P granules in the early stages of embryogenesis [72]. In these stages, *nos-2* is translationally repressed by a series of RNA binding proteins (RBPs) that directly interact with its 3' UTR (Figure 1.1) [73, 74]. Through its RNA binding partners, *nos-2* becomes enriched in P granules and depleted in somatic cells as it concentrates within the P lineage [72]. Once the primordial germ cell has been specified, *nos-2* mRNA emerges from P granules coincident with relief of its translational repression, resulting in NOS-2 protein production exclusively in the germ lineage [72–74]. For these reasons, the hypothesis emerged that RBPs usher *nos-2* mRNA to P granules for the purpose of restricting its protein production in both space and time.

It was long unclear how representative *nos-2* was of P granule transcripts generally. Recently, Lee et al. characterized the P granule transcriptome in early embryos by genome-wide pull-down assay (Figure 1.2) [75]. This was striking as several groups had attempted to characterize P granule

transcriptomes with little success. Those attempts typically relied on RIP-seq of liquid-phase P granule components (personal communication), whereas Lee et al. targeted the gel-phase protein, MEG-3::GFP, using an iCLIP protocol (Figure 1.2). In a complementary approach, my thesis work also expanded the list of P granule transcripts by screening a set of mRNAs that partition through the P lineage in single-cell RNA-seq data (Chapter 2) [76, 77].

The expanded atlas of P granule transcripts affords exploration of their characteristics, functions, and comparisons to *nos-2*. MEG-3::GFP preferentially pulled down messenger RNA and was enriched at 3'UTRs. Indeed, 3'UTRs are sufficient for P granule localization of reporter transcripts [77]. To determine which types of genes associate with MEG-3, we performed gene ontology (GO) analysis on the list of 492 P granule mRNAs identified by Lee et al. (Figure 1.2). We found P granule mRNAs are associated with the terms: "P granules," "germ cell development," "mRNA binding," and "negative regulation of translation." Interestingly, "mitotic cell cycle," "cytokinesis," "microtubule organizing center," and "chaperonin-containing T-complex" terms are also enriched in the P granule transcriptome. It is possible that post-transcriptional regulation of these mRNAs plays a role in timing the comparatively slow cell cycle of the P lineage and leads to their sequestration in P granules in a translationally repressed state [78, 79]. P-body-related transcripts were also prevalent, illustrating the similarity between these ribonucleoprotein (RNP) condensates (see Chapter 1.2.6).

Both Lee et al. and Parker et al. highlight a key observation – mRNAs that concentrate in P granules are associated with low translational status. A comparison of the P granule transcriptome with ribosome profiling data revealed low ribosome occupancy transcripts were enriched in P granules in a sequence-non-specific manner. In contrast, high ribosome occupancy transcripts were depleted from P granules [75].

Whether the function of P granules is to concentrate, asymmetrically localize, surveil, or regulate the translation of their constituent RNAs, P granules can achieve this function by containing only a minority population of any transcript at any given time. While lowly translated mRNAs are enriched in P granules, only between 21 – 75% of any particular transcript were observed within

them at any given time [75, 77]. Curiously, many P granule-localized transcripts undergo degradation and do not re-emerge for translation representing a complex regulatory control that is not understood. Nonetheless, these findings highlight a perennial question: are mRNAs brought to P granules for the purpose of promoting translational repression, or does inhibition of translation promote recruitment to P granules?

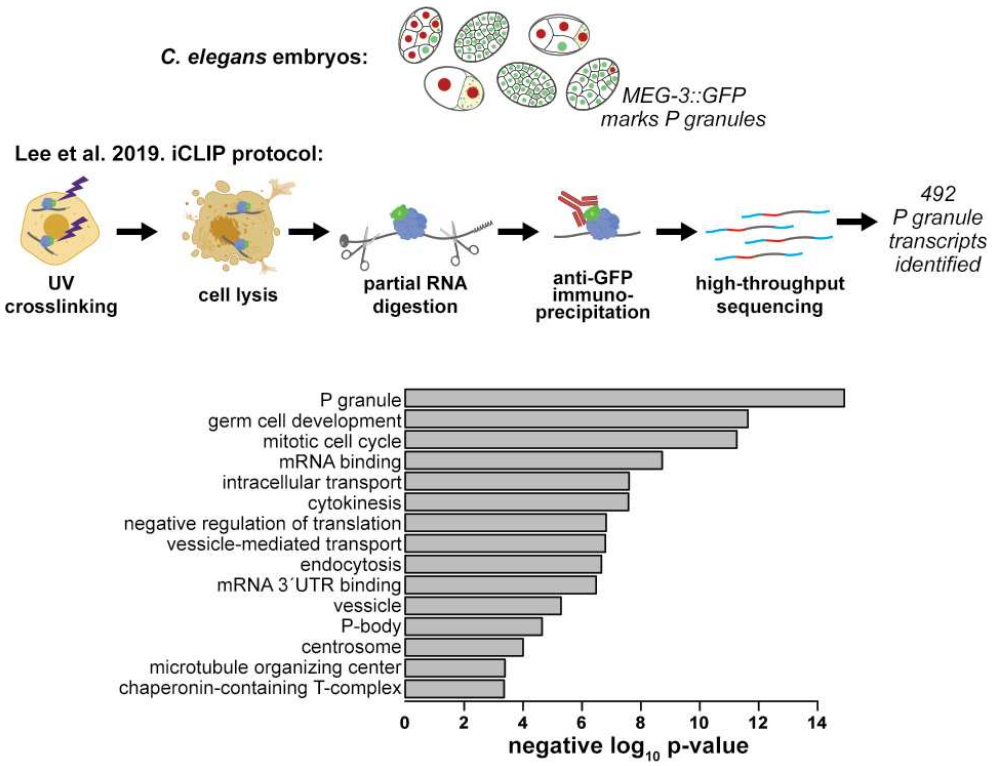

Figure 1.2: The *C. elegans* P granule transcriptome has been characterized. **(A)** Lee et al. identified 492 transcripts enriched in P granules using an individual nucleotide resolution UV- crosslinking and immunoprecipitation (iCLIP) [75]. **(B)** GO terms enriched in the *C. elegans* P granule transcriptome. We used Lee et al's expanded list of 492 MEG-3-associated P granule transcripts to identify enriched categories using the GO::TermFinder [80]. Transcripts with greater than 10 transcripts per million at any embryonic stage from a previous single-cell resolution RNA-seq study [81] were used as a background gene set. The negative $\log_{10}$ of each p-value is shown.

1.2.4 Linking translational status to P granules – repression leads the way

The hypothesis that transcripts are brought to P granules to establish their translationally repressed state is logical given the paucity of ribosomes in P granules [71]. However, observations

from stress granules suggest most transcripts only maintain long-term associations with stress granules if their translational state is already low [82]. Which of these two models occurs in P granules? Single-molecule observations illustrate several natural circumstances where *nos-2* translation repression occurs independently of P granule localization, such as the 1-cell and 2-cell stages of development [77]. Further, depletion of the RBP PIE-1 (Pharynx and Intestine in Excess) prevents *nos-2* from accumulating in P granules but does not lead to precocious NOS-2 protein production [77]. Even when *nos-2* accumulates in P granules, only a fraction of transcripts concentrate there while the majority remain as single, translation-repressed transcripts dispersed in the cytoplasm [77]. Together these findings illustrate that *nos-2* translational repression is independent of P granule localization and may occur prior to it. At the transcriptome-wide scale, depletion of MEG-3 and -4 results in P granule dissolution but fails to increase ribosome occupancy of P granule transcripts [75], illustrating that releasing transcripts from P granules does not result in their translation. Finally, impeding the translation of cytoplasmic transcripts ectopically promotes recruitment to P granules, further implicating mRNA localization as a downstream step following translation regulatory control [75, 77]. Together, these lines of evidence demonstrate that translational repression likely precedes and is sufficient to direct mRNAs to germ granules, not the reverse. However, it is still possible that P granules function in the reinforcement or maintenance of translational repression after transcripts arrive there, but that is yet to be determined.

Though mRNAs are not directed to P granules to repress translation, it should be noted that P granules still regulate gene expression through two major mechanisms. P granules concentrate transcripts in the germ lineage during stages prior to the maternal-to-zygotic transition when RNA Polymerase II transcription is paused [83, 84]. In addition, P granules function to coordinate RNA interference pathways as disruption by *meg-3/4* mutation leads to aberrations in the pool of WAGO-class endo-siRNA, progressive loss of RNAi, and sterility over the course of several generations [85, 86]. Support for the organizational role for P granules comes from similar findings in *Drosophila*. In both *C. elegans* and *Drosophila*, the establishment of translation repression precedes germ granule localization [75, 77, 87, 88], the concentration of particular components in

the germ plasm/germ granules is essential for normal germ cell development [89–92], and RNA interference components concentrate in germ granules [93–95]. These roles are also supported by findings from germ granules of other organisms, suggesting these roles likely conserved among germ granules generally [2].

In summary, P granules function to accumulate translationally repressed transcripts, sequester key mRNAs down the germ lineage, and ultimately coordinate small RNA-mediated regulatory control. Their relative ease of accessibility compared to many other types of germ cells and germ granules has led to their prominence as a quintessential model.

1.2.5 Germ granules serve similar functions

Germ granules across the animal kingdom play widespread roles in RNA regulation. Of these, P granules of *C. elegans* and germ granules of *Drosophila* have been investigated with the greatest scrutiny owing to the ease of imaging these structures microscopically and their facile genetic manipulation. Though the specific names of germ granules, their individual components, and their posited functions are diverse across the animal kingdom, they share several features.

The role of germ granules as hubs of RNA regulatory activity and organization is universal [93–97]. Many of their proteins and RNAs are conserved, with germ granules from all species examined containing Vasa helicases, argonautes, Xrn1, Nanos protein and RNA, and piRNAs, among others [2]. In germ granules of both species, there is a clear structural organization. Germ granules assemble around nucleating proteins (although they differ between species, see below) and are typically near mitochondria [70, 98–100]. Once germ granules nucleate, constituent proteins can oligomerize and RNAs form homotypic clusters, which appear as distinct "domains" within germ granules by microscopy; however, the implications these germ granule domains have on gene regulation are incompletely understood [77, 101, 102].

Differences do exist. Germ granule nucleating factors diverge quickly at the sequence level and are highly species-specific [103]. Moreover, while argonautes are important for germ granule function in both species, their reported roles differ. In *C. elegans*, the argonaute PRG-1 is

implicated in piRNA regulation and germ granule structure, while the *Drosophila* homologue has an additional role in recruiting mRNA to germ granules through a piRNA-dependent templating mechanism [104–106]. Notably, in *Drosophila*, some germ-granule-associated mRNAs are translationally repressed outside the granules and only become translated in association with the germ plasm or germ granules at the posterior pole of the embryo [87, 88].

Further experimentation may reconcile some apparent differences. While germ granule nucleators diverge rapidly, their functions are highly conserved. In fact, many germ granule nucleators from highly divergent species are functionally equivalent. When the *Xenopus* germ granule nucleator, Bucky Ball, is replaced with *Drosophila* Oskar, germ granules assemble, and germ cell specification occurs normally [107]. This functional equivalence indicates even though the primary sequence of germ granules nucleators is not conserved, their functions are.

Recent studies have demonstrated that germ granules in *C. elegans* are composed of spatially separated condensates with distinct functional roles. Some transcripts are thought to transit from P granules to Z granules before being transported to mutator foci to coordinate transgenerational epigenetic inheritance of small RNAs or to SIMR foci to regulate exogenous RNAi [61, 62, 85, 108]. Perturbing the functional organization of P granule-associated condensates by preventing the interaction of PRG-1 and DEPS-1 causes generational loss of P granules [106]. Similarly, when *Drosophila* Aubergine is lost, germ granules fail to form, resulting in sterility [109]. Notably, Aubergine forms a peripheral shell surrounding Tudor labeled germ granules analogous to the various condensates coating P granules [110]. Thus, the generational loss of P granules when PRG-1 association is lost may be due to a loss of piRNA templated recruitment of mRNA to P granules.

Additionally, while *C. elegans* germ granules are associated with translational repression, some transcripts are known to translate only after a period of association with P granules. For instance, translational repression of *nos-2* and *Y51F10.2* occurs even externally to germ granules [75, 77]. They only become translationally activated after a period of association with P granules and components of the germ plasm, similar to the germ plasm-associated activation of specific genes in

Drosophila [87, 88]. Further experiments will determine the degree of conservation among germ granule regulation and organization and which functions are truly distinct to specific animals.

1.2.6 Germ granules share features with stress granules and P-bodies

Germ granules demonstrate striking similarity to two other cytoplasmic biomolecular condensates, stress granules and P-bodies. Stress granules form under stress conditions to store and regulate temporarily translationally repressed mRNA [49, 111, 112]. This reprograms the proteome for stress recovery functions. Processing-bodies, or P-bodies (in contrast to P granules), are associated with translational repression, mRNA metabolism, and mRNA decay [51, 111, 112]. Each of these condensates shows similarities in their behaviors and compositions while also maintaining unique functions (Figure 1.3). These condensates are all rich in RNA content and the concentration and conformation of the RNAs within each condensate also modulates their formation and dissolution [101, 113–116]. They also share protein components. For example, each condensate contains DEAD-box helicases, translation initiation factors, and Argonaute proteins [2, 117, 118] while also housing unique proteins that differentiate their functions, such as the PGL and MEG proteins (P granules), GW182 scaffolding protein (P-bodies), or small ribosomal subunits (stress granules) [2, 48, 65, 111, 112, 118, 119].

What features specify the transcriptomes of these cytoplasmic RNP condensates? Excluding a slight bias for longer RNAs, no specific mRNA attribute results in stress granule, P-body, or P granule localization [75, 120, 121]. These condensates seem only to share the property that they are composed of RNAs that must be post-transcriptionally regulated under various conditions [48, 49, 51, 122–124]. The primary unifying trait of these condensates is their association with predominantly lowly translated transcripts for either temporary storage or eventual decay [77, 125, 126].

It appears that some transcripts may transfer between germ granules, stress granules, and P-bodies, further demonstrating their shared or coordinated functions in gene regulation [48, 49, 127]. Experiments using purified proteins have demonstrated the directional transfer of transcripts from

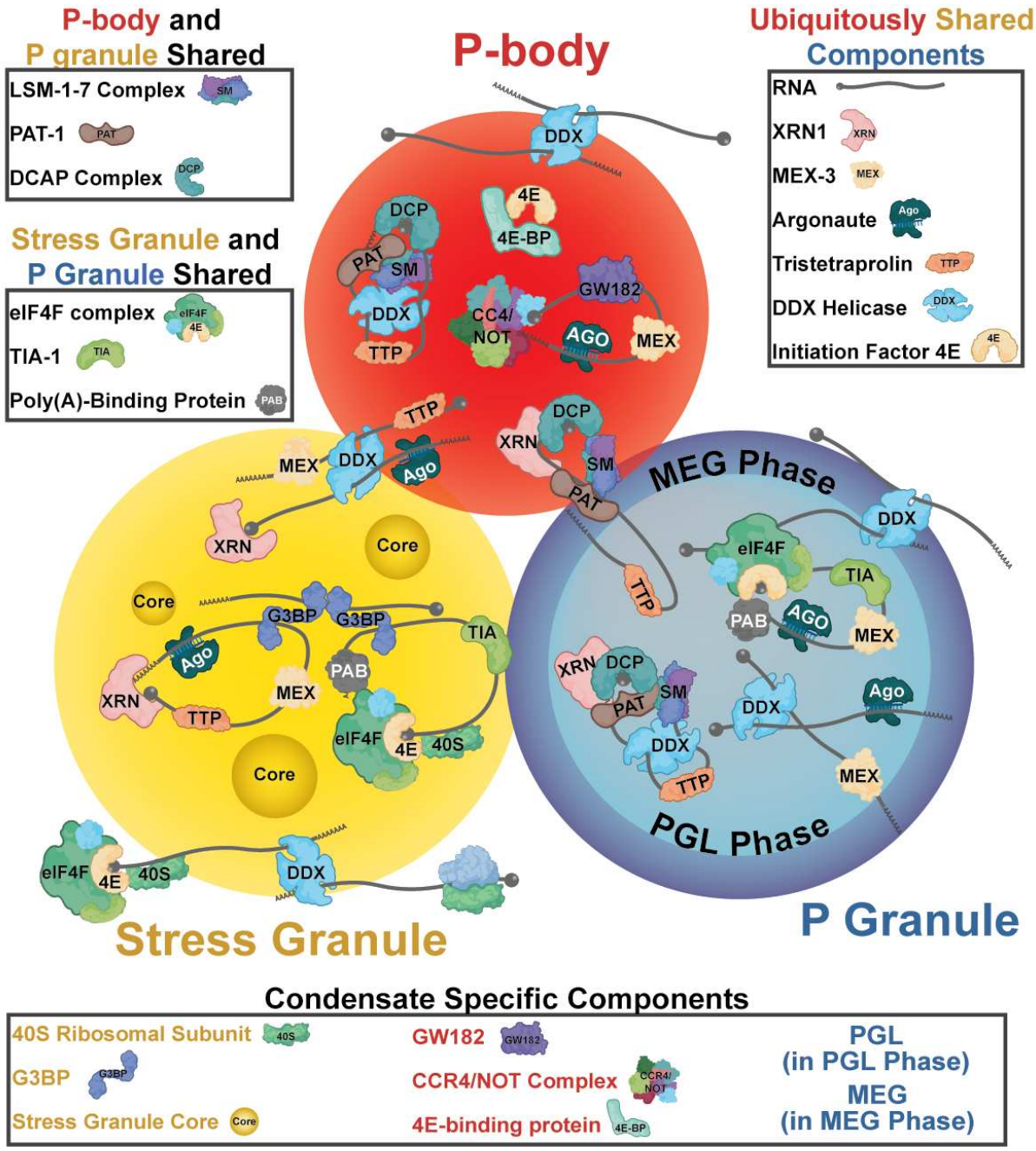

Figure 1.3: Biomolecular condensates organize RNA. Three cytoplasmic RNP condensates– P granules (germ granules), P-bodies, and stress granules – share key components and have some overlapping functions. Some proteins are distinct to each condensate. The components here represent results assimilated from diverse fields of study and are not exhaustive.

Dhh1 condensates to Ded1 condensates, the prototypical helicases of yeast P-bodies and stress granules, respectively [127]. Similarly, stress granule and germ granule components intermix in *C. elegans* normally and grow concurrently under stress [118, 128]. Meanwhile, P-bodies are known to physically associate and partially overlap with both germ granules and stress granules [118, 129]. While the complete roles of these condensates and their interactions are not known, their complexities, functions, and relationships are being studied intently. Recent advances in technology and theory are elucidating surprising modes of regulation and functions in condensates, proving they are more nuanced in their function than simply supporting translation inhibition.

1.3 Condensate mRNAs undergo diverse forms of post-transcriptional regulation

1.3.1 Unlikely translational fates in "repressive" condensates

Most well-studied condensates, including those discussed above, are associated with translational repression. Excluding a small selection of mRNAs, the general theme is that the concentration of mRNA in condensates indicates low translation status. However, recent studies in both well-studied and novel condensates are expanding the diversity and complexity of the functional relationship between the concentration of mRNA in condensates and the regulation of their protein output.

New insights in model condensates are revealing more complex relationships with translation regulation than previously thought. Stress granules and P-bodies have long been thought to house, sequester, and in some instances, degrade translationally repressed transcripts (see Chapter 1.2.1). Several single-molecule studies support a role for these condensates in housing translationally inactive transcripts. Individual transcripts typically associate with stress granules for extended periods only when translation is repressed [82, 125, 130]. Additionally, various translational reporters, protein reporters, proteomics assays, and sequencing assays have yielded significant insight into the RNA, protein, and polysome composition of well-studied condensates like P granules, P-bodies,

and stress granules [75, 77, 120, 121, 131–133]. Due to the enrichment of translation repressive factors and inclusion of only a subset of translation factors as constituents of condensates, these studies have supported the model of condensate-associated translation repression.

However, because these experiments consist of bulk assays, they lack the resolution to determine the translation status of single molecules. Recent advances in *in vivo* single-molecule visualization of translation have suggested that translation of some stress response mRNAs may occur in condensates typically associated with translation repression [134]. Mateju et al. used an in vivo single-molecule translation reporter to demonstrate active translation of a stress response mRNA in G3BP1-labeled stress granules. While they support the widely accepted hypothesis that most stress granule-localized mRNAs are stalled preinitiation complexes, their results show there are exceptions. These results also further support the germ granule models where translationally inactive mRNAs are recruited to condensates rather than causing translational repression.

1.3.2 Translation-associated "Translation factory" condensates and foci

Beyond the occasional translation of mRNA in germ granules, P-bodies, and stress granules, mRNA foci distinct from these generally repressive condensates have been reported. Live observations of these foci have revealed the existence of ribosome-rich, actively-translating puncta, or "translation factories" [135, 136]. These include β-catenin foci, some transcripts in neuronal granules, G-bodies or CoFe granules, and axonemal dynein foci [38–40, 137–141]. Preliminary evidence suggests many of these translation factories behave as biomolecular condensates, although more rigorous studies will be required to confirm whether they are all true phase-separated organelles. It is also likely that the components of specific translation factories vary. Variations in components could lead to some translation factories acting as bona fide biomolecular condensates, while others may be highly-ordered ribonucleoprotein complexes. Regardless of whether they are true biomolecular condensates, it is clear that some transcripts associate with ribosomes and other factors to form translationally active membraneless organelles that perform diverse functions.

Why do some transcripts associate with translation factories and translate in a specific region, while others seem to translate throughout the cytoplasm? As with the repressive condensates discussed above, separating cause and consequence for transcript localization to translation factories is challenging and incompletely understood; however, we can speculate about the various functions of condensate-associated translation based on the data that exists.

In neurons, translation-associated condensates facilitate rapid response to stimuli in distal regions of the cell. Condensates composed of translation factors, translation regulators, and transcripts stalled after translation initiation are quickly switched to a translation promoting fate upon stimulation and are essential for neuronal function [141–145]. This spatial organization of translation-associated condensates appears to be thematic. In yeast, mRNAs encoding translation factors form translation-dependent condensates at regions of growth to support increased translational demand [146]. Translation-associated condensates also support metabolic function by coordinating metabolic pathways. Fermentative conditions in yeast promote the translation of glycolytic mRNAs in condensates termed glycolytic-bodies (G-bodies) or Core Fermentation granules (CoFe granules) [137, 138]. Translation-associated condensates are also being implicated in the misregulation of translation. Recent data has provocatively suggested that solid-like amyloid condensates may facilitate stress-response-induced translation in the nucleus to preserve cell viability [147].

While more rigorous examination is required to prove the condensate behavior of many translation factories and more comprehensive screening is needed to define the breadth of translation factory-associated RNAs, their regulation is interesting nonetheless. Understanding what coordinates the spatial organization of mRNAs and their relationship to the translation state within these clusters/condensates will provide a deeper understanding of the mechanisms regulating gene expression.

1.3.3 mRNA localization in novel condensates highlight diverse condensate functions

In addition to the coordinated, local translational response mediated by translation factories, some novel condensates serve more nuanced functions. Condensates can promote RNA/protein effector interactions, spatial and temporal regulation of organelle assembly, and even cell-cycle-dependent protein turnover. Recent studies are uncovering the mechanisms by which condensates can mediate these myriad functions.

Extensive ER-localized translation has been characterized and typically correlates with the local translation of mRNAs encoding secreted or membrane proteins [148–151]. Recent discoveries have added nuance to this model, however. A novel ER-associated condensate called the TIS granule facilitates local translation and protein-effector assembly near the ER [152]. TIS granules appear as an extraluminal, space-filling condensate interleaved with the ER. TIS granules form from the RBP TIS11B and its RNA targets. TIS11B binds the model transcript CD47 at AU-rich elements present only in the longer of two alternatively-spliced 3'UTR isoforms resulting in localization to the TIGER (TIs Granule ER) domain. This distinct environment promotes CD47 protein interaction with the effector protein, SET, in a splice-variant-specific manner. Ultimately, this condensate-mediated complex formation promotes increased membrane localization of the CD47 protein compared to protein translated from the short, non-TIS granule localized CD47 isoform. The TIS granule condensate environment demonstrates how transcript localization in condensates can mediate specific protein-protein interactions and protein function purely based on mRNA sequence.

Additionally, post-transcriptional regulation in condensates can transcend protein-effector interactions and contribute to the organization of entire organelles. One example is the *PCNT* RNA. At the onset of mitosis, the PCNT protein is vital for the successful condensation of pericentriolar material (PCM) surrounding the centrosome [153, 154]. This condensation is in part organized by the localization of *PCNT* mRNA to centrosomes in a translation- and dynein-dependent manner during centrosome maturation [154]. Due to the short span in which the PCM must form, *PCNT*

RNA condensation appears important to combat the kinetic challenge of transporting and synthesizing this large (3336 amino acids in human) protein to direct PCM and centrosome formation during the short period of early mitosis.

Similarly, axonemal dynein foci, otherwise known as Dynein Axonemal Particles (DynAPs) or kl granules in *Drosophila*, are essential for the assembly of dynein complexes [38–40, 140]. These condensates aid in spatially organizing different dynein components and partners, some of which translate within this translation factory condensate environment [38, 39, 140]. Disruption of these condensates by depleting specific components results in the loss of axonemal dynein complexes [39, 140]. In turn, this loss of axonemal dynein causes defects in cilial beating, cell motility, and in some instances, sterility. These defects demonstrate the importance of translationally active condensates in promoting proper protein function, complex assembly, and the ultimate function of organelles and the cell [40, 140].

One particularly fascinating and complex form of condensate-mediated post-transcriptional regulation is the β-catenin "destruction complex." Throughout the cell cycle, the β-catenin mRNA is perpetually translated, predominantly in translation factory foci [139]. Surprisingly, the β-catenin protein rapidly degrades in these translation factories until mitosis, when sequestration of the "destruction complex" proteins at the cell membrane dissolves the foci [139]. At this point, β-catenin can safely transit to the nucleus to perform Wnt signaling. This constant cycle of protein synthesis and degradation allows for the rapid and specific response required for functional Wnt signaling as the cell cycle progresses. This complex regulation demonstrates how concentrating transcripts can overcome kinetic challenges and facilitating rapid post-translational to meet the needs of the cell.

Overall, cytoplasmic RNP condensate organelles represent dynamic environments. Germ granules, stress granules, and P bodies are enriched for translationally inactive transcripts, but newly discovered roles for biomolecular condensates in post-transcriptional regulation adds complexity to these models. Even condensates long thought to house translationally repressed RNAs can facilitate the translation of a subset of their constituents. As a result, the functional purpose of

organizing RNA and protein into tightly condensed biomolecular condensates is a field of active research with many recent insights and many remaining questions. As the field moves forward, we are interested to see whether RNA accumulation in these granules occurs for the purpose of generating a molecular outcome or as a consequence of their regulatory control.

1.4 Conclusions

mRNA localization and translational control are intimately linked. It is essential to translate proteins when and where they are required and maintain repression when translation would be hazardous to cell viability. It is becoming increasingly apparent that mRNA condensation is an integral contributor to the functional success of the proteins many mRNAs encode.

A recent burst in technologies capable of identifying and characterizing local transcriptomes has led to a surge in the number of known localized condensate RNAs. Genomics approaches, such as RIP-seq, HITS-CLIP/CLIP-seq, iCLIP, irCLIP, and iPAR-CLIP, can capture cohorts of mRNAs that associate with individual RNA Binding Proteins within condensates [155]. Proximity labeling assays, such as APEX2-seq, RNA BioID, and nucleobase oxidation can characterize transcriptomes close to cellular landmarks or distinct locales, which is particularly useful considering the transient structure of many condensates [25, 26, 131]. High-throughput microscopic-sequencing approaches can visualize the localization of the entire transcriptome in fixed cells, or even entire tissues, at single-molecule resolution [156–158]. Complementarily, microscopy-based techniques are now capable of assessing mRNA localization and abundance with unprecedented resolution. *In situ* hybridization techniques, expansion microscopy, and super-resolution microscopy allow for the visualization of transcripts at or beyond the single-molecule level. The advent of nascent chain tracking and viral coat protein-based approaches (MS2 and PP7), Cas13-mediated labeling, riboflour labeling, and other advances in *in vivo* imaging provide a deeper understanding of the constitution, distribution, and dynamics of the transcriptome [82, 159–163]. As these and other technological advances continue, we can visualize just how widespread RNA localization within

condensates is. In doing so, our understanding of the central dogma of biology is becoming more comprehensive.

Many unanswered questions remain. A key challenge will be to determine how essential RNA condensation is. In some classic examples, such as the germ granule RNAs in *Drosophila*, it is clear that this localization is essential for development. However, the functional effects of removing any particular transcript from a condensate are challenging to study. Disruption of condensates can result in the misregulation of many transcripts. Even when experimenting with one transcript, the localization and translation regulatory elements are often difficult to separate or inseparable, leading to pleiotropic effects when inducing their mislocalization [11, 73, 74, 77, 164, 165]. Thus, it is uncertain in many instances whether RNA condensation is a causative, redundant, reinforcing, or symptomatic effect of regulatory control.

Another remaining challenge is understanding the relationships between the cytoplasmic RNP condensates such as stress granules, P-bodies, and germ granules. Do they share an evolutionary origin? Do they communicate with one another? Are there pathways that transfer mRNAs from condensate to condensate? How do these largely repressive condensates relate to translation-associated condensates like translation factories? Decreased reliance on *in situ* microscopy and application of *in vivo* imaging will reveal which mRNAs are true long-term residents of condensates, which are merely migrating through them, and how this correlates with their translational regulation.

Additionally, it will be interesting to continue exploring the structural role of RNA itself in mediating condensation. Long non-coding RNAs are now appreciated for their role in scaffolding structures in both the cytoplasm and nucleus. Several studies have demonstrated that messenger RNA can also scaffold the recruitment of other molecules such as *RPS28B* RNA that recruits its own protein to scaffold P-bodies and the triad of mRNAs *CLN3, BNI1,* and *SPA4* that nucleate Whi3 droplets in *Ashbya gossypia* [37, 166]. Incredibly, some mRNA sequences appear to have intrinsic localization cues. The *BglG* mRNA in *E. coli* may localize to cell membranes through a PolyU tract, which can interact electrostatically with membranes *in vitro* [20, 167]. Further, some

RNAs form homotypic clusters *in vivo* or self-segregate *in vitro* [101,166,168]. Understanding the underlying physics of RNA interactions with cellular components will inevitably provide insight into how condensates form, their internal dynamics, and their ultimate functional effects.

Though a complete understanding of these condensates remains elusive, defects in condensates can result in pronounced phenotypes or even human disease. Defects in mouse germ granule components impair spermatogenesis [169]. In *Drosophila* and *Xenopus*, defects in germ granules prevent germline development, while in *C. elegans*, loss of P granules causes germline transcriptomic changes and can result in immediate, temperature-sensitive, or multi-generational progressive onset of sterility. Stress granules regulate nucleocytoplasmic transport that misfunctions in amyotrophic lateral sclerosis (ALS) and frontotemporal dementia (FTD). These transport defects are rescued by perturbing stress granule components, indicating a functional link between them [170]. Neurological disorders are also associated with P-body dysregulation as mutations in the DDX6 helicase prevent proper assembly of P-bodies and ultimately result in intellectual disability in humans [171]. Further, mutants for the P-body proteins DCP-1 and DCP-2 exhibit phenotypes in pattern-triggered immunity resulting in pathogen susceptibility [172].

By understanding the components and mechanisms cells use to localize RNA and regulate local translation we can begin to better design experiments or treat human diseases. It is not difficult to envision applications stimulated by understating the cues regulating RNA localization and translation. Developing nuanced tools to control the temporal availability of proteins could provide new tunable or inducible expression systems. Further, identifying cis-acting elements sufficient for sequestration of transcripts away from their usual destination will allow for dissecting the functions of RNA localization *in vivo*. Understanding mechanisms underlying the misregulation of condensates implicated in neurological disorders can impact human health by supporting the search for treatments. Perhaps more importantly, it may reveal the underlying genetics and environmental conditions that contribute to the progression of these diseases allowing for more preventative measures to be taken.

As this field matures, insights will continue to emerge. The theme that multiple modes of mRNA regulation can occur concurrently within condensates is likely to continue. The interrelatedness between mRNA localization, translation regulation, decay, and small RNA-mediated regulation will continue to come into focus. Discoveries of highly specialized biomolecular condensates are likely to accelerate as we determine how the biophysical properties of these structures impact the biochemistry of mRNA regulatory control. Further, the linkages between coordinated translational control at each distinct level of initiation, elongation, termination, and recycling are all likely to be important. The field is rich for potential discoveries as mRNA condensation and translation regulatory control emerge from a niche field, studied in a few systems, to a generalizable feature of cell biology.

1.5 Author contributions

This chapter was originally written as a review on RNA localization generally and is currently under review. The original manuscript was co-authored by Dylan M. Parker, Lindsay P. Winkenbach, and Erin Osborne Nishimura. All authors made roughly equal contributions to conceptualization, writing, figure generation, revising, and formatting for the initial submission. All revisions between the original submission and the version presented here were generated by Dylan M. Parker for the purpose of improving the manuscript and tailoring for this chapter.

Chapter 2

mRNA localization is linked to translation regulation in the *Caenorhabditis elegans* germ lineage[2]

2.1 Summary

Caenorhabditis elegans early embryos generate cell-specific transcriptomes despite lacking active transcription, thereby presenting an opportunity to study mechanisms of post-transcriptional regulatory control. We observed that some cell-specific mRNAs accumulate non-homogenously within cells, localizing to membranes, P granules (associated with progenitor germ cells in the P lineage) and P-bodies (associated with RNA processing). The subcellular distribution of transcripts differed in their dependence on 3'UTRs and RNA binding proteins, suggesting diverse regulatory mechanisms. Notably, we found strong but imperfect correlations between low translational status and P granule localization within the progenitor germ lineage. By uncoupling translation from mRNA localization, we untangled a long-standing question: Are mRNAs directed to P granules to be translationally repressed, or do they accumulate there as a consequence of this repression? We found that translational repression preceded P granule localization and could occur independently of it. Further, disruption of translation was sufficient to send homogenously distributed mRNAs to P granules. These results implicate transcriptional repression as a means to deliver essential maternal transcripts to the progenitor germ lineage for later translation.

[2]This chapter was published in July 2020 under the same title

Dylan M. Parker, Lindsay P. Winkenbach, Sam Boyson, Matthew N. Saxton, CamrynDaidone, Zainab A. Al-Mazaydeh, Marc T. Nishimura, Florian Mueller, and Erin Osborne Nishimura. mRNA localization is linked to translation regulation in the *Caenorhabditis elegans* germ lineage. Development, 147(13):dev186817, 2020.

2.2 Introduction

The progression of life from two gametes to an embryo involves the transfer of gene expression responsibilities from the parental to zygotic genomes. In animals, this maternal-to-zygotic transition requires a pause in transcription during late oogenesis, fertilization and the first stages of zygotic development [84, 173–175]. Until zygotic transcription resumes, cell-type transcriptome differences in the early embryo arise through post-transcriptional mechanisms acting on mRNAs inherited from the parental gametes.

In *Caenorhabditis elegans*, transcriptional repression initiates in late oogenesis by an unknown mechanism [176, 177], but is sustained in post-fertilization stages by sequestration of transcriptional machinery to the cytoplasm [178]. Transcription resumes 2 h post-fertilization, initiating in the somatic cells of four-cell embryos and culminating in the P_4 cell of the primordial germ lineage (P lineage) at the 28-cell stage [69, 179].

Even in the absence of *de novo* zygotic transcription, the transcriptomes of early *C. elegans* blastomeres diversify. Single-cell resolution RNA-seq (scRNA-seq) assays have determined that the first two daughter cells (AB and P_1) contain 80 AB-enriched and 201 P_1-enriched transcripts distinguishing them [180]. Similar approaches have identified additional maternally-inherited transcripts with biased representation in different lineages through the first four cell divisions [76]. These cell-specific transcripts likely arise through post-transcriptional mechanisms of mRNA decay, mRNA stabilization or by movement (active or passive) of transcripts into distinct regions of dividing cells.

Interestingly, there is no reason *a priori* for transcriptome diversification to be required for cell-specific protein production. Translational control plays a major role in driving protein production during germline development [181] and into early embryogenesis. Indeed, a major class of mutants that affect early cell fate development are cell-specific RNA binding proteins (RBPs), the target transcripts of which are translated with spatiotemporal specificity [73, 74, 182, 183].

Still, the mRNA encoding Negative Effect on Gut development (NEG-1; a cell fate determinant) has an anterior bias preceding anterior NEG-1 protein production, suggesting that patterns in

mRNA localization can precede or even be amplified at the translation step [180, 184]. Therefore, maternal asymmetric mRNAs appear to be important for cellular diversification in early development. In this study, we explore the mechanisms and functions of this patterning.

We report that several maternally-inherited transcripts localize to subcellular regions within individual cells. In general, the anterior-biased (AB cell-enriched) transcripts tended to localize to cell-peripheral regions, often where the proteins they encode function. In contrast, posterior-biased (P_1 cell-enriched) transcripts formed clustered granules overlapping with P granules, membraneless compartments of RNAs and proteins that form liquid-liquid phase separated condensates or hydrogels that mark the progenitor germ lineage [53, 65].

Understanding the functional roles of P granules (and other phase-separated condensates) is a current major challenge. In early embryos, P granules are dispersed in the cytoplasm and highly dynamic [59, 60], but later grow into larger granules that coalesce around the nucleus [185]. Here, they extend the nuclear pore complex environment and branch into more specialized condensates such as mutator foci [186] and Z-granules [61]. Worms can recover from P granule disruption in early embryonic stages to properly specify the germline [187], but later or sustained dysregulation leads to perturbations in germ-cell development [188], disruption of gene expression regulatory control [189–191] and fertility defects [91, 188, 192]. The reasons why mRNAs associate with P granules may depend on the individual transcript or developmental stage, but functions such as translational repression, RNA processing, small RNA-based regulation or piRNA licensing are possibilities, based on the functions of the proteins that compose P granules.

Here, we identify several new mRNA transcripts associated with P granules and observe that many are lowly translated. Indeed, the well-studied P granule-resident mRNA *nos-2* is also translationally repressed at early embryonic stages. Later, this repression is relieved when NOS-2 becomes essential for germline development [72–74]. It is possible that mRNA transcripts, such as *nos-2* and others, associate with P granules to promote translational repression. Alternatively, transcripts may accumulate in P granules after repression as a downstream step. In this study, we find that translational repression of *nos-2* mRNA precedes *nos-2* mRNA accumulation in P

granules and can persist without P granule localization, supporting the second model. Further, we found that loss of translation can direct homogenously distributed transcripts to P granules, again suggesting that localization is a downstream step.

Overall, our work expands the list of membrane-associated mRNAs (from 0 to 5) and P granule-associated mRNAs (from roughly 10 to 16). Our findings also suggest that the subcellular patterning of maternally-inherited transcripts is a common feature of early embryogenesis. By identifying and studying additional mRNAs with subcellular localization in the *C. elegans* early embryo, we can better determine mechanisms and purposes of their localization in early development.

2.3 Results

2.3.1 Maternally-inherited mRNA transcripts display subcellular localization

scRNA-seq assays have identified transcripts that are differentially abundant between cells before the onset of zygotic transcription in *C. elegans* [76, 81, 180, 193]. To verify the cell-specificity of these mRNAs and visualize their localization, we selected several to image in fixed *C. elegans* embryos using single-molecule resolution imaging [single-molecule fluorescence *in situ* hybridization (smFISH) or single-molecule inexpensive fluorescence *in situ* hybridization (smiFISH)]. We chose eight AB-enriched transcripts, eight P_1-enriched transcripts, four uniformly distributed (maternal) transcripts and eight zygotically expressed transcripts. Single-molecule resolution imaging confirmed the cell-specific patterning predicted by RNA-seq for seven out of eight AB-enriched, seven out of eight P_1-enriched transcripts, and four out of four symmetric transcripts. Strikingly, many maternally-inherited transcripts yielded subcellular localization patterns beyond cell-specific patterning (Table 2.1, Figure 2.1, Figure 2.2).

AB-enriched transcripts tended to localize to cell peripheries (Table 2.1). Specifically, AB-enriched *erm-1 (Ezrin/Radixin/Moesin), lem-3 (LEM domain protein), ape-1 (APoptosis Enhancer)* and *tes-1 (TEStin homolog)* mRNAs accumulated there. ERM-1 protein also accumulates at cell-to-cell contacts where it functions in the remodeling of apical junctions [194]. Similarly, LEM-3,

Table 2.1: A survey of early embryonic mRNA transcripts for localization patterns. Twenty maternally-inherited mRNA imaged by smFISH (or smiFISH). Eight transcripts identified as AB-enriched, eight P_1-enriched and four symmetrically-distributed in scRNA-seq data at the two-cell stage were surveyed [180]. Rankings represent the rank-order cell-enrichment of each transcript in their respective scRNA-seq dataset. Eight zygotically expressed transcripts were also surveyed [76]. A control for P granule localization, *nos-2* mRNA, was included [71, 72]. Note: Clustering of *mex-3* transcripts was observed only in the P lineage; they remained diffuse in somatic cells. *Transcripts that are explored in further detail in this paper.

mRNA	maternal v. zygotic	2-cell enrichment by RNA-seq (ranking)	2-cell enrichment by smFISH	patterning at 1-cell to 16-cell by smFISH	notes
erm-1	maternal	AB-enriched (1)	AB-enriched	**cell periphery**	
C50E3.13	maternal	AB-enriched (3)	AB-enriched	no	
neg-1	maternal	AB-enriched (4)	AB-enriched	no	
lem-3	maternal	AB-enriched (7)	AB-enriched	**cell periphery**	
era-1	maternal	AB-enriched (10)	AB-enriched	no	
ape-1	maternal	AB-enriched (26)	symmetric	**cell periphery**	
mex-3	maternal	AB-enriched (42)	AB-enriched	**granular**	granules are in the P lineage
tes-1	maternal	AB-enriched (75)	AB-enriched	**cell periphery**	variable
chs-1	maternal	P_1-enriched (1)	P_1-enriched	**granular**	
clu-1	maternal	P_1-enriched (4)	P_1-enriched	**granular**	
lpgm-1	maternal	P_1-enriched (25)	P_1-enriched	**granular**	also known as F57B10.3
T24D1.3	maternal	P_1-enriched (40)	P_1-enriched	**granular**	
puf-3	maternal	P_1-enriched (75)	symmetric	**granular**	
cpg-2	maternal	P_1-enriched (30)	P_1-enriched	**granular**	
pgl-3	maternal	P_1-enriched (32)	P_1-enriched	no	
bpl-1	maternal	P_1-enriched (170)	P_1-enriched	no	
set-3	maternal	symmetric	symmetric	no	granular in posterior cells at later stages
gpd-2	maternal	symmetric	symmetric	no	
B0495.7	maternal	symmetric	symmetric	no	
imb-2	maternal	symmetric	symmetric	**nuclear periphery**	
elt-2	zygotic			no	
end-1	zygotic			no	
hlh-27	zygotic			no	
hsp-60	zygotic			no	
ref-1	zygotic			no	
tbx-32	zygotic			no	
tbx-38	zygotic			no	
Y75B12A.2	zygotic			no	
nos-2	maternal	symmetric	symmetric	**granular**	previously reported P granule mRNA

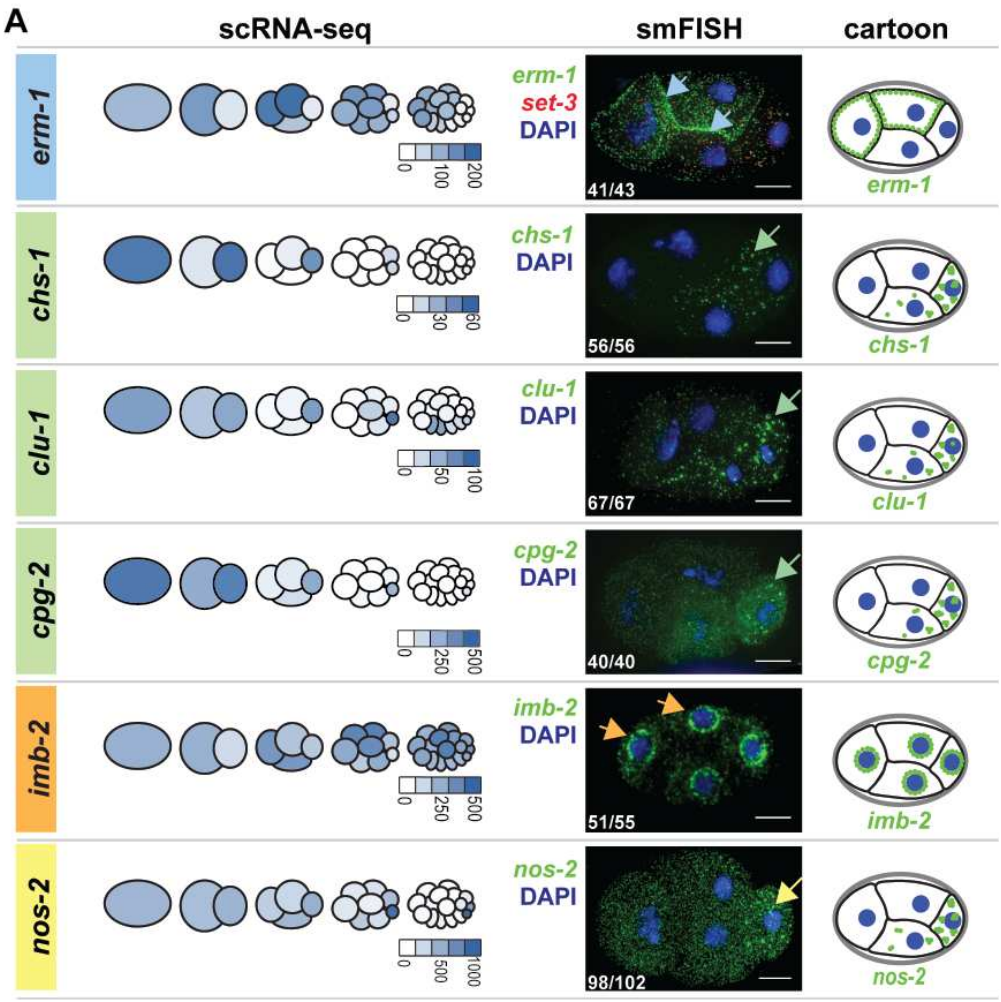

Figure 2.1: Subcellular localization patternsof maternally-inherited mRNAs. (A) mRNA localization patterns for *erm-1, chs-1, clu-1, cpg-2, imb-2* and *nos-2* are shown (Table 2.1). They represent AB-enriched (blue), P_1-enriched (green) and symmetric (orange) maternal mRNA and a known P granule control (yellow). Left column shows the pattern of mRNA abundance through the first four cell divisions as previously reported using scRNA-seq data [76], illustrated as a proportionally colorized pictograph. Normalized transcript abundance values are indicated below each pictograph. Center column shows mRNA imaging using smFISH of a representative four-cell embryo, showing the mRNA of interest (green), DNA (DAPI; blue), and *set-3* [*SET (trithorax/polycomb) domain containing*; red] as a symmetric control. *set-3* was co-probed in each embryo but only shown once for simplicity. mRNAs were found concentrated at cell peripheries (*erm-1*, blue arrows), into clusters (*chs-1, clu-1* and *cpg-2*, green arrows), at nuclear peripheries (*imb-2*, orange arrows) or at known P granules (*nos-2*, yellow arrow). Inset white numbers represent the number of times the pattern was observed out of the total four-cell-stage embryos surveyed over a minimum of five biologically replicated experiments. Right column shows cartoon depictions of each mRNA of interest (green), shown to summarize subcellular distribution patterns. Scale bars: 10 μm.

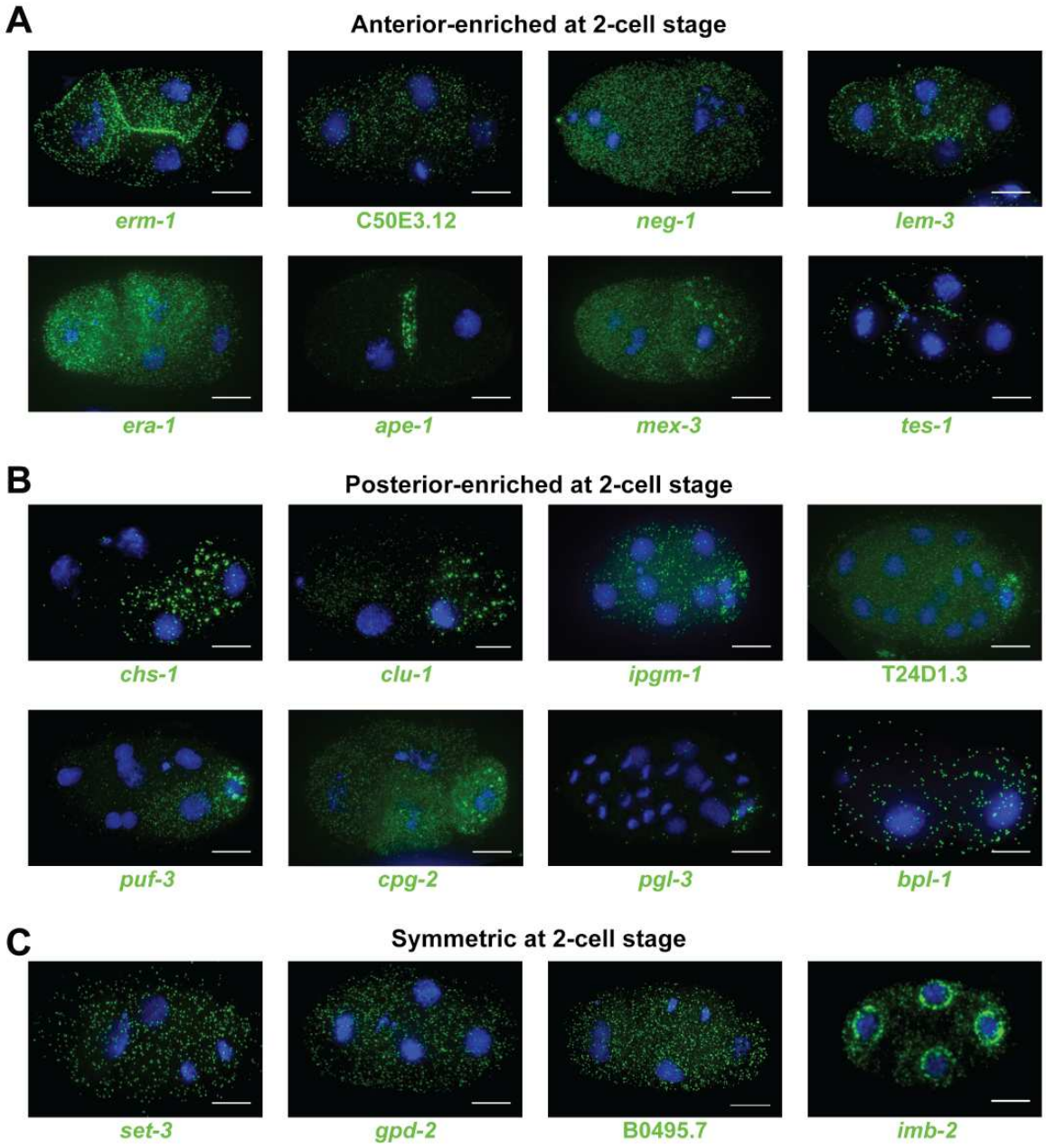

Figure 2.2: Subcellular localization patterns of surveyed transcripts. 8 AB-enriched, 8 P_1-enriched, and 4 symmetric transcripts were selected for verification and examination by smFISH with all transcripts in green and DAPI in blue. **(A)** AB-enriched transcripts *erm-1 (Ezrin/Radixi/Moesin), C50E3.12, neg-1 (Negative Effect on Gut development, lem-3 (LEM domain protein), era-1 (Embryonic mRna Anterior), ape-1 (APoptosis Enhancer), mex-3 (Muscle EXcess),* and *tes-1(TEStin homolog)* are shown. **(B)** P_1-enriched transcripts *chs-1 (CHitin Synthase), clu-1 (yeast CLU related), ipgm-1 (cofactor Independent Phospho-Glycerate Mutase homolog), T24D1.3, puf-3 (PUF domain containing), cpg-2 (Chondroitin ProteoGlycan), pgl-3 (P-GranuLe abnormality),* and *bpl-1 (Biotin Protein Ligase)* are shown. **(C)** Uniformly distributed transcripts *set-3 (SET domain containing), gpd-2 (Glyceraldehyde 3-Phosphate Dehydrogenase), B0495.7,* and *imb-2 (IMportin Beta family)* are shown. Tabulation of the results are in Table 2.1. Scale bars: 10 μm.

a nucleic acid metabolizing enzyme, localizes to cell membranes and cytoplasmic foci [195]. The localization of APE-1 and TES-1 proteins are uncharacterized, but they contain domains known to associate with membranes (ankyrin-repeat domain in APE-1 and PET domain in TES-1) [196,197]. For this chapter, we focused on *erm-1* as a representative of this group (Figure 2.1).

P_1-enriched transcripts primarily aggregated in RNA granules in the P lineage (Table 2.1, Figure 2.1, Figure 2.2). This included transcripts important in eggshell formation such as *chs-1 (CHitin Synthase)* and *cpg-2 (Chondroitin ProteoGlycan)*, mitochondrial distribution and stress response such as *clu-1 [yeast CLU-1 (CLUstered mitochondria) related]*, as well as the carbohydrate-metabolizing enzyme *F57B10.3* (recently renamed *ipgm-1; cofactor-Independent PhosphoGlycerate Mutase homolog*) [198–201].

Of the maternally-inherited transcripts that distribute symmetrically at the two-cell stage, only one of four tested showed subcellular patterning (Table 2.1, Figure 2.2). The transcript *imb-2 (IMportin Beta family)* localized to nuclear peripheries, coincident with its encoded protein, an Importin-β homolog that facilitates nuclear pore complex import (Figure 2.1). In no cases did we observe subcellular localization for mRNAs expressed zygotically, suggesting that subcellular patterning is more common among maternally-inherited transcripts that those zygotically transcribed. However, because zygotically dividing cells subdivide successively, beyond the 16-cell stage their reduced size could potentially obscure our ability to call their localization accurately (Table 2.1).

In addition to these surveyed transcripts, we also used smFISH to image *nos-2*, a previously reported mRNA resident of P granules required for germline maintenance and fertility [72] (Table 2.1, Figure 2.1). smFISH verified P granule localization of *nos-2* mRNA and showed that granular patterning was coincident with P lineage enrichment – both beginning at late four-cell stage (Figure 2.3F).

To explore the dynamics of subcellular patterning through embryogenesis, we imaged key transcripts from the one-cell stage through hatching. The onset and persistence of subcellular mRNA localization varied depending on the transcript and its biology (Figure 2.3). *chs-1* mRNA first localized to posterior clusters at the one- or two-cell stage but degraded over successive cell divisions

until dissipating by the 48-cell stage (Figure 2.3), whereas *imb-2* appeared at or near nuclear membranes in all stages assayed. This is consistent with the roles of the proteins as CHS-1 is essential primarily for deposition of chitin in the eggshell between oogenesis and egg-laying [202], whereas the IMB-2 protein is required throughout the life of the worm for nuclear import [203]. In contrast to *chs-1, nos-2* mRNA distributed homogenously before the four-cell stage and then began clustering in the P lineage, coincident with its degradation in somatic cells. *nos-2* mRNA clusters grew in size until the 28-cell stage (Figure 2.3). At the 28-cell stage, *nos-2* transcripts became visible as individuals in the cytoplasm, concurrent with a decrease in the size of *nos-2* mRNA clusters. Translational regulation of *nos-2* is dynamic during these stages. *nos-2* mRNA is translationally repressed before the 28-cell stage, at which point translation repression is relieved [73, 74]. Therefore, the transition in RNA localization accompanies this transition in regulatory status. What was more surprising is that *nos-2* mRNA could both be observed as individual mRNAs and localized into granules before the 28-cell stage during its phase of translational repression. During the one-, two-, and early 4-cell stages, *nos-2* mRNA fails to produce protein, but also does not localize to clusters, illustrating that these processes can be uncoupled. Altogether, subcellular transcript localization appears transient or persistent depending on the encoded function of the mRNA.

2.3.2 Quantification strategies to characterize mRNA patterning

To better describe the subcellular mRNA patterns we observed, we detected individual mRNA molecules in 3D images using FISH-quant [204] and developed metrics to describe their localizations at membranes or within clusters.

erm-1 mRNA localized to cell peripheries. To characterize this propensity in an unbiased manner, we calculated the frequency with which *erm-1* transcripts accumulated at increasing distances from cell membranes (Figure 2.4). After normalizing for the decreasing volumes of each concentric space, we determined that *erm-1* mRNA were twice as likely to occur within 5 μm of a cell membrane than more than 5 μm from one. In contrast, homogenously distributed *set-3 (SET do-*

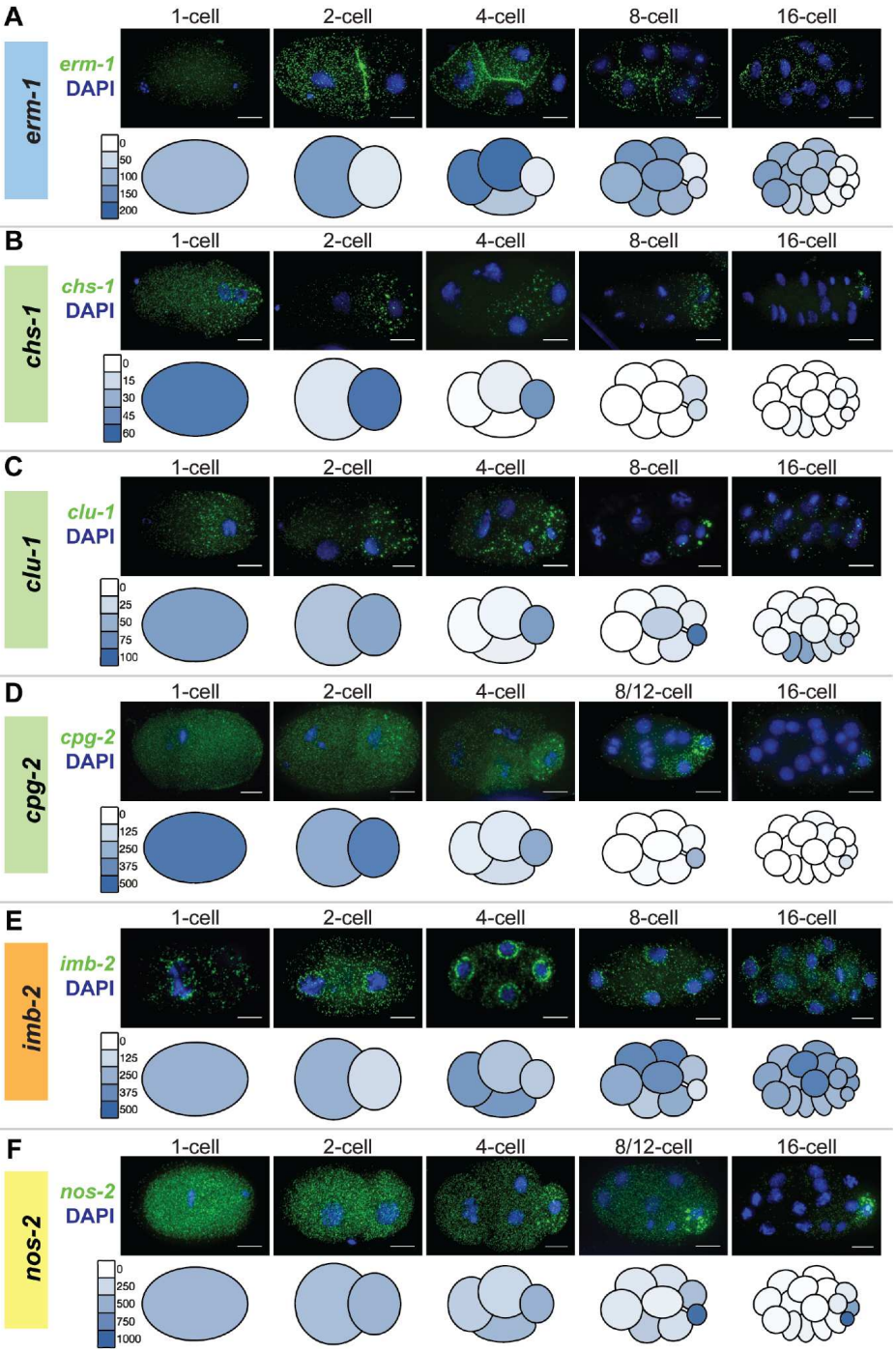

Figure 2.3: Localization patterns of mRNA over developmental time. smFISH microscopy localizations of *erm-1* **(A)**, *chs-1* **(B)**, *clu-1* **(C)**, *cpg-2* **(D)**, *imb-2* **(E)**, and *nos-2* **(F)** shown from 1-cell stage zygotes to the 16-cell stage. mRNA signal is in green. DAPI is in blue. Below each seriesof images is single-cell RNA-seq data from the same transcript [76]. Scale bars: 10 μm.

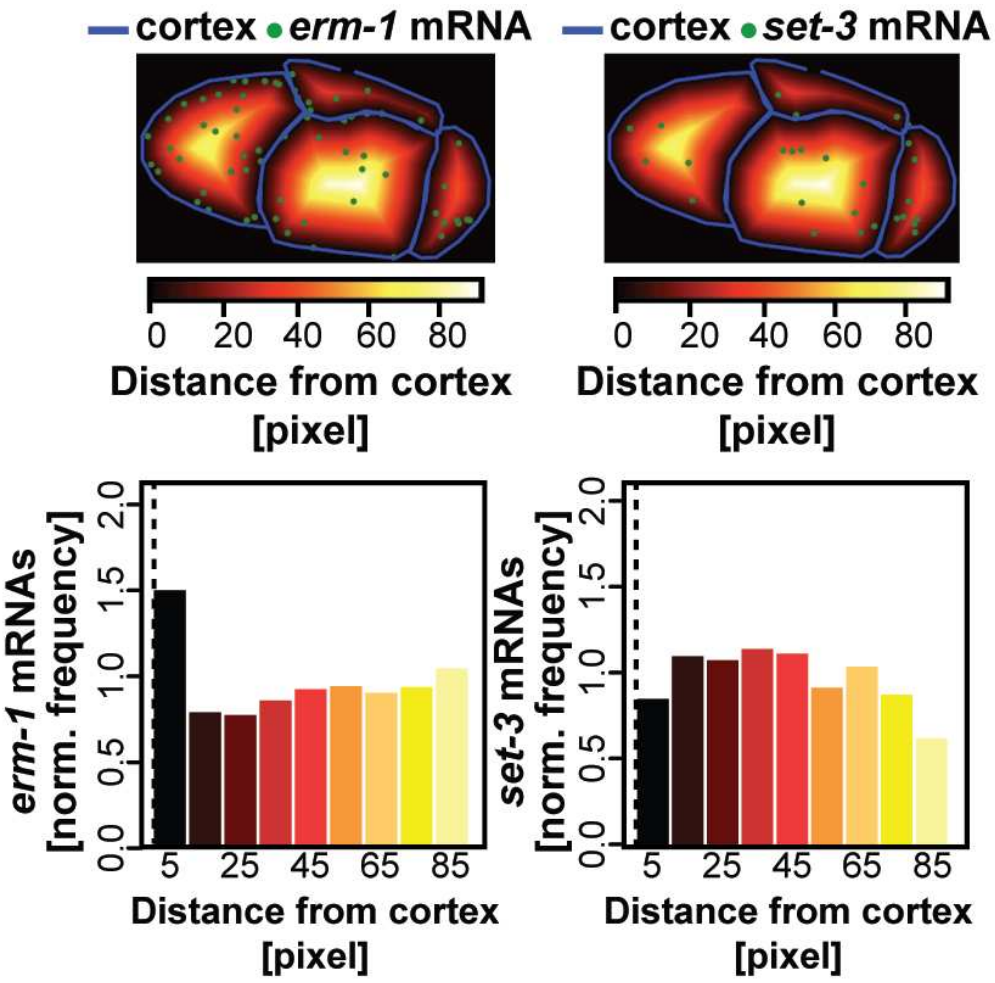

Figure 2.4: Quantification of membrane RNA localization The number of mRNA molecules (green dots) located within binned distances from the cell cortex (blue lines) were tabulated and normalized against the total volume of each concentric space. The frequencies with which *erm-1* mRNA and *set-3* mRNA occurred at varying distances in one embryo are shown.

main containing) transcripts were equally likely to be present at all distances (both measured using 10 μm bin sizes) (Figure 2.4).

Similarly, we calculated the frequency of *imb-2* mRNA at increasing distances from the nuclear periphery (Figure 2.5). *imb-2* transcripts were twice as abundant within 10 μm from the nuclear membrane than at 10 μm or more from a nuclear membrane, again adjusting for volumes of these spaces. The more ubiquitous *set-3* transcripts showed no nuclear peripheral-enrichment.

In developing metrics of mRNA clustering, we found that overlapping mRNA signals complicated the 'single molecule' nature of smFISH, which relies on sufficient spacing between individual

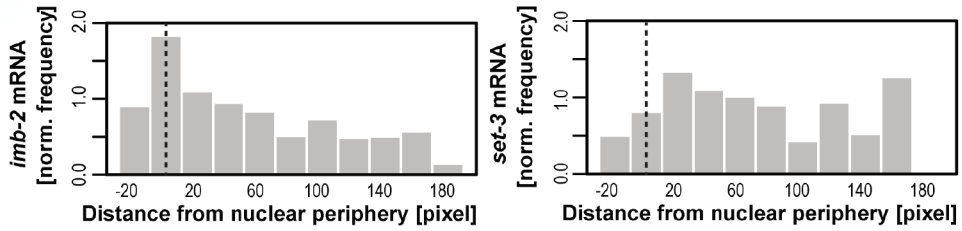

Figure 2.5: Quantification of nuclear peripheral RNA localization The number of mRNA molecules (green dots) located within binned distances from the nuclear periphery (blue lines) were tabulated and normalized against the total volume of each concentric space. The frequencies with which mRNA appeared in relation to the nuclear peripheries in one embryo were similarly calculated for *imb-2* mRNA and *set-3* mRNA.

transcripts. To overcome this, we used a tiered approach, first identifying individual mRNAs [204] before estimating the number of molecules contributing to signal overlap by fitting a Gaussian mixture model (GMM) to the average fluorescence intensities and volumes of the individual molecules (see Chapter 2.5 Materials and Methods). Deconvolved mRNA molecules could then be separated into clusters using a geometric nearest neighbor approach [205].

To characterize mRNA clusters, we quantified total number of mRNA molecules per embryo, total number of mRNA clusters per embryo, fraction of total mRNAs that localize into clusters (as opposed to individuals), and estimated number of mRNAs within each cluster. We calculated these measurements for four clustered transcripts (*chs-1, clu-1, cpg-2* and *nos-2*) at six stages of embryonic development (Figure 2.6). *cpg-2* and *nos-2* were the most abundant transcripts ($\sim$10,000 molecules per embryo) in contrast to *chs-1* or *clu-1* ($\sim$2500 molecules per embryo) at the same time point (two-cell stage). The number of *cpg-2* and *nos-2* mRNA molecules comprising each cluster increased over time, whereas *chs-1* and *clu-1* did not. For *nos-2*, mRNA accumulated to a maximum of 20 molecules per cluster at the 24-cell stage, just before *nos-2* translational activation. After this point, *nos-2* mRNA clusters decreased in size, appearing dispersed in the cytoplasm. All clustered transcripts exhibited marked differences in clustering statistics from the homogenously distributed *set-3* transcripts.

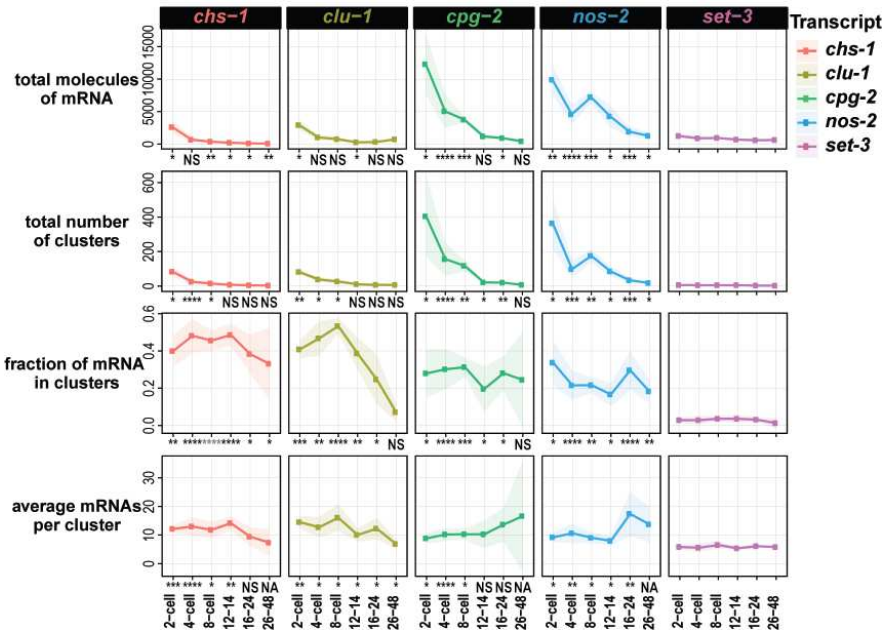

Figure 2.6: Quantification of mRNA clustering patterns Several metrics of clustering were quantified for: *chs-1* (red), *clu-1* (ochre), *cpg-2* (green), the P granule mRNA of *nos-2* (blue) and for comparison *set-3* (purple). We calculated the total number of RNAs in each embryo, the total number of clusters identified in each embryo, the fraction of total mRNAs located within clusters, and the average estimated number of mRNA molecules per cluster within a given embryo. The average of each metric and their standard deviation (shading) for each transcript at six cell stages are shown, representing a minimum of five embryos for each type and time point over a minimum of three replicates. Significance indicates P-values derived from multiple test corrected t-tests comparing the transcript of interest versus the control transcript *set-3* for the metric of interest at the given stage. Adjusted p-value legend: NS>0.05;0.05>*>0.005; 0.005>**>0.0005;0.0005>***>0.00005; 0.00005>****.

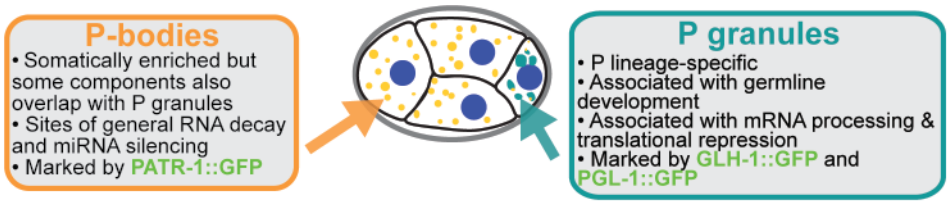

Figure 2.7: P granules are distinct from P-bodies A schematic illustration demonstrating similarities and differences between P granules and P-bodies

2.3.3 Clustered transcripts *chs-1, clu-1, cpg-2* and *nos-2* colocalize with markers of P granules and, less frequently, with markers of P-bodies

mRNA clustering is typically indicative of localization into granules. Many types of condensates exist, such as stress granules (associated with translationally repressed transcripts that accumulate during stress), P-bodies (processing bodies, associated with RNA processing enzymes) and germ granules (associated with regulatory control in animal germ cells). In *C. elegans*, germ granules are specifically called P granules in the early embryo (Figure 2.7) [53, 65] and they segregate to the P lineage with each successive cell division. Dual mechanisms of preferential coalescence/segregation in the P lineage and disassembly/degradation in somatic cells drives their concentration in the P lineage [57, 188, 206].

Given that we observed *chs-1, clu-1* and *cpg-2* mRNAs clustered and progressing down the P lineage, we hypothesized that they might be within P granules. To test this, we imaged *chs-1, clu-1, cpg-2* and, for comparison, *nos-2* by smFISH in worms expressing P granule markers GLH-1::GFP (Figure 2.8) or PGL-1::GFP (Figure 2.9). mRNA clusters overlapped with both P granule markers. Indeed, 23% (*cpg-2*) to 75% (*chs-1*) of identified mRNA clusters overlapped with GLH-1::GFP-marked P granules at the four-cell stage (Figure 2.8), and their co-occurrence increased thereafter. Larger mRNA clusters were more likely to co-occupy space with P granules (Figure 2.10). Conversely, 13-57% of GLH-1::GFP marked P granules contained an mRNA cluster of any specific transcript, suggesting some heterogeneity in their content. Together, these findings illustrate that P-lineage-enriched mRNA clusters in this study are P granule-associated RNAs.

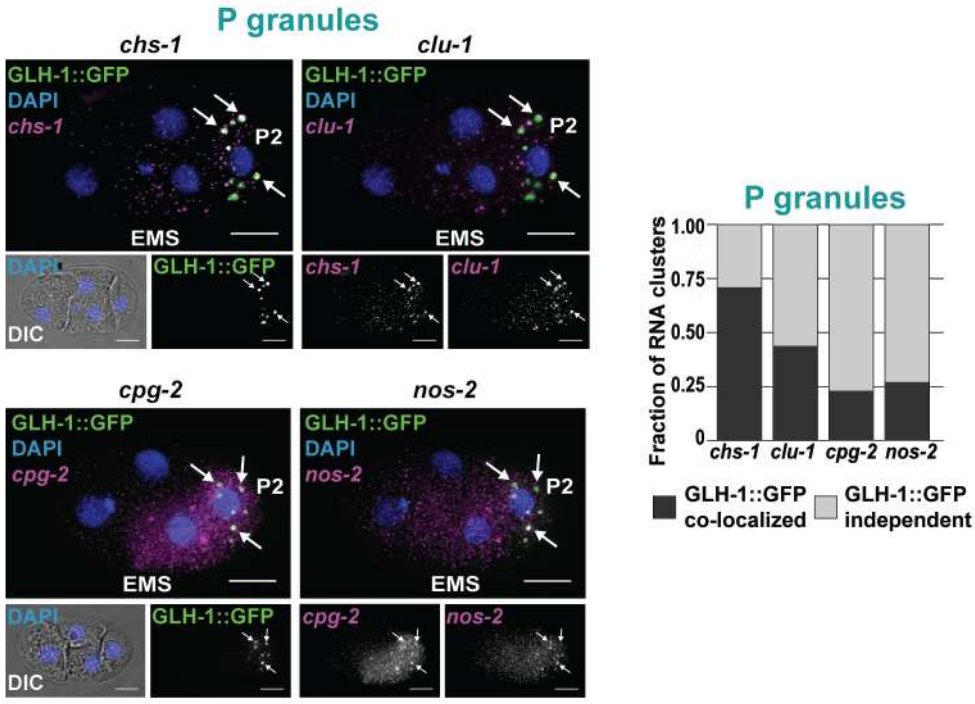

Figure 2.8: P_1-enriched clustered transcripts overlap with the P granule marker GLH-1::GFP. Left) Fixed embryos were imaged for the P granule marker GLH-1::GFP (green) and *chs-1, clu-1, cpg-2,* or *nos-2* transcripts (magenta). DNA (DAPI, blue) and differential interference contrast microscopy (DIC) are also shown. **Right)** The fraction of mRNA clusters overlapping with P granules (dark gray) and P granule-independent clusters (light gray) in four-cell embryos was calculated by assessing spatial overlap between mRNA clusters and GLH-1::GFP-marked P granules. Scale bars: 10 μm.

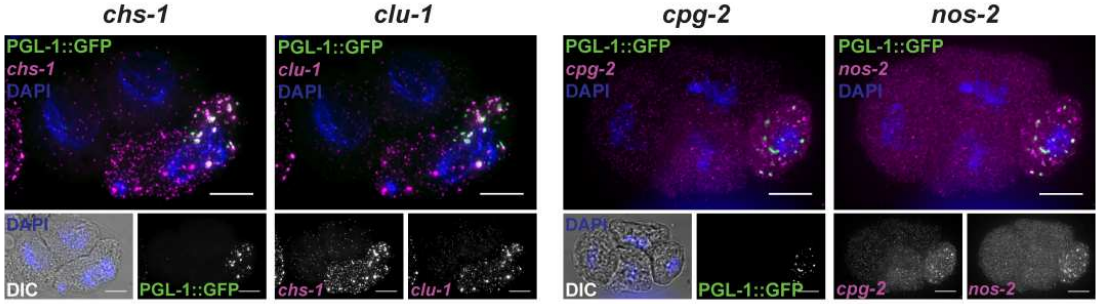

Figure 2.9: P_1-enriched, clustered transcripts co-localize with the P granule marker PGL-1::GFP. In addition to co-localizing with GFP signal in the P granule marker strain containing GLH-1::GFP (Figure 2.8), *chs-1, clu-1, cpg-2,* and *nos-2* mRNAs (all in magenta) also co-localize with a second P granule marker protein, PGL-1::GFP (green). DAPI is illustrated in blue to visualize nuclei and illustrate the 4-cell stage of development. Scale bars: 10 μm.

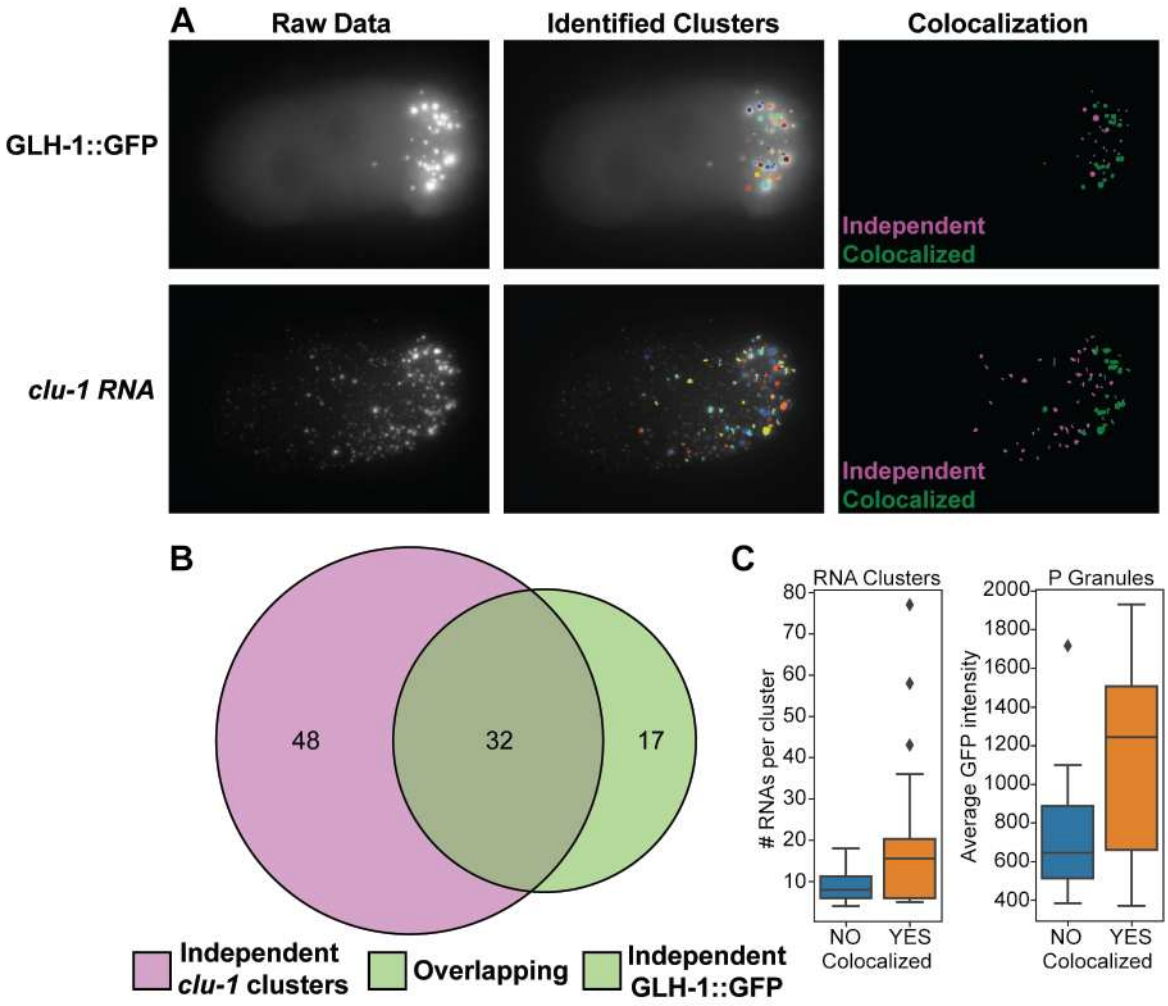

Figure 2.10: Quantification of mRNA cluster overlap with the P granules. mRNA cluster overlap with GLH-1::GFP labeled P granules is calculated using micrographs of GLH-1::GFP and clustered RNAs (*clu-1* shown) **(A, left)**, computationally identifying P granules and RNA clusters **(A, middle)**, and comparing the 3D masks for overlap to identify independent P granules and RNA clusters (magenta) or colocalized clusters (green) **(A, right)**. **(B)** A Venn-Euler diagram illustrating the number of independent *clu-1* mRNA clusters (magenta), independent P granules (light green), and overlapping P granules and mRNA clusters (dark green) in a single embryo (from A). **(C)** Box plots comparing the size of non-over-lapping mRNA clusters and P granules to those overlapping shows larger mRNA clusters more commonly overlap with P granules **(left)** and brighter P granules more commonly overlap with mRNA clusters **(right)**.

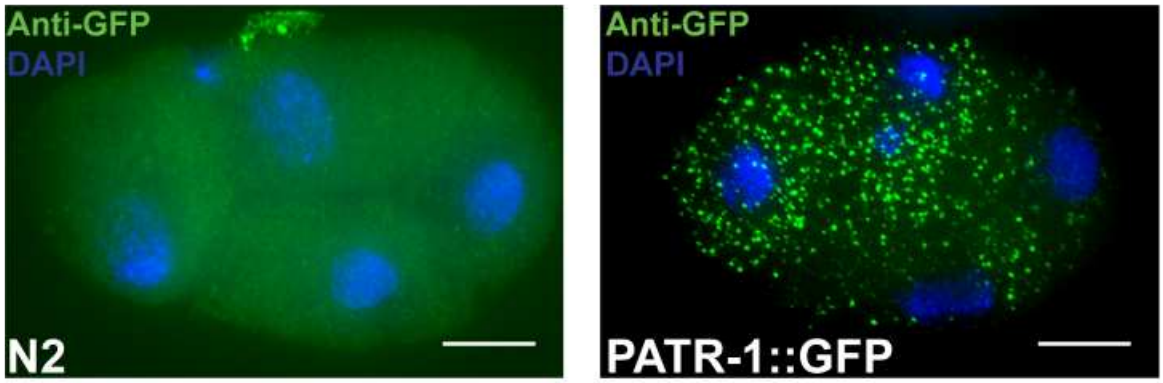

Figure 2.11: Immunofluorescence control images for anti-GFP antibody staining. The anti-GFP antibody reports PATR-1::GFP localization **(green, right)** in PATR-1::GFP containing strains as compared to N2 wild type control strains **(green, left)**. DAPI staining is shown in blue to visualize nuclei and illustrate the 4-cell stage of development. Scale bars: 10 μm.

Depending on the transcript, 25-75% of RNA clusters were distinct from P granule markers at the four-cell stage. These occurred in P cells and their sisters (most evidently in the EMS cell). Because many of the clustered mRNAs (*chs-1, clu-1, cpg-2* and *nos-2*) degrade in early embryogenesis (Figure 2.5), we hypothesized that the RNA clusters that did not overlap with P granule markers were P-bodies. P-bodies – as opposed to P granules – are associated with RNA decay as they contain high concentrations of RNA degrading proteins (DCAP-1, Argonaute, and Xrn-1) [207] (Figure 2.7). In *C. elegans*, P granules and P-bodies share some protein components, but specific proteins distinguish each [2, 118]. To test our hypothesis, we imaged *chs-1, clu-1, cpg-2* and *nos-2* using smFISH concurrently with PATR-1::GFP (yeast PAT-1 Related) amplified by immunofluorescence to mark P-bodies (Figure 2.11, Chapter 2.5 Materials and Methods, Chapter 3). *chs-1* and *clu-1* transcripts were enriched in posterior cells whereas PATR-1::GFP predominantly localized to somatic cells. However, within their regions of overlap, we identified co-localized clusters, indicating that some clusters of *chs-1* and *clu-1* mRNAs reside within P-bodies (Figure 2.12). Some *chs-1* and *clu-1* mRNA clusters failed to overlap with P granule or P-body markers, leaving their identity unknown. Whether these mRNA clusters are stable or short-lived is currently unclear, as fixed smFISH assays cannot resolve their dynamics.

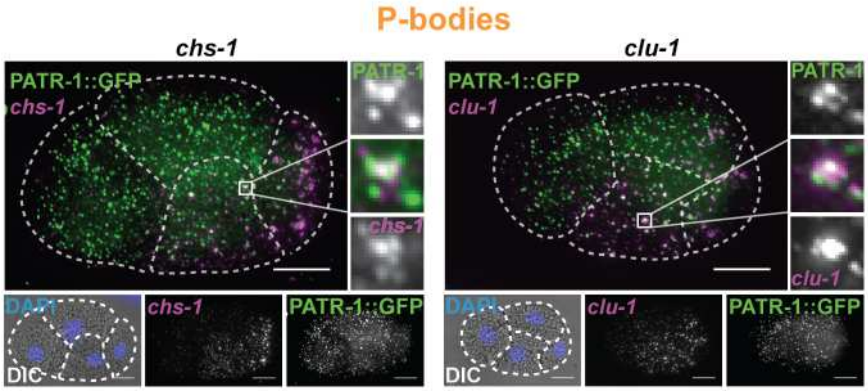

Figure 2.12: Posterior clustered mRNAs partially colocalize with P-bodies. Fixed embryos were imaged for the P-body protein marker PATR-1::GFP amplified using immunofluorescence (green) with smFISH imaging of *chs-1* mRNA or *clu-1* mRNA (magenta), and DNA (DAPI; blue). Enlargements of boxed areas illustrate regions of co-localization. Dashed white lines indicate cell boundaries. Scale bars: 10 μm.

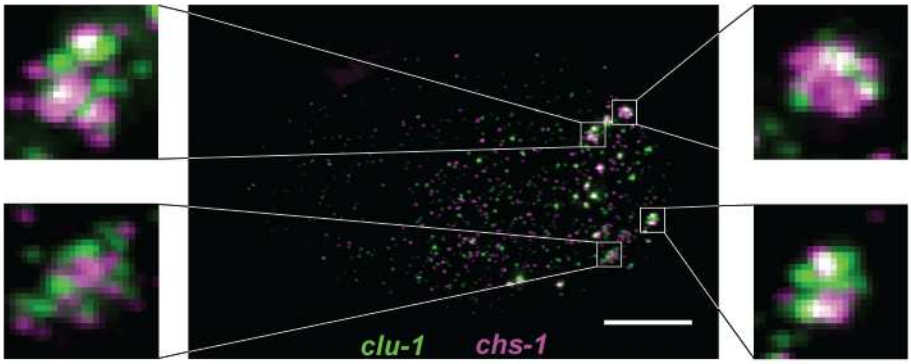

Figure 2.13: mRNA clusters display homotypic clustering within P granules. *chs-1* mRNA (magenta) tend to homotypically cluster in the core of P granules while *clu-1* mRNA (green) also cluster homotypically, but near the peripheries of P granules. Scale bars: 10 μm.

Curiously, we noticed that transcripts did not mix homogenously within P granules but occupied discrete regions within granules. For example, *clu-1* mRNA typically surrounded a *chs-1* mRNA core (Figure 2.13). These observations are echoed by other reports of homotypic mRNA spatial separation within germ granules [101, 208] and suggest a complex organization to granules and the mRNAs they contain.

2.3.4 3'UTRs were sufficient to direct mRNAs to P granules but not membranes

The 3' untranslated regions (UTRs) of transcripts have been implicated in driving subcellular localization of mRNAs in many organisms [209]. To determine whether 3'UTRs of transcripts in our study were sufficient to direct mRNA localization, we appended 3'UTRs of interest onto *mNeonGreen* reporters expressed from the *mex-5* promoter in transgenic strains. We generated single-copy chromosomal integrations using Cas9-mediated insertion into MosSCI integration sites. We imaged *mNeonGreen* mRNA localization using mNeonGreen smFISH probes alongside probe sets for endogenous mRNA in the same embryos.

3'UTRs of *erm-1* and *imb-2* were not sufficient to drive mRNA subcellular localization. Endogenous *erm-1* and *imb-2* mRNAs localize to the cell or nuclear peripheries, respectively, but *mNeonGreen* mRNA appended with *erm-1* or *imb-2* 3'UTRs failed to recapitulate those patterns (Figure 2.14). However, the *imb-2* 3'UTR did show evidence of mRNA destabilization as *Pmex-5::mNeonGreen::imb-2 3'UTR* yielded fewer *mNeonGreen* mRNA than endogenous *imb-2* transcripts or *Pmex-5::mNeonGreen::erm-1 3'UTR* expressed under the same promoter. This suggests that sequences within the body of the *imb-2* mRNA and/or its successful localization are important for mRNA stability. Ultimately, we did not identify sequences within *erm-1* or *imb-2* mRNAs sufficient to direct transcript localization. Either the 5' regions of the mRNA, the coding sequence of the mRNA, the full mRNA, a short N-terminal signal peptide or some larger aspect of the translated protein direct mRNA localization.

In contrast, 3'UTRs of *chs-1, clu-1, cpg-2* and *nos-2* were sufficient to direct *mNeonGreen* mRNA to P granules. Each of the *Pmex-5::mNeonGreen::3'UTR-of-interest* strains yielded *mNeonGreen* mRNA localized to P granules coincident with the localization of their endogenous mRNA (Figure 2.15). The *chs-1* 3'UTR did exhibit hallmarks of transcript destabilization given the comparative low abundance of *mNeonGreen::chs-1 3'UTR* transcripts.

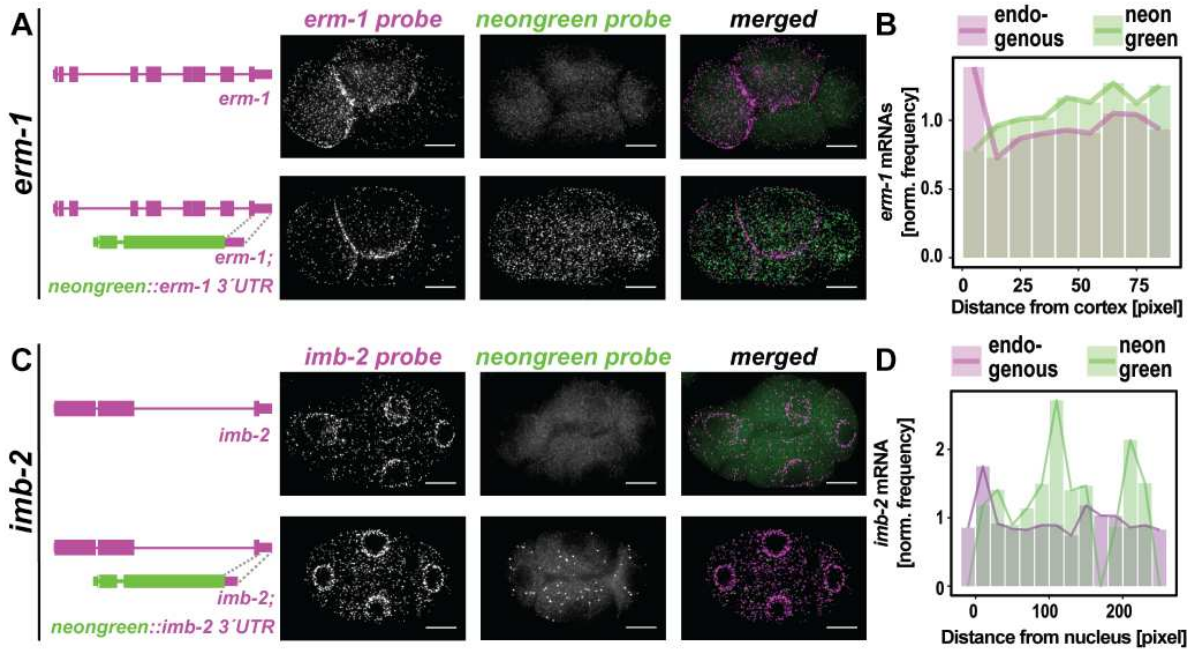

Figure 2.14: The 3'UTRs of membrane associated transcripts are not sufficient for subcellular mRNA localization. The 3'UTRs of *erm-1* **(A)** and *imb-2* **(C)** were appended to monomeric NeonGreen (*mex-5p::mNeonGreen::3'UTR of interest*) and transgenically introduced as a single-copy insert into otherwise wild-type worms. Wild-type control strains **(top panels)** and transgenic strains **(bottom panels)** were imaged by smFISH using probes hybridizing to the endogenous mRNA of interest **(left)** and to *mNeonGreen* mRNA **(middle)** and merged **(right)**. Representative four-cell stage embryos are shown. **(B,D)** Quantification of images shown in A and C indicating the normalized frequency of *erm-1* **(B)** or *imb-2* **(D)** mRNA and *mNeonGreen* mRNA at increasing distances from cell peripheries or nuclear boundaries, respectively, in a single embryo. p-values from multiple test corrected t-tests are shown (NS>0.05; 0.05>*>0.005). Scale bars: 10 μm.

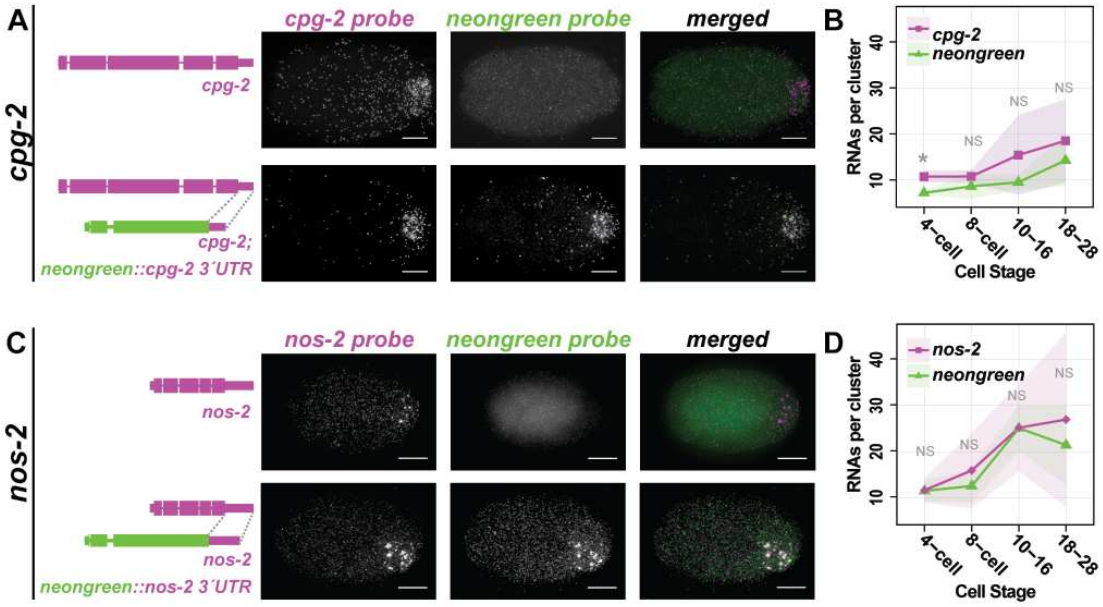

Figure 2.15: The 3'UTRs of posterior-enriched, clustered transcripts are sufficient for subcellular mRNA localization. The 3'UTRs of *cpg-2* **(A)** and *nos-2* **(C)** were appended to monomeric NeonGreen (*mex-5p::mNeonGreen::3'UTR of interest*) and transgenically introduced as a single-copy insert into otherwise wild-type worms. Wild-type control strains **(top panels)** and transgenic strains **(bottom panels)** were imaged by smFISH using probes hybridizing to the endogenous mRNA of interest **(left)** and to *mNeonGreen* mRNA **(middle)** and merged **(right)**. Representative four-cell stage embryos are shown. **(B,D)** The estimated mRNA content per cluster from a minimum of five embryos at each of five binned stages of development from three biological replicates are reported for endogenous *cpg-2* **(B)** or *nos-2* **(D)** (magenta) and *mNeonGreen* reporters (green). P-values from multiple test corrected t-tests are shown (NS>0.05; 0.05>*>0.005). Scale bars: 10 μm.

2.3.5 RNA localization trends with translational status

NOS-2 protein is translationally repressed in germline and early embryonic stages before becoming translationally active in the P_4 cell at the 28-cell stage, with both repression and de-repression being mediated by the *nos-2* 3'UTR [73]. NEONGREEN protein under control of the *nos-2* 3'UTR in our study phenocopied this reported pattern (Figure 2.16A). NEONGREEN fused to 3'UTRs of other transcripts (*erm-1, imb-2, chs-1, clu-1* or *cpg-2*) produced low levels of diffuse fluorescence, preventing interpretation of translational status of these reporter transcripts (Figure 2.16B).

GFP fusions to full-length ERM-1, CHS-1 and CPG-2 proteins were more informative in illustrating the endogenous expression patterns of the proteins encoded by these localized transcripts. ERM-1::GFP localized to the cell cortex throughout embryogenesis, consistent with the role of the ERM-1 protein in linking the cortical actin cytoskeleton to the plasma membrane [194, 210] (Figure 2.17A). CHS-1 and CPG-2 play a transient role in development, evidenced by GFP fusion reporters showing highest signal in the early cell stages followed by their decline (Figure 2.17B, Figure 2.17C). CHS-1 and CPG-2 work together to form two different layers of the trilaminar eggshell. CHS-1 encodes a multipass membrane protein that is exocytosed upon fertilization to polymerize chitin [199, 200]. CHS-1 proteins then internalize, stimulating exocytosis of CPG-1 and CPG-2 proteins that nucleate chondroitin molecules to form the inner eggshell layer – the CPG layer. Indeed, CHS-1::GFP fluoresces at the one-cell stage, but rapidly disappears thereafter (Figure 2.17B). CPG-2::GFP appears to be external to the cells and persists within the extracellular space but declines within cells (Figure 2.17C). mRNAs encoding both *chs-1* and *cpg-2* cluster in P granules and decline in number as development progresses, as evidenced by our smFISH data. Overall, this shows a trend in which transcripts with repressed, declining or low expression tended to accumulate in P granules.

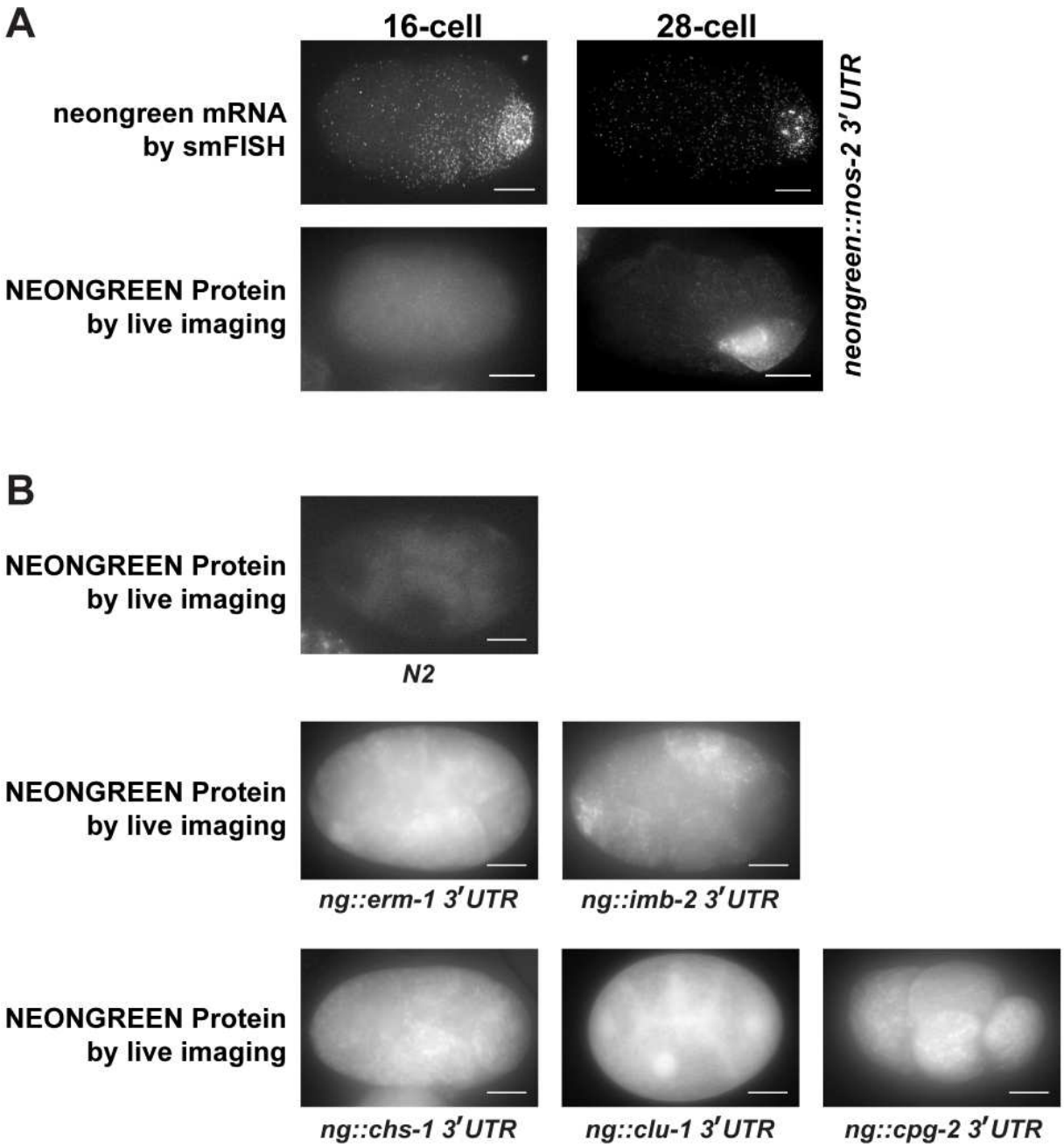

Figure 2.16: *Pmex-5::mNeonGreen::nos-2 3'UTR* RNA recapitulates endogenous translation repression and activation. (A, left) A *Pmex-5::mNeonGreen::nos-2 3'UTR* embryo at the 16-cell stage. smFISH for *mNeonGreen* RNA demonstrated normal RNA localization. Epifluorescent microscopy of living *Pmex-5::mNeonGreen::nos-2 3'UTR* embryos at the 16-cell stage showed no expression of the mNeonGreen reporter protein. **(A, right)** As in **(A)** at the 28-cell stage. Epifluorescent microscopy of living *Pmex-5::mNeonGreen::nos-2 3'UTR* embryos at the 28-cell stage showed P lineage specific expression of the mNeonGreen reporter protein. (B) Epifluorescent microscopy of wildtype N2 embryos demonstrates no apparent fluorescence while *Pmex-5::mNeonGreen::3'UTR* of Interest embryos show low levels of cell-non-specific mNeonGreen fluorescence. Scale bars: 10 μm.

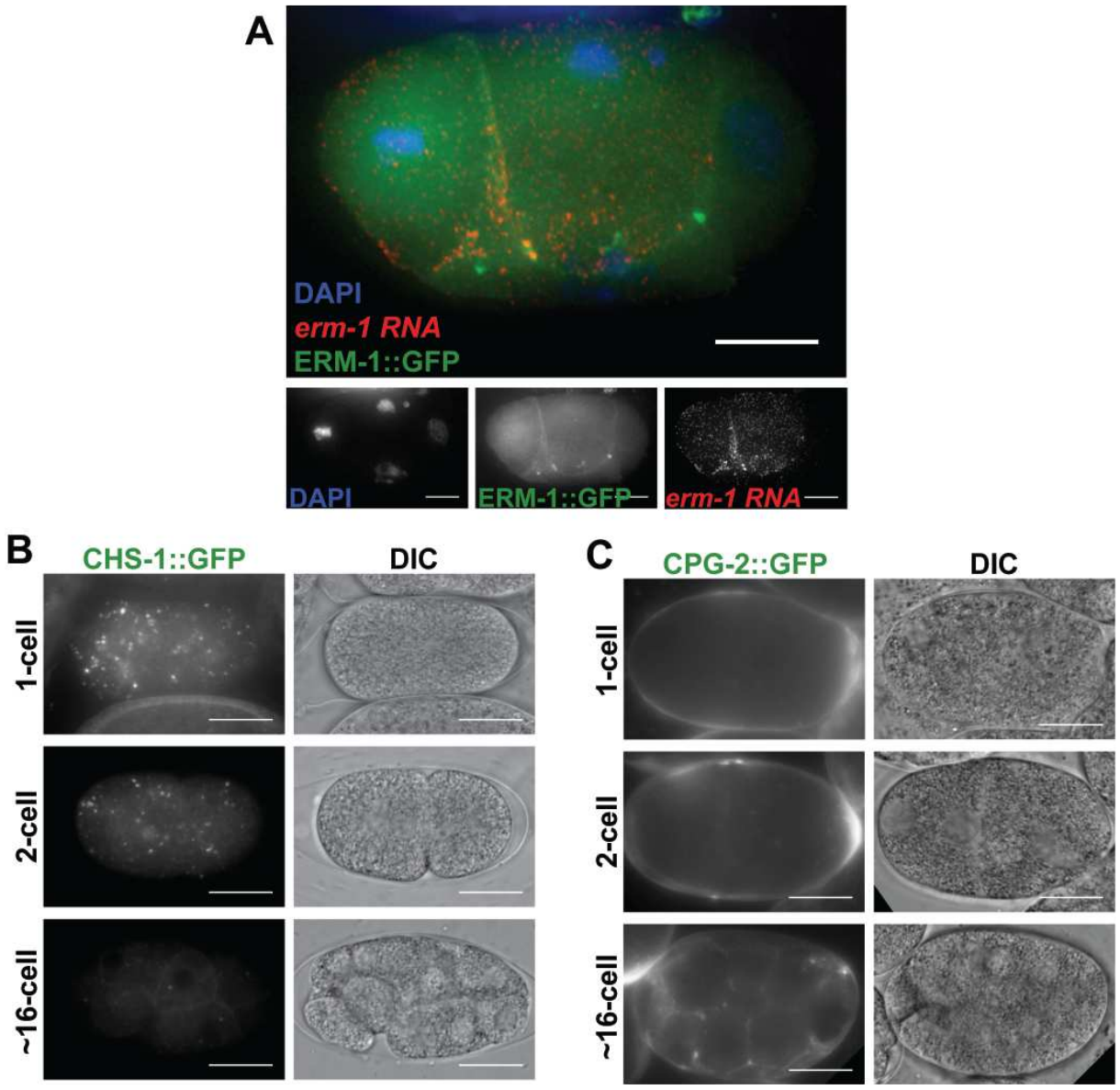

Figure 2.17: *erm-1::gfp* RNA localizes like endogenous *erm-1*. **(A)** smFISH microscopy of *Perm-1::erm-1 ORF::GFP::erm-1 3'UTR* RNA (green) colocalizes with endogenous *erm-1 RNA* (red). **(B)** Epifluorescent microscopy of CHS-1::GFP embryos at the 1-, 2-, and 16-cell stages of embryogenesis show gradual depletion of the CHS-1::GFP protein puncta. **(C)** As in **(B)** imaging CPG-2::GFP embryos. CPG-2::GFP protein can be seen in the extracellular space of the embryo, but not within cells. Scale bars: 10 μm.

2.3.6 Translational repressors of *nos-2* are required for mRNA degradation of multiple transcripts and are required for P granule localization of *nos-2* mRNA

nos-2 is one of three *nanos*-related genes in the *C. elegans* genome and a member of the evolutionarily conserved *nanos* family. Similar to *Drosophila nanos* mRNA, *C. elegans nos-2* mRNA is contributed maternally, concentrates in the progenitor germ lineage, is translationally repressed in oocytes and during early embryogenesis, is translated with spatial specificity and produces a protein that is expressed only in germ cells [72]. *C. elegans nos-2* is required for proper development of the germ cells and is necessary with zygotically-expressed *nos-1* for germ-cell proliferation. Translational repression of *nos-2* is coordinated by four sequential RBPs – OMA-1, OMA-2, MEX-3 and SPN-4 – that directly interact with the *nos-2* 3'UTR [73,74] (Figure 2.18). In oocytes, OMA-1 and OMA-2 are redundantly required to repress translation through direct interactions with the *nos-2* 3'UTR before they are degraded in the zygote. The RBPs MEX-3 and SPN-4 next repress *nos-2* translation throughout the embryo, with SPN-4 being most effective in posterior cells. MEX-3 and SPN-4 both interact with either of two directly repeated RNA sequences in the *nos-2* 3'UTR and function non-redundantly in the early embryo, as RNAi or mutants of either result in premature translation of a *nos-2* reporter. This baton-passing of translational control has been documented for other maternally-inherited transcripts including *zif-1* (an E3 ubiquitin ligase specific to somatic cells) [182] and *mom-2* (the Wnt ligand in P_2) [183].

Though the requirement for OMA-1, OMA-2, MEX-3, and SPN-4 to repress translation of *nos-2* mRNA is clear, owing to a lack of single-molecule resolution FISH data under knockdown conditions it is not known whether they are required to localize *nos-2* mRNA to P granules. To rectify this and to expand the question, we tested how depletion of these RBPs, individually or in combination, impacted the abundance and/or localization of four clustered mRNA transcripts (*chs-1, clu-1, cpg-2* and *nos-2*) (Figure 2.18). True to published reports, individual knockdowns of OMA-1 and OMA-2 had minimal phenotypes, but in combination yielded too few embryos to credibly test as development arrests during oogenesis [211,212]. Depletion of MEX-3 and/or SPN-

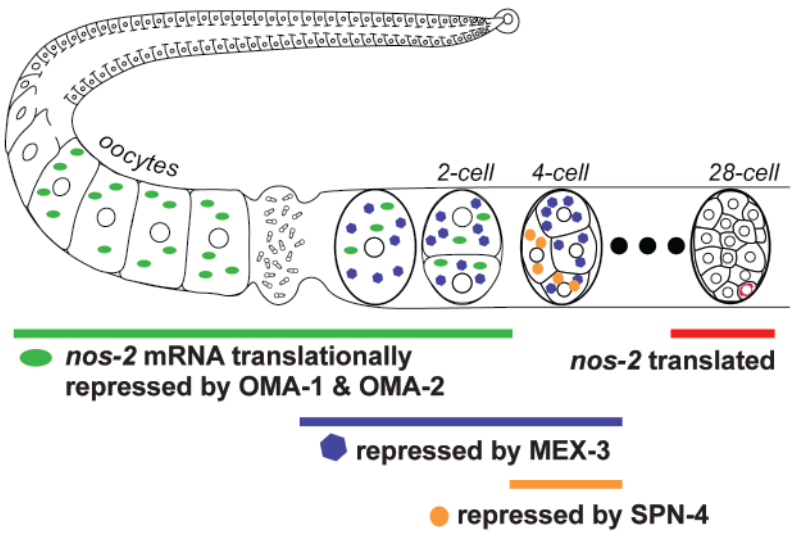

Figure 2.18: A model of *nos-2* mRNA repression by RNA binding proteins. A succession of RBPs cooperatively repress *nos-2* translation from oogenesis through to the 28-cell stage.

4 led to an overabundance of embryo-wide *chs-1, cpg-2* and *nos-2* transcripts compared with mock RNAi control, suggesting that MEX-3 and SPN-4 have a direct or indirect role in mRNA degradation (Figure 2.19, Figure 2.20A, Figure 2.21). MEX-3 and SPN-4 are not required independently to accumulate *chs-1, clu-1*, or *cpg-2* mRNAs in P granules; however, double knockdown of MEX-3 and SPN-4 resulted in a loss of *chs-1* localization to P granules (Figure 2.21). Only the localization of *nos-2* mRNA to P granules was severely disrupted by MEX-3 or SPN-4 loss independently or in combination, as evidenced by the missing *nos-2* clusters in smFISH images (Figure 2.20B, Figure 2.20C) and corresponding decrease in the average number of mRNA molecules per cluster (Figure 2.20A). Together, these findings suggest that MEX-3 and SPN-4 are required for both translational repression and P granule localization of *nos-2* [73, 74]. Further, the role of MEX-3 and SPN-4 in RNA degradation is separable from their role in mRNA localization to P granules, as *chs-1, cpg-2* and *nos-2* require MEX-3 and SPN-4 for RNA clearance, whereas only *nos-2* and *chs-1* rely on them for P granule localization.

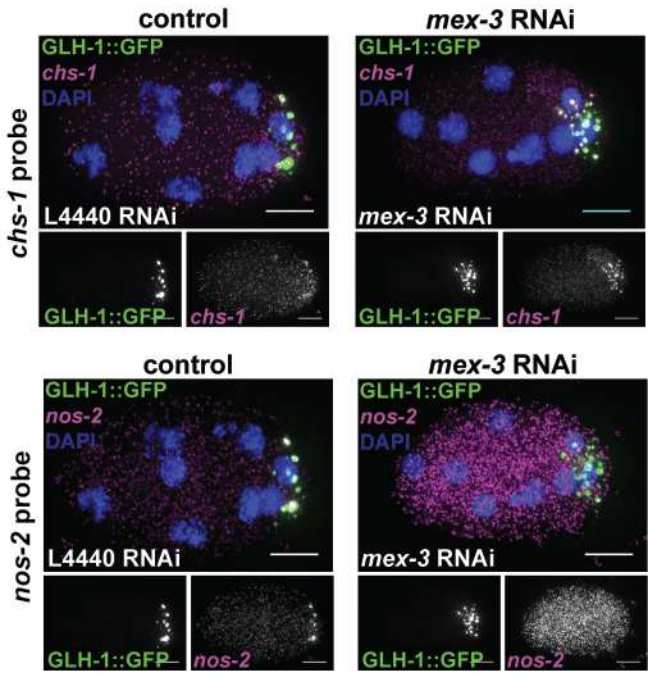

Figure 2.19: Knockdown of the RBP *mex-3* impacts *nos-2* mRNA, but not *chs-1*. *chs-1* mRNA **(magenta, top)** and *nos-2* mRNA **(magenta, bottom)** were imaged by smFISH in a P granule marker strain (GLH-1::GFP, green) under mock (L4440) and *mex-3* RNAi conditions. Scale bars: 10 μm.

2.3.7 RBPs that relieve NOS-2 translational repression impact *nos-2* localization differently

nos-2 mRNA is translationally repressed in the germline, through fertilization, and is only released from repression at the 28-cell stage of development when NOS-2 protein is exclusively produced in the P_4 cell [73,83]. *nos-2* mRNA localizes to P granules in the adult germline [71], but appears distinct from P granules at the one- and two-cell stages (this study). Between the four-cell and 28-cell stages, *nos-2* progressively re-accumulates into P granules, reaching a maximum average density of 20-30 mRNA molecules per P granule before the 28-cell stage (Figure 2.3, Figure 2.5). At the 28-cell stage of development, when NOS-2 translation begins [72], we observed *nos-2* mRNA becoming dispersed in the cytoplasm external to P granules (Figure 2.22A). This could suggest that *nos-2* mRNA emerges from P granules when it becomes actively translated, supported by the fact that P granules are devoid of key ribosomal components required for translation [71].

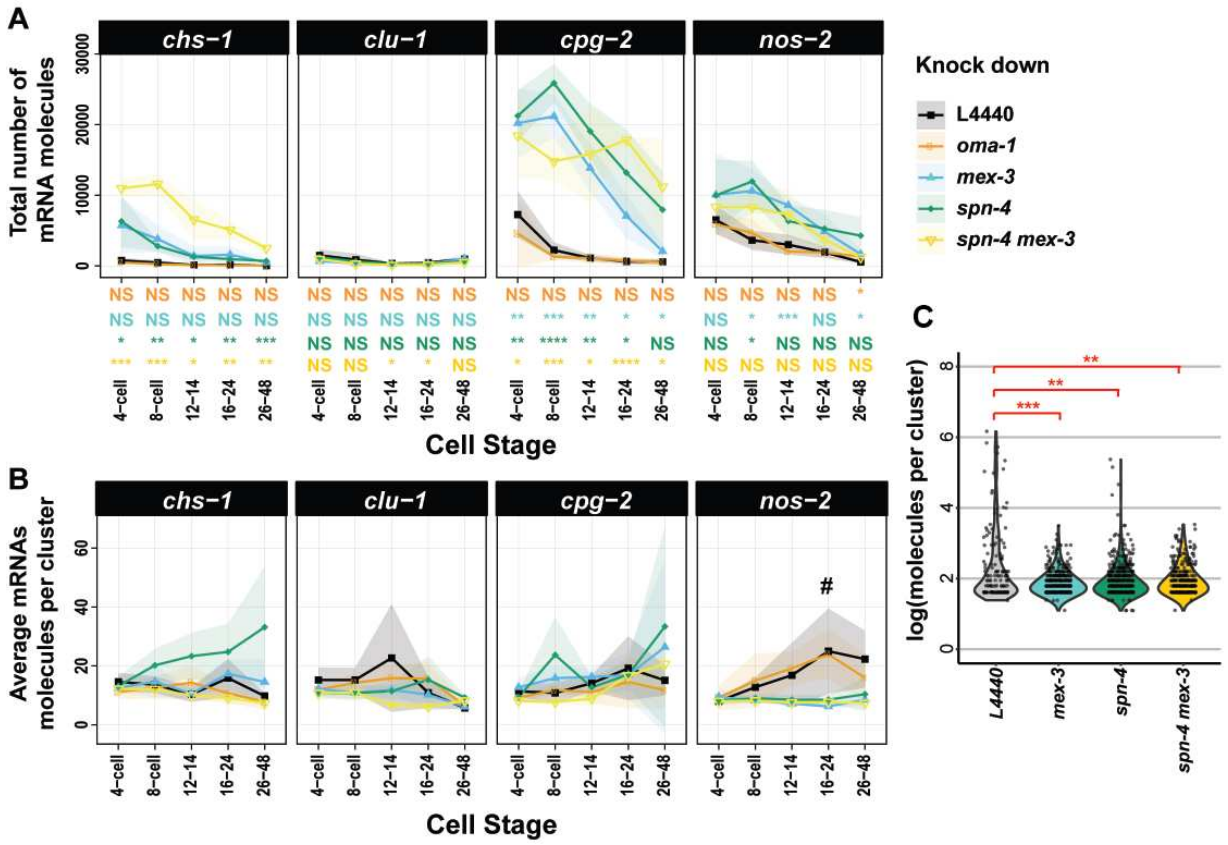

Figure 2.20: Knockdown of maternal RBPs has a variable effect on the regulation of posterior-enriched clustered transcripts. The total number of mRNA molecules **(A)** and average number of mRNA molecules per cluster **(B)** for four different RBP knockdown conditions on five mRNAs at five different developmental stages are shown graphically, compared with the L4440 empty vector RNAi control. At least four embryos were assayed for each data point from three biological replicates. Standard deviations are shown as shaded ribbon regions. # indicates data analyzed in C. **(C)** Distributions of *nos-2* mRNA cluster size under *mex-3, spn-4 (ts)*, and *dual mex-3/spn-4* depletion conditions at the 16- to 24-cell stage demonstrate decreased cluster sizes when compared with mock (L4440) depletion. Significance indicates P-values derived from multiple test corrected t-tests comparing the knockdown condition of interest with vector-only RNAi control (L4440) (0.005>**>0.0005; 0.0005>***>0.00005; 0.00005>****).

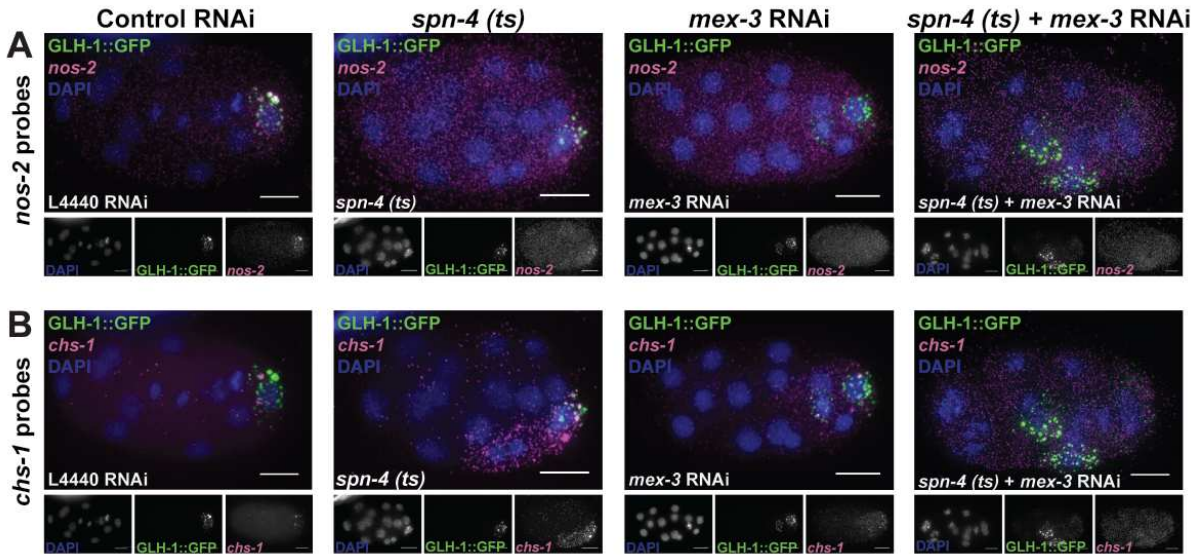

Figure 2.21: Knockdown of *spn-4* and *mex-3* simultaneously resulted in embryonic defects and mislocalization of RNA. GLH-1::GFP and GLH-1::GFP *spn-4(or191)* temperature sensitive embryos raised at 25 °C (GLH-1::GFP shown in green) were treated with L4440 or *mex-3* RNAi and probed for *chs-1* **(A)** and *nos-2* **(B)** mRNAs by smFISH (magenta). DNA was also stained with DAPI (blue). GLH-1::GFP *spn-4(or191)* embryos raised at 15 °C and treated with either L4440 or *mex-3* RNAi phenocopied GLH-1::GFP embryos raised at 25 °C with the same RNAi treatment. Scale bar: 10 μm

Because the translational repression of *nos-2* mRNA correlated with its localization to P granules (Figure 2.18, Figure 2.19, Figure 2.20, Figure 2.21), we sought to determine the effects of prolonged *nos-2* translational repression beyond the 28-cell stage when this repression is typically relieved. We imaged *nos-2* mRNA by smFISH under *pie-1* and *pos-1* RNAi knockdown conditions in which *nos-2* translational repression has been shown to persist [73, 83]. Interestingly, the two knockdown conditions yielded different results. Upon POS-1 depletion, *nos-2* mRNA failed to appear in the cytoplasm after the 28-cell stage and instead remained associated predominantly with P granules (Figure 2.22A), as predicted by its translationally inactive status. In contrast, depletion of PIE-1 had the opposite effect. PIE-1 plays a threefold role by contributing to *nos-2* stabilization, NOS-2 translational activation and germline transcriptional repression [73,83]. Upon disruption of PIE-1, *nos-2* mRNA molecules undergo progressive degradation in the P lineage due to the inappropriate transcription of somatic genes within the P lineage [179]. If this degradation phenotype is abrogated by concurrently blocking somatic gene expression [*pie-1* and *ama-1* (encoding RNA

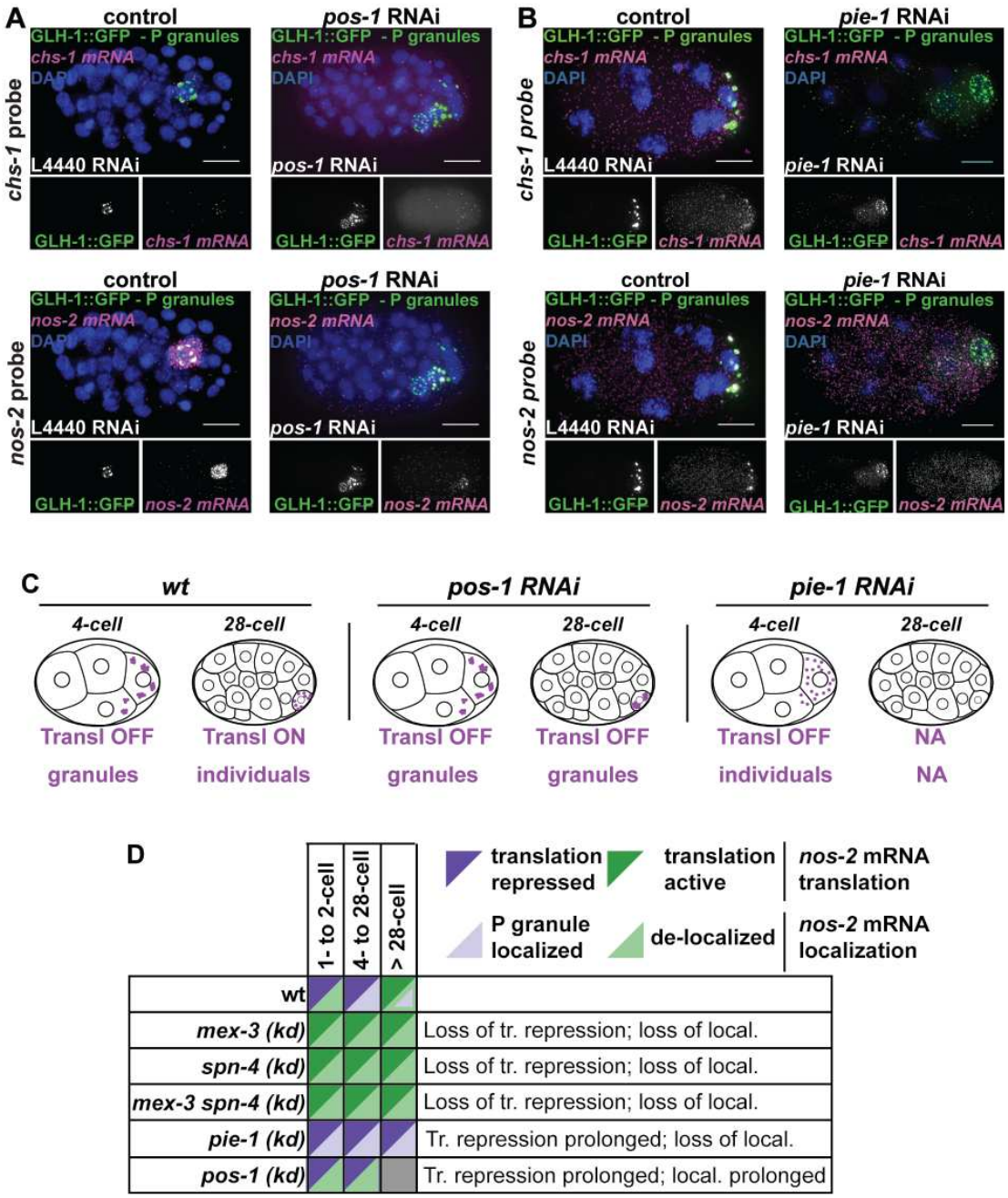

Figure 2.22: RBPs that regulate translation of NOS-2 differentially impact *nos-2* mRNA subcellular localization. **(A, B)** The impact of depleting POS-1 **(A)** or PIE-1 **(B)**, two RBPs important for translation activation of *nos-2* mRNA at the 28-cell stage, was assayed. *chs-1* mRNA **(magenta, top)** and *nos-2* mRNA **(magenta, bottom)** were imaged in knockdown and control conditions using smFISH in a GLH-1::GFP-expressing strain. DAPI-stained DNA illustrates developmental stage. The 28-cell stage, when *nos-2* normally becomes translationally active, is shown for *pos-1* RNAi conditions. The 8-cell-stage embryo is shown for *pie-1* RNAi conditions to illustrate a stage when *nos-2* is normally repressed. **(C)** Pictograph demonstrating *nos-2* behavior under conditions where translation repression is never relieved. **(D)** Schematic showing a summary of localization and translation phenotypes exhibited in knockdown of *nos-2* RBPs. Scale bars: 10 μm.

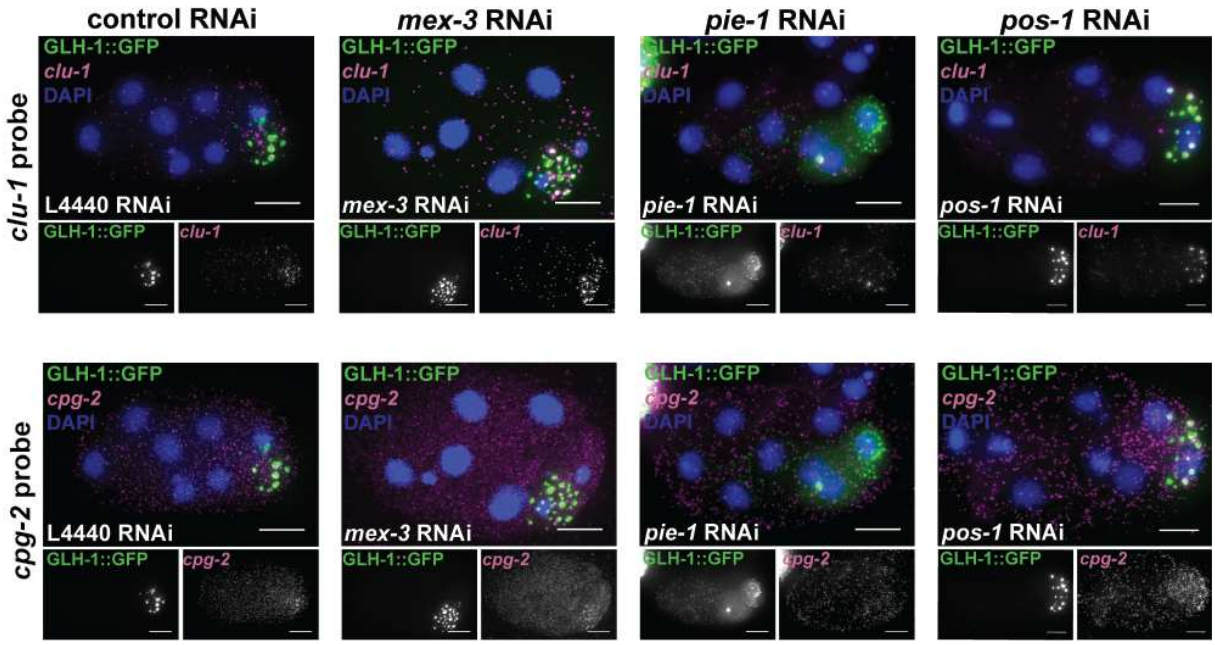

Figure 2.23: Knockdown of RBPs important for *nos-2* transcript localization results in perturbed *cpg-2* and *clu-1* transcript localization. GLH-1::GFP (green) embryos were treated with L4440, *mex-3, pie-1,* or *pos-1* RNAi and probed for *clu-1* **(A)** and *cpg-2* **(B)** mRNAs by smFISH (magenta). DNA was also stained with DAPI (blue). Scale bars: 10 μm

Polymerase II) double knockdown], *nos-2* mRNA molecules survive but fail to produce NOS-2 protein (unlike *ama-1* knockdown alone). The fact that *nos-2* mRNA fails to properly translate after the 28-cell stage under dual *pie-1/ama-1* knockdown conditions illustrates that PIE-1 is required to activate the translation of NOS-2 in the P lineage [83]. Upon *pie-1* depletion, we confirmed premature *nos-2* mRNA degradation; however, we were surprised to see a complete loss of *nos-2* localization to P granules, despite *nos-2* being translationally inactive at these stages [83] (Figure 2.22B). Initially, we suspected that P lineage identity was dysfunctional in these embryos, leading to the loss of wild-type P granule function. However, P granules are clearly present in these embryos (using GLH-1::GFP marker proteins) and they accumulate other mRNAs such as *clu-1* (Figure 2.22, Figure 2.23). As *nos-2* mRNA is not translated upon *pie-1* disruption [83], this suggests that the translational repression of *nos-2* and its localization to P granules can be uncoupled, perhaps mimicking a somatic-cell-like state in the P lineage.

Taken together, RBP knockdown conditions that disrupt *nos-2* mRNA translational repression also disrupt *nos-2* mRNA P granule association [*mex-3* (RNAi) and *spn-4 (ts)*] (Figure 2.18, Figure 2.19, Figure 2.20, Figure 2.21, Figure 2.24). In contrast, an RBP knockdown condition that prolongs *nos-2* translational repression [73, 74] fails to release *nos-2* transcripts from P granules [*pos-1* (RNAi)]. Therefore, the localization of *nos-2* mRNA in P granules is largely coincident with a translationally repressed state (Figure 2.22C, Figure 2.22D). It is not a perfect association, however. We observed several cases where *nos-2* mRNA remains translationally repressed without localizing to P granules: (1) in one- to two-cell stage embryos; (2) in somatic cells of the early embryo; and (3) in *pie-1* mutants in which *nos-2* fails to localize to P granules (*pie-1* depletion retains *nos-2* repression in Tenenhaus et al., 2001). These findings illustrate that *nos-2* translational repression can occur independently of transcript localization and translational repression is not dependent on P granule residency. Further, it illustrates an order of operations in which translational repression precedes P granule localization during development.

2.3.8 Disrupting translation promotes P granule localization

We speculated whether P granule localization was a natural consequence that befalls transcripts experiencing low rates of translation or complete repression. To determine whether altering the translational status of mRNAs could change their localization within the cell, we disrupted translational initiation through heat exposure. Embryos exposed to 30 °C for 25 min repress protein synthesis at the level of translational initiation [213, 214]. We observed that three transcripts that are normally homogenously distributed throughout the cytoplasm coalesced into P granules in response to heat stress (Figure 2.25, Figure 2.26): *set-3, gpd-2 (Glycerol-3-Phosphate Dehydrogenase)* and *B0495.7 (predicted metalloprotease)*. Therefore, loss of protein synthesis was sufficient for otherwise homogenous transcripts to accumulate in P granules.

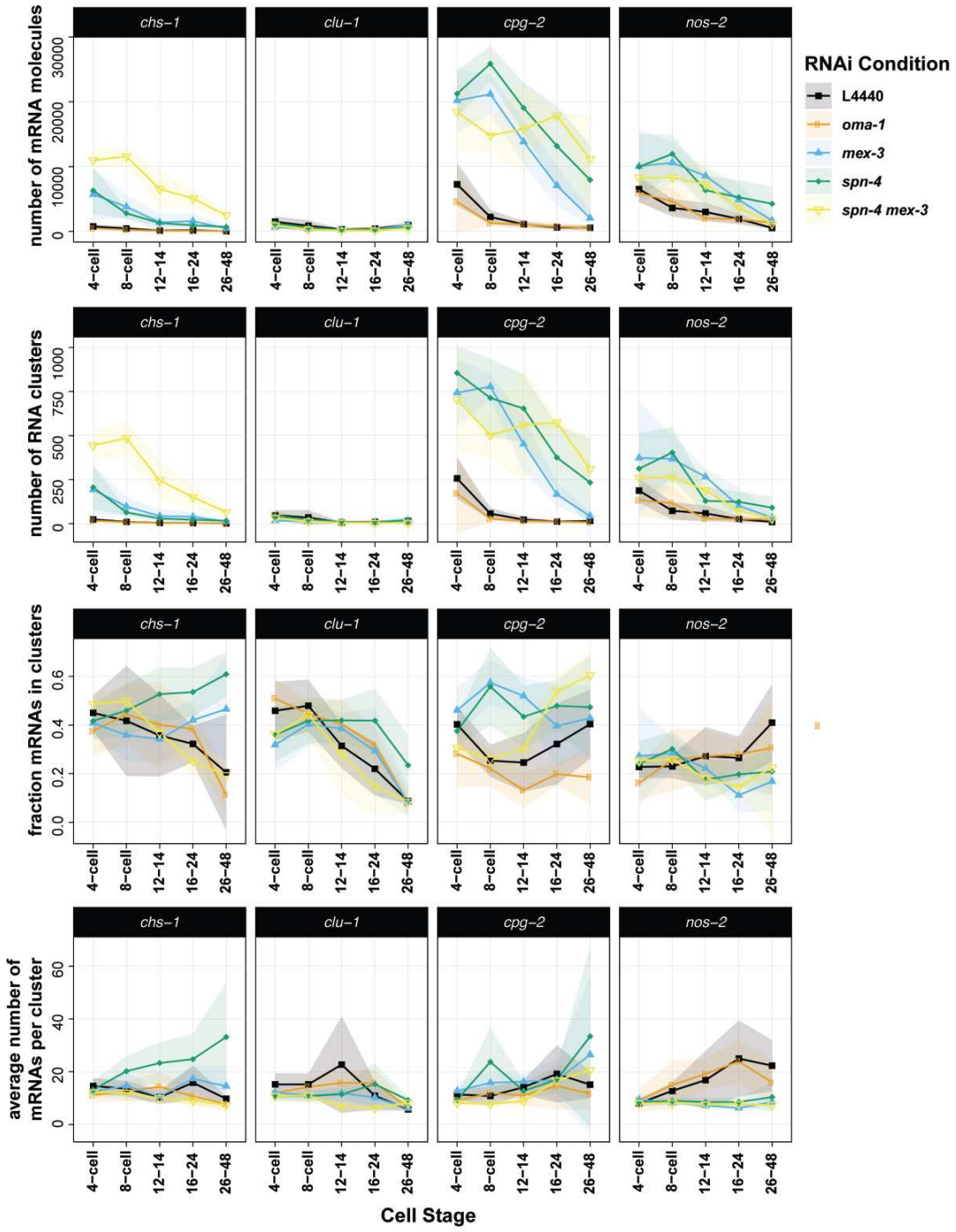

Figure 2.24: Quantification of mRNA clustering under RBP knockdown conditions. Statistical metrics characterizing mRNA clustering are shown: 1) the total number of RNAs in each embryo, 2) the total number of clusters identified in each embryo, 3) the fraction of total mRNAs located within clusters (as opposed to cluster-independent), and 4) the average estimated number of mRNA molecules per cluster within a given embryo. Four transcripts were assayed in five knockdown conditions over 5 developmental time points. The average of each metric (line) and their standard deviation (shading) are shown representing a minimum of 5 embryos assayed over a minimum of 3 biological replicates.

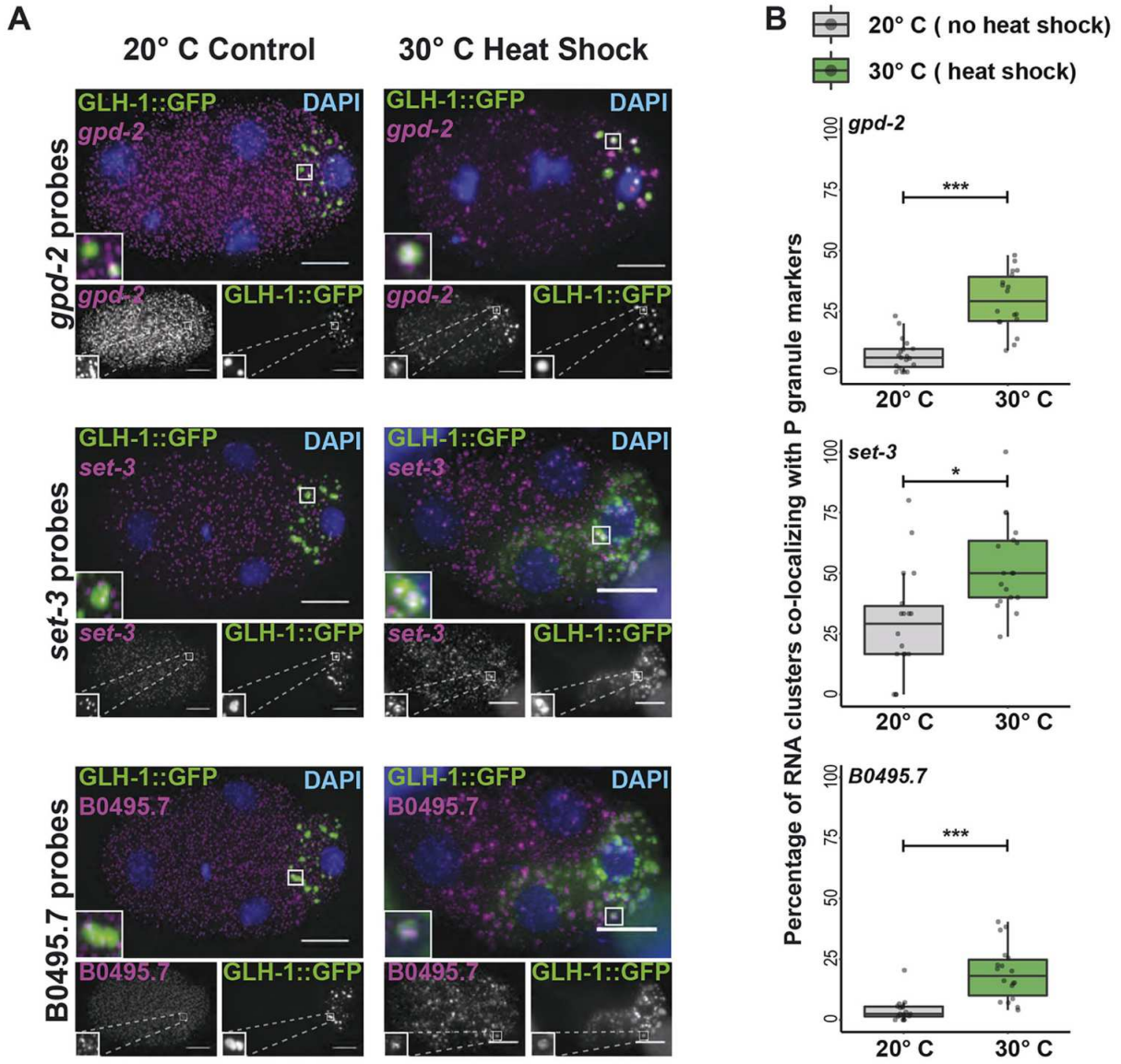

Figure 2.25: Homogenously distributed transcripts form clusters when subjected to heat shock stress. **(A)** The transcripts *gpd-2, set-3,* and *B0495.7* (magenta) are homogenously distributed in four-cell embryos at 20 °C **(left)**. These transcripts become recruited to GLH-1::GFP labeled P granules (green) and other uncharacterized mRNA clusters following a 25 min 30 °C heat shock **(right)**. DAPI-stained DNA illustrates developmental stage. Insets show enlarged views of P granules, demonstrating recruitment of RNA to P granules after heat shock. **(B)** The degree of *gpd-2, set-3,* and *B0495.7* transcript overlap with the P granule marker, GLH-1::GFP, was quantified for embryos cultured at 20 °C or heat-shocked at 30 °C for 25 min. Box plots show the percentage of RNA clusters overlapping with the P granule marker for each transcript, which was found to significantly increase under heat-shock conditions. Median, and first and third quartile ranges, are indicated by the middle bar and box boundaries, respectively. Whiskers indicate 1.5X the interquartile ranges. All included data points are shown as jittered dots. Welch's two sample t-test P-values are shown: 0.05>*>0.005; 0.005>**>0.0005; ***<0.0005. Scale bars: 10 μm.

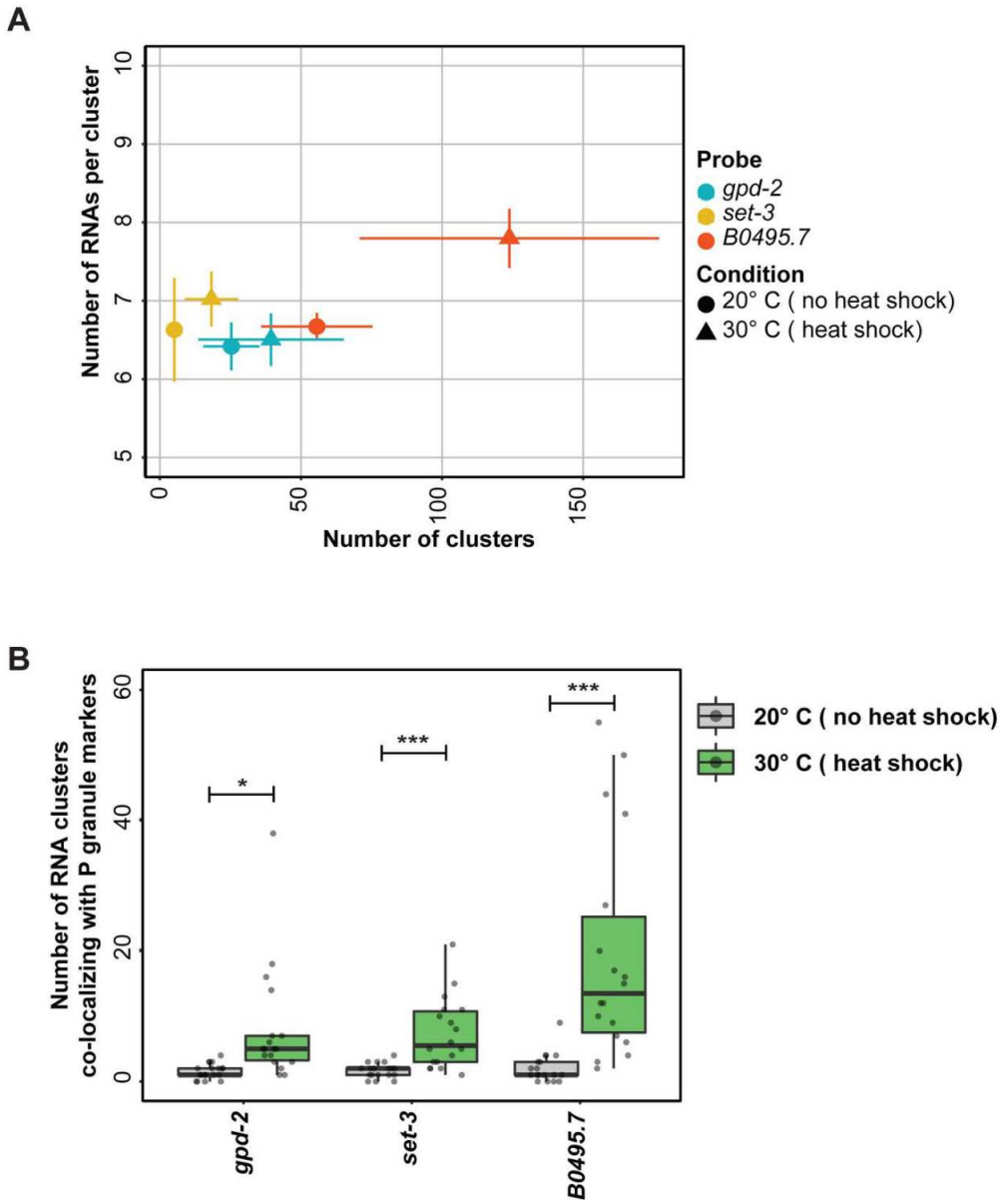

Figure 2.26: Upon heat shock, a greater number of mRNAs clusters co-localize with P granules. Quantification of smFISH assays of *B0495.7, gpd-2,* and *set-3*, three transcripts that are typically not P granule localized. **(A)** Upon heat shock (30 °C), larger and more numerous clusters formed. **(B)** Upon heat shock, more numerous RNA clusters co-localized with the P granule marker protein (GLH-1::GFP). The percentages of clusters overlapping P granule markers are shown in Figure 2.24B. Here, the raw numbers of co-localized clusters are tabulated. Statistics were performed using Welch's Two Sample t-test p-values: $0.05 > * \geq 0.005$; $0.005 > ** \geq 0.0005$; $*** < 0.0005$.

2.4 Discussion

2.4.1 Translational repression of mRNA is necessary and sufficient for P granule localization

In this study, we report several maternally-inherited mRNAs with subcellular localization in early *C. elegans* embryos. Localization patterns were often associated with translational status. P granule transcripts, for example, had repressed or declining translation. We hypothesized that either mRNAs are actively brought to P granules for the purpose of translational repression, or they are translationally repressed in the cytoplasm leading to their accumulation in P granules. In the case of *nos-2*, three lines of evidence support the second model. First, translational downregulation occurred before P granule localization. Second, in situations where *nos-2* translational repression and P granule localization were uncoupled (one-cell stage, somatic cells and upon *pie-1* depletion), translational repression occurred independently of P granule localization. Finally, heat stress-induced translational repression was sufficient to direct P granule localization. Together, these findings support the model that mRNAs of low translational status accumulate in P granules as a downstream step.

A recent publication by Lee et al. corroborates our findings [75]. They identified 492 P granule transcripts that precipitate with the intrinsically-disordered P granule factor MEG-3, and they found them to be of low ribosomal occupancy. Indeed, the P granule transcripts they identified depend both on translational repression and on MEG-3 for nucleation into P granules. Loss of P granule association (through *meg-3 meg-4* disruption) did not lead to loss of translational repression. They also illustrated that translational disruption of homogenous transcripts stimulates their ectopic localization into P granules in a MEG-3-dependent manner. Together, our combined works reinforce the interpretation that P granule accumulation occurs as a secondary step preceded and directed by low translational status.

2.4.2 P granules functionally echo stress granules and P bodies by accumulating transcripts of low translational status

mRNAs that localize to P granules could still be observed as individuals within the cytoplasm, as only 7% (*clu-1*, 26- to 48-cell stage) to 53% (*clu-1*, eight-cell stage) of total mRNAs localized to clusters. This echoes stress granules in which 10% of bulk mRNA and up to 95% of specific transcripts move into stress granules only returning to the cytoplasm after the stress has passed [121]. Though stress granules and germ granules (like P granules) are distinct, they appear to have some functionality in common.

2.4.3 Different transcripts accumulate in P granules through different mechanisms

We identified six new P granule-enriched transcripts. Of the three (*chs-1, clu-1* and *cpg-2*) we selected for further study, all localized to P granules in 3'UTR-dependent manners. However, these transcripts did not rely on the same RBPs for localization into granules as *nos-2* did (MEX-3, SPN-4 and PIE-1). What, then, directs them to P granules? The answer may lie in their biology. CHS-1 and CPG-2 are translationally activated by fertilization but their mRNA and protein levels decline shortly thereafter. Therefore, whether translation is repressed temporarily (*nos-2*) or permanently and followed by degradation (*chs-1* or *cpg-2*), P granule accumulation results. Different sets of RBPs likely interpret the 3'UTR sequence information of each transcript to direct regulation.

2.4.4 mRNA degradation plays a role in shaping transcript localization patterns

Transcripts of *chs-1, clu-1, cpg-2* and *nos-2* accumulate in the P granules of progenitor germ cells at the same time they disappear from somatic cells. These linked mechanisms concentrate transcripts down the P lineage. All transcripts tested required MEX-3 and SPN-4 for degradation in somatic cells, yet *nos-2* (and to a lesser extent *chs-1* and *cpg-2*) specifically required both RBPs for strong accumulation in P granules. Together, these findings suggest a mechanism in which

P granule localization protects mRNAs from MEX-3 and SPN-4-dependent degradation. Local protection coupled to generalized degradation has also been evoked to explain how *Drosophila nanos* concentrates at posterior regions of the embryonic syncytium [12]. Similarly, we found the 3'UTR of *imb-2* fused to *mNeonGreen* elicited *mNeonGreen* mRNA decay, suggesting that *imb-2* localizes to nuclei by a 3'UTR-independent mechanism that protects it from its own 3'UTR-dependent degradation. Together, these findings illustrate how subcellular localization can preserve mRNAs in specific regions of the cell and embryo.

Altogether, translational status directs P granule residency of key transcripts, and P granule residency, in turn, directs enrichment down the P lineage. This explains how mRNAs may be retained and concentrated in specific lineages even in the absence of *de novo* transcription. Indeed, we found that *nos-2* mRNAs within P granules were exceptionally numerous. Whereas other P granule associated transcripts were estimated at 8-12 molecules per granule, *nos-2* mRNAs accumulated to >20 molecules per granule just before the onset of *nos-2* translation. This suggests a possible functional reason why transcripts important for germ cell biology accumulate in P granules – to direct cell-specific protein production even in the absence of *de novo* transcription.

2.4.5 Peripheral transcripts often encode membrane-associated proteins

Half of the anterior AB-enriched transcripts we surveyed by smFISH accumulated at the cell periphery. Of these, ERM-1 and LEM-3 proteins also localize to apical plasma membranes [194, 195]. The localizations of APE-1 and TES-1 are currently uncharacterized, but these proteins harbor domains associated with membrane localization [196, 197]. In addition, symmetrically-distributed *imb-2* mRNA localized preferentially at nuclear membranes, the same localization at which the protein it encodes functions [203]. The concordance between localization of mRNA and the proteins they encode suggest that either the transcripts are directed to membranes for the purpose of local translation or they are passively dragged along behind the growing peptide as it localizes to its final destination. Current genomics assays have illustrated that mRNAs can associate with the endoplasmic reticulum in both translationally-dependent and -independent ways

[215], suggesting that both models are possible. Although *erm-1* and *imb-2* lack discernible signal peptides at their N-termini, they both contain membrane-associated domains. Future studies will determine whether these could act to co-translationally direct transcripts to membranes, possibly for the purpose of efficiently generating secondary rounds of translation.

2.4.6 mRNA localization is a widespread feature of cell biology

Diverse examples of transcript-specific mRNA localization have been described across the tree of life ranging from bacteria [18] to humans [216]. Although early discoveries of localized mRNAs were thought to represent exceptional cases, recent advances in mRNA proximity labeling suggest that mRNA localization may be more widespread than previously thought [23, 25]. A new perspective is emerging to encompass mRNA localization control as a general feature of cell biology.

2.5 Materials and Methods

2.5.1 Ethics and oversight

All experiments were subject to oversight by the Colorado State University Institutional Biosafety Committee and were conducted in accordance with National Institutes of Health guidelines.

2.5.2 *C. elegans* maintenance

C. elegans strains were maintained using standard procedures [217]. Worms were grown at 20 °C and reared on nematode growth medium (NGM: 3 g/l NaCl; 17 g/l agar; 2.5 g/l peptone; 5 mg/l cholesterol; 1 mM $CaCl_2$; 1 mM $MgSO_4$; 2.7 g/l KH_2PO_4; 0.89 g/l K_2HPO_4). *C. elegans* strains generated in this study were derived from the standard laboratory strain, Bristol N2. Strains used in this study are listed in Table 2.2.

Table 2.2: Worm strains used in this study.

Strain	Description	Genotype	Reference/Source	Verification
N2	N2	*C. elegans* wildtype	CGC	
DUP64	GLH-1:: GFP	*glh-1(sam24 [glh-1::gfp:: 3xFlag]) I*	Andraloje et al., 2017; obtained from Dustin Updike	verified by true breeding GFP fluorescence pattern
DUP75	PGL-1:: GFP	*pgl-1(sam33 [pgl-1::gfp:: 3xFlag]) IV*	Andraloje et al., 2017; obtained from Dustin Updike	verified by true breeding GFP fluorescence pattern
DUP98	PATR-1:: GFP	*patr-1(sam50 [patr-1::gfp:: 3xFlag])II*	Andraloje et al., 2017; obtained from Dustin Updike	verified by true breeding GFP fluorescence pattern
LP306	GFP::PH	*cpIs53 [mex-5p:: GFP-C1::PLC (delta)-PH::tbb-2 3'UTR + unc-119 (+)] II*	Heppert JK, et al. Mol Biol Cell. 2016; obtained from Jason Lieb Lab	verified by true breeding GFP fluorescence pattern
wDMP014	erm-1:: GFP	*erm-1 [Perm-1:: erm-1::GFP::erm-1 3'UTR] I*	Personal Com., Mike Boxem Lab; obtained from Mike Boxem	verified by true breeding GFP fluorescence pattern
EU923	spn-4 TS	*spn-4(or191) V*	CGC (Isolated in the Bowerman Lab); obtained from CGC	sequence verified & phenotype verified
wDMP005	NG::erm-1 3'UTR	*ttTi5605 [Pmex-5:: mNeonGreen:: erm-1 3'UTR] II*	This study	verified by PCR & sequencing
wDMP006	NG::imb-2 3'UTR	*ttTi5605 [Pmex-5:: mNeonGreen:: imb-2 3'UTR] II*	This study	verified by PCR & sequencing
wDMP047	NG::clu-1 3'UTR	*ttTi5605 [Pmex-5:: mNeonGreen:: clu-1 3'UTR] II*	This study	verified by PCR & sequencing
wDMP038	NG::cpg-2 3'UTR	*ttTi5605 [Pmex-5:: mNeonGreen:: cpg-2 3'UTR] II*	This study	verified by PCR & sequencing
wDMP039	NG::chs-1 3'UTR	*ttTi5605 [Pmex-5:: mNeonGreen:: chs-1 3'UTR] II*	This study	verified by PCR & sequencing
wDMP011	NG::nos-2 3'UTR	*ttTi5605 [Pmex-5:: mNeonGreen:: nos-2 3'UTR] II*	This study	verified by PCR & sequencing

2.5.3 3'UTR reporter constructs

The plasmid pMTNCSU7 was generated to express *mNeonGreen* as an N-terminal fluorescent reporter. Starting with a *Pmex-5::neongreen::neg-1::neg-1-3'UTR* plasmid derived from the MosSCI-based plasmid pCFJ150, we replaced the *neg-1* sequences with an NheI/BglII/EcoRV multiple cloning site using inverse PCR. 3'UTRs were PCR amplified and cloned into the NheI site of pMTNCSU7 using Gibson cloning (New England Biolabs) to create pDMP45 (*Pmex-5::mNeonGreen::nos-2 3'UTR*), pDMP47 (*Pmex-5::mNeonGreen::cpg-2 3'UTR*), pDMP48 (*Pmex-5::mNeonGreen::chs-1 3'UTR*), pDMP91 (*Pmex-5::mNeonGreen::clu-1 3'UTR*), pDMP111 (*Pmex-5::mNeonGreen::imb-2 3'UTR*) and pDMP112 (*Pmex-5::mNeonGreen::erm-1 3'UTR*). Plasmids used in this study are listed in Table 2.3. Primers used for 3'UTR amplification can be found in Table 2.4.

Table 2.4: Oligonucleotide primers used in this study.

Primer Name	Primer Sequence	Target	Gene ID	Isoform	Usage/Goal
oMTNCSU_0001b	GTCTTGATGGTTGTGCGCATTG	pEO98	NA	NA	Remove *neg-1* gene fragment from pEO98
oMTNCSU_0004	gatatcagatctgctagCTTGTACAGCTCGTCCATTCC	pEO98	NA	NA	Remove *neg-1* gene fragment from pEO98
oMTNCSU_0003b	ctagcagatctgatatcGTCTTGATGGTTGTGCGCATTG	pEO98	NA	NA	Remove *neg-1* gene fragment from pEO98
oMTNCSU_0002	CTTGTACAGCTCGTCCATTCC	pEO98	NA	NA	Remove *neg-1* gene fragment from pEO98

Table 2.4: Oligonucleotide primers used in this study.

Primer Name	Primer Sequence	Target	Gene ID	Isoform	Usage/Goal
oMTNCSU_0007	tatgggaatggacgagctgtacaagtaaAAGATCCAATTTCTCAATACTTTTTTATATCG	*nos-2* 3'UTR	WBGene00003784	ZK1127.1.1	Amplify *nos-2* 3'UTR for Gibson assembly
oMTNCSU_0008b	caaccatcaagacgatatcagatctgctagCGAATTGTAAATTTTTATTTTCAGAGCTAT	*nos-2* 3'UTR	WBGene00003784	ZK1127.1.1	Amplify *nos-2* 3'UTR for Gibson assembly
oMTNCSU_0015	tgggaatggacgagctgtacaagtaaTTGTACCCATTTTTTTTACAAAATTACACACTAA	*cpg-2* 3'UTR	WBGene00015102	B0280.5.1	Amplify *cpg-2* 3'UTR for Gibson assembly
oMTNCSU_0016b	cacaaccatcaagacgatatcagatctgctagTCAGAGTTCTAGTCAGGCAGTTTCATTT	*cpg-2* 3'UTR	WBGene00015102	B0280.5.1	Amplify *cpg-2* 3'UTR for Gibson assembly

Table 2.4: Oligonucleotide primers used in this study.

Primer Name	Primer Sequence	Target	Gene ID	Isoform	Usage/Goal
oMTNCSU_0017	gggaatggacgagctgtacaagtaaTGCTAAAATTGATTTTTATTTTTTATTTATTGCAT	*chs-1* 3'UTR	WBGene00000496	T25G3.2.1	Amplify *chs-1* 3'UTR for Gibson assembly
oMTNCSU_0018b	aatgcgcacaaccatcaagacgatatcagatctgctagAGAATGACCCTGCAAACGTGCT	*chs-1* 3'UTR	WBGene00000496	T25G3.2.1	Amplify *chs-1* 3'UTR for Gibson assembly
DMP175	accatcaagacgatatcagatctgctagagattttcagattttattattggagaaagaac	*clu-1* 3'UTR	WBGene00000550	F55H2.6.1	Amplify *clu-1* 3'UTR for Gibson assembly
DMP176	tgatgttatgggaatggacgagctgtacaagaattgattagatatcacccaatttttgg	*clu-1* 3'UTR	WBGene00000550	F55H2.6.1	Amplify *clu-1* 3'UTR for Gibson assembly
oMTNCSU_0009	ttatgggaatggacgagctgtacaagtaaGGAAAACGAGTATCTAGATATGCAATTTTC	*imb-2* 3'UTR	WBGene00002076	R06A4.4a.1	Amplify *imb-2* 3'UTR for Gibson assembly

Table 2.4: Oligonucleotide primers used in this study.

Primer Name	Primer Sequence	Target	Gene ID	Isoform	Usage/Goal
oMTNCSU_0010b	caaccatcaagacgatatcagatctgctagCATGAATCATTAAAAAATGAAGGATAGAAA	*imb-2* 3'UTR	WBGene00002076	R06A4.4a.1	Amplify *imb-2* 3'UTR for Gibson assembly
oMTNCSU_0013	tatgggaatggacgagctgtacaagtaaTTATTTGTTCTATCGTATTTCCTTTTATTTTT	*erm-1* 3'UTR	WBGene00001333	C01G8.5	Amplify *erm-1* 3'UTR for Gibson assembly
oMTNCSU_0014b	ccatcaagacgatatcagatctgctagCATGTCACGTATTCATATTTATCATAATATCAT	*erm-1* 3'UTR	WBGene00001333	C01G8.5	Amplify *erm-1* 3'UTR for Gibson assembly

2.5.4 *C. elegans* single-copy transgenesis by CRISPR

Pmex-5::mNeonGreen::3'UTR strains were generated from N2 worms by CRISPR targeting to the ttTi5605 MosSCI site [218]. Guide RNA targeting the ttTi5605 MosSCI site and Cas9 protein were co-expressed from the plasmid pDD122, whereas plasmids pDMP45, pDMP47, pDMP48, pDMP91, pDMP111 and pDMP112 were used as repair templates. Three vectors containing mCherry-tagged pGH8 (*Prab-8::mCherry* neuronal co-injection marker), pCFJ104 (*Pmyo-3::mCherry* body wall muscle co-injection marker) and pCFJ90 (*Pmyo-2::mCherry* pharyngeal co-injection marker) as well as one containing the heat-shock activated PEEL-1 counter-selectable marker (pMA122) were co-injected. *mNeonGreen*- and *mCherry*-positive animals were identified

Table 2.3: *E.coli* strains and plasmids used in this study.

Strain description	Plasmid description	Detailed description	Reference
OP50	NA	OP50	
L4440	pPD129.36	empty worm RNAi plasmid	Fire Lab *C. elegans* Vector Kit 1999 (unpublished)
oma-1 RNAi	IV-4F01 from the Ahringer library	worm RNAi plasmid + *oma-1* gene fragment	Fraser et al, 2000, Nature
oma-2 RNAi	V-5D12 from the Ahringer library	worm RNAi plasmid + *oma-2* gene fragment	Fraser et al, 2000, Nature
mex-3 RNAi	I-1A23 from the Ahringer library	worm RNAi plasmid + *mex-3* gene fragment	Fraser et al, 2000, Nature
pie-1 RNAi	III-6E08 from the Ahringer library	worm RNAi plasmid + *pie-1* gene fragment	Fraser et al, 2000, Nature
pos-1 RNAi	V-6A23 from the Ahringer library	worm RNAi plasmid + *pos-1* gene fragment	Fraser et al, 2000, Nature
pEO98	*mNeonGreen::neg-1*	*ttTi5605 Pmex-5:: mNeonGreen::neg-1:: neg-1 3'UTR*	This study
pDMP112	*mNeonGreen::erm-1*	*ttTi5605 Pmex-5:: mNeonGreen::erm-1 3'UTR*	This study
pDMP111	*mNeonGreen::imb-2*	*ttTi5605 Pmex-5:: mNeonGreen::imb-2 3'UTR*	This study
pDMP48	*mNeonGreen::chs-1*	*ttTi5605 Pmex-5:: mNeonGreen::chs-1 3'UTR*	This study
pDMP91	*mNeonGreen::clu-1*	*ttTi5605 Pmex-5:: mNeonGreen::clu-2 3'UTR*	This study
pDMP47	*mNeonGreen::cpg-2*	*ttTi5605 Pmex-5:: mNeonGreen::cpg-2 3'UTR*	This study
pDMP45	*mNeonGreen::nos-2*	*ttTi5605 Pmex-5:: mNeonGreen::nos-2 3'UTR*	This study

as F1 progeny and singled to new plates until starvation. Starved plates were then subjected to a 4 h incubation at 34 °C to counterselect, followed by an overnight recovery at 25 °C. Plates were then screened for living worms that did not express the mCherry co-injection markers. Worms that showed no fluorescence from the presence of extrachromosomal arrays were singled to establish lines, which were confirmed for single-copy insertion by PCR using the primers in Table 2.4.

2.5.5 smFISH

smFISH was performed based on the TurboFish protocol, with updates specific to *C. elegans* and using new Biosearch reagents [180, 219–222]. Custom Stellaris FISH Probes were designed against target transcripts (Table A.1) using the Stellaris RNA FISH Probe Designer (Biosearch Technologies; www.biosearchtech.com/stellarisdesigner; version 4.2). The embryos were hybridized with Stellaris RNA FISH Probe sets labeled with CalFluor 610 or Quasar 670 (Biosearch Technologies) following the manufacturer's instructions (www.biosearchtech.com/stellarisprotocols). Briefly, young adult worms were bleached for embryos, suspended in 1 ml -20 °C methanol, quickly vortexed and freeze cracked in liquid nitrogen. Embryos were stored in methanol at -20 °C for 1-24 h. After fixation, embryos were equilibrated briefly in Stellaris Wash Buffer A (Biosearch Technologies, SMF-WA1-60) before hybridization in 100 µl Stellaris Hybridization buffer (Biosearch Technologies, SMF-HB1-10) containing 10% formamide and 50 pmol of each primer set. The hybridization reaction was incubated at 37 °C overnight. Hybridized embryos were then washed twice for 30 min in Stellaris Wash Buffer A, with the second wash containing 1 µg/ml of DAPI. Following counterstaining, a final wash in Stellaris Wash Buffer B (Biosearch Technologies, SMF-WB1-20) was carried out before storage with N-propyl gallate antifade [10 ml 100% glycerol, 100 mg N-propyl gallate, 400 µl 1 M Tris (pH 8.0), 9.6 ml DEPC-treated H2O] before slide preparation. Embryos were mounted based on original descriptions in Ji and van Oudenaarden (2012) [223], using equal volumes of hybridized embryos resuspended in N-propyl gallate antifade and Vectashield antifade (Vector Laboratories, H-1000). smFISH image stacks were acquired on a Photometrics Cool Snap HQ2 camera using a DeltaVi-

sion Elite inverted microscope (GE Healthcare), with an Olympus PLAN APO 60X (1.42 NA, PLAPON60XOSC2) objective, an Insight SSI 7-Color Solid State Light Engine and SoftWorx software (Applied Precision) using 0.2 μm z-stacks. Representative images were deconvolved using Deltavision (SoftWorx) deconvolution software. Images were further processed using FIJI [224]. Initial characterization of subcellular localization for the transcripts *erm-1, imb-2, chs-1, clu-1, cpg-2* and *nos-2* was performed in conjunction with the homogenous transcript *set-3* as a negative control for subcellular localization (data not shown; see http://dx.doi.org/10.25675/10217/201623 for raw microscopy images). In all instances, a minimum of five embryos, but often many more, were imaged for each genetic condition and time point. All raw microscopy images are deposited on Mountain Scholar, a digital, open access data repository associated with Colorado State University Libraries (http://dx.doi.org/10.25675/10217/201623).

2.5.6 smiFISH

smiFISH was performed as in Tsanov et al. [225] using FLAPY primary probe extensions and secondary probes. Briefly, between 12 and 24 primary probes were designed using Oligostan [225] and ordered in 25 nmol 96-well format from Integrated DNA Technologies diluted to 100 μM in IDTE buffer (pH 8.0). Secondary FLAPY probes were ordered from Stellaris LGC with dual 5' and 3' fluorophore labeling using either Cal Fluor 610 or Quasar 670 (Biosearch Technologies, BNS-5082 and FC-1065, respectively). Individual probes were combined to a final concentration of 0.833 μM, and 2 μl of primary probe mixture were mixed with 1 μl 50 μM FLAPY secondary probe, 1 μl NEB buffer 3 and 6 μl DEPC-treated H2O. The primary and secondary probe mixtures were then incubated in a thermocycler at 85 °C for 3 min, 65 °C for 3 min and 25 °C for 5 min to anneal. Then 2 μl of annealed probe mixtures were used as normal smFISH probe sets as above. smiFISH probe sequences are listed in Table A.1.

2.5.7 smFISH plus immunofluorescence

smFISH combined with immunofluorescence was performed similarly to smFISH with slight modifications. N2 and DUP98 *patr-1(sam50[patr-1::GFP::3xFLAG])II* [226] embryos were har-

vested as above with the exception that they were resuspended in methanol, freeze cracked in liquid nitrogen for 1 min, and transferred to acetone after ∼5 min total in methanol. Embryos were then incubated in acetone for 25 min before proceeding to hybridization/immunofluorescence. smFISH was then performed as above with the exception that a final concentration of 2.37 µg/ml Janelia Fluor 549 (Tocris, 6147) conjugated anti-GFP nanobody (Chromotek, gt-250) was incubated with the embryos overnight in hybridization buffer.

2.5.8 Initial quantification of smFISH micrographs

Initial characterization of mRNA counts from smFISH micrographs was performed using a standard FISH-quant analysis [204]. Briefly, embryos were manually outlined, 3D LoG filtered using default FISH-quant parameters (size=5, s.d.=1), spots were pre-detected using a local maximum fitting and RNAs were detected using a manually determined image-dependent intensity and quality threshold, with sub-region fitting of 2 pixels in the x- and y-axes and 3 pixels in the z-axis.

Post-processing to calculate the different location metrics was performed as described below with custom-written Matlab and Python code. The Python code is implemented as plugins for the image processing platform ImJoy [227]. Source code and detailed description are provided at https://github.com/muellerflorian/parker-rna-loc-elegans.

2.5.9 Quantification of cortical RNA localization

Quantification of transcript localization to the cell cortex was performed using the web application ImJoy [227]. RNAs were first detected as above using FISH-quant. Individual cell outlines were then manually annotated in FIJI for each z-stack in the micrograph, excluding the uppermost and lowermost stacks where cells are flattened against the slide or coverslip. The distance of each RNA was then measured from the nearest annotated membrane and binned in 10 µm increments. The total number of RNAs per bin was then normalized by the volume of the concentric spheres they occupied. After this normalization, values larger than 1 indicate that for this distance more RNAs are found compared with a randomly distributed sample.

2.5.10 Quantification of nuclear peripheral RNA localization

Quantification of transcript localization to the nuclear periphery was also performed using ImJoy. RNAs were first detected as above using FISH-quant. Embryos were then manually outlined to create an upper limit for RNA distance from the nucleus. Individual nuclei were then annotated by binarizing DAPI micrographs to create a nuclear mask. The distance of each RNA was then measured from the nearest annotated nuclear membrane and binned in 10 μm increments. Negative distance indicates positioning within the nuclear mask. The total number of RNAs per bin was then normalized for volume as described above for cell membrane localization.

2.5.11 Quantification of RNA clustering

Detection of RNA molecules was performed in the 3D image stacks using FISH-quant [204]. Positions of individual RNA molecules within dense clusters were determined with a recently developed approach using the signal of isolated RNAs to decompose these clusters [228]. Post-processing to calculate the different location metrics was performed as described below with custom-written Matlab and Python code. The Python code is implemented in user-friendly plugins for the image processing platform ImJoy [227]. Source code and all scripts used for analysis and figure generation are available at https://github.com/muellerflorian/parker-rna-loc-elegans.

To quantify the number of individual mRNAs in mRNA clusters, the total number of clusters per embryo and the fraction of mRNAs in clusters, a custom MATLAB script was implemented. FISH-quant detection settings were used to identify candidate mRNA clusters from smFISH micrographs using GMM. The GMM differentiates independent, single mRNAs from groups of clustered mRNAs by probabilistically fitting a predicted RNA of average intensity and size over each FISH-quant detected RNA. GMM fitting then provided coordinates of both independent RNAs and the modeled coordinates of each RNA that composes a cluster. The decomposed coordinates of each RNA in the embryo were then used by a density-based spatial clustering of applications with noise (DBSCAN) algorithm to quantitatively analyze cluster size and number. Quantifying RNA cluster overlap with GLH-1::GFP

To determine the degree of overlap between RNA clusters and P granules labeled with GLH-1::GFP a hybrid Matlab-ImJoy pipeline was implemented. RNA clusters were identified as described above. The occupied volume of these clusters in the image was calculated as the convex hull around all RNA positions within a cluster with the SciPy function ConvexHull. The location of P granules was determined in 3D with a Laplacian of Gaussian (LoG) blob detection method (with the scikit-image function blog_log). RNA clusters and P granules were considered to co-localize when their 3D volumes at least partly overlap. This allowed quantification of the number of independent P granules, RNA clusters, and RNA clusters that overlap with P granules.

2.5.12 RNAi feeding for smFISH microscopy

dsRNA feeding was executed as previously described [229]. Mixed-stage worms were bleached to harvest and synchronize embryos. Harvested embryos were deposited on RNAi feeding plates and grown at 25 °C until gravid. Embryos were harvested and smFISH was conducted. For each gene targeted by RNAi, we performed at least three independent replicates of feeding and smFISH using L4440 empty vector as a negative control and *pop-1* RNAi as a 100% embryonic lethal positive control. For experiments using the *spn-4* temperature sensitive allele, *spn-4(or191)* V, worms were grown at 15 °C until gravid, bleached for embryos, and split into 15 °C negative control and 25 °C query conditions while plating on L4440, *mex-3* or *pop-1* RNAi conditions.

2.6 Author contributions

This chapter was a collaborative project originally written for publication. Dylan M. Parker and Erin Osborne Nishimura led the project. Marc T. Nishimura designed the original cloning strategy to produce 3'UTR reporter plasmids and produced several of the final plasmids. Marc also contributed feedback on the conceptualization of many experiments performed in this chapter. Florian Mueller collaboratively and iteratively designed the Matlab and ImJoy RNA localization analysis pipelines with Dylan and Erin and generated the code to perform the analysis. Lindsay P. Winkenbach optimized the RNAi feeding followed by smFISH protocol and performed many of

the initial replicates of those experiments. Lindsay also performed multiple replicates of heatshock experiments. Sam Boyson optimized smiFISH and screened several transcripts for subcellular localization using this method. Matt N. Saxton, Camryn Daidone, and Zainab A. Al-Mazaydeh all screened transcripts for subcellular localization using either smFISH or smiFISH. All authors contributed to manuscript editing. All other work performed in this chapter was solely performed by Dylan M. Parker.

Chapter 3

Improved methods for protein and single-molecule RNA detection in *C. elegans* embryos[3]

3.1 Summary

Visualization of gene products in *Caenorhabditis elegans* has provided insights into the molecular and biological functions of many novel genes in their native contexts. Single-molecule Fluorescence *In Situ* Hybridization (smFISH) and Immunofluorescence (IF) visualize the abundance and localization of mRNAs and proteins, respectively, allowing researchers to elucidate the localization, dynamics, and functions of many genes. Here, we describe several improvements and optimizations to existing IF and smFISH approaches specifically for use in *C. elegans* embryos. We present 1) optimized fixation and permeabilization steps to preserve cellular morphology while maintaining probe and antibody accessibility, 2) a streamlined, in-tube approach that negates freeze-cracking, 3) the smiFISH (single molecule inexpensive FISH) adaptation that reduces cost, 4) an assessment of optimal anti-fade products, and 5) straightforward quantification and data analysis methods. Most importantly, published IF and smFISH protocols have predominantly been mutually exclusive, preventing exploration of relationships between an mRNA and a relevant protein in the same sample. Here, we present methods to combine IF and smFISH protocols in *C. elegans* embryos including an efficient method harnessing nanobodies. Finally, we discuss tricks and tips to help the reader optimize and troubleshoot individual steps in each protocol.

[3]This chapter was published as a preprint in May 2021 under the same title pending manuscript submission

Dylan M. Parker, Lindsay P. Winkenbach, Annemarie Parker, Sam Boyson, Erin Osborne Nishimura, Improved methods for protein and single-molecule RNA detection in *C. elegans* embryos, bioRxiv 2021.05.07.443170; doi: https://doi.org/10.1101/2021.05.07.443170

3.2 Introduction

3.2.1 1.1 Microscopic methods for RNA and protein visualization in *C. elegans*

The spatial and temporal patterns of gene expression in *C. elegans* can provide fundamental insights into their function and importance. By querying the abundance and spatial patterning of mRNA and their protein products in whole animals it is possible to gain insight to their transcription and translation, mRNA stability, modification states of protein, developmental regulation, and their functional roles [77, 230–233]. Visualizing RNA and protein in the same intact animal requires methods that are sensitive, non-perturbative, and, most importantly, compatible with one another. Traditional approaches to visualizing mRNA and protein simultaneously have either relied on the visibility of a GFP-tagged protein to persist under RNA labeling conditions; or they involve combining IF with low resolution FISH protocols. Here, we introduce methods that improve upon existing *in situ* RNA and protein visualization protocols allowing for concurrent imaging of a wide array of proteins and mRNA with state-of-the-art resolution.

The current gold standard for *in situ* single-molecule RNA detection is single-molecule Fluorescence *in situ* hybridization (smFISH). In smFISH, single-molecule RNA visualization occurs by annealing a series of 24-48 fluorescently-labeled short antisense oligonucleotide probes to a transcript of interest in fixed animals [219, 221, 234]. Annealing multiple fluorescent probes to an RNA produces a discrete, punctate signal for each individual molecule of RNA *in situ*. Labeling each RNA in this manner permits quantification of both the abundance and localization of individual molecules of RNA. Conventional smFISH protocols have successfully characterized RNA expression in *C. elegans*; however, they are challenged by low signal due to poor photostability for some fluorophores and high background [223]. The probes are also costly. We remedy these issues by optimizing the standard smFISH protocol for *C. elegans*, including comparisons of commercial and homemade reagents, rigorous testing of various antifade compounds, and implementation

of a recently developed protocol, single molecule inexpensive Fluorscence *In Situ* Hybridization (smiFISH) to reduce cost [225].

Visualization of endogenous protein expression by immunofluorescence (IF) has also proved to be an indispensible biological tool in *C. elegans*. IF has several benefits in contrast to other protein detection assays. For instance, western blots provide protein abundance and biochemical information but lack any spatial resolution. However, worm embryos pose a challenge for IF experiments due to their strong eggshell and robust permeability barrier [200, 235]. Ultimately, this has resulted in adapted protocols requiring harsh fixatives (aldehydes, picric acid), reducing reagents (β-mercaptoethanol, DTT), enzymatic treatments (collagenase), and demanding a high degree of finesse for freeze-crack permeabilization [235, 236]. To overcome these challenges, we have adapted strategies for use in the *C. elegans* embryo with comparatively mild chemical treatments allowing antibody penetrance while leaving protein epitopes intact using a simple one-tube protocol.

Perhaps most importantly, **we provide a protocol that combines both IF and smFISH in *C. elegans* embryos.** While it is sometimes possible to visualize RNA and protein simultaneously with a standard smFISH protocol through the use of fluorescently tagged proteins, tags like GFP can often bleach during fixation. Moreover, conventional methods of smFISH and IF in worms have been challenging to perform in the same sample, resulting in few published protocols. By optimizing the combined protocol, we have co-imaged single-molecules of RNA in conjunction with the proteins they produce *in situ* in whole animals. Our approach is to first perform immunofluorescence followed by smFISH, with key modifications. RNA quality and FISH probe permeability are maintained by using mild fixation conditions and chemical treatments compatible with immunofluorescence while employing RNAse free reagents throughout the protocol. Notably, for some antibody variants, such as nanobodies, a simplified protocol can sometime be utilized.

We present the technical details for each protocol individually, in combination, user-friendly ways to analyze the data, standard controls, and some options for troubleshooting. We present several related protocols for the reader to choose between (Figure 3.1). This includes a compre-

hensive protocol to perform sample prep, immunofluorescence, smFISH, and slide preparation in series (Figure 3.1, Protocol 1). Additional protocols also describe smFISH or smiFISH alone (Protocol 2), immunofluorescence alone (Protocol 3), or an alternative simultaneous immunofluorescence/smFISH approach using nanobodies (Protocol 4).

3.3 Experimental design, considerations, and data analysis

3.3.1 Sample preparation and fixation

IF and smFISH have been performed using various fixation conditions in *C. elegans* and other model systems. Common fixatives include formaldehyde/formalin or organic solvents such as methanol, ethanol, and acetone. Formaldehyde/formalin acts by creating crosslinked, covalent chemical bonds in the sample, primarily at lysine residues. Formalin can also cause C-T and G-A mutations on DNA sequences as characterized by PCR [237]. Moreover, formaldehyde/formalin-fixation affects tertiary amines in RNA sequences resulting in modification of up to nearly 40 % of As and Cs in formalin-fixed tissues [238]. Due to the high degree of alteration that occurs on nucleic acids, formaldehyde/formalin-fixation is not an ideal fixative for nucleic acid visualization. As an alternative to crosslinking-fixatives, alcohols and other organic solvents have been identified as superior nucleic acid-fixatives [239]. Alcohols and organic solvents, such as ethanol, methanol, and acetone, function by dehydrating clathrate water molecules around proteins and nucleic acids, thus precipitating biological molecules into a fixed state without significant chemical alteration. As with crosslinking fixatives, alcohols and organic solvents have their detriments. These fixatives can disrupt cell membrane structures, cytoplasmic organelles, and soluble cell structural elements such as microtubules [240, 241]. However, due to their preservation of nucleic acid composition, they are ideal fixatives for single-molecule RNA detection assays. Further, we have found that short fixations using these types of fixatives allow efficient antibody penetration and do not appear to cause disruption to the protein epitopes we have targeted through IF as some previous studies have shown [242].

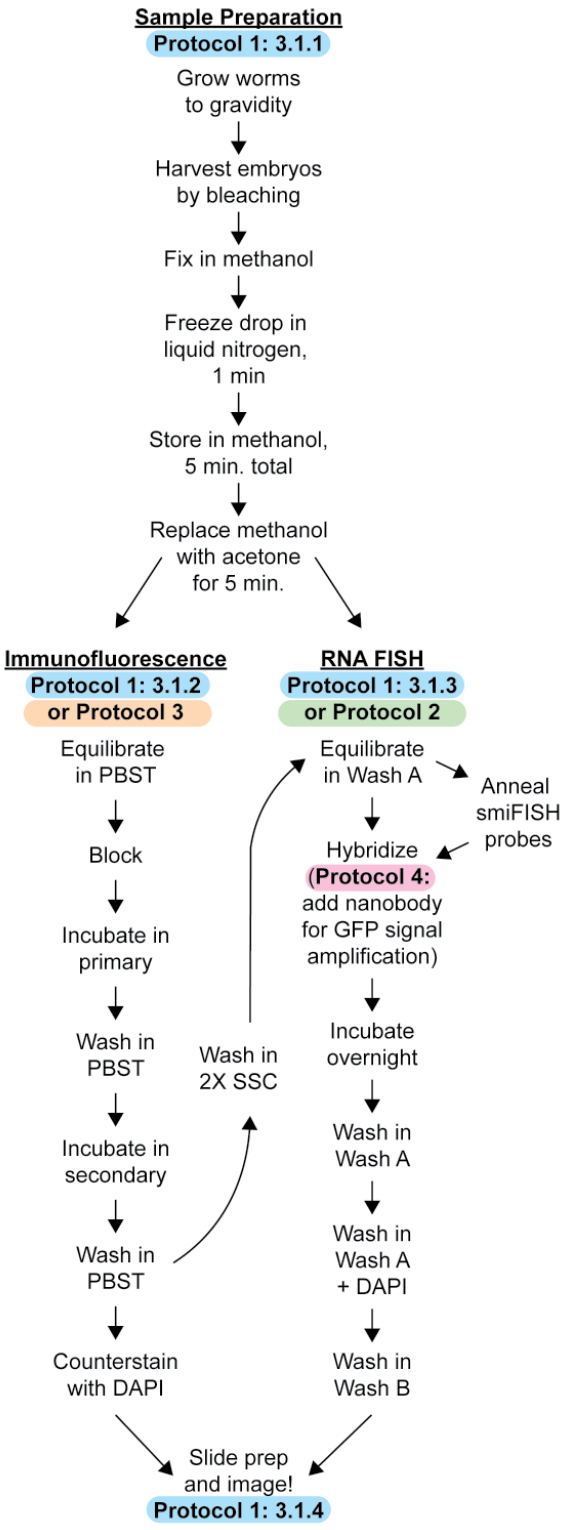

Figure 3.1: Schematic illustration of IF, FISH, and IF/FISH protocols An overview illustrating the workflow of the sequential IF/FISH (Protocol 1), RNA FISH (Protocol 2), IF (Protocol 3), and simultaneous IF/FISH (Protocol 4) protocols from sample preparation to slide preparation.

3.3.2 Immunofluorescence

IF has been a staple of *C. elegans* experimentation for decades. As a result, a variety of methods for performing IF have been developed, providing information and protocols for antigen production, peptide coupling, antibody purification, fixation conditions, and protocols related to IF in *C. elegans* [59, 235, 243]. However, the majority of these methods have focused on the use of larval stages of development, and are not optimized for embyos. Most protocols use some combination of reducing reagents, enzymatic treatments, formaldehyde fixation, and "Freeze-Cracking" mechanical disruption — compressing samples between slides, not to be confused with freeze-cracking of the eggshell in liquid nitrogen — [236]. Here we present a single-tube protocol requiring no reducing reagents or enzymatic treatments and utilizing a light methanol/acetone fixation and liquid nitrogen cracking to permeabilize the eggshell. We demonstrate this protocol using the anti-PGL-1 antibody K76 [59] (DHSB, Antibody registry ID AB_531836) and the anti-ELT-2 antibody 455-2A4 [244] (DHSB, Antibody Registry ID: AB_2618114) (Figure 3.2).

3.3.3 smFISH and smiFISH

Single-molecule RNA Fluorsecence *In Situ* Hybridization (smFISH) has provided insights into the regulation of transcripts in *C. elegans* at all stages of development. smFISH probes can be designed and synthesized in the lab [221, 223] or ordered as a set from Biosearch Technologies (Novato, CA). Some typical fluorophores include Cy5, Quasar 670, Alexa 594, Cal Fluor 610, and Fluorescein, among many others. In general, we have had the best signal to noise and most photostable fluorescence using Quasar 670 and Cal Fluor 610, which also work well in experiments probing for two RNAs. Fluorescein tends to have very low signal-to-noise ratios.

Because each probe in a set requires chemical conjugation with fluorophores for each specific transcript to be imaged, smFISH probe sets are relatively expensive [219,225,234]. Targeting a single RNA typically costs in the range of $\sim$\$500. Recently, Tsanov et al. outlined a straightforward, flexible method for reducing the cost of single-molecule RNA detection: single-molecule inexpensive Fluorescence *In Situ* Hybridization (smiFISH). smiFISH brings down the cost of single

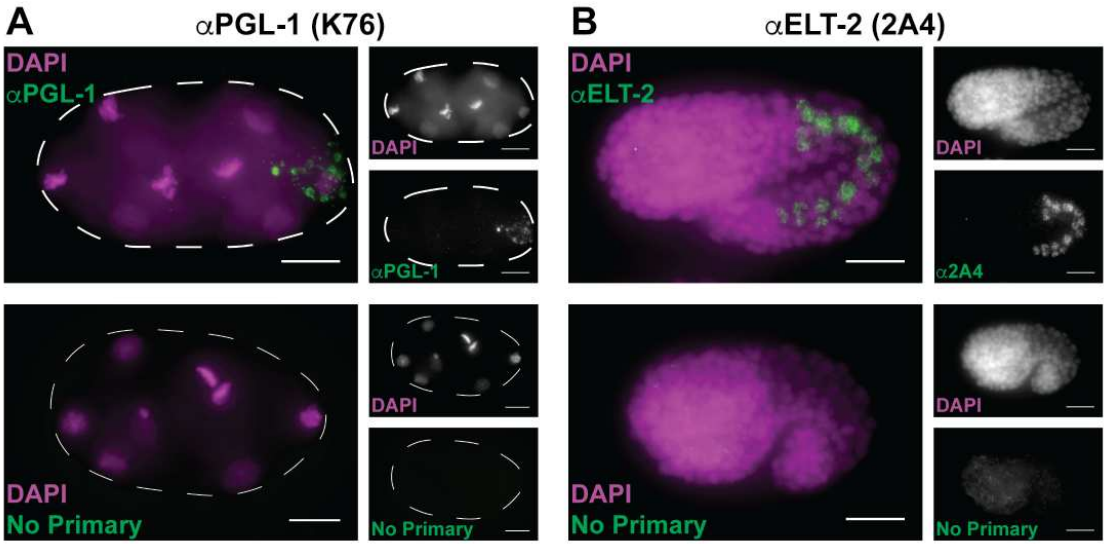

Figure 3.2: Simplified immunofluorescence in *C. elegans* embryos. Immunofluorescence was performed on N2 embryos as described (Protocol 3). Embryos were incubated with 1:20 dilutions of K76 (DHSB, Antibody registry ID AB_531836) **(A)** or 1:1000 dilutions 2A4 (DHSB, Antibody Registry ID: AB_2618114) **(B)** primary antibodies followed by incubation with 1:250 dilutions of Alexa Fluor Goat Anti-Mouse secondary antibody (Jackson ImmunoResearch, Antibody Registry ID: AB_2338840) (green). In the presence of K76 (anti-PGL-1), P granules are observed **(A, top)**, while 2A4 (anti-ELT-2) stained the intestine-specific ELT-2 transcription factor **(B, top)**. Non-specific binding of the secondary was not observed in either instance **(A, B, bottom)**. Three biological replicates were performed for each experiment. Scale bars represent 10 μm.

molecule RNA detection by taking advantage of a single, universal fluorophore-labeled secondary probe annealed *in vitro* to gene-specific primary probes (Figure 3.3A). Primary smiFISH probes contain two main parts facilitating efficacy and cost reduction: the gene-specific region complementary to the transcript of interest and the FLAP region complementary to the fluorescently-labeled secondary probe. *In situ*, the complementary region of the primary probes bind to the target RNA while it's FLAP region is annealed to a fluorophore-labeled secondary FLAP probe. This regime significantly reduces the cost of single-molecule RNA visualization by eliminating the need to create chemically conjugated probe sets for each specific target RNA. To test whether smiFISH performs as well as traditional smFISH in *C. elegans* embryos, we compared *nos-2* or *imb-2* smFISH and smiFISH probes in the same sample (Figure 3.3). We found that smiFISH faithfully reproduces the sensitivity, spatial resolution, and reliability of smFISH probes. We have found that in larval stages smiFISH is less effective than smFISH using our standard protocols, possibly due to lower larval permeability preventing smiFISH probe entry.

3.3.4 smiFISH probe design

smiFISH primary probes can be designed as described Tsanov et al. 2016 using the R script Oligostan. Primary probes can be ordered in 96-well plates from IDT on the 25 nmol scale prediluted to 100 μM in IDTE buffer pH 8.0. Alternatively, if ordering 96 or more individual probes, oligos can be ordered on the 500 pm scale, which still provides ample primary probes for hundreds of experiments. For most experiments, 12-16 primary probes per transcript is sufficient, although testing as few as 8 primary probes has produced discernable single-molecule spots in *C. elegans* embryos. An increased number of primary probes typically increases the signal-to-noise ratio for any given transcript. Secondary FLAP probes (see smiFISH below) can also be ordered as 5' and/or 3' single- or dual-fluorophore-labeled oligos from either Biosearch Technologies or IDT (Coralville, Iowa).

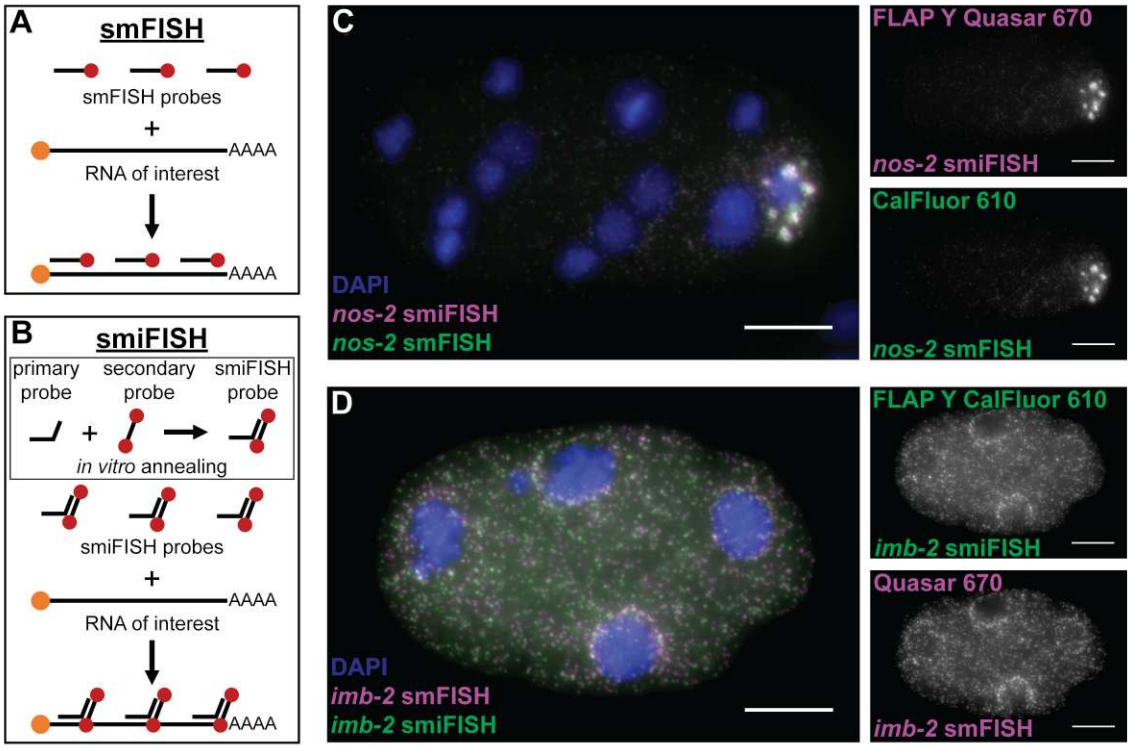

Figure 3.3: smFISH and smiFISH in *C. elegans* embryos. (A) Schematic illustration of smFISH probes. **(B)** Schematic illustration of smiFISH probes. **(C)** *nos-2* RNA was visualized using smiFISH (magenta) and smFISH (green). *nos-2* smiFISH primary probes used FLAP-Y sequences and the secondary FLAP-Y probe was 5' and 3' dual-conjugated with Quasar 670 fluorophores. *nos-2* smFISH probes were 3' single-conjugated with Cal Fluor 610. **(D)** *imb-2* RNA was visualized using smFISH (magenta) and smiFISH (green). *imb-2* smFISH probes were 3' single-conjugated with Quasar 670 fluorophores. *imb-2* smiFISH primary probes used FLAP-Y sequences and the secondary FLAP-Y probe was 5' and 3' dual-conjugated with Cal Fluor 610. Embryos were counterstained with DAPI in blue **(C, D)**. Three biological replicates were performed for each experiment using newly annealed smiFISH probes for each replicate. Scale bars represent 10 μm.

3.3.5 Optimizing signal-to-noise in smFISH and smiFISH samples

In RNA FISH experiments, it is crucial to obtain the highest possible signal-to-noise ratio (SNR) to ensure reliable interpretation of the data. One common question surrounding smFISH is whether commercial reagents (i.e., Stellaris) are superior to homemade reagents [219, 234]. By comparing the signal-to-noise ratio of four transcripts imaged by smFISH using homemade buffers or Stellaris buffers, we found Stellaris buffers perform significantly better for all four transcripts, ranging from 15-25% improvement in average SNR compared with homemade buffers. (Figure 3.4). Another common concern with smFISH experiments is photolability. Due to the relatively low signal, high laser powers, and small number of fluorophores (24-48) utilized in smFISH experiments, photobleaching can occur rapidly. Photobleaching is of particular concern with thick samples that must be imaged through many Z-stacks, as is the case with *C. elegans* embryos (12-20 μm thickness as prepared in Protocol 1: 3.1.4, or 60-100 stacks per embryo at 0.2 μm spacing between Z-stacks). One of the primary causes of photobleaching is degradation of fluorophore molecules by oxygen radicals produced upon laser excitation [245]. Therefore, free-radical scavenging antifades are commonly used to reduce the degree of experimentally-induced photobleaching. We tested combinations of antifades to determine the optimal reagents for maintaining high signal-to-noise throughout an experiment. Through these experiments, we found that the optimal antifade solution can vary depending on the probe set or fluorophore (Figure 3.5). In our hands, VECTASHIELD, N-propyl gallate, or a mixture of the two, provided the best signal stability for Cal Fluor 610 and Quasar 670 labeled RNAs in *C. elegans* embryos.

3.3.6 Sequential IF/FISH protocol

Simultaneous detection of an RNA and its cognate protein reveals a wealth of information regarding the expression patterns, regulation, and functions of genes. However, the combination of IF and FISH is often challenging due to slight incompatibilities in traditional protocols. Typically combined IF/FISH protocols require specific tailoring to the system of interest [246–248]. This includes one protocol designed for the extruded *C. elegans* gonad, which requires hand dissection

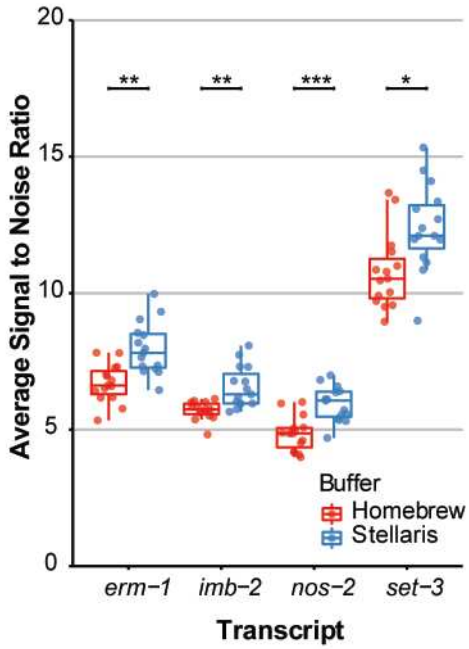

Figure 3.4: Stellaris buffers provide higher signal-to-noise ratios than homebrew buffers. Signal-to-noise ratios were calculated for each RNA puncta identified when smFISH was performed using homebrew (red) or commercial Stellaris (blue) buffers. The signal-to-noise ratio was calculated by identifying RNA spots using FISHquant [204] before using the ImJoy SNR plugin. In short, the SNR plugin compares the intensity at the coordinates of RNA puncta identified by FISHquant to the average intensity of a sphere surrounding the spot to calculate SNR. Four Stellaris smFISH probe sets were used, *erm-1* conjugated to Cal Fluor 610, *imb-2* conjugated to Quasar 670, *nos-2* conjugated to Quasar 670, and *set-3* conjugated to Cal Fluor 610. Individual dots represent the average SNR in one embryo. Three biological replicates were performed for each experiment, and 15 embryos were quantified for each condition. P values from Benjamini-Hochberg corrected t-tests are shown ($0.05 > * > 0.005 > ** > 0.0005 > *** > 0.00005$).

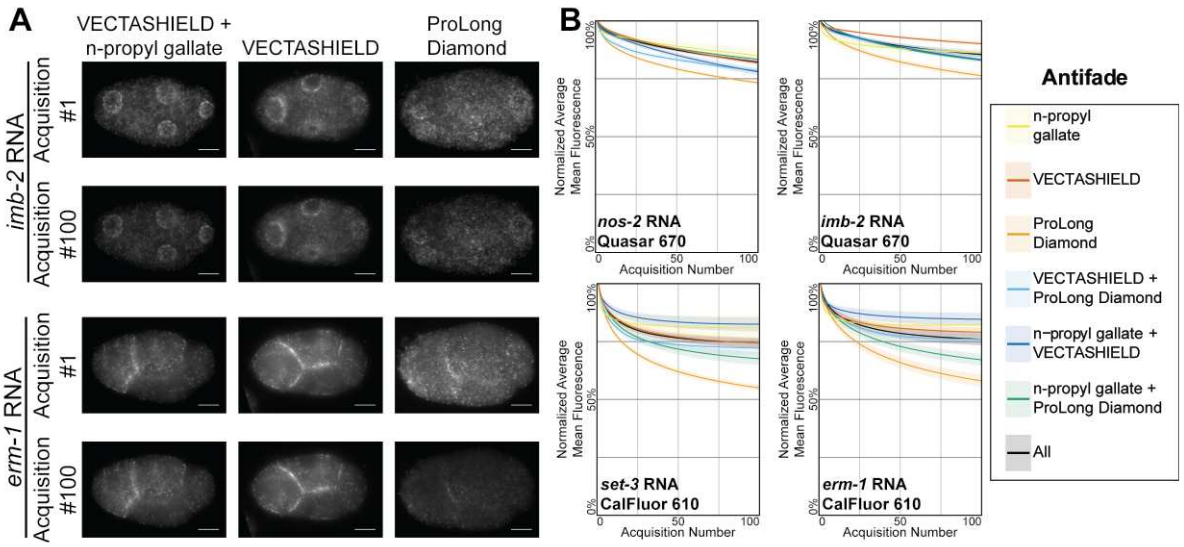

Figure 3.5: Effect of anti-fade composition on smFISH signal intensity. The mean fluorescence intensity of smFISH signal over 100 exposures was measured in embryos using various antifades and their combinations. Experiments were performed using four different smFISH probe sets: *erm-1* conjugated to Cal Fluor 610, *imb-2* conjugated to Quasar 670, *nos-2* conjugated to Quasar 670, and *set-3* conjugated to Cal Fluor 610). **(A)** The average mean intensity throughout imaging was normalized to the intensity of first acquisition for each embryo. The shaded region represents the standard error of the mean for each exposure. Three biological replicates were performed for each experiment, and no less than nine embryos were quantified for each condition. **(B)** Representative images of the first and final acquisitions for *imb-2* (top) and *erm-1* (bottom) RNAs using VECTASHIELD and N-propyl gallate (left), VECTASHIELD only (middle), and ProLong Diamond (right) anti-fades. Scale bars represent 10 μm.

of individual animals and careful slide preparation [249]. When immunofluorescence is performed in series with smFISH all reagents must be RNAse free where possible. Steps containing BSA must be treated with an RNAse inhibitor to prevent RNA degradation. We demonstrate a sequential IF/FISH protocol using the anti-PGL-1 antibody, K76 and smFISH probes against the P granule RNAs *nos-2* (Figure 3.6A) and *cpg-2* (Figure 3.6B). Additionally we show IF/FISH results in embryos stained with the ELT-2 antibody, 2A4 and hybridized with smFISH probes targeting *elt-2* RNA (Figure 3.6C)

3.3.7 Simultaneous IF/FISH protocol

If performing IF with a high-affinity nanobody or single chain variable fragment (ScFv), a simplified protocol can often be utilized. Under these circumstances, the FISH protocol (Protocol 3) can be followed with the caveat that fluorescently labeled nanobody or ScFv can be added directly to the hybridization buffer in step 4 and incubated with the FISH probes and sample overnight to perform IF. It is unclear why some nanobodies and ScFv work with this simplified protocol, but it is possible that their small size compared to traditional antibodies allows better permeation during hybridization while the high-affinity of some common nanobodies/ScFv facilitate antigen recognition at the higher temperatures required for RNA FISH probe hybridization. Here we present results for simulataneous IF/FISH from embryos containing PATR-1::GFP (Figure 3.7). The embryos were stained with a Janelia Fluor 549 (Tocris cat. no. 6147) labeled anti-GFP nanobody (Chromotek, gt-250) in hybridization buffer along with smFISH probes targeting *nos-2* RNA.

3.3.8 smFISH and smiFISH data analysis

Depending on the biological questions at hand, there are several routes for the interpretation of smFISH data. These analyses range from simply characterizing the quality of the data, counting the number of RNAs in the samples, or even identifying spatial distributions of RNA within cells of interest.

The most common method for quantification of smFISH data is counting the number of RNAs within the sample. Some commonly used tools for this purpose are FISH-quant [204] and

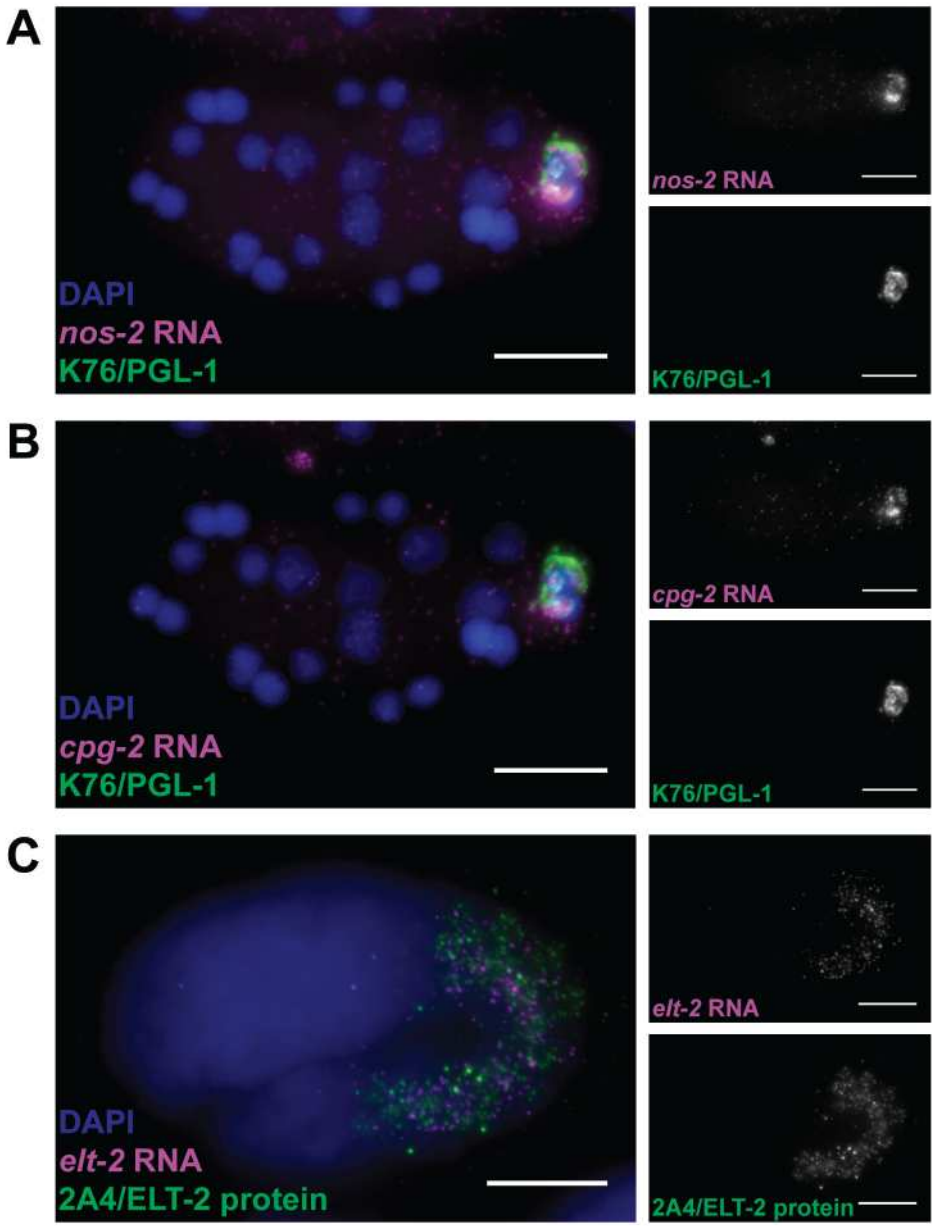

Figure 3.6: Sequential IF/FISH. Immunofluorescence followed by smFISH was performed on N2 embryos. IF was performed using K76 **(A and B)** or 2A4 **(C)** primary antibodies to identify PGL-1 containing P granules and ELT-2 protein (magenta), respectively. smFISH was used to simultaneously detect the P granule constituent RNAs *nos-2* **(A)** and *cpg-2* **(B)**, or *elt-2* mRNA **(C)**, all in magenta. Embryos were counterstained with DAPI (blue). Three biological replicates were performed for each experiment. Scale bars represent 10 μm.

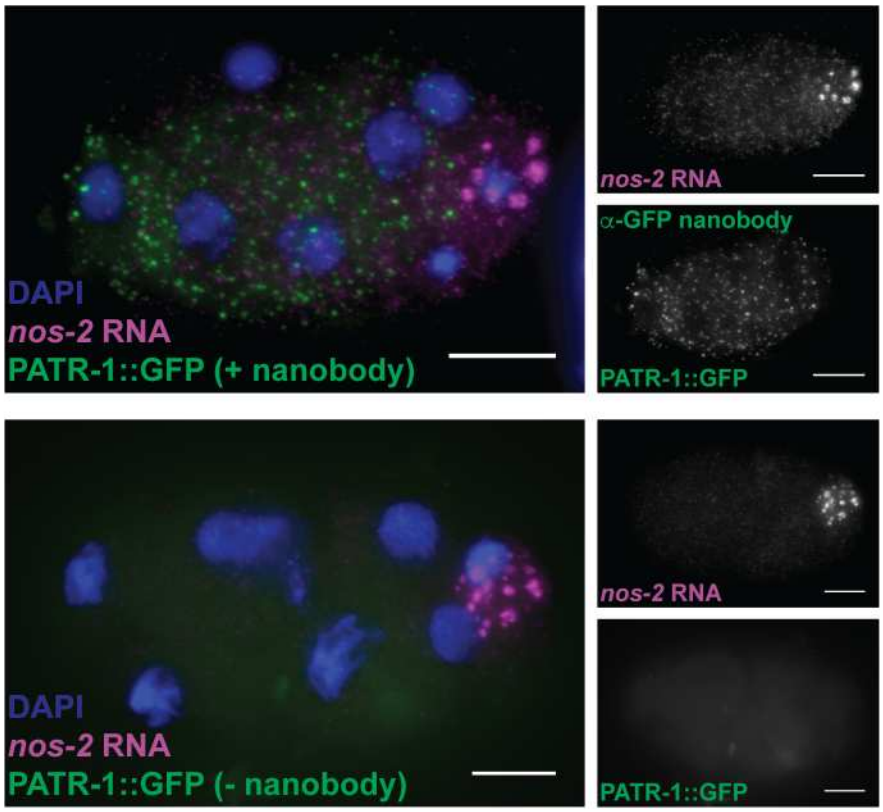

Figure 3.7: Simultaneous IF/FISH. smFISH was performed on N2 embryos with the addition of anti-GFP nanobody to hybridization buffer. *nos-2* mRNA (magenta) was probed using smFISH probes conjugated to Quasar 670. PATR-1::GFP (green) signal was visualized using 2.37 μg/ml Janelia Fluor 549 (Tocris 6147) conjugated anti-GFP nanobody (Chromotek, gt-250) (top). A no nanobody control is also shown (bottom). DNA was counterstained with DAPI (blue). Three biological replicates were performed for each experiment. Scale bars represent 10 μm.

StarSearch [221]. These algorithms function by enhancing spot signals through various filtering methods, setting a threshold for RNA spot detection, and identifying individual spots. Thresholds are often set manually by testing a range of intensity values. When plotting these values against the number of detected spots, a plateau can often be seen corresponding to threshold values separating RNA spots from lower intensity noise. When performing spot detection analysis of smFISH data, it is imperative to ensure the SNR of the data is sufficient to identify spots unambiguously. SNR can be calculated using an ImJoy plugin, which compares the intensity of a detected spot to the surrounding background intensities (https://github.com/fish-quant). In our experience, if SNR values are below $\sim$3-4, spot detection becomes less reliable. When analyzing smFISH data using FISH-quant or StarSearch, if there is no clear plateau of RNA counts over various threshold values, the SNR is likely too low for accurate RNA spot detection.

As smFISH has become more widely utilized, novel methods of analysis beyond spot counting are rapidly developing. For instance, FISH-quant has been ported from Matlab to an open-source implementation in Python and successfully applied to two large-scale screening projects [139,250]. This package includes methods for detecting, deconvolving overlapping RNAs to increase the counting accuracy of highly abundant or clustered RNAs [77, 139], measuring the signal-to-noise ratio of an image (https://github.com/fish-quant), and even identifying diverse subcellular localization patterns of RNA [139, 228]. Further, to facilitate its usage by non-specialists, several plugins providing user-interfaces for the data analysis platform ImJoy [227] were developed. As more labs adopt smFISH methodologies and more high-throughput methods of *in situ* RNA detection develop [158, 251–254], more sophisticated analysis methods are likely to arise. An exciting initiative is Starfish, an open-source software suite with the goal to build a unified data-analysis tool and file format for several spatial transcriptomic techniques [255].

3.3.9 IF data analysis

Standard methods of analysis for IF experiments include measuring the total internal fluorescence and measuring colocalization between different markers. These methods require that

imaging conditions, such as laser intensity and exposure times, are held constant across samples and replicates. We will highlight publicly available tools for analysis here; however, most microscopes ship with instrument-specific software packages capable of performing these analyses. Total internal fluorescence compares the intensity of a protein visualized by IF in a control sample and an experimental condition, such as an RNAi knockdown or protein knockout. Total internal fluorescence can be measured over the total volume of the embryo, or regions of interest can be masked either automatically or manually if specific regions must be analyzed. Regardless of whether particular segmentations are required, these analyses can be performed relatively quickly in FIJI Is Just ImageJ (FIJI) [224,256]. Additionally, several FIJI plugins are available to analyze a protein of interest's colocalization with another fluorescent marker. It is crucial when performing colocalization analyses to consider optimal uses for any given colocalization metric, as there are well-documented circumstances where these metrics can be misleading [257]. Helpful instructions for segmentation, colocalization analysis, and much more can be found at https://imagej.net/.

3.3.10 Combined IF/FISH data analysis

As with the analysis of IF data, colocalization analyses may be performed on combined IF/FISH data. However, due to the punctate nature of FISH signal, RNA spots may not overlap with a colocalization marker as well as expected, resulting in deceptively low colocalization coefficients. This can occur for several reasons. First, the small total volume of RNA puncta can lead to high variability in colocalization. This variability is compounded by the low temporal resolution of fixed cell experiments and the stochastic movements of RNA in the cell, even for tightly localized transcripts. Moreover, because it is often not known what proteins an RNA may be directly interacting with, it can be more desirable to compare RNA distributions to a nearby landmark rather than an overlapping component. For these reasons, several groups are developing novel metrics for comparing RNA and protein data and analyzing the spatial relationships between them. For instance, by spatially modeling the coordinates of each RNA puncta and comparing their distributions to other RNAs or organelles, it is possible to identify RNA patterning at vari-

ous cellular features such as cortical membranes, nuclear membranes, condensates/puncta, cellular protrusions, centrosomes, and more [77, 139, 228, 250].

3.4 Procedures

3.4.1 Protocol 1: Sequential IF/smFISH Protocol (Embryo preparation + fixation, immunofluorescence, smFISH, slide preparation)

This protocol describes methods for isolating *C. elegans* embryos and fixing them in a manner compatible with both immunofluorescence and RNA FISH. Steps for performing immunofluorescence subsequently followed by smFISH are then outlined. Finally, slide preparation is described. This approach can be used for simultaneous visualization of RNA transcripts and a protein of interest in the same sample provided the FISH probes and fluorescent antibody are selected in distinct channels.

3.4.1.1 Embryo preparation and fixation

Reagents:

1. 100% reagent grade acetone (Fisher cat. no. A18-500)
2. 100% reagent grade methanol (Fisher cat. no. A412-500)
3. Bleaching solution for use when imaging embryos (per 50 ml, make fresh):
   a. 40 ml deionized, distilled water
   b. 7.2 ml 5 M NaOH (Fisher cat. no. S318-400)
   c. 4.5 ml 5% NaHOCl (Ricca cat. no. 7495.5-32)
4. M9 buffer
   a. 3 g KH_2O_4 (Sigma cat. no. P0662-500G)
   b. 6 g Na_2HPO_4 (Sigma cat. no. RDD022-500G)
   c. 5 g NaCl (Fisher cat. no. S271-500)

   Deionized, distilled water (ddH_2O) to 1 l final volume

   Sterilize by autoclaving.

d. Add 1 ml 1 M $MgSO_4$ (Millipore cat. no. MX0075-1) using sterile technique

Wait until the solution cools to prevent precipitation.

Embryo Preparation and Fixation Protocol:

1. Grow worms to gravidity on OP50 seeded NGM plates.
   - Synchronize by bleaching if necessary.
   - We typically harvest one or two gravid 10 cm NGM plates seeded with 2 ml OP50 for each slide to be made.
   - Other bacterial stocks, such as inducible RNAi vector containing *E. coli*, can be used if desired.

2. Harvest gravid worms by washing them off of plates using M9 and collect in a 15 ml conical tube in 15 ml total volume.
   - Aggressive pipetting will increase yield by releasing more worms from the plates. Be sure not to pierce the plate's surface as agar carried into the sample will persist.

3. Spin conical at 2000 x g for 1 minute to pellet gravid worms.
   - Alternatively, allow gravid worms to settle over time.

4. Remove supernatant using a pipette or aspirator, being careful not to disturb worm pellet.

5. Resuspend worm pellet in 15 ml M9.

6. Spin to pellet again as above (3).

7. Repeat steps 4 - 6 until the supernatant is clear, removing supernatant after the final wash.

8. Add $\sim$15 ml of bleaching solution to the worms and nutate or hand-shake for 6-8 minutes until embryos are released from the mothers.
   - Check on the condition of worms periodically throughout bleaching. The gravid adults should be broken into about two pieces before continuing. If worms are bleached for too long, some early-stage embryos may be damaged.
   - For tips on harvesting embryos, see Porta-de-la-Riva et al., 2012 [258].

9. Centrifuge conical at 2000 x g for 1 minute to pellet. Immediately remove supernatant and quench bleaching with 15 ml M9.

- At this point, embryos typically stick to the tube, and the supernatant can be carefully decanted to decrease the time before quenching.

10. After adding M9, vortex the pellet to release remaining worm fragments before centrifuging at 2000 x g for 1 minute.

11. Wash with 15 ml M9 two more times (for a total of 3 washes), vortexing the pellet after the addition of M9 each time.

- The aroma of bleach should be completely gone by the end of washing.

12. Transfer remaining embryos to a 1.7 ml microcentrifuge tube and pellet in a tabletop centrifuge for 30 seconds at 2000 x g. Turn tube 180° and repeat until a pellet has formed. Remove any remaining M9.

13. Add 1 ml pure methanol cooled to -20 °C, vortex to break up the pellet, and immediately submerge in liquid nitrogen for 1 minute to crack the eggshell and promote permeabilization.

14. Remove the tube from liquid nitrogen and immediately begin pelleting at 2000 x g in 30 sec intervals, rotating the tube 180° between each spin.

- The sample will still be partially frozen for the first spins, but it is best to get the sample pelleting early to prevent over-fixation.

15. Once the embryos are pelleted, and the sample has been in methanol for 5 min, remove the methanol and replace it with 1 ml pure acetone cooled to -20 °C. Store the sample at -20 °C for $\sim$3 min.

16. Pellet embryos by centrifugation as in step 14.

17. After embryos have fixed in acetone for 5 min, remove the acetone and immediately continue to IF, smFISH, smiFISH, or IF/FISH protocol.

3.4.1.2 Immunofluorescence

Reagents:

1. 10X PBST

   a. 80 g NaCl (Fisher cat. no. S271-500)

   b. 2 g KCl (Sigma cat. no. P3911-500G)

c. 14.2 g Na_2HPO_4 (Sigma cat. no. RDD022-500G)

d. 2.4 g KH_2PO_4 (Sigma cat. no. P0662-500G)

e. 1% Tween 20 detergent (w/v) (Sigma cat. no. P1379-500ML)

Deionized, distilled water to 1 l final volume

Sterilize by autoclaving

Dilute to 1X in sterile deionized, distilled water

2. Bovine Serum Albumin (Sigma cat. no. A9418-5G)

a. RNAse free BSA can be used if issues with RNA degradation occur with sequential IF/smFISH protocols; however, it is much more expensive.

3. Primary antibody or fluorescently labeled nanobody/ScFv

4. Fluorescent secondary antibody (if using an unlabeled primary antibody)

5. DAPI, 4',6-Diamidino-2-Phenylindole, Dihydrochloride (Invitrogen cat. no. D1306)

6. RNasin Ribonuclease Inhibitor (If performing IF/FISH) (Promega cat. no. N2111)

7. 20X SSC (If performing IF/FISH)

a. 800 ml deionized, distilled water

b. 175.2 g NaCl (Fisher cat. no. S271-500)

c. 88.2 g sodium citrate tribasic dihydrate (Sigma cat. no. S4641-500G)

pH to 7.0 with 1 M HCl.

Deionized, distilled water to 1 l and autoclave.

Dilute to 2X in sterile deionized, distilled water.

PRELIMINARY NOTES: If performing IF/FISH, all reagents must be RNAse free where possible. Steps containing BSA must be treated with an RNAse inhibitor to prevent RNA degradation (see step 6 and 8). Once a fluorescent antibody has been added (either primary or secondary) all subsequent steps should be carried out in the dark, ie covered in foil, to minimize fluorophore bleaching.

Immunofluorescence Protocol:

1. Prepare fixed embryo samples as described in Chapter 3.4.1.1 steps 1-17.

2. Add 1 ml 1X PBST to sample and nutate for 5 min to wash.

3. Pellet embryos by centrifuging at 2000 x g in 30 sec intervals, rotating the tube 180° between each spin until pellet forms.

4. Pipet or aspirate as much of the supernatant PBST as possible without disrupting the pellet.

5. Repeat steps 2-5 two more times (3 washes total).

6. Block for 30 min. at 37 °C in 50-250 µl 1X PBST containing 1% w/v BSA with nutation.

   IMPORTANT: If FISH will be performed subsequently, it is essential to add 1 unit/µl RNasin (Promega) to prevent RNA degradation during steps where BSA is included.

7. Centrifuge embryos at 2000 x g in 30 sec intervals, rotating the tube 180° between each spin until pellet forms.

8. Pipet or aspirate as much of the supernatant as possible without disrupting the pellet.

9. Apply 25-100 µl 1° antibody diluted in 1X PBST with 1% w/v BSA (and 1 unit/µl RNasin if FISH will be performed subsequently). Nutate at room temperature for at least 1-2 hrs, or overnight at 4 °C.

   - Overnight incubations will give better IF signal, but can increase RNA degradation.
   - Optimal antibody concentrations must be determined for each antibody.

10. Add 1 ml 1X PBST directly to sample and nutate for 5 min to wash out free antibody.

11. Centrifuge embryos at 2000 x g in 30 sec intervals, rotating the tube 180° between each spin until pellet forms.

12. Pipet or aspirate as much of the supernatant PBST as possible without disrupting the pellet.

13. Repeat steps 9-11 two more times (3 washes total).

14. Apply 25-250 µl fluorescently labeled 2° antibody diluted in 1X PBST and incubate for 1-2 hrs in the dark at room temperature with nutation.

   - Optimal antibody concentrations must be determined for each antibody.

15. Add 1 ml 1X PBST and nutate for 5 min to wash out excess antibody.

16. Centrifuge embryos at 2000 x g in 30 sec intervals, rotating the tube 180° between each spin until pellet forms.

17. Pipet or aspirate as much of the supernatant PBST as possible without disrupting the pellet.

18. Repeat steps 15-17.

19. Add 1 ml 2X SSC and nutate for 5 min to equilibrate embyros in an smFISH compatible solution.

20. Centrifuge embryos at 2000 x g in 30 sec intervals, rotating the tube 180° between each spin until pellet forms.

21. Pipet or aspirate as much of the supernatant SSC as possible without disrupting the pellet.

22. Repeat steps 19-21.

23. Continue to 3.4.1.3, smFISH protocol

3.4.1.3 smFISH

Reagents:

1. Wash Buffer A (10% volume/volume formamide)

   a. 600 µL Stellaris Wash Buffer A (Biosearch Technologies cat. no. SMF-WA1-60)

   b. 2.1 mL DEPC treated RNAse free water (Invitrogen cat. no. AM9922)

   c. 300 µL deionized formamide (Millipore cat. no. S4117)

   Prepare 3 mL for each sample to be hybridized.

   Prepare Wash Buffer A fresh for each experiment.

2. Wash Buffer B

   a. Stellaris Wash Buffer B (Biosearch Technologies cat. no. SMF-WB1-20

   Add 88 ml RNAse free water (Invitrogen cat. no. AM9922) to Wash Buffer B stock before use.

3. Hybridization Buffer (10% volume/volume formamide)

   Prepare 110 µl for each sample in an experiment

   Prepare hybridization buffer fresh for each experiment

   a. 99 µl Stellaris Hybridization Buffer (Biosearch Technologies cat. no. SMF-HB1-10)

b. 11 µl deionized formamide (Millipore cat. no. S4117)

4. Mounting Medium (5 mL)

a. 2.5 mL 100% glycerol (Sigma cat. no. G5516-100ML)

b. 100 mg N-propyl gallate (Sigma cat. no. 02370-100G)

c. 400 µl 1 M Tris pH 8.0 (Sigma cat. no. 10708976001)

N-propyl gallate is toxic.

Vortex until N-propyl gallate has dissolved.

Store mounting medium in amber tubes or covered in foil at either 4 or -20 °C.

The solution is light sensitive.

Throw mounting medium away if it begins to yellow or crystalize.

5. smFISH probes and/or annealed smiFISH probes

6. DAPI, 4',6-Diamidino-2-Phenylindole, Dihydrochloride (Invitrogen cat. no. D1306)

7. RNAse free water (Invitrogen cat. no. AM9922)

smFISH Protocol:

1. Prepare fresh buffers by adding formamide to Wash Buffer A and Hybridization Buffer.

- Wash Buffer A and Hybridization Buffer should always have formamide added immediately preceding the experiment. Formamide can decompose over time, particularly at higher temperatures, leading to less stringent probe binding. It can also acidify when exposed to air resulting in fluorophore quenching.
- Formamide stocks should be stored frozen and their pH monitored periodically (pH 7-8 is ideal)

2. Add 2 µl 1.25 µM smFISH probes (1:20 dilution of 25 µM stocks) to 110 µl hybridization buffer. If performing experiments using multiple probe sets with different fluorophores, add 2 µL of each probe set.

- Mix well. Hybridization buffer is viscous.

Optional step: If performing Protocol 4 (simultaneous IF/FISH) using a compatible ScFv or nanobody, additionally add the appropriate concentration of ScFv or nanobody to the hybridization buffer.

Note: Although 2 μL has worked well for most of the probe sets we have used, it is helpful to perform a titration over ∼1 order of magnitude of concentrations to identify optimal probe concentrations on an individual probe set basis.

3. Centrifuge embryos at 2000 x g in 30 sec intervals, rotating the tube 180° between each spin until pellet forms.

4. Pipet or aspirate as much supernatant as possible without disturbing the pellet.

5. Prehybridize sample in 1 mL Wash Buffer A and incubate at room temperature for ∼5 minutes.

6. Centrifuge embryos at 2000 x g in 30 sec intervals, rotating the tube 180° between each spin until pellet forms.

7. Pipet or aspirate as much supernatant as possible without disturbing the pellet.

8. Add 100 μL hybridization buffer with probes to the pelleted embryos and hybridize at 37 °C in the dark for 8-48 hours.

- Store prepared Wash Buffer A at room temperature or 37 °C during this incubation. Warm buffer will increase the stringency of probe binding and decrease background and non-specific binding.
- If available, use a thermomixer to shake the hybridization solution and all subsequent washes at 450 rpm during incubation to ensure even probe penetration.

9. Add 1 mL Wash Buffer A directly to the embryos in hybridization solution.

10. Incubate at 37 °C in the dark for 30 minutes.

11. Centrifuge embryos at 2000 x g in 30 sec intervals, rotating the tube 180° between each spin until pellet forms.

12. Pipet or aspirate as much supernatant as possible without disturbing the pellet.

13. Add 1 mL Wash Buffer A containing 1 ng/μL DAPI to the sample.

14. Incubate at 37 °C in the dark for 30 minutes.

15. Centrifuge embryos at 2000 x g in 30 sec intervals, rotating the tube 180° between each spin

until pellet forms.

16. Pipet or aspirate as much supernatant as possible without disturbing the pellet.

17. Add 1 mL Wash Buffer B and incubate for ∼5 minutes.

18. Repeat step 15 and 16.

19. Resuspend in 50 µL of mounting medium (or less if the sample is small) and incubate at 4 °C for 30 minutes to ensure antifade penetrance.

20. Move to slide preparation.

3.4.1.4 Slide preparation

Reagents:

1. VECTASHIELD mounting medium (Vector Laboratories cat. no. H-1000-10)

2. 8mm 1.5 thickness round cover glass (Electron Microscopy Sciences, cat. no. 72296-08)

3. Glass microscope slides (VWR cat. no. 48312-401)

4. 1.5 thickness, 22X22 mm coverglass (VWR cat. no. 48366-227)

5. Grace Bio-Lab Press-To-Seal silicon isolator (Sigma cat. no. GBL664504-25ea)

Slide preparation protocol:

1. Working at a dissecting microscope, drop 2 – 6 µl of embryos suspended in mounting medium onto a single 8 mm 1.5 thickness round cover glass resting on a glass slide.

- Always wear gloves when handling slides and cover slips to prevent smudging and contamination.

2. Add the same volume of VECTASHIELD antifade solution and pipet up and down to mix thoroughly.

- Try to keep the final volume to 4-6 µl by removing some of the mixture.
- This is a good time to break up any large clumps of embryos by pipetting.

3. Place a 1.5 thickness 22 mm x 22 mm square cover glass on top trying to avoid bubbles.

- Do not let the coverslip touch the slide. The sample solution will pour over the edge of the round coverslip and seal it to the slide beneath through surface tension. Having the round

coverslip close to the edge of the slide can provide some extra working height. Additionally, gently lowering the square coverslip from front to back over the round coverslip until surface tension pulls the round cover slip up will help prevent spillover.

4. Flip the coverslips so the square coverslip is on the bottom. Remove as much liquid as possible from between the two cover glasses using a torn kimwipe placed against the round one.

- The aim is to flatten the embryos as much as possible without damaging them.
- Samples can be firmly pressed on with a pipette tip as long as the coverslip doesn't slide from side to side.
- The ideal depth of an embryo on the slide is $\sim$12-20 μm. Signal-to-noise ratio will decrease and photobleaching will increase with increasing thickness due to out-of-focus light and more image acquisitions, respectively.

5. Affix the cover slip sandwich to a microscope slide using a Grace Bio-Lab Press-To-Seal silicon isolator such that the embryos will be imaged through the square coverslip.

6. Head off to the microscope!

3.4.2 Protocol 2: smFISH or smiFISH alone (Embryo preparation + fixation, smFISH or smiFISH, slide preparation)

This protocol describes the workflow for performing smFISH or smiFISH in embryos, from sample preparation to slide preparation.

3.4.2.1 Embryo preparation and fixation

Perform Embryo prep and fixation as in Chapter 3.4.1.1

3.4.2.2 smFISH

Perform smFISH as in Chapter 3.4.1.3

3.4.2.3 smiFISH

Perform smiFISH as in 3.4.1.3 with the following considerations/exceptions: The following reagents and protocol is required to generate annealed primary + secondary smiFISH probes.

Reagents:

1. 8-24 gene specific primary probes resuspended at 100 μM in IDTE pH 8.0 (or Tris pH 8.0)
2. 1 Fluorophore-labeled FLAP probe resuspended at 50 μM in Tris pH. 8.0
3. New England Bio Labs Buffer 3 (or 3.1) (NEB cat. no. B7203S)

smiFISH probe annealing:

i. Combine primary probes at equimolar ratio and dilute to 0.833 μM in Tris pH 8.0.

In a PCR tube, prepare a solution of:

ii. 2 μL primary probe set
iii. 1 μL 50 μM FLAP secondary probe
iv. 1 μL NEB Buffer 3 (or 3.1)
v. 6 μL RNAse free water

Anneal primary probe set to fluorophore-labeled secondary probes using the following thermocycling conditions:

vi. 1 cycle at 85 °C for 3 minutes
vii. 1 cycle at 65 °C for 3 minutes
viii. 1 cycle at 25 °C for 5 minutes

The primary probe mixture is stable at -20 °C indefinitely.

Annealed smiFISH probes are viable at -20 °C for up to at least a week.

Treat annealed smiFISH probes as diluted smFISH probes.

2 μl annealed smiFISH probe works well for most hybridizations

3.4.2.4 Slide preparation

Prepare slides as in 3.4.1.4

3.4.3 Protocol 3: Immunofluorescence alone (Embryo preparation + fixation, immunofluorescence, slide preparation)

This protocol describes the steps to perform immunofluorescence in *C. elegans* embryos from harvesting embryos to preparing slides.

3.4.3.1 Embryo preparation and fixation

Perform Embryo preparation and fixation as in 3.4.1.1

3.4.3.2 Immunofluorescence

Perform immunofluorescence as in 3.4.1.2 with the following exceptions:

1. At step 15, nutate the sample in 1X PBST for 10 minutes instead of 5.
2. Pellet embryos by centrifuging at 2000 x g in 30 sec intervals, rotating the tube 180° between each spin until pellet forms.
3. Pipet or aspirate as much of the supernatant PBST as possible without disrupting the pellet.
4. Counterstain with 1X PBST containing 2 µl 500 ng/mL DAPI for 10 min.
5. Pellet embryos by centrifuging at 2000 x g in 30 sec intervals, rotating the tube 180° between each spin until pellet forms.
6. Pipet or aspirate as much of the supernatant PBST as possible without disrupting the pellet.
7. Add 1 ml 1X PBST directly to sample and nutate for 10 min to wash out excess DAPI.
8. Repeat steps 5-7, followed by steps 5 and 6 (for two 1X PBST washes).
9. Resuspend in 50 µL of mounting medium (or less if the sample is small) and incubate at 4 °C for 30 minutes to ensure antifade penetrance.

3.4.3.3 Slide preparation

Prepare slides as in 3.4.1.4

3.4.4 Protocol 4: Abreviated protocol for IF/smiFISH for use with nanobodies. (Embryo preparation + fixation, simultaneous IF/smiFISH, slide preparation)

This protocol describes a simplified method for performing immunofluorescence at the same time as smFISH with select antibodies

3.4.4.1 Embryo preparation and fixation

Perform Embryo prep and fixation as in 3.4.1.1.

3.4.4.2 Simultaneous immunofluorescence and smFISH

Perform smFISH as in 3.4.1.3 with the following exceptions and considerations:

1. At step 2, when preparing the hybridization buffer mix, incorporate the appropriate concentration of antibody and proceed normally.

- This protocol only works with a subset of antibodies.
- We have had the best results using high-affinity nanobodies, ScFv, or fragmented antibodies [259]. High-affinity, small sized antibodies have improved the success of this simplified protocol in our hands.
- We have only had success with primary staining using this protocol. Immunofluorescence using secondary antibody amplification during wash steps has not succeded.

3.4.4.3 Slide preparation

Prepare slides as in 3.4.1.4

3.5 Controls and Troubleshooting

3.5.1 Validating new probe sets

There are several ways to validate new probe sets for target specificity and labeling efficiency. The most straightforward test for target specificity is to use the probes in a wildtype and deletion strain for the target of interest to ensure the probe set is binding only when the RNA is present. If a deletion allele is not available, RNAi can be utilized to a similar end. However, it is important to note that residual fluorescent signal may be present after RNAi because the knockdown may be incomplete or may only partially degrade the targets. Target specificity can also be determined by targeting a gene with two separate probe sets in different colors, which should colocalize if the probes are specific. Labeling efficiency of a probe set can be determined by comparing transcript

abundance found using smFISH data to other sources, such as qRT-PCR, digital-droplet PCR, or quantitative sequencing data.

3.5.2 Positive controls

Positive control smFISH probe sets should be consistently employed to ensure the protocol is working. These probe sets have the added benefit of marking specific cell lineages or developmental stages and thereby identify the embryo's orientation or stage. By comparing the performance across replicates, researchers can identify outliers or problems in protocol execution. When troubleshooting, the use of smFISH probe sets that anneal to highly abundant RNAs, such as the polyA sequence of mRNA, or using previously validated probes can be useful to ensure the FISH protocol is successful.

3.5.3 Photobleaching

Due to the small number of fluorophores on any single RNA, the photolabile nature of common fluorophores, and the common use of widefield microscopy for FISH experiments, FISH can often suffer from rapid photobleaching. If a sample has clear puncta that disappear throughout imaging or the mean intensity of the sample drops rapidly during acquisition, photobleaching is likely reducing the data's quality. Anti-fade should always be included in slide preparation and given time to permeate the sample before imaging to prevent photobleaching. Further, imaging from long, low energy wavelength lasers to short, higher-energy (i.e., from far-red to UV) can help preserve fluorescence.

3.5.4 Low Signal to Noise

Since *C. elegans* embryos are relatively thick ($\sim$20-30 μm), the use of widefield microscopy will capture a large amount of out-of-focus signals from non-focal Z-planes in the sample. Embryos can be flattened during slide preparation to improve SNR. We have found that samples from $\sim$12-20 μm thick have an optimal signal-to-noise ratio without obviously perturbing sample morphology. While pressing down on embryos does not seem to affect their morphology, any lateral

motion during slide preparation will shear embryos, so it is essential to press directly down when making slides.

3.5.5 Crosstalk of smiFISH secondary probes

Tsanov et al. demonstrated that multiple primary probe sets containing the same FLAP sequence could be utilized in the same experiment without observable mislabeling by annealing them to secondary probes labeled with distinct fluorophores (i.e., probe-set-1 FLAP-Y-Cal Fluor 610, probe-set-2 FLAP-Y-Quasar 670). We have validated this in the *C. elegans* embryo.

3.5.6 Probing for short transcripts

If a transcript is too short to design ample FISH probes, it can be worrisome to order probe sets. We have obtained clear punctate signal for probe sets using as few as eight smiFISH probes. If a transcript is too short for even eight probes, it is worth considering amplification-based FISH methods [254, 260–262], which have been utilized in *C. elegans* [263]. However, quantification of amplification-based FISH is far less accurate due to variability in signal strength from single RNA molecules.

3.5.7 smiFISH secondary aggregates

In some instances, we and other groups (personal comm) have observed large aggregates of fluorescently labeled secondary smiFISH probes on the surface of cells or adhered to slides. In our experience, vortexing annealed smiFISH probes followed by a quick centrifugation in a microfuge before hybridization and vigorous vortexing of samples after hybridization are sufficient to remove these large aggregates.

3.5.8 Validation of antibodies

With any IF experiment, it is essential to validate the antibodies' function and specificity. Primary antibodies can be validated using null or RNAi strains to ensure that the antibody is binding specifically to the target antigen. Secondary antibodies can be tested for specificity by incubating

them in the absence of primary antibodies to ensure that there is no staining of endogenous antigens. Should an antibody have some non-specific binding, it may be possible to increase specificity by depleting the antibody using a null allele [235]. It is also necessary to test every antibody's sensitivity over a range of concentrations to identify the optimal concentration for detecting the antigen of interest without promoting non-specific staining, typically over at least one to two orders of magnitude. Most commercial antibodies have a range of suggested optimal concentrations for immunofluorescence that can be used as a starting point. It is wise to test these concentrations for each experiment or experimental condition because changes in protein concentration or antigen accessibility can lead to different optimal concentrations of antibodies on a case-by-case basis. It is important to be aware that this can make downstream quantification inaccurate; however, so it is beneficial to use identical staining conditions when possible.

3.5.9 Low yield

If embryo yield is low after performing IF, ensure that detergent is being used in the wash steps as it strongly reduces adherence to pipette tips and plastic tubes.

3.5.10 Positive controls

If a protein can not be detected using a validated antibody, it is crucial to ensure that IF is working correctly. Staining common cytoskeletal components such as actin or microtubules can both verify the efficacy of the IF protocol in a sample while simultaneously demonstrating the sample is morphologically intact. Alternatively, a fluorescent protein, such as GFP, can be targeted for immunofluorescence using a different color and colocalization analyzed to ensure effective staining.

3.5.11 RNA degradation

The most common issue in performing combined IF/FISH is RNA degradation. It is essential to use RNase-free reagents throughout the protocol and, when necessary, to add RNase inhibitors such as RNasin. In our experience, RNase inhibitor was only necessary during steps where BSA

is present (which contains RNases). However, if RNA is not visible after performing IF/FISH, it is likely due to RNase contamination. Remaking reagents with RNase-free components or adding RNase inhibitors at each step will likely remedy this issue. As RNase inhibitor is relatively expensive, it is best to ensure the purity of reagents where possible. If RNA degradation continues to be an issue, reducing the duration of the IF steps of the protocol tends to improve RNA signal at the cost of protein signal. For example, performing a two-hour incubation with primary antibody instead of overnight can reduce RNA degradation.

3.5.12 Permeabilization and fixation

C. elegans embryos are highly effective at preventing environmental contaminants from entering. This is in part due to the permeability barrier, a membranous barrier that prevents fluid exchange between the embryo and the environment [200]. The choice of fixative and fixation duration appear to be highly important for permeabilizing the embryo to antibodies, which are roughly 20X the mass and radius of smFISH probes (Ab $\sim$ 150 kDa and $\sim$ 60 Å, 20mer oligo $\sim$ 7.5 kDa and $\sim$ 3 Å [264, 265]. In our experience, a brief methanol fixation, liquid nitrogen freeze cracking, followed by a quick acetone fixation, was most effective at allowing antibodies to pass through the eggshell and permeability barrier while maintaining antigen recognition and FISH probe accessibility. The use of acetone was necessary for antibody staining. We interpret this result as acetone solubilizing permeability barrier components, thus increasing the size of molecules that can enter the embryo, although we have not rigorously examined the effective pore size under different fixation conditions. Our experiments with longer fixation times with both methanol and acetone reduced antigen recognition by antibodies (as well as GFP fluorescence for protein fusions). Moreover, the use of formalin/formaldehyde reduces the binding and photostability of FISH probes. Some antigens are likely more compatible with different fixatives, however. Should the fixation conditions presented here be incompatible with an antigen of interest, Duerr 2006 describes alternative fixation strategies. If alternative fixation strategies must be pursued, it is crucial to keep in mind the effect they will have on the permeability of the eggshell and permeability bar-

rier. If IF still fails, it may be worth using 150kDa fluorescent dextran to determine whether the embryo is permeable to antibodies.

3.5.13 Clumps

For reasons unknown, in our experiments, *C. elegans* embryos that have undergone IF/FISH form aggregates of embryos that do not occur with either protocol alone. While some clumping seems inevitable, vigorous vortexing after fixation and every wash/pelleting step, as well as constant rocking during incubations, reduces the number and size of clumps. Clumps can also be disrupted by pipetting when preparing slides.

3.6 Author contributions

This chapter was a collaborative project originally written for publication. Dylan M. Parker and Erin Osborne Nishimura led the project. Sam Boyson optimized the smiFISH method used in this chapter. Lindsay P. Winkenbach performed smFISH for antifade optimization experiments. Annemarie Parker performed image analysis for antifade optimization experiments. All authors contributed to manuscript editing. All other work performed in this chapter was solely performed by Dylan M. Parker.

Chapter 4

Conclusions

4.1 mRNA localization is a widespread form of post-transcriptional regulation

Since subcellular mRNA localization was first characterized in 1983 [7], nearly 200,000 transcripts from diverse species have been annotated as having subcellular localization [29]. These localized transcripts have been identified in virtually every imaginable region of the cell, from the cortical membrane to the nuclear membrane, to centrosomes, and even in intercellular compartments [29, 266]. The explosion in the number of identified localized RNAs and patterns they can adopt has led to a corresponding growth in understanding the regulatory functions of mRNA localization.

Many of the first studies identifying mRNA localization were performed in embryos where localized transcripts function to set up embryonic polarity and define cell fates in the absence of zygotic transcription by controlling the spatial and temporal translation of mRNAs [12]. As the functions of mRNA localization became clear in systems aside from embryogenesis, this theme of spatially and temporally regulating translation continued. In neurons, mRNA localization contributes to neuronal function by preventing the expression of proteins when and where they would be toxic to the cell [33]. Moreover, mRNA localization in neurons also facilitates the rapid response to stimuli by rapidly synthesizing proteins required for synaptic plasticity [141–145]. The spatial and temporal control mediated through mRNA localization is best illustrated in intestinal epithelial cells. In these cells, the presence of food after a period of starvation repolarizes the mRNA content of the cell, resulting in a positive feedback loop of ribosomal biogenesis to promote a rapid increase in protein output and nutrient uptake [36]. While much has been learned from the abundance of localized transcripts that have been identified and the mechanisms that have been characterized, many questions remain. In this thesis, I set out to further our understanding of

mRNA localization by developing *C. elegans* as a tractable, whole-animal model for characterizing the diversity of mRNA localization patterns, dissecting the mechanisms that lead to patterning, and identifying the ultimate functions of mRNA localization.

4.2 *C. elegans* is a tractable model for exploring mRNA localization patterns, mechanisms, and functions

In Chapter 2, we set out to use *C. elegans* as a model organism for exploring the patterns, mechanisms, and functions of mRNA localization. Prior to this work, instances of subcellular mRNA localization in *C. elegans* were sparse. Roughly six transcripts had been shown to have distinct localization patterns, all in P granules [71].

Using single-cell RNA-sequencing data from 2-cell embryos [180] and 1- to 16-cell embryos [76], we developed a candidate approach to screen *C. elegans* transcripts for subcellular localization using single-molecule microscopy. By performing single-molecule Fluorescence *In Situ* Hybridization on transcripts that were enriched in the anterior or posterior cell of the 2-cell stage embryo, symmetrically distributed between those cells, or zygotically activated later in development by single-cell RNA-sequencing data, we found that maternally-loaded transcripts were enriched for subcellular localization compared to zygotic transcripts.

The identification of subcellular mRNA localization in *C. elegans* was striking for two reasons. First, our observations from this initial screen more than doubled the number of transcripts known to have subcellular localization in *C. elegans* and demonstrated localization patterns that had never been reported in this animal. Second, and more strikingly, these observations demonstrated that localization of maternally-loaded mRNAs is likely to be a widespread feature of embryos. The majority of studies exploring subcellular mRNA localization in embryos have been performed in *Drosophila*. It has long been posited that mRNA localization in the development of *Drosophila* is only prevalent because early embryogenesis in *Drosophila* occurs in a syncytial environment. This led researchers to hypothesize that mRNA localization was required for development in the absence of cellularization, while in the development of cellularized organisms like *C. elegans* partitioning

transcripts in a cell-specific manner without subcellular localization could be sufficient to guide cell fate decisions. We definitively proved that subcellular localization to diverse locales is prevalent in embryogenesis, even in those with cellularized development.

In Chapter 3, we further developed *C. elegans* embryos as a model for exploring mRNA localization by improving methods for detecting single-molecules of RNA and generating simplified protocols for fluorescent staining of proteins *in situ*. With the knowledge that mRNA localization is common in *C. elegans* embryos, these protocols will allow other researchers to determine whether subcellular localization plays a role in the post-transcriptional regulation of their gene of interest. These methodological improvements have already spurred collaborations between our lab and others. For instance, we found that the *erm-1* transcript localizes to the cell cortex in embryos, where its encoded protein functions in organizing the cytoskeleton and cellular structure. The discovery of *erm-1* RNA localization has led to an ongoing collaboration aimed at determining how localization of the *erm-1* transcript can regulate its protein function and ultimately guide cell structure and organogenesis.

In addition to optimizing smFISH and immunofluorescence, in Chapter 3, we also developed a protocol to combine these two assays. By analyzing the localization of a transcript in relation to the protein it encodes it is possible to gain much deeper insights into the regulation of mRNA localization, its effects on protein production, and the functional effects of localizing any given transcript. The distribution of this protocol allows researchers to better define the role of mRNA localization as a means of post-transcriptional regulation in this model organism.

In addition to the work presented in this thesis, *C. elegans* more generally makes for a strong model organism for several reasons. It is inexpensive, easy to culture, and one of the few animals capable of surviving indefinitely as a frozen stock, making it highly accessible. The developmental lineage of *C. elegans* is invariable and mapped from the 1-cell stage to the final stage of development. Combined with the well-annotated genome and ease of genetic manipulation, this allows the effects of genetic perturbation to be characterized by changes in cell fates. *C. elegans* is also transparent and embryos can survive outside of the mothers, making microscopy of early embryos

favorable. Together, these advantages and the developments presented in this thesis position *C. elegans* as a highly favorable model for the study of mRNA localization moving forward.

4.3 mRNA accumulates in P granules as a consequence of translation repression

In addition to developing *C. elegans* as a model organism for the study of mRNA localization, in Chapter 2, we aimed to answer a long-standing question in the P granule field: Do P granules recruit transcripts to repress their translation or as a downstream consequence of translation repression by other factors.

We performed several experiments to determine the directionality of translation repression and transcript accumulation in P granules. We first determined what cis-acting elements are sufficient to direct P granule localization. We found that the 3'UTRs, where translation regulatory elements are commonly housed, were sufficient for the P granule localization of every transcript we tested. We then identified trans-acting factors that are necessary for P granule recruitment. In these experiments, we demonstrated that loss of trans-acting RBPs that mediate translation repression also results in a failure to accumulate in P granules. These results indicate that translation repression is likely required for recruitment to P granules. This is supported by the fact that many P granule-associated transcripts do not exist solely in P granules but maintain a translationally-repressed state even when they are distinct from P granules. Finally, by ectopically inducing a translationally inactive state through heat stress, we showed that otherwise diffuse transcripts become recruited to P granules. These findings were bolstered by a contemporary study demonstrating that P granules predominately accumulate transcripts with low ribosome occupancy [75]. Ultimately, these lines of evidence demonstrate that translation repression precedes and is sufficient for the accumulation of transcripts in P granules.

That translation repression precedes P granule localization is of particular importance for several reasons:

1) In *C. elegans* defects in P granule assembly and function are known to cause defects in transgenerational epigenetic inheritance, transgenerational sterility, temperature-sensitive sterility, and in some instances transdifferentiation of the germ lineage into neuron-like cells [190]. These defects all occur even while P granules are not strictly required for viability and fertility [188]. Understanding that these phenotypes do not result from a failure to initiate translation repression of maternally-loaded transcripts is informative. It indicates that ectopic translation of somatic proteins in the germline is likely not the only cause of these phenotypes. Moreover, that P granule defects result from a failure to accumulate repressed transcripts suggests that P granules play a multifaceted role in germ cell biology.

2) P granules are known to recruit two general classes of translationally repressed transcripts: those destined for degradation and those required for germ lineage development [77]. Knowing that translation repression is the cause of P granule localization narrows the search for factors that differentiate the fates of P granule localized transcripts. As the translational repression of P granule transcripts is mediated through interactions with trans-acting RBPs that first occur in the cytoplasm, we can start identifying components that promote degradation or preservation once a transcript arrives at a P granule.

3) P granules are highly similar to, and partially overlap with, two other condensate environments: stress granules and P-bodies [118]. Demonstrating that P granules recruit transcripts after translation repression adds to the similarities between these condensate environments. Importantly, stress granules and P-bodies are tightly linked to several neurological disorders. Often these disorders manifest as runaway accumulation of component proteins and RNAs, which disrupts the phase state of the condensates. Understanding the physical and biological principles that underlie the assembly and disassembly of these highly homologous condensates will aid in the development of treatments and prophylactic measures to reduce the toll of these diseases.

Thanks in part to the work in this thesis we now have a better understanding of the form and function of P granules. With this knowledge, studies are beginning to dissect the multifaceted role P granules have on their translationally-repressed constituent RNAs. Current hypotheses suggest

that P granules function to concentrate and protect transcripts required for germline development, mediate the degradation of somatic transcripts in the germline, reinforce the translationally inactive state of their constituent RNAs, structurally organize both the nuclear pore environment and the small RNA machinery, and ultimately facilitate the temporal activation of a subset of germline required genes in the primordial germ cells. However, more experiments are required to definitively characterize the extent to which P granules actively function in each of these processes, whether they are a passive hub where the products of these processes accumulate, or if they serve to reinforce and strengthen the effects of each of these processes.

4.4 Perspectives and future directions

In this thesis, we have developed the *C. elegans* embryo as a model for the study of RNA localization, developed and optimized protocols to expand the repertoire of localized transcripts and understand their functions, characterized diverse mRNA localization patterns in *C. elegans*, and unraveled long-standing questions surrounding P granule biology. These discoveries and contemporary advances in the fields of mRNA localization, condensate biology, sequencing technologies, and microscopy have opened new doors for the continued exploration of this fascinating form of post-transcriptional regulation.

Moving forward, continuing to screen maternally-loaded transcripts for subcellular localization will continue to provide deeper insights into the diversity of patterns occurring in embryonic development. Already, we have discovered many more transcripts with subcellular localization than are discussed in this thesis, including some with patterns we have not observed previously. Characterizing the spatial organization of the complete maternal transcriptome will provide a rich source of data for future researchers to develop hypotheses around.

It will also be deeply insightful to dissect the roles of various RNA binding proteins in the function and organization of P granules. For instance, in Chapter 2, we found that knockdown of the RBP PIE-1 results in a loss of P granule localization for the *nos-2* transcript while maintaining translation repression. How this protein contributes to the assembly of P granules and recruitment

of translationally repressed RNAs will further elucidate the modes of regulation occurring there. Further, the RBP POS-1 is required for the translational activation of *nos-2* upon the development of the primordial germ cell [73, 74]. How this occurs, however, unknown. Identifying the mechanism by which POS-1 can promote translation in the repressive environment of P granules will provide insights into how transcripts can escape these organelles to perform their functions.

Some of the P granule-associated RBPs are also associated with other condensates or protein complexes. The RBP TIAR-1 localizes to both P granules and stress granules and simultaneously accumulates in both under stress conditions [118]. Characterizing the overlap between different condensate compartments, their shared functions, and their divergent functions will help define their true roles in post-transcriptional regulation and put long-standing questions regarding their specific functions to rest. Of interest in this regard is the RBP SPN-4. SPN-4 is a known P granule component, which has recently been shown to interact with the entire CCR4/NOT deadenylation complex, a known P-body component (Data not published). We are currently working to define the role this RBP has in defining whether P granule transcripts undergo degradation or temporary repression within P granules and how its functions differ in somatic and germ cells.

Finally, the advent of live-cell RNA imaging techniques will provide an unprecedented temporal resolution for exploring RNA localization. Visualizing an RNA in real-time as it transits to its destination will expose never-before-seen details of the localization mechanisms. Do P granule transcripts diffuse in and out of the condensate? Do certain classes of transcripts use specific cytoskeletal components? How long does it take for a transcript to be recruited to P granules after translation is repressed? All of these questions and many more will be answered with these revolutionary technologies.

Ultimately, the field of mRNA localization is rich for discovery. The work presented here provides a new platform for researchers around the world to explore questions surrounding this exciting and beautiful form of post-transcriptional regulation.

Bibliography

[1] Ritter R. Die Entwicklung Der Geschlechtsorgane Und Des Darmes Bei Chiromomus. *Bd. Z furr WZ*, Vol 50, 1890.

[2] Ekaterina Voronina, Geraldine Seydoux, Paolo Sassone-Corsi, and Ippei Nagamori. RNA Granules in Germ Cells. *Cold Spring Harbor Perspectives in Biology*, 3(12):a002774, 2011.

[3] M.R. Rebagliati, D.L. Weeks, R.P. Harvey, and D.A. Melton. Identification and cloning of localized maternal RNAs from xenopus eggs. *Cell*, 42(3):769–777, 1985.

[4] Ruth Lehmann and Christiane Nüsslein-Volhard. Abdominal segmentation, pole cell formation, and embryonic polarity require the localized activity of oskar, a maternal gene in drosophila. *Cell*, 47(1):141–152, 1986.

[5] Craig C. Garner, Richard P. Tucker, and Andrew Matus. Selective localization of messenger RNA for cytoskeletal protein MAP2 in dendrites. *Nature*, 336(6200):674–677, 1988.

[6] Roy M. Long, Robert H. Singer, Xiuhua Meng, Isabel Gonzalez, Kim Nasmyth, and Ralf-Peter Jansen. Mating Type Switching in Yeast Controlled by Asymmetric Localization of ASH1 mRNA. *Science*, 277(5324):383–387, 1997.

[7] William R. Jeffery, Craig R. Tomlinson, and Richard D. Brodeur. Localization of actin messenger RNA during early ascidian development. *Developmental Biology*, 99(2):408–417, 1983.

[8] Jeanne Bentley Lawrence and Robert H. Singer. Intracellular localization of messenger RNAs for cytoskeletal proteins. *Cell*, 45(3):407–415, 1986.

[9] E H Kislauskis, X Zhu, and R H Singer. Sequences responsible for intracellular localization of beta-actin messenger RNA also affect cell phenotype. *The Journal of Cell Biology*, 127(2):441–451, 1994.

[10] A F Ross, Y Oleynikov, E H Kislauskis, K L Taneja, and R H Singer. Characterization of a beta-actin mRNA zipcode-binding protein. *Molecular and Cellular Biology*, 17(4):2158–2165, 1997.

[11] Stefan Hüttelmaier, Daniel Zenklusen, Marcell Lederer, Jason Dictenberg, Mike Lorenz, XiuHua Meng, Gary J. Bassell, John Condeelis, and Robert H. Singer. Spatial regulation of β-actin translation by Src-dependent phosphorylation of ZBP1. *Nature*, 438(7067):512–515, 2005.

[12] Paul Lasko. mRNA Localization and Translational Control in Drosophila Oogenesis. *Cold Spring Harbor Perspectives in Biology*, 4(10):a012294, 2012.

[13] Zehra Ali-Murthy and Thomas B Kornberg. Bicoid gradient formation and function in the Drosophila pre-syncytial blastoderm. *eLife*, 5:e13222, 2016.

[14] Sarah C. Hughes and Andrew J. Simmonds. Drosophila mRNA Localization During Later Development: Past, Present, and Future. *Frontiers in Genetics*, 10:135, 2019.

[15] O Steward and WB Levy. Preferential localization of polyribosomes under the base of dendritic spines in granule cells of the dentate gyrus. *Journal of Neuroscience*, 2(3):284–291, 1982.

[16] Malgorzata Kloc, N.Ruth Zearfoss, and Laurence D. Etkin. Mechanisms of Subcellular mRNA Localization. *Cell*, 108(4):533–544, 2002.

[17] Kathi Zarnack and Michael Feldbrügge. Microtubule-Dependent mRNA Transport in Fungi. *Eukaryotic Cell*, 9(7):982–990, 2010.

[18] Jingyi Fei and Cynthia M Sharma. Regulating with RNA in Bacteria and Archaea. *Microbiology spectrum*, 6(5):421–439, 2019.

[19] Li Tian, Hong-Li Chou, Masako Fukuda, Toshihiro Kumamaru, and Thomas W Okita. mRNA localization in plant cells. *Plant Physiology*, 182(1):pp.00972.2019, 2019.

[20] Keren Nevo-Dinur, Anat Nussbaum-Shochat, Sigal Ben-Yehuda, and Orna Amster-Choder. Translation-Independent Localization of mRNA in *E. coli*. *Science*, 331(6020):1081–1084, 2011.

[21] J. L. Marrison, PHD. Schunmann, H. J. Ougham, and R. M. Leech. Subcellular Visualization of Gene Transcripts Encoding Key Proteins of the Chlorophyll Accumulation Process in Developing Chloroplasts. *Plant Physiology*, 110(4):1089–1096, 1996.

[22] LCD. Gibson, J. L. Marrison, R. M. Leech, P. E. Jensen, D. C. Bassham, M. Gibson, and C. N. Hunter. A Putative Mg Chelatase Subunit from Arabidopsis thaliana cv C24 (Sequence and Transcript Analysis of the Gene, Import of the Protein into Chloroplasts, and in Situ Localization of the Transcript and Protein. *Plant Physiology*, 111(1):61–71, 1996.

[23] J. Matthew Taliaferro, Marina Vidaki, Ruan Oliveira, Sara Olson, Lijun Zhan, Tanvi Saxena, Eric T. Wang, Brenton R. Graveley, Frank B. Gertler, Maurice S. Swanson, and Christopher B. Burge. Distal Alternative Last Exons Localize mRNAs to Neural Projections. *Molecular Cell*, 61(6):821–833, 2016.

[24] Andreas Mayer and L. Stirling Churchman. A Detailed Protocol for Subcellular RNA Sequencing (subRNA-seq). *Current Protocols in Molecular Biology*, 120(1):4.29.1–4.29.18, 2017.

[25] Furqan M. Fazal, Shuo Han, Kevin R. Parker, Pornchai Kaewsapsak, Jin Xu, Alistair N. Boettiger, Howard Y. Chang, and Alice Y. Ting. Atlas of Subcellular RNA Localization Revealed by APEX-Seq. *Cell*, 178(2):473–490.e26, 2019.

[26] Ying Li, Mahima B Aggarwal, Ke Ke, Kim Nguyen, and Robert C Spitale. Improved Analysis of RNA Localization by Spatially Restricted Oxidation of RNA–Protein Complexes. *Biochemistry*, 57(10):1577–1581, 2018.

[27] Ronit Wilk, Jack Hu, Dmitry Blotsky, and Henry M. Krause. Diverse and pervasive subcellular distributions for both coding and long noncoding RNAs. *Genes & Development*, 30(5):594–609, 2016.

[28] Eric Lécuyer, Hideki Yoshida, Neela Parthasarathy, Christina Alm, Tomas Babak, Tanja Cerovina, Timothy R. Hughes, Pavel Tomancak, and Henry M. Krause. Global Analysis of mRNA Localization Reveals a Prominent Role in Organizing Cellular Architecture and Function. *Cell*, 131(1):174–187, 2007.

[29] Ting Zhang, Puwen Tan, Liqiang Wang, Nana Jin, Yana Li, Lin Zhang, Huan Yang, Zhenyu Hu, Lining Zhang, Chunyu Hu, Chunhua Li, Kun Qian, Changjian Zhang, Yan Huang, Kongning Li, Hao Lin, and Dong Wang. RNALocate: a resource for RNA subcellular localizations. *Nucleic Acids Research*, 45(D1):D135–D138, 2017.

[30] Florence Besse and Anne Ephrussi. Translational control of localized mRNAs: restricting protein synthesis in space and time. *Nature Reviews Molecular Cell Biology*, 9(12):971–980, 2008.

[31] Pearl V. Ryder and Dorothy A. Lerit. RNA localization regulates diverse and dynamic cellular processes. *Traffic*, 19(7):496–502, 2018.

[32] Christine E. Holt and Simon L. Bullock. Subcellular mRNA Localization in Animal Cells and Why It Matters. *Science*, 326(5957):1212–1216, 2009.

[33] Lisbeth S. Laursen, Colin W. Chan, and Charles ffrench Constant. Translation of myelin basic protein mRNA in oligodendrocytes is regulated by integrin activation and hnRNP-K. *The Journal of Cell Biology*, 192(5):797–811, 2011.

[34] Hans Georg Frohnhöfer and Christiane Nüsslein-Volhard. Organization of anterior pattern in the Drosophila embryo by the maternal gene bicoid. *Nature*, 324(6093):120–125, 1986.

[35] Jeffrey L. Smith, Joan E. Wilson, and Paul M. Macdonald. Overexpression of oskar directs ectopic activation of nanos and presumptive pole cell formation in Drosophila embryos. *Cell*, 70(5):849–859, 1992.

[36] Andreas E. Moor, Matan Golan, Efi E. Massasa, Doron Lemze, Tomer Weizman, Rom Shenhav, Shaked Baydatch, Orel Mizrahi, Roni Winkler, Ofra Golani, Noam Stern-Ginossar, and Shalev Itzkovitz. Global mRNA polarization regulates translation efficiency in the intestinal epithelium. *Science*, 357(6357):1299–1303, 2017.

[37] Nikita Fernandes and J Ross Buchan. RPS28B mRNA acts as a scaffold promoting cis-translational interaction of proteins driving P-body assembly. *Nucleic Acids Research*, 48(11):6265–6279, 2020.

[38] Ryan L Huizar, Chanjae Lee, Alexander A Boulgakov, Amjad Horani, Fan Tu, Edward M Marcotte, Steven L Brody, and John B Wallingford. A liquid-like organelle at the root of motile ciliopathy. *eLife*, 7:e38497, 2018.

[39] Chanjae Lee, Rachael M Cox, Ophelia Papoulas, Amjad Horani, Kevin Drew, Caitlin C Devitt, Steven L Brody, Edward M Marcotte, and John B Wallingford. Functional partitioning of a liquid-like organelle during assembly of axonemal dyneins. *eLife*, 9:e58662, 2020.

[40] Isabella Aprea, Johanna Raidt, Inga Marlena Höben, Niki Tomas Loges, Tabea Nöthe-Menchen, Petra Pennekamp, Heike Olbrich, Thomas Kaiser, Luisa Biebach, Frank Tüttelmann, Judit Horvath, Maria Schubert, Claudia Krallmann, Sabine Kliesch, and Heymut Omran. Defects in the cytoplasmic assembly of axonemal dynein arms cause morphological abnormalities and dysmotility in sperm cells leading to male infertility. *PLOS Genetics*, 17(2):e1009306, 2021.

[41] Salman F. Banani, Hyun O. Lee, Anthony A. Hyman, and Michael K. Rosen. Biomolecular condensates: organizers of cellular biochemistry. *Nature Reviews Molecular Cell Biology*, 18(5):285–298, 2017.

[42] Simon Alberti, Amy Gladfelter, and Tanja Mittag. Considerations and Challenges in Studying Liquid-Liquid Phase Separation and Biomolecular Condensates. *Cell*, 176(3):419–434, 2019.

[43] Celestin N. Mudogo, Sven Falke, Hévila Brognaro, Michael Duszenko, and Christian Betzel. Protein phase separation and determinants of in cell crystallization. *Traffic*, 21(2):220–230, 2020.

[44] Yuntao S. Mao, Bin Zhang, and David L. Spector. Biogenesis and function of nuclear bodies. *Trends in Genetics*, 27(8):295–306, 2011.

[45] Karla M. Neugebauer. Special focus on the Cajal Body. *RNA Biology*, 14(6):669–670, 2017.

[46] Shinichi Nakagawa, Tomohiro Yamazaki, and Tetsuro Hirose. Molecular dissection of nuclear paraspeckles: towards understanding the emerging world of the RNP milieu. *Royal Society Open Biology*, 8(10):180150, 2018.

[47] Run-Wen Yao, Guang Xu, Ying Wang, Lin Shan, Peng-Fei Luan, Yang Wang, Man Wu, Liang-Zhong Yang, Yu-Hang Xing, Li Yang, and Ling-Ling Chen. Nascent Pre-rRNA Sorting via Phase Separation Drives the Assembly of Dense Fibrillar Components in the Human Nucleolus. *Molecular Cell*, 76(5):767–783.e11, 2019.

[48] J. Ross Buchan and Roy Parker. Eukaryotic Stress Granules: The Ins and Outs of Translation. *Molecular Cell*, 36(6):932–941, 2009.

[49] David S.W. Protter and Roy Parker. Principles and Properties of Stress Granules. *Trends in Cell Biology*, 26(9):668–679, 2016.

[50] Jeffrey B. Woodruff, Anthony A. Hyman, and Elvan Boke. Organization and Function of Non-dynamic Biomolecular Condensates. *Trends in Biochemical Sciences*, 43(2):81–94, 2017.

[51] Yang Luo, Zhenkun Na, and Sarah A Slavoff. P-Bodies: Composition, Properties, and Functions. *Biochemistry*, 57(17):2424–2431, 2018.

[52] Tatjana Trcek and Ruth Lehmann. Germ granules in Drosophila. *Traffic*, 20(9):650–660, 2019.

[53] Elisabeth A. Marnik and Dustin L. Updike. Membraneless organelles: P granules in Caenorhabditis elegans. *Traffic*, 20(6):373–379, 2019.

[54] Allison Jamieson-Lucy and Mary C. Mullins. The vertebrate Balbiani body, germ plasm, and oocyte polarity. *Current Topics in Developmental Biology*, 135:1–34, 2019.

[55] Laura R. Ganser and Sua Myong. Methods to Study Phase-Separated Condensates and the Underlying Molecular Interactions. *Trends in Biochemical Sciences*, 45(J. Mol. Biol. 430 2018):1004–1005, 2020.

[56] David T. McSwiggen, Mustafa Mir, Xavier Darzacq, and Robert Tjian. Evaluating phase separation in live cells: diagnosis, caveats, and functional consequences. *Genes & Development*, 33(23-24):1619–1634, 2019.

[57] Clifford P. Brangwynne, Christian R. Eckmann, David S. Courson, Agata Rybarska, Carsten Hoege, Jöbin Gharakhani, Frank Jülicher, and Anthony A. Hyman. Germline P Granules Are Liquid Droplets That Localize by Controlled Dissolution/Condensation. *Science*, 324(5935):1729–1732, 2009.

[58] Jennifer T. Wang and Geraldine Seydoux. P granules. *Current Biology*, 24(14):R637–R638, 2014.

[59] S Strome and W B Wood. Immunofluorescence visualization of germ-line-specific cytoplasmic granules in embryos, larvae, and adults of Caenorhabditis elegans. *Proceedings of the National Academy of Sciences*, 79(5):1558–1562, 1982.

[60] S N Hird, J E Paulsen, and S Strome. Segregation of germ granules in living Caenorhabditis elegans embryos: cell-type-specific mechanisms for cytoplasmic localisation. *Development (Cambridge, England)*, 122(4):1303–12, 1996.

[61] Gang Wan, Brandon D. Fields, George Spracklin, Aditi Shukla, Carolyn M. Phillips, and Scott Kennedy. Spatiotemporal regulation of liquid-like condensates in epigenetic inheritance. *Nature*, 557(7707):679–683, 2018.

[62] Celja J. Uebel, Dana Agbede, Dylan C. Wallis, and Carolyn M. Phillips. Mutator Foci Are Regulated by Developmental Stage, RNA, and the Germline Cell Cycle in Caenorhabditis elegans. *G3: Genes, Genomes, Genetics*, 10(10):g3.401514.2020, 2020.

[63] Susan Strome. Specification of the germ line. *WormBook*, pages 1–10, 2005.

[64] Dustin Updike and Susan Strome. P Granule Assembly and Function in Caenorhabditis elegans Germ Cells. *Journal of Andrology*, 31(1):53–60, 2010.

[65] Geraldine Seydoux. The P Granules of C. elegans: A Genetic Model for the Study of RNA-Protein Condensates. *Journal of Molecular Biology*, 430(23):4702–4710, 2018.

[66] Wenjun Chen, Yabing Hu, Charles F. Lang, Jordan S. Brown, Sierra Schwabach, Xiaoyan Song, Ying Zhang, Edwin Munro, Karen Bennett, Donglei Zhang, and Heng-Chi Lee. The Dynamics of P Granule Liquid Droplets Are Regulated by the Caenorhabditis elegans Germline RNA Helicase GLH-1 via Its ATP Hydrolysis Cycle. *Genetics*, 215(2):genetics.303052.2020, 2020.

[67] Yunqi Yang, Zhiwei Fang, Xuan Chen, Weiwang Zhang, Yangmei Xie, Yinghui Chen, Zhenguo Liu, and Weien Yuan. An Overview of Pickering Emulsions: Solid-Particle Materials, Classification, Morphology, and Applications. *Frontiers in Pharmacology*, 08:287, 2017.

[68] Andrea Putnam, Madeline Cassani, Jarrett Smith, and Geraldine Seydoux. A gel phase promotes condensation of liquid P granules in Caenorhabditis elegans embryos. *Nature Structural & Molecular Biology*, 26(3):220–226, 2019.

[69] G Seydoux and A Fire. Soma-germline asymmetry in the distributions of embryonic RNAs in Caenorhabditis elegans. *Development (Cambridge, England)*, 120(10):2823–34, 1994.

[70] Jason N. Pitt, Jennifer A. Schisa, and James R. Priess. P Granules in the Germ Cells of Caenorhabditis elegans Adults Are Associated with Clusters of Nuclear Pores and Contain RNA. *Developmental Biology*, 219(2):315–333, 2000.

[71] J A Schisa, J N Pitt, and J R Priess. Analysis of RNA associated with P granules in germ cells of C. elegans adults. *Development*, 128(8):1287–1298, 2001.

[72] K Subramaniam and G Seydoux. nos-1 and nos-2, two genes related to Drosophila nanos, regulate primordial germ cell development and survival in Caenorhabditis elegans. *Development (Cambridge, England)*, 126(21):4861–71, 1999.

[73] Ingrid D'Agostino, Chris Merritt, Pei-Lung Chen, Geraldine Seydoux, and Kuppuswamy Subramaniam. Translational repression restricts expression of the C. elegans Nanos homolog NOS-2 to the embryonic germline. *Developmental Biology*, 292(1):244–252, 2006.

[74] Shreyas Jadhav, Mainpal Rana, and Kuppuswamy Subramaniam. Multiple maternal proteins coordinate to restrict the translation of C. elegans nanos-2 to primordial germ cells. *Development*, 135(10):1803–1812, 2008.

[75] Chih-Yung S Lee, Andrea Putnam, Tu Lu, ShuaiXin He, John Paul T Ouyang, and Geraldine Seydoux. Recruitment of mRNAs to P granules by condensation with intrinsically-disordered proteins. *eLife*, 9:e52896, 2020.

[76] Sophia C. Tintori, Erin Osborne Nishimura, Patrick Golden, Jason D. Lieb, and Bob Goldstein. A Transcriptional Lineage of the Early C. elegans Embryo. *Developmental Cell*, 38(4):430–444, 2016.

[77] Dylan M. Parker, Lindsay P. Winkenbach, Sam Boyson, Matthew N. Saxton, Camryn Daidone, Zainab A. Al-Mazaydeh, Marc T. Nishimura, Florian Mueller, and Erin Osborne

Nishimura. mRNA localization is linked to translation regulation in the Caenorhabditis elegans germ lineage. *Development*, 147(13):dev186817, 2020.

[78] Shin-ichi Yokota, Hideki Yanagi, Takashi Yura, and Hiroshi Kubota. Cytosolic chaperonin-containing t-complex polypeptide 1 changes the content of a particular subunit species concomitant with substrate binding and folding activities during the cell cycle. *European Journal of Biochemistry*, 268(17):4664–4673, 2001.

[79] Edward T. Kipreos and Sander van den Heuvel. Developmental Control of the Cell Cycle: Insights from Caenorhabditis elegans. *Genetics*, 211(3):797–829, 2019.

[80] Elizabeth I. Boyle, Shuai Weng, Jeremy Gollub, Heng Jin, David Botstein, J. Michael Cherry, and Gavin Sherlock. GO::TermFinder—open source software for accessing Gene Ontology information and finding significantly enriched Gene Ontology terms associated with a list of genes. *Bioinformatics*, 20(18):3710–3715, 2004.

[81] Tamar Hashimshony, Florian Wagner, Noa Sher, and Itai Yanai. CEL-Seq: Single-Cell RNA-Seq by Multiplexed Linear Amplification. *Cell Reports*, 2(3):666–673, 2012.

[82] Stephanie L. Moon, Tatsuya Morisaki, Anthony Khong, Kenneth Lyon, Roy Parker, and Timothy J. Stasevich. Multicolour single-molecule tracking of mRNA interactions with RNP granules. *Nature Cell Biology*, 21(2):162–168, 2019.

[83] C Tenenhaus, K Subramaniam, M A Dunn, and G Seydoux. PIE-1 is a bifunctional protein that regulates maternal and zygotic gene expression in the embryonic germ line of Caenorhabditis elegans. *Genes & Development*, 15(8):1031–1040, 2001.

[84] Scott Robertson and Rueyling Lin. Chapter One The Maternal-to-Zygotic Transition in C. elegans. *Current Topics in Developmental Biology*, 113:1–42, 2015.

[85] John Paul T. Ouyang, Andrew Folkmann, Lauren Bernard, Chih-Yung Lee, Uri Seroussi, Amanda G. Charlesworth, Julie M. Claycomb, and Geraldine Seydoux. P Granules Pro-

tect RNA Interference Genes from Silencing by piRNAs. *Developmental Cell*, 50(6):716–728.e6, 2019.

[86] Anne E. Dodson and Scott Kennedy. Germ Granules Coordinate RNA-Based Epigenetic Inheritance Pathways. *Developmental Cell*, 50(6):704–715.e4, 2019.

[87] Elizabeth R. Gavis and Ruth Lehmann. Translational regulation of nanos by RNA localization. *Nature*, 369(6478):315–318, 1994.

[88] Prashanth Rangan, Matthew DeGennaro, Kean Jaime-Bustamante, Rémi-Xavier Coux, Rui G. Martinho, and Ruth Lehmann. Temporal and Spatial Control of Germ-Plasm RNAs. *Current Biology*, 19(1):72–77, 2009.

[89] Anne Ephrussi, Laura K. Dickinson, and Ruth Lehmann. oskar organizes the germ plasm and directs localization of the posterior determinant nanos. *Cell*, 66(1):37–50, 1991.

[90] Kathryn E Kistler, Tatjana Trcek, Thomas R Hurd, Ruoyu Chen, Feng-Xia Liang, Joseph Sall, Masato Kato, and Ruth Lehmann. Phase transitioned nuclear Oskar promotes cell division of Drosophila primordial germ cells. *eLife*, 7:e37949, 2018.

[91] Ichiro Kawasaki, Yhong-Hee Shim, Jay Kirchner, Joshua Kaminker, William B Wood, and Susan Strome. PGL-1, a Predicted RNA-Binding Component of Germ Granules, Is Essential for Fertility in C. elegans. *Cell*, 94(5):635–645, 1998.

[92] Ichiro Kawasaki, Anahita Amiri, Yuan Fan, Nicole Meyer, Steve Dunkelbarger, Tomoko Motohashi, Takeshi Karashima, Olaf Bossinger, and Susan Strome. The PGL Family Proteins Associate With Germ Granules and Function Redundantly in Caenorhabditis elegans Germline Development. *Genetics*, 167(2):645–661, 2004.

[93] Xiawei Huang, Katalin Fejes Tóth, and Alexei A. Aravin. piRNA Biogenesis in Drosophila melanogaster. *Trends in Genetics*, 33(11):882–894, 2017.

[94] En-Zhi Shen, Hao Chen, Ahmet R. Ozturk, Shikui Tu, Masaki Shirayama, Wen Tang, Yue-He Ding, Si-Yuan Dai, Zhiping Weng, and Craig C. Mello. Identification of piRNA Binding Sites Reveals the Argonaute Regulatory Landscape of the C. elegans Germline. *Cell*, 172(5):937–951.e18, 2018.

[95] Donglei Zhang, Shikui Tu, Michael Stubna, Wei-Sheng Wu, Wei-Che Huang, Zhiping Weng, and Heng-Chi Lee. The piRNA targeting rules and the resistance to piRNA silencing in endogenous genes. *Science*, 359(6375):587–592, 2018.

[96] James A. Toombs, Yuliya A. Sytnikova, Gung-wei Chirn, Ignatius Ang, Nelson C. Lau, and Michael D. Blower. Xenopus Piwi proteins interact with a broad proportion of the oocyte transcriptome. *RNA*, 23(4):504–520, 2017.

[97] Chen Chen, Jing Jin, D. Andrew James, Melanie A. Adams-Cioaba, Jin Gyoon Park, Yahong Guo, Enrico Tenaglia, Chao Xu, Gerald Gish, Jinrong Min, and Tony Pawson. Mouse Piwi interactome identifies binding mechanism of Tdrkh Tudor domain to arginine methylated Miwi. *Proceedings of the National Academy of Sciences*, 106(48):20336–20341, 2009.

[98] Jarrett Smith, Deepika Calidas, Helen Schmidt, Tu Lu, Dominique Rasoloson, and Geraldine Seydoux. Spatial patterning of P granules by RNA-induced phase separation of the intrinsically-disordered protein MEG-3. *eLife*, 5:e21337, 2016.

[99] Scott Takeo Aoki, Tina R. Lynch, Sarah L. Crittenden, Craig A. Bingman, Marvin Wickens, and Judith Kimble. C. elegans germ granules require both assembly and localized regulators for mRNA repression. *Nature Communications*, 12(1):996, 2021.

[100] Anthony P. Mahowald. Polar granules of Drosophila. II. Ultrastructural changes during early embryogenesis. *Journal of Experimental Zoology*, 167(2):237–261, 1968.

[101] Tatjana Trcek, Markus Grosch, Andrew York, Hari Shroff, Timothée Lionnet, and Ruth Lehmann. Drosophila germ granules are structured and contain homotypic mRNA clusters. *Nature Communications*, 6(1):7962, 2015.

[102] Matthew G. Niepielko, Whitby V.I. Eagle, and Elizabeth R. Gavis. Stochastic Seeding Coupled with mRNA Self-Recruitment Generates Heterogeneous Drosophila Germ Granules. *Current Biology*, 28(12):1872–1881.e3, 2018.

[103] Arpita Kulkarni and Cassandra G. Extavour. Convergent evolution of germ granule nucleators: A hypothesis. *Stem Cell Research*, 24:188–194, 2017.

[104] Anastassios Vourekas, Panagiotis Alexiou, Nicholas Vrettos, Manolis Maragkakis, and Zissimos Mourelatos. Sequence-dependent but not sequence-specific piRNA adhesion traps mRNAs to the germ plasm. *Nature*, 531(7594):390–394, 2016.

[105] Piergiuseppe Quarato, Meetali Singh, Eric Cornes, Blaise Li, Loan Bourdon, Florian Mueller, Celine Didier, and Germano Cecere. Germline inherited small RNAs facilitate the clearance of untranslated maternal mRNAs in C. elegans embryos. *Nature Communications*, 12(1):1441, 2021.

[106] Kin Man Suen, Fabian Braukmann, Richard Butler, Dalila Bensaddek, Alper Akay, Chi-Chuan Lin, Dovilė Milonaitytė, Neel Doshi, Alexandra Sapetschnig, Angus Lamond, John Edward Ladbury, and Eric Alexander Miska. DEPS-1 is required for piRNA-dependent silencing and PIWI condensate organisation in Caenorhabditis elegans. *Nature Communications*, 11(1):4242, 2020.

[107] Pritesh Krishnakumar, Stephan Riemer, Roshan Perera, Thomas Lingner, Alexander Goloborodko, Hazem Khalifa, Franck Bontems, Felix Kaufholz, Mohamed A. El-Brolosy, and Roland Dosch. Functional equivalence of germ plasm organizers. *PLOS Genetics*, 14(11):e1007696, 2018.

[108] Kevin I Manage, Alicia K Rogers, Dylan C Wallis, Celja J Uebel, Dorian C Anderson, Dieu An H Nguyen, Katerina Arca, Kristen C Brown, Ricardo J Cordeiro Rodrigues, Bruno F M de Albuquerque, Rene F Ketting, Taiowa A Montgomery, and Carolyn Marie Phillips. A

Tudor domain protein, SIMR-1, promotes siRNA production at piRNA-targeted mRNAs in C. elegans. *eLife*, 9:e56731, 2020.

[109] H. Bahar Sahin, Omer Faruk Karatas, Valeria Specchia, Silvia Di Tommaso, Céline Diebold, Maria Pia Bozzetti, and Angela Giangrande. Novel mutants of the aubergine gene. *Fly*, 10(2):81–90, 2016.

[110] Hieu D. L. Vo, Wahiduzzaman, Samuel J. Tindell, Jimiao Zheng, Ming Gao, and Alexey L. Arkov. Protein components of ribonucleoprotein granules from Drosophila germ cells oligomerize and show distinct spatial organization during germline development. *Scientific Reports*, 9(1):19190, 2019.

[111] Ji-Young Youn, Boris J.A. Dyakov, Jianping Zhang, James D.R. Knight, Robert M. Vernon, Julie D. Forman-Kay, and Anne-Claude Gingras. Properties of Stress Granule and P-Body Proteomes. *Molecular Cell*, 76(2):286–294, 2019.

[112] Claire L. Riggs, Nancy Kedersha, Pavel Ivanov, and Paul Anderson. Mammalian stress granules and P bodies at a glance. *Journal of Cell Science*, 133(16):jcs242487, 2020.

[113] Yuan Lin, David S.W. Protter, Michael K. Rosen, and Roy Parker. Formation and Maturation of Phase-Separated Liquid Droplets by RNA-Binding Proteins. *Molecular Cell*, 60(2):208–219, 2015.

[114] Shambaditya Saha, Christoph A. Weber, Marco Nousch, Omar Adame-Arana, Carsten Hoege, Marco Y. Hein, Erin Osborne-Nishimura, Julia Mahamid, Marcus Jahnel, Louise Jawerth, Andrej Pozniakovski, Christian R. Eckmann, Frank Jülicher, and Anthony A. Hyman. Polar Positioning of Phase-Separated Liquid Compartments in Cells Regulated by an mRNA Competition Mechanism. *Cell*, 166(6):1572–1584.e16, 2016.

[115] Jacob C. Schwartz, Xueyin Wang, Elaine R. Podell, and Thomas R. Cech. RNA Seeds Higher-Order Assembly of FUS Protein. *Cell Reports*, 5(4):918–925, 2013.

[116] Daniela Teixeira, Ujwal Sheth, Marco A. Valencia-Sanchez, Muriel Brengues, and Roy Parker. Processing bodies require RNA for assembly and contain nontranslating mRNAs. *RNA*, 11(4):371–382, 2005.

[117] Nancy Kedersha and Paul Anderson. Mammalian Stress Granules and Processing Bodies. *Methods in Enzymology*, 431:61–81, 2007.

[118] Christopher M. Gallo, Edwin Munro, Dominique Rasoloson, Christopher Merritt, and Geraldine Seydoux. Processing bodies and germ granules are distinct RNA granules that interact in C. elegans embryos. *Developmental Biology*, 323(1):76–87, 2008.

[119] Jidong Liu, Marco Antonio Valencia-Sanchez, Gregory J. Hannon, and Roy Parker. MicroRNA-dependent localization of targeted mRNAs to mammalian P-bodies. *Nature Cell Biology*, 7(7):719–723, 2005.

[120] Arnaud Hubstenberger, Maïté Courel, Marianne Bénard, Sylvie Souquere, Michèle Ernoult-Lange, Racha Chouaib, Zhou Yi, Jean-Baptiste Morlot, Annie Munier, Magali Fradet, Maëlle Daunesse, Edouard Bertrand, Gérard Pierron, Julien Mozziconacci, Michel Kress, and Dominique Weil. P-Body Purification Reveals the Condensation of Repressed mRNA Regulons. *Molecular Cell*, 68(1):144–157.e5, 2017.

[121] Anthony Khong, Tyler Matheny, Saumya Jain, Sarah F. Mitchell, Joshua R. Wheeler, and Roy Parker. The Stress Granule Transcriptome Reveals Principles of mRNA Accumulation in Stress Granules. *Molecular Cell*, 68(4):808–820.e5, 2017.

[122] Shih-Peng Chan and Frank J Slack. microRNA-Mediated Silencing Inside P Bodies. *RNA Biology*, 3(3):97–100, 2006.

[123] Pedro J. Batista, J. Graham Ruby, Julie M. Claycomb, Rosaria Chiang, Noah Fahlgren, Kristin D. Kasschau, Daniel A. Chaves, Weifeng Gu, Jessica J. Vasale, Shenghua Duan, Darryl Conte, Shujun Luo, Gary P. Schroth, James C. Carrington, David P. Bartel, and

Craig C. Mello. PRG-1 and 21U-RNAs Interact to Form the piRNA Complex Required for Fertility in C. elegans. *Molecular Cell*, 31(1):67–78, 2008.

[124] Guilin Wang and Valerie Reinke. A C. elegans Piwi, PRG-1, Regulates 21U-RNAs during Spermatogenesis. *Current Biology*, 18(12):861–867, 2008.

[125] Adva Aizer, Alon Kalo, Pinhas Kafri, Amit Shraga, Rakefet Ben-Yishay, Avi Jacob, Noa Kinor, and Yaron Shav-Tal. Quantifying mRNA targeting to P-bodies in living human cells reveals their dual role in mRNA decay and storage. *J Cell Sci*, 127(20):4443–4456, 2014.

[126] Sethuramasundaram Pitchiaya, Marcio D.A. Mourao, Ameya P. Jalihal, Lanbo Xiao, Xia Jiang, Arul M. Chinnaiyan, Santiago Schnell, and Nils G. Walter. Dynamic Recruitment of Single RNAs to Processing Bodies Depends on RNA Functionality. *Molecular Cell*, 74(3):521–533.e6, 2019.

[127] Maria Hondele, Ruchika Sachdev, Stephanie Heinrich, Juan Wang, Pascal Vallotton, Beatriz M. A. Fontoura, and Karsten Weis. DEAD-box ATPases are global regulators of phase-separated organelles. *Nature*, 573(7772):144–148, 2019.

[128] Gabriela Huelgas-Morales, Carlos Giovanni Silva-García, Laura S. Salinas, David Greenstein, and Rosa E. Navarro. The Stress Granule RNA-Binding Protein TIAR-1 Protects Female Germ Cells from Heat Shock in Caenorhabditis elegans. *G3: Genes|Genomes|Genetics*, 6(4):1031–1047, 2016.

[129] Nancy Kedersha, Georg Stoecklin, Maranatha Ayodele, Patrick Yacono, Jens Lykke-Andersen, Marvin J. Fritzler, Donalyn Scheuner, Randal J. Kaufman, David E. Golan, and Paul Anderson. Stress granules and processing bodies are dynamically linked sites of mRNP remodeling. *The Journal of Cell Biology*, 169(6):871–884, 2005.

[130] Stephanie Mollet, Nicolas Cougot, Ania Wilczynska, François Dautry, Michel Kress, Edouard Bertrand, and Dominique Weil. Translationally Repressed mRNA Transiently Cy-

cles through Stress Granules during Stress. *Molecular Biology of the Cell*, 19(10):4469–4479, 2008.

[131] Hagai Marmor-Kollet, Aviad Siany, Nancy Kedersha, Naama Knafo, Natalia Rivkin, Yehuda M. Danino, Thomas G. Moens, Tsviya Olender, Daoud Sheban, Nir Cohen, Tali Dadosh, Yoseph Addadi, Revital Ravid, Chen Eitan, Beata Toth Cohen, Sarah Hofmann, Claire L. Riggs, Vivek M. Advani, Adrian Higginbottom, Johnathan Cooper-Knock, Jacob H. Hanna, Yifat Merbl, Ludo Van Den Bosch, Paul Anderson, Pavel Ivanov, Tamar Geiger, and Eran Hornstein. Spatiotemporal Proteomic Analysis of Stress Granule Disassembly Using APEX Reveals Regulation by SUMOylation and Links to ALS Pathogenesis. *Molecular Cell*, 80(5):876–891.e6, 2020.

[132] Saumya Jain, Joshua R. Wheeler, Robert W. Walters, Anurag Agrawal, Anthony Barsic, and Roy Parker. ATPase-Modulated Stress Granules Contain a Diverse Proteome and Substructure. *Cell*, 164(3):487–498, 2016.

[133] Sim Namkoong, Allison Ho, Yu Mi Woo, Hojoong Kwak, and Jun Hee Lee. Systematic Characterization of Stress-Induced RNA Granulation. *Molecular Cell*, 70(1):175–187.e8, 2018.

[134] Daniel Mateju, Bastian Eichenberger, Franka Voigt, Jan Eglinger, Gregory Roth, and Jeffrey A. Chao. Single-Molecule Imaging Reveals Translation of mRNAs Localized to Stress Granules. *Cell*, 183(7):1801–1812.e13, 2020.

[135] James Eberwine, Kevin Miyashiro, Janet Estee Kacharmina, and Christy Job. Local translation of classes of mRNAs that are targeted to neuronal dendrites. *Proceedings of the National Academy of Sciences*, 98(13):7080–7085, 2001.

[136] Jeremy Dufourt, Maelle Bellec, Antonio Trullo, Matthieu Dejean, Sylvain De Rossi, Cyril Favard, and Mounia Lagha. Imaging translation dynamics in live embryos reveals spatial heterogeneities. *Science*, page eabc3483, 2021.

[137] Fabian Morales-Polanco, Christian Bates, Jennifer Lui, Joseph Casson, Clara A. Solari, Mariavittoria Pizzinga, Gabriela Forte, Claire Griffin, Kirsten E.L. Garner, Harriet E. Burt, Hannah L. Dixon, Simon Hubbard, Paula Portela, and Mark P. Ashe. Core Fermentation (CoFe) granules focus coordinated glycolytic mRNA localization and translation to fuel glucose fermentation. *iScience*, 24(2):102069, 2021.

[138] Gregory G Fuller, Ting Han, Mallory A Freeberg, James J Moresco, Amirhossein Ghanbari Niaki, Nathan P Roach, John R Yates, Sua Myong, and John K Kim. RNA promotes phase separation of glycolysis enzymes into yeast G bodies in hypoxia. *eLife*, 9:e48480, 2020.

[139] Racha Chouaib, Adham Safieddine, Xavier Pichon, Arthur Imbert, Oh Sung Kwon, Aubin Samacoits, Abdel-Meneem Traboulsi, Marie-Cécile Robert, Nikolay Tsanov, Emeline Coleno, Ina Poser, Christophe Zimmer, Anthony Hyman, Hervé Le Hir, Kazem Zibara, Marion Peter, Florian Mueller, Thomas Walter, and Edouard Bertrand. A Dual Protein-mRNA Localization Screen Reveals Compartmentalized Translation and Widespread Co-translational RNA Targeting. *Developmental Cell*, 54(6):773–791.e5, 2020.

[140] Jaclyn M. Fingerhut and Yukiko M. Yamashita. mRNA localization mediates maturation of cytoplasmic cilia in Drosophila spermatogenesis. *Journal of Cell Biology*, 219(9), 2020.

[141] Baskar Bakthavachalu, Joern Huelsmeier, Indulekha P. Sudhakaran, Jens Hillebrand, Amanjot Singh, Arnas Petrauskas, Devasena Thiagarajan, M. Sankaranarayanan, Laura Mizoue, Eric N. Anderson, Udai Bhan Pandey, Eric Ross, K. VijayRaghavan, Roy Parker, and Mani Ramaswami. RNP-Granule Assembly via Ataxin-2 Disordered Domains Is Required for Long-Term Memory and Neurodegeneration. *Neuron*, 98(4):754–766.e4, 2018.

[142] Hosung Jung, Byung C. Yoon, and Christine E. Holt. Axonal mRNA localization and local protein synthesis in nervous system assembly, maintenance and repair. *Nature Reviews Neuroscience*, 13(5):308–324, 2012.

[143] Yoshimitsu Kanai, Naoshi Dohmae, and Nobutaka Hirokawa. Kinesin Transports RNA Isolation and Characterization of an RNA-Transporting Granule. *Neuron*, 43(4):513–525, 2004.

[144] Hovy Ho-Wai Wong, Julie Qiaojin Lin, Florian Ströhl, Cláudio Gouveia Roque, Jean-Michel Cioni, Roberta Cagnetta, Benita Turner-Bridger, Romain F. Laine, William A. Harris, Clemens F. Kaminski, and Christine E. Holt. RNA Docking and Local Translation Regulate Site-Specific Axon Remodeling In Vivo. *Neuron*, 95(4):852–868.e8, 2017.

[145] Brian Tsang, Jason Arsenault, Robert M. Vernon, Hong Lin, Nahum Sonenberg, Lu-Yang Wang, Alaji Bah, and Julie D. Forman-Kay. Phosphoregulated FMRP phase separation models activity-dependent translation through bidirectional control of mRNA granule formation. *Proceedings of the National Academy of Sciences*, 116(10):201814385, 2019.

[146] Mariavittoria Pizzinga, Christian Bates, Jennifer Lui, Gabriella Forte, Fabián Morales-Polanco, Emma Linney, Barbora Knotkova, Beverley Wilson, Clara A. Solari, Luke E. Berchowitz, Paula Portela, and Mark P. Ashe. Translation factor mRNA granules direct protein synthetic capacity to regions of polarized growth. *Journal of Cell Biology*, 218(5):1564–1581, 2019.

[147] Phaedra R. Theodoridis, Michael Bokros, Dane Marijan, Nathan C. Balukoff, Dazhi Wang, Chloe C. Kirk, Taylor D. Budine, Harris D. Goldsmith, Miling Wang, Timothy E. Audas, and Stephen Lee. Local translation in nuclear condensate amyloid bodies. *Proceedings of the National Academy of Sciences*, 118(7):e2014457118, 2021.

[148] P Walter and A E Johnson. Signal Sequence Recognition and Protein Targeting to the Endoplasmic Reticulum Membrane. *Annual Review of Cell Biology*, 10(1):87–119, 1994.

[149] P Walter and G Blobel. Translocation of proteins across the endoplasmic reticulum III. Signal recognition protein (SRP) causes signal sequence-dependent and site-specific arrest

of chain elongation that is released by microsomal membranes. *The Journal of Cell Biology*, 91(2):557–561, 1981.

[150] David Akopian, Kuang Shen, Xin Zhang, and Shu-ou Shan. Signal Recognition Particle: An Essential Protein-Targeting Machine. *Annual Review of Biochemistry*, 82(1):693–721, 2013.

[151] Tslil Ast, Galit Cohen, and Maya Schuldiner. A Network of Cytosolic Factors Targets SRP-Independent Proteins to the Endoplasmic Reticulum. *Cell*, 152(5):1134–1145, 2013.

[152] Weirui Ma and Christine Mayr. A Membraneless Organelle Associated with the Endoplasmic Reticulum Enables 3'UTR-Mediated Protein-Protein Interactions. *Cell*, 175(6):1492–1506.e19, 2018.

[153] Jeffrey B. Woodruff, Beatriz Ferreira Gomes, Per O. Widlund, Julia Mahamid, Alf Honigmann, and Anthony A. Hyman. The Centrosome Is a Selective Condensate that Nucleates Microtubules by Concentrating Tubulin. *Cell*, 169(6):1066–1077.e10, 2017.

[154] Guadalupe Sepulveda, Mark Antkowiak, Ingrid Brust-Mascher, Karan Mahe, Tingyoung Ou, Noemi M Castro, Lana N Christensen, Lee Cheung, Xueer Jiang, Daniel Yoon, Bo Huang, and Li-En Jao. Co-translational protein targeting facilitates centrosomal recruitment of PCNT during centrosome maturation in vertebrates. *eLife*, 7:e34959, 2018.

[155] Emily C. Wheeler, Eric L. Van Nostrand, and Gene W. Yeo. Advances and challenges in the detection of transcriptome-wide protein–RNA interactions. *Wiley Interdisciplinary Reviews: RNA*, 9(1):e1436, 2018.

[156] Je Hyuk Lee, Evan R Daugharthy, Jonathan Scheiman, Reza Kalhor, Thomas C Ferrante, Richard Terry, Brian M Turczyk, Joyce L Yang, Ho Suk Lee, John Aach, Kun Zhang, and George M Church. Fluorescent in situ sequencing (FISSEQ) of RNA for gene expression profiling in intact cells and tissues. *Nature Protocols*, 10(3):442–458, 2015.

[157] Sheel Shah, Eric Lubeck, Wen Zhou, and Long Cai. In Situ Transcription Profiling of Single Cells Reveals Spatial Organization of Cells in the Mouse Hippocampus. *Neuron*, 92(2):342–357, 2016.

[158] Chee-Huat Linus Eng, Michael Lawson, Qian Zhu, Ruben Dries, Noushin Koulena, Yodai Takei, Jina Yun, Christopher Cronin, Christoph Karp, Guo-Cheng Yuan, and Long Cai. Transcriptome-scale super-resolved imaging in tissues by RNA seqFISH+. *Nature*, 568(7751):235–239, 2019.

[159] Adina R. Buxbaum, Bin Wu, and Robert H. Singer. Single β-Actin mRNA Detection in Neurons Reveals a Mechanism for Regulating Its Translatability. *Science*, 343(6169):419–422, 2014.

[160] Bin Wu, Carolina Eliscovich, Young J. Yoon, and Robert H. Singer. Translation dynamics of single mRNAs in live cells and neurons. *Science*, 352(6292):1430–1435, 2016.

[161] Jeremy S. Paige, Karen Y. Wu, and Samie R. Jaffrey. RNA Mimics of Green Fluorescent Protein. *Science*, 333(6042):642–646, 2011.

[162] Tatsuya Morisaki, Kenneth Lyon, Keith F. DeLuca, Jennifer G. DeLuca, Brian P. English, Zhengjian Zhang, Luke D. Lavis, Jonathan B. Grimm, Sarada Viswanathan, Loren L. Looger, Timothee Lionnet, and Timothy J. Stasevich. Real-time quantification of single RNA translation dynamics in living cells. *Science*, 352(6292):1425–1429, 2016.

[163] Esther Braselmann, Colin Rathbun, Erin M. Richards, and Amy E. Palmer. Illuminating RNA Biology: Tools for Imaging RNA in Live Mammalian Cells. *Cell Chemical Biology*, 27(8):891–903, 2020.

[164] Nicolas Paquin, Marie Ménade, Guillaume Poirier, Damiane Donato, Emmanuel Drouet, and Pascal Chartrand. Local Activation of Yeast ASH1 mRNA Translation through Phosphorylation of Khd1p by the Casein Kinase Yck1p. *Molecular Cell*, 26(6):795–809, 2007.

[165] Pascal Chartrand, Xiu Hua Meng, Stefan Huttelmaier, Damiane Donato, and Robert H. Singer. Asymmetric Sorting of Ash1p in Yeast Results from Inhibition of Translation by Localization Elements in the mRNA. *Molecular Cell*, 10(6):1319–1330, 2002.

[166] Erin M. Langdon, Yupeng Qiu, Amirhossein Ghanbari Niaki, Grace A. McLaughlin, Chase Weidmann, Therese M. Gerbich, Jean A. Smith, John M. Crutchley, Christina M. Termini, Kevin M. Weeks, Sua Myong, and Amy S. Gladfelter. MRNA structure determines specificity of a polyQ-driven phase separation. *Science*, 360(6391):eaar7432, 2018.

[167] Neha P. Kamat, Sylvia Tobé, Ian T. Hill, and Jack W. Szostak. Electrostatic Localization of RNA to Protocell Membranes by Cationic Hydrophobic Peptides. *Angewandte Chemie International Edition*, 54(40):11735–11739, 2015.

[168] Shawn C. Little, Kristina S. Sinsimer, Jack J. Lee, Eric F. Wieschaus, and Elizabeth R. Gavis. Independent and coordinate trafficking of single Drosophila germ plasm mRNAs. *Nature Cell Biology*, 17(5):558–568, 2015.

[169] Tiina Lehtiniemi and Noora Kotaja. Germ granule-mediated RNA regulation in male germ cells. *Reproduction*, 155(2):R77–R91, 2018.

[170] Ke Zhang, J. Gavin Daigle, Kathleen M. Cunningham, Alyssa N. Coyne, Kai Ruan, Jonathan C. Grima, Kelly E. Bowen, Harsh Wadhwa, Peiguo Yang, Frank Rigo, J. Paul Taylor, Aaron D. Gitler, Jeffrey D. Rothstein, and Thomas E. Lloyd. Stress Granule Assembly Disrupts Nucleocytoplasmic Transport. *Cell*, 173(4):958–971.e17, 2018.

[171] Chris Balak, Marianne Benard, Elise Schaefer, Sumaiya Iqbal, Keri Ramsey, Michèle Ernoult-Lange, Francesca Mattioli, Lorida Llaci, Véronique Geoffroy, Maité Courel, Marcus Naymik, Kristine K. Bachman, Rolph Pfundt, Patrick Rump, Johanna ter Beest, Ingrid M. Wentzensen, Kristin G. Monaghan, Kirsty McWalter, Ryan Richholt, Antony Le Béchec, Wayne Jepsen, Matt De Both, Newell Belnap, Anne Boland, Ignazio S. Piras, Jean-François Deleuze, Szabolcs Szelinger, Hélène Dollfus, Jamel Chelly, Jean Muller, Arthur

Campbell, Dennis Lal, Sampathkumar Rangasamy, Jean-Louis Mandel, Vinodh Narayanan, Matt Huentelman, Dominique Weil, and Amélie Piton. Rare De Novo Missense Variants in RNA Helicase DDX6 Cause Intellectual Disability and Dysmorphic Features and Lead to P-Body Defects and RNA Dysregulation. *The American Journal of Human Genetics*, 105(3):509–525, 2019.

[172] Xiao Yu, Bo Li, Geng-Jen Jang, Shan Jiang, Daohong Jiang, Jyan-Chyun Jang, Shu-Hsing Wu, Libo Shan, and Ping He. Orchestration of Processing Body Dynamics and mRNA Decay in Arabidopsis Immunity. *Cell Reports*, 28(8):2194–2205.e6, 2019.

[173] Danielle C. Hamm and Melissa M. Harrison. Regulatory principles governing the maternal-to-zygotic transition: insights from Drosophila melanogaster. *Royal Society Open Biology*, 8(12):180183, 2018.

[174] Katharine N. Schulz and Melissa M. Harrison. Mechanisms regulating zygotic genome activation. *Nature Reviews Genetics*, 20(4):221–234, 2019.

[175] Nadine L. Vastenhouw, Wen Xi Cao, and Howard D. Lipshitz. The maternal-to-zygotic transition revisited. *Development*, 146(11):dev161471, 2019.

[176] M A Gibert, J Starck, and B Beguet. Role of the gonad cytoplasmic core during oogenesis of the nematode Caenorhabditis elegans. *Biology of the Cell*, 50(1):77–85, 1984.

[177] Amy K. Walker, Peter R. Boag, and T. Keith Blackwell. Transcription reactivation steps stimulated by oocyte maturation in C. elegans. *Developmental Biology*, 304(1):382–393, 2007.

[178] Tugba Guven-Ozkan, Scott M. Robertson, Yuichi Nishi, and Rueyling Lin. zif-1 translational repression defines a second, mutually exclusive OMA function in germline transcriptional repression. *Development*, 137(20):3373–3382, 2010.

[179] Geraldine Seydoux, Craig C. Mello, Jonathan Pettitt, William B. Wood, James R. Priess, and Andrew Fire. Repression of gene expression in the embryonic germ lineage of C. elegans. *Nature*, 382(6593):713–716, 1996.

[180] Erin Osborne Nishimura, Jay C. Zhang, Adam D. Werts, Bob Goldstein, and Jason D. Lieb. Asymmetric Transcript Discovery by RNA-seq in C. elegans Blastomeres Identifies neg-1, a Gene Important for Anterior Morphogenesis. *PLOS Genetics*, 11(4):e1005117, 2015.

[181] Christopher Merritt, Dominique Rasoloson, Darae Ko, and Geraldine Seydoux. 3' UTRs Are the Primary Regulators of Gene Expression in the C. elegans Germline. *Current Biology*, 18(19):1476–1482, 2008.

[182] Marieke Oldenbroek, Scott M. Robertson, Tugba Guven-Ozkan, Steven Gore, Yuichi Nishi, and Rueyling Lin. Multiple RNA-binding proteins function combinatorially to control the soma-restricted expression pattern of the E3 ligase subunit ZIF-1. *Developmental Biology*, 363(2):388–398, 2012.

[183] Marieke Oldenbroek, Scott M. Robertson, Tugba Guven-Ozkan, Caroline Spike, David Greenstein, and Rueyling Lin. Regulation of maternal Wnt mRNA translation in C. elegans embryos. *Development*, 140(22):4614–4623, 2013.

[184] Ahmed Elewa, Masaki Shirayama, Ebru Kaymak, Paul F. Harrison, David R. Powell, Zhuo Du, Christopher D. Chute, Hannah Woolf, Dongni Yi, Takao Ishidate, Jagan Srinivasan, Zhirong Bao, Traude H. Beilharz, Sean P. Ryder, and Craig C. Mello. POS-1 Promotes Endomesoderm Development by Inhibiting the Cytoplasmic Polyadenylation of neg-1 mRNA. *Developmental Cell*, 34(1):108–118, 2015.

[185] Ujwal Sheth, Jason Pitt, Shannon Dennis, and James R. Priess. Perinuclear P granules are the principal sites of mRNA export in adult C. elegans germ cells. *Development*, 137(8):1305–1314, 2010.

[186] Carolyn M. Phillips, Taiowa A. Montgomery, Peter C. Breen, and Gary Ruvkun. MUT-16 promotes formation of perinuclear Mutator foci required for RNA silencing in the C. elegans germline. *Genes & Development*, 26(13):1433–1444, 2012.

[187] Christopher M. Gallo, Jennifer T. Wang, Fumio Motegi, and Geraldine Seydoux. Cytoplasmic Partitioning of P Granule Components Is Not Required to Specify the Germline in C. elegans. *Science*, 330(6011):1685–1689, 2010.

[188] Jennifer T Wang, Jarrett Smith, Bi-Chang Chen, Helen Schmidt, Dominique Rasoloson, Alexandre Paix, Bramwell G Lambrus, Deepika Calidas, Eric Betzig, and Geraldine Seydoux. Regulation of RNA granule dynamics by phosphorylation of serine-rich, intrinsically disordered proteins in C. elegans. *eLife*, 3:e04591, 2014.

[189] Anne C. Campbell and Dustin L. Updike. CSR-1 and P granules suppress sperm-specific transcription in the C. elegans germline. *Development*, 142(10):1745–1755, 2015.

[190] Dustin L. Updike, Andrew Kekūpa'a Knutson, Thea A. Egelhofer, Anne C. Campbell, and Susan Strome. Germ-Granule Components Prevent Somatic Development in the C. elegans Germline. *Current Biology*, 24(9):970–975, 2014.

[191] Ekaterina Voronina, Alexandre Paix, and Geraldine Seydoux. The P granule component PGL-1 promotes the localization and silencing activity of the PUF protein FBF-2 in germline stem cells. *Development*, 139(20):3732–3740, 2012.

[192] Caroline A. Spike, Donna Coetzee, Yuichi Nishi, Tugba Guven-Ozkan, Marieke Oldenbroek, Ikuko Yamamoto, Rueyling Lin, and David I. Greenstein. Translational Control of the Oogenic Program by Components of OMA Ribonucleoprotein Particles in Caenorhabditis elegans. *Genetics*, 198(4):genetics.114.168823, 2014.

[193] Tamar Hashimshony, Martin Feder, Michal Levin, Brian K. Hall, and Itai Yanai. Spatiotemporal transcriptomics reveals the evolutionary history of the endoderm germ layer. *Nature*, 519(7542):219–222, 2015.

[194] Daniela van Furden, Kevin Johnson, Christoph Segbert, and Olaf Bossinger. The C. elegans ezrin-radixin-moesin protein ERM-1 is necessary for apical junction remodelling and tubulogenesis in the intestine. *Developmental Biology*, 272(1):262–276, 2004.

[195] Christina M. Dittrich, Katja Kratz, Ataman Sendoel, Yosef Gruenbaum, Josef Jiricny, and Michael O. Hengartner. LEM-3 – A LEM Domain Containing Nuclease Involved in the DNA Damage Response in C. elegans. *PLoS ONE*, 7(2):e24555, 2012.

[196] Vann Bennett and Anthony J. Baines. Spectrin and Ankyrin-Based Pathways: Metazoan Inventions for Integrating Cells Into Tissues. *Physiological Reviews*, 81(3):1353–1392, 2001.

[197] Matthew Sweede, Gayatri Ankem, Boonta Chutvirasakul, Hugo F Azurmendi, Souhad Chbeir, Justin Watkins, Richard F Helm, Carla V Finkielstein, and Daniel G S Capelluto. Structural and Membrane Binding Properties of the Prickle PET Domain †. *Biochemistry*, 47(51):13524–13536, 2008.

[198] S D Fields, M N Conrad, and M Clarke. The S. cerevisiae CLU1 and D. discoideum cluA genes are functional homologues that influence mitochondrial morphology and distribution. *Journal of Cell Science*, 111(12):1717–1727, 1998.

[199] Rika Maruyama, Nathalie V. Velarde, Richard Klancer, Scott Gordon, Pavan Kadandale, Jean M. Parry, Julie S. Hang, Jacob Rubin, Allison Stewart-Michaelis, Peter Schweinsberg, Barth D. Grant, Fabio Piano, Asako Sugimoto, and Andrew Singson. EGG-3 Regulates Cell-Surface and Cortex Rearrangements during Egg Activation in Caenorhabditis elegans. *Current Biology*, 17(18):1555–1560, 2007.

[200] Sara K. Olson, Garrett Greenan, Arshad Desai, Thomas Müller-Reichert, and Karen Oegema. Hierarchical assembly of the eggshell and permeability barrier in C. elegans. *The Journal of Cell Biology*, 198(4):731–748, 2012.

[201] Yinhua Zhang, Jeremy M. Foster, Sanjay Kumar, Marjorie Fougere, and Clotilde K.S. Carlow. Cofactor-independent Phosphoglycerate Mutase Has an Essential Role in Caenorhab-

ditis elegans and Is Conserved in Parasitic Nematodes*. *Journal of Biological Chemistry*, 279(35):37185–37190, 2004.

[202] Yinhua Zhang, Jeremy M. Foster, Laura S. Nelson, Dong Ma, and Clotilde K.S. Carlow. The chitin synthase genes chs-1 and chs-2 are essential for C. elegans development and responsible for chitin deposition in the eggshell and pharynx, respectively. *Developmental Biology*, 285(2):330–339, 2005.

[203] Marrit Putker, Tobias Madl, Harmjan R. Vos, Hesther de Ruiter, Marieke Visscher, Maaike C.W. van den Berg, Mohammed Kaplan, Hendrik C. Korswagen, Rolf Boelens, Michiel Vermeulen, Boudewijn M.T. Burgering, and Tobias B. Dansen. Redox-Dependent Control of FOXO/DAF-16 by Transportin-1. *Molecular Cell*, 49(4):730–742, 2013.

[204] Florian Mueller, Adrien Senecal, Katjana Tantale, Hervé Marie-Nelly, Nathalie Ly, Olivier Collin, Eugenia Basyuk, Edouard Bertrand, Xavier Darzacq, and Christophe Zimmer. FISH-quant: automatic counting of transcripts in 3D FISH images. *Nature Methods*, 10(4):277–278, 2013.

[205] Xiaowei Xu, M. Ester, H.-P. Kriegel, and J. Sander. A distribution-based clustering algorithm for mining in large spatial databases. *Proceedings 14th International Conference on Data Engineering*, pages 324–331, 1998.

[206] Cynthia DeRenzo, Kimberly J. Reese, and Geraldine Seydoux. Exclusion of germ plasm proteins from somatic lineages by cullin-dependent degradation. *Nature*, 424(6949):685–689, 2003.

[207] Roy Parker and Ujwal Sheth. P Bodies and the Control of mRNA Translation and Degradation. *Molecular Cell*, 25(5):635–646, 2007.

[208] Whitby V. I. Eagle, Daniel K. Yeboah-Kordieh, Matthew G. Niepielko, and Elizabeth R. Gavis. Distinct cis-acting elements mediate targeting and clustering of Drosophila polar granule mRNAs. *Development*, 145(22):dev164657, 2018.

[209] Kelsey C. Martin and Anne Ephrussi. mRNA Localization: Gene Expression in the Spatial Dimension. *Cell*, 136(4):719–730, 2009.

[210] Verena Göbel, Peter L Barrett, David H Hall, and John T Fleming. Lumen Morphogenesis in C. elegans Requires the Membrane-Cytoskeleton Linker erm-1. *Developmental Cell*, 6(6):865–873, 2004.

[211] Michelle R. Detwiler, Melanie Reuben, Xiumin Li, Eric Rogers, and Rueyling Lin. Two Zinc Finger Proteins, OMA-1 and OMA-2, Are Redundantly Required for Oocyte Maturation in C. elegans. *Developmental Cell*, 1(2):187–199, 2001.

[212] Masumi Shimada, Hiroyuki Kawahara, and Hirofumi Doi. Novel family of CCCH-type zinc-finger proteins, MOE-1, -2 and -3, participates in C. elegans oocyte maturation. *Genes to Cells*, 7(9):933–947, 2002.

[213] R Cuesta, G Laroia, and R J Schneider. Chaperone hsp27 inhibits translation during heat shock by binding eIF4G and facilitating dissociation of cap-initiation complexes. *Genes & development*, 14(12):1460–70, 2000.

[214] Shannin C. Zevian and Judith L. Yanowitz. Methodological considerations for heat shock of the nematode Caenorhabditis elegans. *Methods*, 68(3):450–457, 2014.

[215] Justin W. Chartron, Katherine C. L. Hunt, and Judith Frydman. Cotranslational signal-independent SRP preloading during membrane targeting. *Nature*, 536(7615):224–228, 2016.

[216] Bilal Khalil, Dmytro Morderer, Phillip L. Price, Feilin Liu, and Wilfried Rossoll. mRNP assembly, axonal transport, and local translation in neurodegenerative diseases. *Brain Research*, 1693(Pt A):75–91, 2018.

[217] S Brenner. The genetics of Caenorhabditis elegans. *Genetics*, 77(1):71–94, 1974.

[218] Daniel J Dickinson, Jordan D Ward, David J Reiner, and Bob Goldstein. Engineering the Caenorhabditis elegans genome using Cas9-triggered homologous recombination. *Nature Methods*, 10(10):1028–1034, 2013.

[219] Andrea M. Femino, Fredric S. Fay, Kevin Fogarty, and Robert H. Singer. Visualization of Single RNA Transcripts in Situ. *Science*, 280(5363):585–590, 1998.

[220] Arjun Raj and Sanjay Tyagi. Chapter 17 Detection of Individual Endogenous RNA Transcripts In Situ Using Multiple Singly Labeled Probes. *Methods in Enzymology*, 472:365–386, 2010.

[221] Arjun Raj, Patrick van den Bogaard, Scott A Rifkin, Alexander van Oudenaarden, and Sanjay Tyagi. Imaging individual mRNA molecules using multiple singly labeled probes. *Nature Methods*, 5(10):877–879, 2008.

[222] Sydney M. Shaffer, Min-Tzu Wu, Marshall J. Levesque, and Arjun Raj. Turbo FISH: A Method for Rapid Single Molecule RNA FISH. *PLoS ONE*, 8(9):e75120, 2013.

[223] Ni Ji and Alexander van Oudenaarden. Single molecule fluorescent in situ hybridization (smFISH) of C. elegans worms and embryos. *WormBook*, pages 1–16, 2012.

[224] Johannes Schindelin, Ignacio Arganda-Carreras, Erwin Frise, Verena Kaynig, Mark Longair, Tobias Pietzsch, Stephan Preibisch, Curtis Rueden, Stephan Saalfeld, Benjamin Schmid, Jean-Yves Tinevez, Daniel James White, Volker Hartenstein, Kevin Eliceiri, Pavel Tomancak, and Albert Cardona. Fiji: an open-source platform for biological-image analysis. *Nature Methods*, 9(7):676–682, 2012.

[225] Nikolay Tsanov, Aubin Samacoits, Racha Chouaib, Abdel-Meneem Traboulsi, Thierry Gostan, Christian Weber, Christophe Zimmer, Kazem Zibara, Thomas Walter, Marion Peter, Edouard Bertrand, and Florian Mueller. smiFISH and FISH-quant – a flexible single RNA detection approach with super-resolution capability. *Nucleic Acids Research*, 44(22):e165–e165, 2016.

[226] Karolina M. Andralojc, Anne C. Campbell, Ashley L. Kelly, Markus Terrey, Paige C. Tanner, Ian M. Gans, Michael J. Senter-Zapata, Eraj S. Khokhar, and Dustin L. Updike. ELLI-1, a novel germline protein, modulates RNAi activity and P-granule accumulation in Caenorhabditis elegans. *PLOS Genetics*, 13(2):e1006611, 2017.

[227] Wei Ouyang, Florian Mueller, Martin Hjelmare, Emma Lundberg, and Christophe Zimmer. ImJoy: an open-source computational platform for the deep learning era. *Nature Methods*, 16(12):1199–1200, 2019.

[228] Aubin Samacoits, Racha Chouaib, Adham Safieddine, Abdel-Meneem Traboulsi, Wei Ouyang, Christophe Zimmer, Marion Peter, Edouard Bertrand, Thomas Walter, and Florian Mueller. A computational framework to study sub-cellular RNA localization. *Nature Communications*, 9(1):4584, 2018.

[229] Jacob M. Sawyer, Stephanie Glass, Trudy Li, Gidi Shemer, Noor D. White, Natalia G. Starostina, Edward T. Kipreos, Corbin D. Jones, and Bob Goldstein. Overcoming Redundancy: An RNAi Enhancer Screen for Morphogenesis Genes in Caenorhabditis elegans. *Genetics*, 188(3):549–564, 2011.

[230] Maria I Toki, Fabiola Cecchi, Todd Hembrough, Konstantinos N Syrigos, and David L Rimm. Proof of the quantitative potential of immunofluorescence by mass spectrometry. *Laboratory Investigation*, 97(3):329–334, 2017.

[231] Marshall J Levesque and Arjun Raj. Single-chromosome transcriptional profiling reveals chromosomal gene expression regulation. *Nature Methods*, 10(3):246–248, 2013.

[232] Laura Perez-Burgos, Antoine H.F.M Peters, Susanne Opravil, Monika Kauer, Karl Mechtler, and Thomas Jenuwein. Generation and Characterization of Methyl-Lysine Histone Antibodies. *Methods in Enzymology*, 376:234–254, 2003.

[233] Tatjana Trcek, Samir Rahman, and Daniel Zenklusen. mRNA Decay, Methods and Protocols. *Methods in Molecular Biology*, 1720:35–54, 2017.

[234] Arturo Orjalo, Hans E Johansson, and Jerry L Ruth. Stellaris^{TM} fluorescence in situ hybridization (FISH) probes: a powerful tool for mRNA detection. *Nature Methods*, 8(10):i–ii, 2011.

[235] Janet Duerr. Immunohistochemistry. *WormBook*, 2006.

[236] Janet S Duerr. Antibody Staining in *C. Elegans* Using Freeze-Cracking. *Journal of Visualized Experiments*, (80), 2013.

[237] Cecilia Williams, Fredrik Pontén, Catherine Moberg, Peter Söderkvist, Mathias Uhlén, Jan Pontén, Gisela Sitbon, and Joakim Lundeberg. A High Frequency of Sequence Alterations Is Due to Formalin Fixation of Archival Specimens. *The American Journal of Pathology*, 155(5):1467–1471, 1999.

[238] Norikazu Masuda, Tadashi Ohnishi, Shoko Kawamoto, Morito Monden, and Kousaku Okubo. Analysis of chemical modification of RNA from formalin-fixed samples and optimization of molecular biology applications for such samples. *Nucleic Acids Research*, 27(22):4436–4443, 1999.

[239] Mythily Srinivasan, Daniel Sedmak, and Scott Jewell. Effect of Fixatives and Tissue Processing on the Content and Integrity of Nucleic Acids. *The American Journal of Pathology*, 161(6):1961–1971, 2002.

[240] Rob W.M. Hoetelmans, Frans A. Prins, Ingrid Cornelese-ten Velde, Joke van der Meer, Cornelis J.H. van de Velde, and Jan Hein van Dierendonck. Effects of Acetone, Methanol, or Paraformaldehyde on Cellular Structure, Visualized by Reflection Contrast Microscopy and Transmission and Scanning Electron Microscopy. *Applied Immunohistochemistry & Molecular Morphology*, 9(4):346–351, 2001.

[241] U. Vielkind and S. H. Swierenga. A simple fixation procedure for immunofluorescent detection of different cytoskeletal components within the same cell. *Histochemistry*, 91(1):81–88, 1989.

[242] Daniel Levitt and Marina King. Methanol fixation permits flow cytometric analysis of immunofluorescent stained intracellular antigens. *Journal of Immunological Methods*, 96(2):233–237, 1987.

[243] Samuel Ward and Michael Klass. The location of the major protein in Caenorhabditis elegans sperm and spermatocytes. *Developmental Biology*, 92(1):203–208, 1982.

[244] Tobias Wiesenfahrt, Janette Y. Berg, Erin Osborne Nishimura, Adam G. Robinson, Barbara Goszczynski, Jason D. Lieb, and James D. McGhee. The function and regulation of the GATA factor ELT-2 in the C. elegans endoderm. *Development*, 143(3):483–491, 2015.

[245] Lior Greenbaum, Chana Rothmann, Ronit Lavie, and Zvi Malik. Green Fluorescent Protein Photobleaching: a Model for Protein Damage by Endogenous and Exogenous Singlet Oxygen. *Biological Chemistry*, 381(12):1251–1258, 2000.

[246] Livia V. Bayer, Mona Batish, Stephen K. Formel, and Diana P. Bratu. Drosophila Oogenesis, Methods and Protocols. *Methods in Molecular Biology*, 1328:125–136, 2015.

[247] Ikuhiro Okamoto. X-Chromosome Inactivation, Methods and Protocols. *Methods in Molecular Biology*, 1861:149–159, 2018.

[248] Llilians Calvo, Matthew Ronshaugen, and Tom Pettini. smiFISH and embryo segmentation for single-cell multi-gene RNA quantification in arthropods. *Communications Biology*, 4(1):352, 2021.

[249] Dong Suk Yoon, DeQwon L. Pendergrass, and Myon-Hee Lee. A simple and rapid method for combining fluorescent in situ RNA hybridization (FISH) and immunofluorescence in the C. elegans germline. *MethodsX*, 3:378–385, 2016.

[250] Adham Safieddine, Emeline Coleno, Soha Salloum, Arthur Imbert, Abdel-Meneem Traboulsi, Oh Sung Kwon, Frederic Lionneton, Virginie Georget, Marie-Cécile Robert, Thierry Gostan, Charles-Henri Lecellier, Racha Chouaib, Xavier Pichon, Hervé Le Hir, Kazem

Zibara, Florian Mueller, Thomas Walter, Marion Peter, and Edouard Bertrand. A choreography of centrosomal mRNAs reveals a conserved localization mechanism involving active polysome transport. *Nature Communications*, 12(1):1352, 2021.

[251] Emmanuelle Querido, Lynda Dekakra-Bellili, and Pascal Chartrand. RNA fluorescence in situ hybridization for high-content screening. *Methods*, 126:149–155, 2017.

[252] Jeffrey R. Moffitt, Junjie Hao, Guiping Wang, Kok Hao Chen, Hazen P. Babcock, and Xiaowei Zhuang. High-throughput single-cell gene-expression profiling with multiplexed error-robust fluorescence in situ hybridization. *Proceedings of the National Academy of Sciences*, 113(39):11046–11051, 2016.

[253] Eric Lubeck, Ahmet F Coskun, Timur Zhiyentayev, Mubhij Ahmad, and Long Cai. Single-cell in situ RNA profiling by sequential hybridization. *Nature Methods*, 11(4):360–361, 2014.

[254] Chenglong Xia, Hazen P. Babcock, Jeffrey R. Moffitt, and Xiaowei Zhuang. Multiplexed detection of RNA using MERFISH and branched DNA amplification. *Scientific Reports*, 9(1):7721, 2019.

[255] Jeffrey M. Perkel. Starfish enterprise: finding RNA patterns in single cells. *Nature*, 572(7770):549–551, 2019.

[256] Caroline A Schneider, Wayne S Rasband, and Kevin W Eliceiri. NIH Image to ImageJ: 25 years of image analysis. *Nature Methods*, 9(7):671–675, 2012.

[257] Kenneth W. Dunn, Malgorzata M. Kamocka, and John H. McDonald. A practical guide to evaluating colocalization in biological microscopy. *American Journal of Physiology-Cell Physiology*, 300(4):C723–C742, 2011.

[258] Montserrat Porta-de-la Riva, Laura Fontrodona, Alberto Villanueva, and Julián Cerón. Basic Caenorhabditis elegans Methods: Synchronization and Observation. *Journal of Visualized Experiments*, (64):e4019, 2012.

[259] Rupak Doshi, Beverly R. Chen, Cecile Rose T. Vibat, Norman Huang, Chang-Wook Lee, and Geoffrey Chang. In vitro nanobody discovery for integral membrane protein targets. *Scientific Reports*, 4(1):6760, 2014.

[260] Harry M. T. Choi, Maayan Schwarzkopf, Mark E. Fornace, Aneesh Acharya, Georgios Artavanis, Johannes Stegmaier, Alexandre Cunha, and Niles A. Pierce. Third-generation in situ hybridization chain reaction: multiplexed, quantitative, sensitive, versatile, robust. *Development*, 145(12):dev165753, 2018.

[261] Salvatore A. E. Marras, Yuri Bushkin, and Sanjay Tyagi. High-fidelity amplified FISH for the detection and allelic discrimination of single mRNA molecules. *Proceedings of the National Academy of Sciences*, 116(28):13921–13926, 2019.

[262] Fay Wang, John Flanagan, Nan Su, Li-Chong Wang, Son Bui, Allissa Nielson, Xingyong Wu, Hong-Thuy Vo, Xiao-Jun Ma, and Yuling Luo. RNAscope A Novel in Situ RNA Analysis Platform for Formalin-Fixed, Paraffin-Embedded Tissues. *The Journal of Molecular Diagnostics*, 14(1):22–29, 2012.

[263] Harry M. T. Choi, Colby R. Calvert, Naeem Husain, David Huss, Julius C. Barsi, Benjamin E. Deverman, Ryan C. Hunter, Mihoko Kato, S. Melanie Lee, Anna C. T. Abelin, Adam Z. Rosenthal, Omar S. Akbari, Yuwei Li, Bruce A. Hay, Paul W. Sternberg, Paul H. Patterson, Eric H. Davidson, Sarkis K. Mazmanian, David A. Prober, Matt van de Rijn, Jared R. Leadbetter, Dianne K. Newman, Carol Readhead, Marianne E. Bronner, Barbara Wold, Rusty Lansford, Tatjana Sauka-Spengler, Scott E. Fraser, and Niles A. Pierce. Mapping a multiplexed zoo of mRNA expression. *Development*, 143(19):3632–3637, 2016.

[264] M. X. Fernandes, A. Ortega, M. C. López Martínez, and J. García de la Torre. Calculation of hydrodynamic properties of small nucleic acids from their atomic structure. *Nucleic Acids Research*, 30(8):1782–1788, 2002.

[265] Andrea Hawe, Wendy L. Hulse, Wim Jiskoot, and Robert T. Forbes. Taylor Dispersion Analysis Compared to Dynamic Light Scattering for the Size Analysis of Therapeutic Peptides and Proteins and Their Aggregates. *Pharmaceutical Research*, 28(9):2302–2310, 2011.

[266] Xuelin Wu, Detlef Weigel, and Philip A. Wigge. Signaling in plants by intercellular RNA and protein movement. *Genes & Development*, 16(2):151–158, 2002.

Appendix A

FISH probes

Table A.1: smFISH and smiFISH probe sets used in this thesis

Transcript_name	Sequence_ID	Wormbase_ID	Probe_sequence	Fluorophore
erm-1	C01G8.5	WBGene 00001333	gtttgaactgctggaccaat	Cal Fluor 610
erm-1	C01G8.5	WBGene 00001333	ccgcaaccatttttctattt	Cal Fluor 610
erm-1	C01G8.5	WBGene 00001333	gacacgcacattgatatcgc	Cal Fluor 610
erm-1	C01G8.5	WBGene 00001333	aaaagttgctttcctgtggt	Cal Fluor 610
erm-1	C01G8.5	WBGene 00001333	cggagaccaatggttttgac	Cal Fluor 610
erm-1	C01G8.5	WBGene 00001333	gtcagtgtactgaagtccaa	Cal Fluor 610
erm-1	C01G8.5	WBGene 00001333	ttcttgttcaatttcagcca	Cal Fluor 610
erm-1	C01G8.5	WBGene 00001333	cttcttaacgtcctgagaca	Cal Fluor 610
erm-1	C01G8.5	WBGene 00001333	ggatagaatttggcgcggaa	Cal Fluor 610
erm-1	C01G8.5	WBGene 00001333	attccatctttcacttggag	Cal Fluor 610

Table A.1: smFISH and smiFISH probe sets used in this thesis

Transcript_name	Sequence_ID	Wormbase_ID	Probe_sequence	Fluorophore
erm-1	C01G8.5	WBGene 00001333	aagaacagaggtttccggtg	Cal Fluor 610
erm-1	C01G8.5	WBGene 00001333	atttagcttgcatcgcgtaa	Cal Fluor 610
erm-1	C01G8.5	WBGene 00001333	gtgtctctggaacatagtct	Cal Fluor 610
erm-1	C01G8.5	WBGene 00001333	gatcagcagtaagacatccg	Cal Fluor 610
erm-1	C01G8.5	WBGene 00001333	agaacgcgttgaggaagcag	Cal Fluor 610
erm-1	C01G8.5	WBGene 00001333	acgtgtagttgcacgatgat	Cal Fluor 610
erm-1	C01G8.5	WBGene 00001333	gactccatacatctcgagat	Cal Fluor 610
erm-1	C01G8.5	WBGene 00001333	tagagatcagttccctttt	Cal Fluor 610
erm-1	C01G8.5	WBGene 00001333	cgactttcggcgaaagacga	Cal Fluor 610
erm-1	C01G8.5	WBGene 00001333	gccttcttatcaattggttt	Cal Fluor 610
erm-1	C01G8.5	WBGene 00001333	cgtttgttgatacggagtcg	Cal Fluor 610
erm-1	C01G8.5	WBGene 00001333	tcgtgatttcccatacacaa	Cal Fluor 610

Table A.1: smFISH and smiFISH probe sets used in this thesis

Transcript_name	Sequence_ID	Wormbase_ID	Probe_sequence	Fluorophore
erm-1	C01G8.5	WBGene 00001333	caatggtatctggctttctt	Cal Fluor 610
erm-1	C01G8.5	WBGene 00001333	cggcaatcttaagagcacga	Cal Fluor 610
erm-1	C01G8.5	WBGene 00001333	tgcttcagccaattcaagac	Cal Fluor 610
erm-1	C01G8.5	WBGene 00001333	tgcaattgcttgagttgagc	Cal Fluor 610
erm-1	C01G8.5	WBGene 00001333	tctgttccaatgcttgttta	Cal Fluor 610
erm-1	C01G8.5	WBGene 00001333	tgaagttgagcagtgagctc	Cal Fluor 610
erm-1	C01G8.5	WBGene 00001333	atcactcattgctttttcgg	Cal Fluor 610
erm-1	C01G8.5	WBGene 00001333	gtctctcaaatgacgtctct	Cal Fluor 610
erm-1	C01G8.5	WBGene 00001333	ttcacgttcacgagcatcaa	Cal Fluor 610
erm-1	C01G8.5	WBGene 00001333	cgacttcttctctcatcgaa	Cal Fluor 610
erm-1	C01G8.5	WBGene 00001333	tctgtgtctgaagttgtctt	Cal Fluor 610
erm-1	C01G8.5	WBGene 00001333	gtagtgttgagtgtgttgtt	Cal Fluor 610

Table A.1: smFISH and smiFISH probe sets used in this thesis

Transcript_name	Sequence_ID	Wormbase_ID	Probe_sequence	Fluorophore
erm-1	C01G8.5	WBGene 00001333	gtgtccattggaaacgtgat	Cal Fluor 610
erm-1	C01G8.5	WBGene 00001333	tatcttcatcatcagtggca	Cal Fluor 610
erm-1	C01G8.5	WBGene 00001333	catttgtgagttcagttgct	Cal Fluor 610
erm-1	C01G8.5	WBGene 00001333	ttgtggcacattctgatcag	Cal Fluor 610
erm-1	C01G8.5	WBGene 00001333	atccagcttattcttgatct	Cal Fluor 610
erm-1	C01G8.5	WBGene 00001333	ttaacactgtcaagctcgcg	Cal Fluor 610
erm-1	C01G8.5	WBGene 00001333	ccatatgcagaacgtcgtag	Cal Fluor 610
erm-1	C01G8.5	WBGene 00001333	cacggatttgacggagagtc	Cal Fluor 610
erm-1	C01G8.5	WBGene 00001333	attcttcgttttgtgtttcc	Cal Fluor 610
erm-1	C01G8.5	WBGene 00001333	tttggaagttggtgggagac	Cal Fluor 610
erm-1	C01G8.5	WBGene 00001333	gtaaaaggcactgatggggt	Cal Fluor 610
erm-1	C01G8.5	WBGene 00001333	tttggcggcggatttaacaa	Cal Fluor 610

Table A.1: smFISH and smiFISH probe sets used in this thesis

Transcript_name	Sequence_ID	Wormbase_ID	Probe_sequence	Fluorophore
erm-1	C01G8.5	WBGene 00001333	gtctttgcgcgagaaattcg	Cal Fluor 610
erm-1	C01G8.5	WBGene 00001333	gtttgatggggagagagagg	Cal Fluor 610
neg-1	F32D1.6	WBGene 00017985	ctgaggtgaagaaggtcaca	Cal Fluor 590
neg-1	F32D1.6	WBGene 00017985	gcagtgctggatgagaatac	Cal Fluor 590
neg-1	F32D1.6	WBGene 00017985	caaaagattcggagttcccg	Cal Fluor 590
neg-1	F32D1.6	WBGene 00017985	gtggactgtacgcagtgtat	Cal Fluor 590
neg-1	F32D1.6	WBGene 00017985	cgggaatcattgaagatcga	Cal Fluor 590
neg-1	F32D1.6	WBGene 00017985	gttatttaccgaagaagccg	Cal Fluor 590
neg-1	F32D1.6	WBGene 00017985	ccgatttctggaatgaattg	Cal Fluor 590
neg-1	F32D1.6	WBGene 00017985	ttgaatggagcattgcaatc	Cal Fluor 590
neg-1	F32D1.6	WBGene 00017985	cgtcattggaaaggatgtgc	Cal Fluor 590
neg-1	F32D1.6	WBGene 00017985	tactgctctccgttgtcgag	Cal Fluor 590

Table A.1: smFISH and smiFISH probe sets used in this thesis

Transcript_name	Sequence_ID	Wormbase_ID	Probe_sequence	Fluorophore
neg-1	F32D1.6	WBGene 00017985	gatgaatttccggcgtgctc	Cal Fluor 590
neg-1	F32D1.6	WBGene 00017985	tcttctttgcaggtgcattg	Cal Fluor 590
neg-1	F32D1.6	WBGene 00017985	ccgatatcaacacaagtgga	Cal Fluor 590
neg-1	F32D1.6	WBGene 00017985	cttgtcacattcctcatcgg	Cal Fluor 590
neg-1	F32D1.6	WBGene 00017985	gaatcctccgttttctgctt	Cal Fluor 590
neg-1	F32D1.6	WBGene 00017985	gcgagacttcttcgaagatt	Cal Fluor 590
neg-1	F32D1.6	WBGene 00017985	gtttcctgctcttacggatc	Cal Fluor 590
neg-1	F32D1.6	WBGene 00017985	tctttcggtagtctgatgct	Cal Fluor 590
neg-1	F32D1.6	WBGene 00017985	ctgccttcaaaagttcccag	Cal Fluor 590
neg-1	F32D1.6	WBGene 00017985	catcagcttcagcacgattt	Cal Fluor 590
neg-1	F32D1.6	WBGene 00017985	aagcgactattcagctttgt	Cal Fluor 590
neg-1	F32D1.6	WBGene 00017985	atccagcttatattggggtt	Cal Fluor 590

Table A.1: smFISH and smiFISH probe sets used in this thesis

Transcript_name	Sequence_ID	Wormbase_ID	Probe_sequence	Fluorophore
neg-1	F32D1.6	WBGene 00017985	gctttctatcattccaagtg	Cal Fluor 590
neg-1	F32D1.6	WBGene 00017985	ttcccgatgatgaatgatct	Cal Fluor 590
neg-1	F32D1.6	WBGene 00017985	agtacgggcgttgttgtcaa	Cal Fluor 590
neg-1	F32D1.6	WBGene 00017985	tcgacacgaagatgaggaat	Cal Fluor 590
neg-1	F32D1.6	WBGene 00017985	agaaaagagaagagctccag	Cal Fluor 590
neg-1	F32D1.6	WBGene 00017985	tcggaagaagagaagtcgtc	Cal Fluor 590
neg-1	F32D1.6	WBGene 00017985	acgagagaaacggagagaac	Cal Fluor 590
neg-1	F32D1.6	WBGene 00017985	cgcagaaagcgagatgatcg	Cal Fluor 590
neg-1	F32D1.6	WBGene 00017985	ccgaagtgcgtctggagatc	Cal Fluor 590
neg-1	F32D1.6	WBGene 00017985	acgtcttccagaagacatag	Cal Fluor 590
neg-1	F32D1.6	WBGene 00017985	tggagaacgagaatcggatc	Cal Fluor 590
neg-1	F32D1.6	WBGene 00017985	gcccacatagagatagagac	Cal Fluor 590

Table A.1: smFISH and smiFISH probe sets used in this thesis

Transcript_name	Sequence_ID	Wormbase_ID	Probe_sequence	Fluorophore
neg-1	F32D1.6	WBGene 00017985	cggaagcgatcccgatcaag	Cal Fluor 590
neg-1	F32D1.6	WBGene 00017985	tgaggagagaagaagctccc	Cal Fluor 590
neg-1	F32D1.6	WBGene 00017985	tttcgacggttagtgatgac	Cal Fluor 590
neg-1	F32D1.6	WBGene 00017985	gaagtctcatgggatctggt	Cal Fluor 590
ape-1	F46F3.4	WBGene 00000146	cgtacagaatccgacgagtg	Cal Fluor 610
ape-1	F46F3.4	WBGene 00000146	ggtatattggggcagttgaa	Cal Fluor 610
ape-1	F46F3.4	WBGene 00000146	cgtagatgccattgatgacg	Cal Fluor 610
ape-1	F46F3.4	WBGene 00000146	ggagccgtcgaagatttatg	Cal Fluor 610
ape-1	F46F3.4	WBGene 00000146	cattcgttgatttgcggaga	Cal Fluor 610
ape-1	F46F3.4	WBGene 00000146	tgggacaatgcttgtggatg	Cal Fluor 610
ape-1	F46F3.4	WBGene 00000146	tggtgcggaatacatcatca	Cal Fluor 610
ape-1	F46F3.4	WBGene 00000146	cggaataacgtgtggtcgtg	Cal Fluor 610

Table A.1: smFISH and smiFISH probe sets used in this thesis

Transcript_name	Sequence_ID	Wormbase_ID	Probe_sequence	Fluorophore
ape-1	F46F3.4	WBGene 00000146	agggttctgaaactgtgcat	Cal Fluor 610
ape-1	F46F3.4	WBGene 00000146	cgtaatcggcgatcatttca	Cal Fluor 610
ape-1	F46F3.4	WBGene 00000146	ttctactgactgcggtttta	Cal Fluor 610
ape-1	F46F3.4	WBGene 00000146	gaacagctcgaactctttgc	Cal Fluor 610
ape-1	F46F3.4	WBGene 00000146	tcttattttgaagctgtgcc	Cal Fluor 610
ape-1	F46F3.4	WBGene 00000146	atggatccttgcacattcaa	Cal Fluor 610
ape-1	F46F3.4	WBGene 00000146	cctcattgaagcatttctca	Cal Fluor 610
ape-1	F46F3.4	WBGene 00000146	ccggtacatttcttccaaat	Cal Fluor 610
ape-1	F46F3.4	WBGene 00000146	atttttcgttgttccacgag	Cal Fluor 610
ape-1	F46F3.4	WBGene 00000146	gtggatacttgatttgcagc	Cal Fluor 610
ape-1	F46F3.4	WBGene 00000146	gacagaagcacgaggtctta	Cal Fluor 610
ape-1	F46F3.4	WBGene 00000146	tcgatagcatcataactgcc	Cal Fluor 610

Table A.1: smFISH and smiFISH probe sets used in this thesis

Transcript_name	Sequence_ID	Wormbase_ID	Probe_sequence	Fluorophore
ape-1	F46F3.4	WBGene 00000146	ccgtcggtatttttgatga	Cal Fluor 610
ape-1	F46F3.4	WBGene 00000146	ctttacatggtgccaagtac	Cal Fluor 610
ape-1	F46F3.4	WBGene 00000146	tgccattttacttaactccg	Cal Fluor 610
ape-1	F46F3.4	WBGene 00000146	agaatcccgagtcattgtag	Cal Fluor 610
ape-1	F46F3.4	WBGene 00000146	attcgtctagactatcacca	Cal Fluor 610
ape-1	F46F3.4	WBGene 00000146	aatcagtctttccacttctc	Cal Fluor 610
ape-1	F46F3.4	WBGene 00000146	ttcgtagctttcagggaatc	Cal Fluor 610
ape-1	F46F3.4	WBGene 00000146	ttgaagtaccttcggaagca	Cal Fluor 610
ape-1	F46F3.4	WBGene 00000146	tcttcttgtgatgttggcaa	Cal Fluor 610
ape-1	F46F3.4	WBGene 00000146	tgtttctgatgttattgccg	Cal Fluor 610
ape-1	F46F3.4	WBGene 00000146	ccgaacttgtagcaacttgt	Cal Fluor 610
ape-1	F46F3.4	WBGene 00000146	catttgttcggttggcaatt	Cal Fluor 610

Table A.1: smFISH and smiFISH probe sets used in this thesis

Transcript_name	Sequence_ID	Wormbase_ID	Probe_sequence	Fluorophore
ape-1	F46F3.4	WBGene 00000146	gaacttgcatcttcttctgt	Cal Fluor 610
ape-1	F46F3.4	WBGene 00000146	agattctgtccatcatcaga	Cal Fluor 610
ape-1	F46F3.4	WBGene 00000146	cagttcttctttcaatcgca	Cal Fluor 610
ape-1	F46F3.4	WBGene 00000146	aggtcttctcaaaatgcctt	Cal Fluor 610
ape-1	F46F3.4	WBGene 00000146	gacctttgttcatcttttca	Cal Fluor 610
ape-1	F46F3.4	WBGene 00000146	ttctaaagcagcatcgagca	Cal Fluor 610
ape-1	F46F3.4	WBGene 00000146	caaatcgcattgtgcaacgc	Cal Fluor 610
ape-1	F46F3.4	WBGene 00000146	aaccatcggaatcttgagca	Cal Fluor 610
ape-1	F46F3.4	WBGene 00000146	ggttattacaggaagctgca	Cal Fluor 610
ape-1	F46F3.4	WBGene 00000146	tccacaagttgtctaaccat	Cal Fluor 610
ape-1	F46F3.4	WBGene 00000146	tagtgtcgaagcgagaacgc	Cal Fluor 610
ape-1	F46F3.4	WBGene 00000146	tccagtattaattgatcccg	Cal Fluor 610

Table A.1: smFISH and smiFISH probe sets used in this thesis

Transcript_name	Sequence_ID	Wormbase_ID	Probe_sequence	Fluorophore
ape-1	F46F3.4	WBGene 00000146	tcatatccataagcagcgta	Cal Fluor 610
ape-1	F46F3.4	WBGene 00000146	tcacatgtccaccaattttt	Cal Fluor 610
ape-1	F46F3.4	WBGene 00000146	ttaacgatgggtacaacgcc	Cal Fluor 610
ape-1	F46F3.4	WBGene 00000146	gacattgttgttcgattcca	Cal Fluor 610
mex-3	F53G12.5	WBGene 00003229	gcgatttgttcttccttcat	Cal Fluor 590
mex-3	F53G12.5	WBGene 00003229	ccaagcccctggcaatttat	Cal Fluor 590
mex-3	F53G12.5	WBGene 00003229	gatcgctgactggagagcac	Cal Fluor 590
mex-3	F53G12.5	WBGene 00003229	agaaactgcgcaatatcctc	Cal Fluor 590
mex-3	F53G12.5	WBGene 00003229	gcctatcgacgttctgtagt	Cal Fluor 590
mex-3	F53G12.5	WBGene 00003229	acggactctgtgacattttg	Cal Fluor 590
mex-3	F53G12.5	WBGene 00003229	cttgacgaccaacaatctcg	Cal Fluor 590
mex-3	F53G12.5	WBGene 00003229	cgcagtgccttaattttgca	Cal Fluor 590

Table A.1: smFISH and smiFISH probe sets used in this thesis

Transcript_name	Sequence_ID	Wormbase_ID	Probe_sequence	Fluorophore
mex-3	F53G12.5	WBGene 00003229	gaaccggtgtcttgatgtag	Cal Fluor 590
mex-3	F53G12.5	WBGene 00003229	tgaccacgaaaattggatct	Cal Fluor 590
mex-3	F53G12.5	WBGene 00003229	cagtcgatctctcgtttcgc	Cal Fluor 590
mex-3	F53G12.5	WBGene 00003229	cggatctgtgtgaagtgctc	Cal Fluor 590
mex-3	F53G12.5	WBGene 00003229	ctcctggaacaacttgtgta	Cal Fluor 590
mex-3	F53G12.5	WBGene 00003229	tctgacatagctcgtgatct	Cal Fluor 590
mex-3	F53G12.5	WBGene 00003229	gagtccgacaactcttaacg	Cal Fluor 590
mex-3	F53G12.5	WBGene 00003229	gatagtcgctcctttcggtc	Cal Fluor 590
mex-3	F53G12.5	WBGene 00003229	tgggtgtcctgttgaattcg	Cal Fluor 590
mex-3	F53G12.5	WBGene 00003229	ggctcggcgtaatgatgtac	Cal Fluor 590
mex-3	F53G12.5	WBGene 00003229	tcaaaaacgggctcccttc	Cal Fluor 590
mex-3	F53G12.5	WBGene 00003229	aagatgtgcgtctcgatctc	Cal Fluor 590

Table A.1: smFISH and smiFISH probe sets used in this thesis

Transcript_name	Sequence_ID	Wormbase_ID	Probe_sequence	Fluorophore
mex-3	F53G12.5	WBGene 00003229	gtttctggaagatttccggt	Cal Fluor 590
mex-3	F53G12.5	WBGene 00003229	aactgtccggcaaagtcatt	Cal Fluor 590
mex-3	F53G12.5	WBGene 00003229	cttctgcaccatcaacgaga	Cal Fluor 590
mex-3	F53G12.5	WBGene 00003229	catttgttgttgagcctgtt	Cal Fluor 590
mex-3	F53G12.5	WBGene 00003229	agaacatcgattgttgctga	Cal Fluor 590
mex-3	F53G12.5	WBGene 00003229	gattactgttgccgaatgct	Cal Fluor 590
mex-3	F53G12.5	WBGene 00003229	cgacgacatctccttctgat	Cal Fluor 590
mex-3	F53G12.5	WBGene 00003229	gagctctccattccgaatgg	Cal Fluor 590
mex-3	F53G12.5	WBGene 00003229	caacgaactacgcatcgatg	Cal Fluor 590
mex-3	F53G12.5	WBGene 00003229	cagtaccggaaagagattcc	Cal Fluor 590
mex-3	F53G12.5	WBGene 00003229	aacgatggacgagaagacag	Cal Fluor 590
mex-3	F53G12.5	WBGene 00003229	gtttcgccgattgtcctcct	Cal Fluor 590

Table A.1: smFISH and smiFISH probe sets used in this thesis

Transcript_name	Sequence_ID	Wormbase_ID	Probe_sequence	Fluorophore
mex-3	F53G12.5	WBGene 00003229	tagtcgtaggttggcagatc	Cal Fluor 590
mex-3	F53G12.5	WBGene 00003229	ttaagcgagttgttggttcc	Cal Fluor 590
mex-3	F53G12.5	WBGene 00003229	gctgagaatttcgttctcca	Cal Fluor 590
mex-3	F53G12.5	WBGene 00003229	cggacagggcatcgtacttg	Cal Fluor 590
mex-3	F53G12.5	WBGene 00003229	gattcctcgcgtttctccaa	Cal Fluor 590
mex-3	F53G12.5	WBGene 00003229	ggacatgagcccattggttg	Cal Fluor 590
mex-3	F53G12.5	WBGene 00003229	cagattgtgctgagaagacc	Cal Fluor 590
mex-3	F53G12.5	WBGene 00003229	gggctcagattcatgtttcc	Cal Fluor 590
mex-3	F53G12.5	WBGene 00003229	agatgctgaagccaacgatc	Cal Fluor 590
mex-3	F53G12.5	WBGene 00003229	gtatgatcgttgtgatcgca	Cal Fluor 590
mex-3	F53G12.5	WBGene 00003229	cttatccattgatcggcacg	Cal Fluor 590
mex-3	F53G12.5	WBGene 00003229	ggaatgatgaatggatccac	Cal Fluor 590

Table A.1: smFISH and smiFISH probe sets used in this thesis

Transcript_name	Sequence_ID	Wormbase_ID	Probe_sequence	Fluorophore
mex-3	F53G12.5	WBGene 00003229	gctagatgagagtctacacg	Cal Fluor 590
mex-3	F53G12.5	WBGene 00003229	cgtacaccgatgaacaaagt	Cal Fluor 590
mex-3	F53G12.5	WBGene 00003229	ccaaaaaaacctactgtagg	Cal Fluor 590
mex-3	F53G12.5	WBGene 00003229	tgagttggtcgtcctatcat	Cal Fluor 590
chs-1	T25G3.2	WBGene 00000496	cttgctgtttcgttgattga	Cal Fluor 610
chs-1	T25G3.2	WBGene 00000496	gttcatcctggtaacgaacg	Cal Fluor 610
chs-1	T25G3.2	WBGene 00000496	cagatcttttgtgcgatcga	Cal Fluor 610
chs-1	T25G3.2	WBGene 00000496	gtcgcctgtaaaactgtgac	Cal Fluor 610
chs-1	T25G3.2	WBGene 00000496	tagcgacagatatattcccg	Cal Fluor 610
chs-1	T25G3.2	WBGene 00000496	tgacttgacgagttgaccac	Cal Fluor 610
chs-1	T25G3.2	WBGene 00000496	ccgattgctcgaagagattc	Cal Fluor 610
chs-1	T25G3.2	WBGene 00000496	ttcggaatgatcttcctgtt	Cal Fluor 610

Table A.1: smFISH and smiFISH probe sets used in this thesis

Transcript_name	Sequence_ID	Wormbase_ID	Probe_sequence	Fluorophore
chs-1	T25G3.2	WBGene 00000496	agaatgcgttgtgtcaatcc	Cal Fluor 610
chs-1	T25G3.2	WBGene 00000496	cttccgtacagcatatttga	Cal Fluor 610
chs-1	T25G3.2	WBGene 00000496	acgatgcgcatgagggaaac	Cal Fluor 610
chs-1	T25G3.2	WBGene 00000496	agtagaagaagcctcgtgtg	Cal Fluor 610
chs-1	T25G3.2	WBGene 00000496	tgaaatccctcgcatgacaa	Cal Fluor 610
chs-1	T25G3.2	WBGene 00000496	gggtgcacgaaagagaacgg	Cal Fluor 610
chs-1	T25G3.2	WBGene 00000496	gggtgattggcaagcataac	Cal Fluor 610
chs-1	T25G3.2	WBGene 00000496	gctttggaaccattgatcac	Cal Fluor 610
chs-1	T25G3.2	WBGene 00000496	aaagtccggagatgcgattc	Cal Fluor 610
chs-1	T25G3.2	WBGene 00000496	ttcttgccgattcagtgaat	Cal Fluor 610
chs-1	T25G3.2	WBGene 00000496	tcatccgatatgtcttcttc	Cal Fluor 610
chs-1	T25G3.2	WBGene 00000496	tcgtttcgaattcgtagctc	Cal Fluor 610

Table A.1: smFISH and smiFISH probe sets used in this thesis

Transcript_name	Sequence_ID	Wormbase_ID	Probe_sequence	Fluorophore
chs-1	T25G3.2	WBGene 00000496	atctcggtttctgtttcatg	Cal Fluor 610
chs-1	T25G3.2	WBGene 00000496	cttgttgttcatacgtgtcg	Cal Fluor 610
chs-1	T25G3.2	WBGene 00000496	cttccaatcggtatcgaagt	Cal Fluor 610
chs-1	T25G3.2	WBGene 00000496	ttctctattccatcttcttc	Cal Fluor 610
chs-1	T25G3.2	WBGene 00000496	catgtacataacttggctcc	Cal Fluor 610
chs-1	T25G3.2	WBGene 00000496	taaacgtgttgtcagccatc	Cal Fluor 610
chs-1	T25G3.2	WBGene 00000496	gaaaacatgttcagcagcct	Cal Fluor 610
chs-1	T25G3.2	WBGene 00000496	gaaacatccaggcgcacaaa	Cal Fluor 610
chs-1	T25G3.2	WBGene 00000496	ttgtcatccatcaatgcaga	Cal Fluor 610
chs-1	T25G3.2	WBGene 00000496	ggtcttagtatacttgtgca	Cal Fluor 610
chs-1	T25G3.2	WBGene 00000496	taggcgatgtaggcatatga	Cal Fluor 610
chs-1	T25G3.2	WBGene 00000496	aaagcagcaacttgggcgaa	Cal Fluor 610

Table A.1: smFISH and smiFISH probe sets used in this thesis

Transcript_name	Sequence_ID	Wormbase_ID	Probe_sequence	Fluorophore
chs-1	T25G3.2	WBGene 00000496	cacatcagatcctcgaagtt	Cal Fluor 610
chs-1	T25G3.2	WBGene 00000496	tacgaacgcgtacgcaatcg	Cal Fluor 610
chs-1	T25G3.2	WBGene 00000496	taaattgttccataggcgct	Cal Fluor 610
chs-1	T25G3.2	WBGene 00000496	atctgaatccctttttcaca	Cal Fluor 610
chs-1	T25G3.2	WBGene 00000496	ttcttttccattttctctcg	Cal Fluor 610
chs-1	T25G3.2	WBGene 00000496	tctgcagtttgagtttcttc	Cal Fluor 610
chs-1	T25G3.2	WBGene 00000496	ctacgttctcttcaatcgga	Cal Fluor 610
chs-1	T25G3.2	WBGene 00000496	atgacttgtcatccacacat	Cal Fluor 610
chs-1	T25G3.2	WBGene 00000496	gttttcctcgttcacaaact	Cal Fluor 610
chs-1	T25G3.2	WBGene 00000496	gaaaacctttccgcacttt	Cal Fluor 610
chs-1	T25G3.2	WBGene 00000496	tttcgtagagaagccaatcc	Cal Fluor 610
chs-1	T25G3.2	WBGene 00000496	ttggcgagaacttgatgctg	Cal Fluor 610

Table A.1: smFISH and smiFISH probe sets used in this thesis

Transcript_name	Sequence_ID	Wormbase_ID	Probe_sequence	Fluorophore
chs-1	T25G3.2	WBGene 00000496	ttaatggttcatcggtttcc	Cal Fluor 610
chs-1	T25G3.2	WBGene 00000496	cttcttggaaagctcctatc	Cal Fluor 610
chs-1	T25G3.2	WBGene 00000496	ggtgaaactccgtattcgta	Cal Fluor 610
chs-1	T25G3.2	WBGene 00000496	gagacgagccttttgaagtt	Cal Fluor 610
chs-1	T25G3.2	WBGene 00000496	cttgctgtttcgttgattga	Quasar 670
chs-1	T25G3.2	WBGene 00000496	gttcatcctggtaacgaacg	Quasar 670
chs-1	T25G3.2	WBGene 00000496	cagatcttttgtgcgatcga	Quasar 670
chs-1	T25G3.2	WBGene 00000496	gtcgcctgtaaaactgtgac	Quasar 670
chs-1	T25G3.2	WBGene 00000496	tagcgacagatatattcccg	Quasar 670
chs-1	T25G3.2	WBGene 00000496	tgacttgacgagttgaccac	Quasar 670
chs-1	T25G3.2	WBGene 00000496	ccgattgctcgaagagattc	Quasar 670
chs-1	T25G3.2	WBGene 00000496	ttcggaatgatcttcctgtt	Quasar 670

Table A.1: smFISH and smiFISH probe sets used in this thesis

Transcript_name	Sequence_ID	Wormbase_ID	Probe_sequence	Fluorophore
chs-1	T25G3.2	WBGene 00000496	agaatgcgttgtgtcaatcc	Quasar 670
chs-1	T25G3.2	WBGene 00000496	cttccgtacagcatatttga	Quasar 670
chs-1	T25G3.2	WBGene 00000496	acgatgcgcatgagggaaac	Quasar 670
chs-1	T25G3.2	WBGene 00000496	agtagaagaagcctcgtgtg	Quasar 670
chs-1	T25G3.2	WBGene 00000496	tgaaatccctcgcatgacaa	Quasar 670
chs-1	T25G3.2	WBGene 00000496	gggtgcacgaaagagaacgg	Quasar 670
chs-1	T25G3.2	WBGene 00000496	gggtgattggcaagcataac	Quasar 670
chs-1	T25G3.2	WBGene 00000496	gctttggaaccattgatcac	Quasar 670
chs-1	T25G3.2	WBGene 00000496	aaagtccggagatgcgattc	Quasar 670
chs-1	T25G3.2	WBGene 00000496	ttcttgccgattcagtgaat	Quasar 670
chs-1	T25G3.2	WBGene 00000496	tcatccgatatgtcttcttc	Quasar 670
chs-1	T25G3.2	WBGene 00000496	tcgtttcgaattcgtagctc	Quasar 670

Table A.1: smFISH and smiFISH probe sets used in this thesis

Transcript_name	Sequence_ID	Wormbase_ID	Probe_sequence	Fluorophore
chs-1	T25G3.2	WBGene 00000496	atctcggtttctgtttcatg	Quasar 670
chs-1	T25G3.2	WBGene 00000496	cttgttgttcatacgtgtcg	Quasar 670
chs-1	T25G3.2	WBGene 00000496	cttccaatcggtatcgaagt	Quasar 670
chs-1	T25G3.2	WBGene 00000496	ttctctattccatcttcttc	Quasar 670
chs-1	T25G3.2	WBGene 00000496	catgtacataacttggctcc	Quasar 670
chs-1	T25G3.2	WBGene 00000496	taaacgtgttgtcagccatc	Quasar 670
chs-1	T25G3.2	WBGene 00000496	gaaaacatgttcagcagcct	Quasar 670
chs-1	T25G3.2	WBGene 00000496	gaaacatccaggcgcacaaa	Quasar 670
chs-1	T25G3.2	WBGene 00000496	ttgtcatccatcaatgcaga	Quasar 670
chs-1	T25G3.2	WBGene 00000496	ggtcttagtatacttgtgca	Quasar 670
chs-1	T25G3.2	WBGene 00000496	taggcgatgtaggcatatga	Quasar 670
chs-1	T25G3.2	WBGene 00000496	aaagcagcaacttgggcgaa	Quasar 670

Table A.1: smFISH and smiFISH probe sets used in this thesis

Transcript_name	Sequence_ID	Wormbase_ID	Probe_sequence	Fluorophore
chs-1	T25G3.2	WBGene 00000496	cacatcagatcctcgaagtt	Quasar 670
chs-1	T25G3.2	WBGene 00000496	tacgaacgcgtacgcaatcg	Quasar 670
chs-1	T25G3.2	WBGene 00000496	taaattgttccataggcgct	Quasar 670
chs-1	T25G3.2	WBGene 00000496	atctgaatccctttttcaca	Quasar 670
chs-1	T25G3.2	WBGene 00000496	ttcttttccattttctctcg	Quasar 670
chs-1	T25G3.2	WBGene 00000496	tctgcagtttgagtttcttc	Quasar 670
chs-1	T25G3.2	WBGene 00000496	ctacgttctcttcaatcgga	Quasar 670
chs-1	T25G3.2	WBGene 00000496	atgacttgtcatccacacat	Quasar 670
chs-1	T25G3.2	WBGene 00000496	gttttcctcgttcacaaact	Quasar 670
chs-1	T25G3.2	WBGene 00000496	gaaaacctttccgcacttt	Quasar 670
chs-1	T25G3.2	WBGene 00000496	tttcgtagagaagccaatcc	Quasar 670
chs-1	T25G3.2	WBGene 00000496	ttggcgagaacttgatgctg	Quasar 670

Table A.1: smFISH and smiFISH probe sets used in this thesis

Transcript_name	Sequence_ID	Wormbase_ID	Probe_sequence	Fluorophore
chs-1	T25G3.2	WBGene 00000496	ttaatggttcatcggtttcc	Quasar 670
chs-1	T25G3.2	WBGene 00000496	cttcttggaaagctcctatc	Quasar 670
chs-1	T25G3.2	WBGene 00000496	ggtgaaactccgtattcgta	Quasar 670
chs-1	T25G3.2	WBGene 00000496	gagacgagccttttgaagtt	Quasar 670
cpg-2	B0280.5	WBGene 00015102	caaaagccaggagtgtgagt	Cal Fluor 610
cpg-2	B0280.5	WBGene 00015102	tgaaggaactgtccattggc	Cal Fluor 610
cpg-2	B0280.5	WBGene 00015102	catcgagagcgtttgtacag	Cal Fluor 610
cpg-2	B0280.5	WBGene 00015102	gcattcaccaagagcgtaaa	Cal Fluor 610
cpg-2	B0280.5	WBGene 00015102	tcccgagcaagtcagaaatt	Cal Fluor 610
cpg-2	B0280.5	WBGene 00015102	tgggcaatccatgattcttg	Cal Fluor 610
cpg-2	B0280.5	WBGene 00015102	gctcgttgtagatgagatca	Cal Fluor 610
cpg-2	B0280.5	WBGene 00015102	cgccagtcgcagataagaag	Cal Fluor 610

Table A.1: smFISH and smiFISH probe sets used in this thesis

Transcript_name	Sequence_ID	Wormbase_ID	Probe_sequence	Fluorophore
cpg-2	B0280.5	WBGene 00015102	cttcgcaaccaatcacgttg	Cal Fluor 610
cpg-2	B0280.5	WBGene 00015102	tgaggtctcaccagatgatt	Cal Fluor 610
cpg-2	B0280.5	WBGene 00015102	gaagattcaccagatccttc	Cal Fluor 610
cpg-2	B0280.5	WBGene 00015102	aacattttcgactgtctcct	Cal Fluor 610
cpg-2	B0280.5	WBGene 00015102	taagtggtacaaccacctga	Cal Fluor 610
cpg-2	B0280.5	WBGene 00015102	ccgtgtttgttgtacagaag	Cal Fluor 610
cpg-2	B0280.5	WBGene 00015102	agaagagtggagttgggcaa	Cal Fluor 610
cpg-2	B0280.5	WBGene 00015102	gcacttctgagaatcagcat	Cal Fluor 610
cpg-2	B0280.5	WBGene 00015102	ttgcattcctcgacaagaga	Cal Fluor 610
cpg-2	B0280.5	WBGene 00015102	cagatccttcaccagaagtc	Cal Fluor 610
cpg-2	B0280.5	WBGene 00015102	cagaagattctccagatgct	Cal Fluor 610
cpg-2	B0280.5	WBGene 00015102	gcaaactccatttggatgga	Cal Fluor 610

Table A.1: smFISH and smiFISH probe sets used in this thesis

Transcript_name	Sequence_ID	Wormbase_ID	Probe_sequence	Fluorophore
cpg-2	B0280.5	WBGene 00015102	gagcaagtgaggaagttggt	Cal Fluor 610
cpg-2	B0280.5	WBGene 00015102	catgatgcgagcaattccac	Cal Fluor 610
cpg-2	B0280.5	WBGene 00015102	gaagacgagagaagctgggc	Cal Fluor 610
cpg-2	B0280.5	WBGene 00015102	gtggccagtcacaaacaaga	Cal Fluor 610
cpg-2	B0280.5	WBGene 00015102	gaatgagaagtatccgtcct	Cal Fluor 610
cpg-2	B0280.5	WBGene 00015102	gcagtgaatgacgatgagca	Cal Fluor 610
cpg-2	B0280.5	WBGene 00015102	agaacatgacgatggcacgg	Cal Fluor 610
cpg-2	B0280.5	WBGene 00015102	agactcggagaacttgagtc	Cal Fluor 610
cpg-2	B0280.5	WBGene 00015102	gactcgtagtcgcaacgtac	Cal Fluor 610
cpg-2	B0280.5	WBGene 00015102	tctcttggcattcggaaaca	Cal Fluor 610
cpg-2	B0280.5	WBGene 00015102	gaagcttctccagattcttc	Cal Fluor 610
cpg-2	B0280.5	WBGene 00015102	agatccttctccagattgtt	Cal Fluor 610

Table A.1: smFISH and smiFISH probe sets used in this thesis

Transcript_name	Sequence_ID	Wormbase_ID	Probe_sequence	Fluorophore
cpg-2	B0280.5	WBGene 00015102	acgcattgattttgctcttc	Cal Fluor 610
cpg-2	B0280.5	WBGene 00015102	gatagcatgaagtccattgt	Cal Fluor 610
cpg-2	B0280.5	WBGene 00015102	gagagaacacgtggagagca	Cal Fluor 610
cpg-2	B0280.5	WBGene 00015102	tatcaacgtgtccattctgg	Cal Fluor 610
cpg-2	B0280.5	WBGene 00015102	atcgttgaaaaccaggctgg	Cal Fluor 610
cpg-2	B0280.5	WBGene 00015102	atgtttgtgggtaatcgcag	Cal Fluor 610
cpg-2	B0280.5	WBGene 00015102	tgtcttcgatgaggcatttc	Cal Fluor 610
cpg-2	B0280.5	WBGene 00015102	cagcaattggagtctcatca	Cal Fluor 610
cpg-2	B0280.5	WBGene 00015102	aaaggccatcggagaagagg	Cal Fluor 610
cpg-2	B0280.5	WBGene 00015102	tgcactgatgataagtggca	Cal Fluor 610
cpg-2	B0280.5	WBGene 00015102	aagttaatgagttgtccggc	Cal Fluor 610
cpg-2	B0280.5	WBGene 00015102	tgttggcagctgagaagacg	Cal Fluor 610

Table A.1: smFISH and smiFISH probe sets used in this thesis

Transcript_name	Sequence_ID	Wormbase_ID	Probe_sequence	Fluorophore
cpg-2	B0280.5	WBGene 00015102	cattgaagcagggtcgatga	Cal Fluor 610
cpg-2	B0280.5	WBGene 00015102	cggggttagtcaattagtgt	Cal Fluor 610
cpg-2	B0280.5	WBGene 00015102	tctatgggggcaatagtttt	Cal Fluor 610
cpg-2	B0280.5	WBGene 00015102	caggcagtttcatttctcaa	Cal Fluor 610
cpg-2	B0280.5	WBGene 00015102	caaaagccaggagtgtgagt	Quasar 670
cpg-2	B0280.5	WBGene 00015102	tgaaggaactgtccattggc	Quasar 670
cpg-2	B0280.5	WBGene 00015102	catcgagagcgtttgtacag	Quasar 670
cpg-2	B0280.5	WBGene 00015102	gcattcaccaagagcgtaaa	Quasar 670
cpg-2	B0280.5	WBGene 00015102	tcccgagcaagtcagaaatt	Quasar 670
cpg-2	B0280.5	WBGene 00015102	tgggcaatccatgattcttg	Quasar 670
cpg-2	B0280.5	WBGene 00015102	gctcgttgtagatgagatca	Quasar 670
cpg-2	B0280.5	WBGene 00015102	cgccagtcgcagataagaag	Quasar 670

Table A.1: smFISH and smiFISH probe sets used in this thesis

Transcript_name	Sequence_ID	Wormbase_ID	Probe_sequence	Fluorophore
cpg-2	B0280.5	WBGene 00015102	cttcgcaaccaatcacgttg	Quasar 670
cpg-2	B0280.5	WBGene 00015102	tgaggtctcaccagatgatt	Quasar 670
cpg-2	B0280.5	WBGene 00015102	gaagattcaccagatccttc	Quasar 670
cpg-2	B0280.5	WBGene 00015102	aacattttcgactgtctcct	Quasar 670
cpg-2	B0280.5	WBGene 00015102	taagtggtacaaccacctga	Quasar 670
cpg-2	B0280.5	WBGene 00015102	ccgtgtttgttgtacagaag	Quasar 670
cpg-2	B0280.5	WBGene 00015102	agaagagtggagttgggcaa	Quasar 670
cpg-2	B0280.5	WBGene 00015102	gcacttctgagaatcagcat	Quasar 670
cpg-2	B0280.5	WBGene 00015102	ttgcattcctcgacaagaga	Quasar 670
cpg-2	B0280.5	WBGene 00015102	cagatccttcaccagaagtc	Quasar 670
cpg-2	B0280.5	WBGene 00015102	cagaagattctccagatgct	Quasar 670
cpg-2	B0280.5	WBGene 00015102	gcaaactccatttggatgga	Quasar 670

Table A.1: smFISH and smiFISH probe sets used in this thesis

Transcript_name	Sequence_ID	Wormbase_ID	Probe_sequence	Fluorophore
cpg-2	B0280.5	WBGene 00015102	gagcaagtgaggaagttggt	Quasar 670
cpg-2	B0280.5	WBGene 00015102	catgatgcgagcaattccac	Quasar 670
cpg-2	B0280.5	WBGene 00015102	gaagacgagagaagctgggc	Quasar 670
cpg-2	B0280.5	WBGene 00015102	gtggccagtcacaaacaaga	Quasar 670
cpg-2	B0280.5	WBGene 00015102	gaatgagaagtatccgtcct	Quasar 670
cpg-2	B0280.5	WBGene 00015102	gcagtgaatgacgatgagca	Quasar 670
cpg-2	B0280.5	WBGene 00015102	agaacatgacgatggcacgg	Quasar 670
cpg-2	B0280.5	WBGene 00015102	agactcggagaacttgagtc	Quasar 670
cpg-2	B0280.5	WBGene 00015102	gactcgtagtcgcaacgtac	Quasar 670
cpg-2	B0280.5	WBGene 00015102	tctcttggcattcggaaaca	Quasar 670
cpg-2	B0280.5	WBGene 00015102	gaagcttctccagattcttc	Quasar 670
cpg-2	B0280.5	WBGene 00015102	agatccttctccagattgtt	Quasar 670

Table A.1: smFISH and smiFISH probe sets used in this thesis

Transcript_name	Sequence_ID	Wormbase_ID	Probe_sequence	Fluorophore
cpg-2	B0280.5	WBGene 00015102	acgcattgattttgctcttc	Quasar 670
cpg-2	B0280.5	WBGene 00015102	gatagcatgaagtccattgt	Quasar 670
cpg-2	B0280.5	WBGene 00015102	gagagaacacgtggagagca	Quasar 670
cpg-2	B0280.5	WBGene 00015102	tatcaacgtgtccattctgg	Quasar 670
cpg-2	B0280.5	WBGene 00015102	atcgttgaaaaccaggctgg	Quasar 670
cpg-2	B0280.5	WBGene 00015102	atgtttgtgggtaatcgcag	Quasar 670
cpg-2	B0280.5	WBGene 00015102	tgtcttcgatgaggcatttc	Quasar 670
cpg-2	B0280.5	WBGene 00015102	cagcaattggagtctcatca	Quasar 670
cpg-2	B0280.5	WBGene 00015102	aaaggccatcggagaagagg	Quasar 670
cpg-2	B0280.5	WBGene 00015102	tgcactgatgataagtggca	Quasar 670
cpg-2	B0280.5	WBGene 00015102	aagttaatgagttgtccggc	Quasar 670
cpg-2	B0280.5	WBGene 00015102	tgttggcagctgagaagacg	Quasar 670

Table A.1: smFISH and smiFISH probe sets used in this thesis

Transcript_name	Sequence_ID	Wormbase_ID	Probe_sequence	Fluorophore
cpg-2	B0280.5	WBGene 00015102	cattgaagcagggtcgatga	Quasar 670
cpg-2	B0280.5	WBGene 00015102	cggggttagtcaattagtgt	Quasar 670
cpg-2	B0280.5	WBGene 00015102	tctatgggggcaatagtttt	Quasar 670
cpg-2	B0280.5	WBGene 00015102	caggcagtttcatttctcaa	Quasar 670
pgl-3	C18G1.4	WBGene 00003994	aatttcttcattgcttgggc	Quasar 670
pgl-3	C18G1.4	WBGene 00003994	agtcatttggcaggatcatc	Quasar 670
pgl-3	C18G1.4	WBGene 00003994	atccccgagaataaggcaaa	Quasar 670
pgl-3	C18G1.4	WBGene 00003994	atcgaactttggtcgcaacg	Quasar 670
pgl-3	C18G1.4	WBGene 00003994	tcatcgatgattggagccaa	Quasar 670
pgl-3	C18G1.4	WBGene 00003994	ctttagctttgtttttcggg	Quasar 670
pgl-3	C18G1.4	WBGene 00003994	agaatcttggcgtcattcga	Quasar 670
pgl-3	C18G1.4	WBGene 00003994	ctcgacaaacttctcttccg	Quasar 670

Table A.1: smFISH and smiFISH probe sets used in this thesis

Transcript_name	Sequence_ID	Wormbase_ID	Probe_sequence	Fluorophore
pgl-3	C18G1.4	WBGene 00003994	gccaagacatagacgtcgaa	Quasar 670
pgl-3	C18G1.4	WBGene 00003994	cgatgcaaatccaagcagtt	Quasar 670
pgl-3	C18G1.4	WBGene 00003994	tttcaatttcttcctggagc	Quasar 670
pgl-3	C18G1.4	WBGene 00003994	aaacgcatctgtgacgttgt	Quasar 670
pgl-3	C18G1.4	WBGene 00003994	acagaatcaatcttcggtcc	Quasar 670
pgl-3	C18G1.4	WBGene 00003994	cagaagttgggtgaatgggt	Quasar 670
pgl-3	C18G1.4	WBGene 00003994	tgggatacagctttttcgat	Quasar 670
pgl-3	C18G1.4	WBGene 00003994	ttcttcgaagcgagcaacga	Quasar 670
pgl-3	C18G1.4	WBGene 00003994	agtgattcatcatcctcgac	Quasar 670
pgl-3	C18G1.4	WBGene 00003994	atcctagctgagatttcagg	Quasar 670
pgl-3	C18G1.4	WBGene 00003994	tcagcaagtgagcgaacgac	Quasar 670
pgl-3	C18G1.4	WBGene 00003994	cgattggattgtcctggaag	Quasar 670

Table A.1: smFISH and smiFISH probe sets used in this thesis

Transcript_name	Sequence_ID	Wormbase_ID	Probe_sequence	Fluorophore
pgl-3	C18G1.4	WBGene 00003994	tgcaatccgggaaacacttc	Quasar 670
pgl-3	C18G1.4	WBGene 00003994	atatggcttgcgaggaacac	Quasar 670
pgl-3	C18G1.4	WBGene 00003994	tcctcgaatgacttcatgga	Quasar 670
pgl-3	C18G1.4	WBGene 00003994	caattcagcgattgctcttc	Quasar 670
pgl-3	C18G1.4	WBGene 00003994	aagcactgctcgagaacaga	Quasar 670
pgl-3	C18G1.4	WBGene 00003994	ttcaactcgctttgagggag	Quasar 670
pgl-3	C18G1.4	WBGene 00003994	attctcgatgacagtttcgt	Quasar 670
pgl-3	C18G1.4	WBGene 00003994	gtagaactctgtgatccaca	Quasar 670
pgl-3	C18G1.4	WBGene 00003994	gagtgatttcttctcactct	Quasar 670
pgl-3	C18G1.4	WBGene 00003994	gggcttaggaattgaagctg	Quasar 670
pgl-3	C18G1.4	WBGene 00003994	tgggcgaacttttgaagct	Quasar 670
pgl-3	C18G1.4	WBGene 00003994	cagaaggttccgacgaactg	Quasar 670

Table A.1: smFISH and smiFISH probe sets used in this thesis

Transcript_name	Sequence_ID	Wormbase_ID	Probe_sequence	Fluorophore
pgl-3	C18G1.4	WBGene 00003994	tggaagttgtggtctgtttt	Quasar 670
pgl-3	C18G1.4	WBGene 00003994	acagttactacttgagctgc	Quasar 670
pgl-3	C18G1.4	WBGene 00003994	gacgactgaatggcatcttt	Quasar 670
pgl-3	C18G1.4	WBGene 00003994	tgttccttcacatggaatcg	Quasar 670
pgl-3	C18G1.4	WBGene 00003994	gaattgagcacattcgccaa	Quasar 670
pgl-3	C18G1.4	WBGene 00003994	cactttctccgatgatcttt	Quasar 670
pgl-3	C18G1.4	WBGene 00003994	agtttctccggaatgacatc	Quasar 670
pgl-3	C18G1.4	WBGene 00003994	gaggcagttgatggagtatt	Quasar 670
pgl-3	C18G1.4	WBGene 00003994	cccaaccatcgctagaaaat	Quasar 670
pgl-3	C18G1.4	WBGene 00003994	ggcagagcaacagattttgt	Quasar 670
pgl-3	C18G1.4	WBGene 00003994	ctccaaagtcgagatcttcg	Quasar 670
pgl-3	C18G1.4	WBGene 00003994	tggtgatcgttgtatcttct	Quasar 670

Table A.1: smFISH and smiFISH probe sets used in this thesis

Transcript_name	Sequence_ID	Wormbase_ID	Probe_sequence	Fluorophore
pgl-3	C18G1.4	WBGene 00003994	tcttgtggttgcggagaaac	Quasar 670
pgl-3	C18G1.4	WBGene 00003994	tcgttaaccggagtagcaag	Quasar 670
pgl-3	C18G1.4	WBGene 00003994	aaactgtccgaatcccgaag	Quasar 670
pgl-3	C18G1.4	WBGene 00003994	acgggatccaccaaagaatc	Quasar 670
set-3	C07A9.7	WBGene 00007403	aagacggaacttccaccata	Quasar 670
set-3	C07A9.7	WBGene 00007403	agagctgtgggaaatgttca	Quasar 670
set-3	C07A9.7	WBGene 00007403	catttgaccgtgactttgtc	Quasar 670
set-3	C07A9.7	WBGene 00007403	gcttctacaaatcttccacg	Quasar 670
set-3	C07A9.7	WBGene 00007403	gtttccacacagacaacagt	Quasar 670
set-3	C07A9.7	WBGene 00007403	ttgtggatcaacgttcacgg	Quasar 670
set-3	C07A9.7	WBGene 00007403	cgcattttcggttattttca	Quasar 670
set-3	C07A9.7	WBGene 00007403	gcagtttttgcagtatgcaa	Quasar 670

Table A.1: smFISH and smiFISH probe sets used in this thesis

Transcript_name	Sequence_ID	Wormbase_ID	Probe_sequence	Fluorophore
set-3	C07A9.7	WBGene 00007403	ttcgtctggctcgtaaaact	Quasar 670
set-3	C07A9.7	WBGene 00007403	agctcatcaaattctccaca	Quasar 670
set-3	C07A9.7	WBGene 00007403	gatgcgcagcgagtttgaaa	Quasar 670
set-3	C07A9.7	WBGene 00007403	agcgatgcaatatccgcaaa	Quasar 670
set-3	C07A9.7	WBGene 00007403	gttctggatcactcgattga	Quasar 670
set-3	C07A9.7	WBGene 00007403	tatcctgagtggaaagtgct	Quasar 670
set-3	C07A9.7	WBGene 00007403	ggtgtcaactggaagattgc	Quasar 670
set-3	C07A9.7	WBGene 00007403	agcttctccaatttctggaa	Quasar 670
set-3	C07A9.7	WBGene 00007403	tattgcattttgaatcgccg	Quasar 670
set-3	C07A9.7	WBGene 00007403	aatcttccccaattttcatc	Quasar 670
set-3	C07A9.7	WBGene 00007403	agatctttcggccattattc	Quasar 670
set-3	C07A9.7	WBGene 00007403	atgctgtatattgtgtgtgc	Quasar 670

Table A.1: smFISH and smiFISH probe sets used in this thesis

Transcript_name	Sequence_ID	Wormbase_ID	Probe_sequence	Fluorophore
set-3	C07A9.7	WBGene 00007403	cttcttggctttctatttgt	Quasar 670
set-3	C07A9.7	WBGene 00007403	gaaaagtccagtagccatcg	Quasar 670
set-3	C07A9.7	WBGene 00007403	tgttccggacaaagaatcca	Quasar 670
set-3	C07A9.7	WBGene 00007403	ccctggctgacaaagatgaa	Quasar 670
set-3	C07A9.7	WBGene 00007403	atcaagaagctcctctcttg	Quasar 670
set-3	C07A9.7	WBGene 00007403	gttgatgatatgtgactcca	Quasar 670
set-3	C07A9.7	WBGene 00007403	atcctgatacacttgcaagg	Quasar 670
set-3	C07A9.7	WBGene 00007403	ggtttttcgagtaccttcaa	Quasar 670
set-3	C07A9.7	WBGene 00007403	cgtcgcaatagtttcaggat	Quasar 670
set-3	C07A9.7	WBGene 00007403	tgtcggtaaagcaacttgca	Quasar 670
set-3	C07A9.7	WBGene 00007403	acgtggtatattctcagtgt	Quasar 670
set-3	C07A9.7	WBGene 00007403	agttctcaagttccttcgat	Quasar 670

Table A.1: smFISH and smiFISH probe sets used in this thesis

Transcript_name	Sequence_ID	Wormbase_ID	Probe_sequence	Fluorophore
set-3	C07A9.7	WBGene 00007403	ctccgagcgaatgcaatgat	Quasar 670
set-3	C07A9.7	WBGene 00007403	cgtgtaggtttctgaatcgg	Quasar 670
set-3	C07A9.7	WBGene 00007403	cgcattttccacaaacttct	Quasar 670
set-3	C07A9.7	WBGene 00007403	ggatcataagtgattccacg	Quasar 670
set-3	C07A9.7	WBGene 00007403	atctcgacatagggacgtac	Quasar 670
set-3	C07A9.7	WBGene 00007403	cttgttccatgcaagtatcg	Quasar 670
set-3	C07A9.7	WBGene 00007403	agcaattccgaagaagtcga	Quasar 670
set-3	C07A9.7	WBGene 00007403	gaacatactccgagagtgga	Quasar 670
set-3	C07A9.7	WBGene 00007403	tttttctgcgtctccataat	Quasar 670
set-3	C07A9.7	WBGene 00007403	gagtttgacgacgagccaaa	Quasar 670
set-3	C07A9.7	WBGene 00007403	tcagcattctgattggcaac	Quasar 670
set-3	C07A9.7	WBGene 00007403	agtttttctagcgttctgtt	Quasar 670

Table A.1: smFISH and smiFISH probe sets used in this thesis

Transcript_name	Sequence_ID	Wormbase_ID	Probe_sequence	Fluorophore
set-3	C07A9.7	WBGene 00007403	acagcattcttgctcgtaat	Quasar 670
set-3	C07A9.7	WBGene 00007403	ctctgattgttccgagtatt	Quasar 670
set-3	C07A9.7	WBGene 00007403	agggtggagatcagttttga	Quasar 670
set-3	C07A9.7	WBGene 00007403	gaactagttcaatggcggga	Quasar 670
set-3	C07A9.7	WBGene 00007403	aagacggaacttccaccata	Cal Fluor 610
set-3	C07A9.7	WBGene 00007403	agagctgtgggaaatgttca	Cal Fluor 610
set-3	C07A9.7	WBGene 00007403	catttgaccgtgactttgtc	Cal Fluor 610
set-3	C07A9.7	WBGene 00007403	gcttctacaaatcttccacg	Cal Fluor 610
set-3	C07A9.7	WBGene 00007403	gtttccacacagacaacagt	Cal Fluor 610
set-3	C07A9.7	WBGene 00007403	ttgtggatcaacgttcacgg	Cal Fluor 610
set-3	C07A9.7	WBGene 00007403	cgcattttcggttattttca	Cal Fluor 610
set-3	C07A9.7	WBGene 00007403	gcagtttttgcagtatgcaa	Cal Fluor 610

Table A.1: smFISH and smiFISH probe sets used in this thesis

Transcript_name	Sequence_ID	Wormbase_ID	Probe_sequence	Fluorophore
set-3	C07A9.7	WBGene 00007403	ttcgtctggctcgtaaaact	Cal Fluor 610
set-3	C07A9.7	WBGene 00007403	agctcatcaaattctccaca	Cal Fluor 610
set-3	C07A9.7	WBGene 00007403	gatgcgcagcgagtttgaaa	Cal Fluor 610
set-3	C07A9.7	WBGene 00007403	agcgatgcaatatccgcaaa	Cal Fluor 610
set-3	C07A9.7	WBGene 00007403	gttctggatcactcgattga	Cal Fluor 610
set-3	C07A9.7	WBGene 00007403	tatcctgagtggaaagtgct	Cal Fluor 610
set-3	C07A9.7	WBGene 00007403	ggtgtcaactggaagattgc	Cal Fluor 610
set-3	C07A9.7	WBGene 00007403	agcttctccaatttctggaa	Cal Fluor 610
set-3	C07A9.7	WBGene 00007403	tattgcattttgaatcgccg	Cal Fluor 610
set-3	C07A9.7	WBGene 00007403	aatcttccccaattttcatc	Cal Fluor 610
set-3	C07A9.7	WBGene 00007403	agatctttcggccattattc	Cal Fluor 610
set-3	C07A9.7	WBGene 00007403	atgctgtatattgtgtgtgc	Cal Fluor 610

Table A.1: smFISH and smiFISH probe sets used in this thesis

Transcript_name	Sequence_ID	Wormbase_ID	Probe_sequence	Fluorophore
set-3	C07A9.7	WBGene 00007403	cttcttggctttctatttgt	Cal Fluor 610
set-3	C07A9.7	WBGene 00007403	gaaaagtccagtagccatcg	Cal Fluor 610
set-3	C07A9.7	WBGene 00007403	tgttccggacaaagaatcca	Cal Fluor 610
set-3	C07A9.7	WBGene 00007403	ccctggctgacaaagatgaa	Cal Fluor 610
set-3	C07A9.7	WBGene 00007403	atcaagaagctcctctcttg	Cal Fluor 610
set-3	C07A9.7	WBGene 00007403	gttgatgatatgtgactcca	Cal Fluor 610
set-3	C07A9.7	WBGene 00007403	atcctgatacacttgcaagg	Cal Fluor 610
set-3	C07A9.7	WBGene 00007403	ggtttttcgagtaccttcaa	Cal Fluor 610
set-3	C07A9.7	WBGene 00007403	cgtcgcaatagtttcaggat	Cal Fluor 610
set-3	C07A9.7	WBGene 00007403	tgtcggtaaagcaacttgca	Cal Fluor 610
set-3	C07A9.7	WBGene 00007403	acgtggtatattctcagtgt	Cal Fluor 610
set-3	C07A9.7	WBGene 00007403	agttctcaagttccttcgat	Cal Fluor 610

Table A.1: smFISH and smiFISH probe sets used in this thesis

Transcript_name	Sequence_ID	Wormbase_ID	Probe_sequence	Fluorophore
set-3	C07A9.7	WBGene 00007403	ctccgagcgaatgcaatgat	Cal Fluor 610
set-3	C07A9.7	WBGene 00007403	cgtgtaggtttctgaatcgg	Cal Fluor 610
set-3	C07A9.7	WBGene 00007403	cgcattttccacaaacttct	Cal Fluor 610
set-3	C07A9.7	WBGene 00007403	ggatcataagtgattccacg	Cal Fluor 610
set-3	C07A9.7	WBGene 00007403	atctcgacatagggacgtac	Cal Fluor 610
set-3	C07A9.7	WBGene 00007403	cttgttccatgcaagtatcg	Cal Fluor 610
set-3	C07A9.7	WBGene 00007403	agcaattccgaagaagtcga	Cal Fluor 610
set-3	C07A9.7	WBGene 00007403	gaacatactccgagagtgga	Cal Fluor 610
set-3	C07A9.7	WBGene 00007403	tttttctgcgtctccataat	Cal Fluor 610
set-3	C07A9.7	WBGene 00007403	gagtttgacgacgagccaaa	Cal Fluor 610
set-3	C07A9.7	WBGene 00007403	tcagcattctgattggcaac	Cal Fluor 610
set-3	C07A9.7	WBGene 00007403	agtttttctagcgttctgtt	Cal Fluor 610

Table A.1: smFISH and smiFISH probe sets used in this thesis

Transcript_name	Sequence_ID	Wormbase_ID	Probe_sequence	Fluorophore
set-3	C07A9.7	WBGene 00007403	acagcattcttgctcgtaat	Cal Fluor 610
set-3	C07A9.7	WBGene 00007403	ctctgattgttccgagtatt	Cal Fluor 610
set-3	C07A9.7	WBGene 00007403	agggtggagatcagttttga	Cal Fluor 610
set-3	C07A9.7	WBGene 00007403	gaactagttcaatggcggga	Cal Fluor 610
nos-2	ZK1127.1	WBGene 00003784	acccagagacatctttcaag	Quasar 670
nos-2	ZK1127.1	WBGene 00003784	gattcgagagtcgaagtcgg	Quasar 670
nos-2	ZK1127.1	WBGene 00003784	gtggcggaaaggaatacatc	Quasar 670
nos-2	ZK1127.1	WBGene 00003784	aatcaaatgttggcgacggc	Quasar 670
nos-2	ZK1127.1	WBGene 00003784	atccgaaagtgatggatccg	Quasar 670
nos-2	ZK1127.1	WBGene 00003784	ggtgaccattcactgtcaaa	Quasar 670
nos-2	ZK1127.1	WBGene 00003784	gtctttctattgagcatgga	Quasar 670
nos-2	ZK1127.1	WBGene 00003784	ttgatgatgttgaggtctcc	Quasar 670

Table A.1: smFISH and smiFISH probe sets used in this thesis

Transcript_name	Sequence_ID	Wormbase_ID	Probe_sequence	Fluorophore
nos-2	ZK1127.1	WBGene 00003784	gggtctagcttcaaacgaga	Quasar 670
nos-2	ZK1127.1	WBGene 00003784	agattttcttaccgttttga	Quasar 670
nos-2	ZK1127.1	WBGene 00003784	ggtggcggctaaataatatt	Quasar 670
nos-2	ZK1127.1	WBGene 00003784	ggaagtcgaagatattcggc	Quasar 670
nos-2	ZK1127.1	WBGene 00003784	tccggaattattcgttgaca	Quasar 670
nos-2	ZK1127.1	WBGene 00003784	ccgaagcgacaactgaatcg	Quasar 670
nos-2	ZK1127.1	WBGene 00003784	gaacttcccgtacaaattga	Quasar 670
nos-2	ZK1127.1	WBGene 00003784	tgctgtcattcaaccaatca	Quasar 670
nos-2	ZK1127.1	WBGene 00003784	cgcaaacgatccactgcgag	Quasar 670
nos-2	ZK1127.1	WBGene 00003784	gagctcttcagcagattcaa	Quasar 670
nos-2	ZK1127.1	WBGene 00003784	agcgagtttctcttggattc	Quasar 670
nos-2	ZK1127.1	WBGene 00003784	gccttttgaacaatgatggc	Quasar 670

Table A.1: smFISH and smiFISH probe sets used in this thesis

Transcript_name	Sequence_ID	Wormbase_ID	Probe_sequence	Fluorophore
nos-2	ZK1127.1	WBGene 00003784	taccagcaaacttactccat	Quasar 670
nos-2	ZK1127.1	WBGene 00003784	cgacagtatccacactggaa	Quasar 670
nos-2	ZK1127.1	WBGene 00003784	catcgcatatatccaacgga	Quasar 670
nos-2	ZK1127.1	WBGene 00003784	ttcttacgtgtatgcgtttc	Quasar 670
nos-2	ZK1127.1	WBGene 00003784	aatgagctgagcttgtcgca	Quasar 670
nos-2	ZK1127.1	WBGene 00003784	ccacaaattttacatggagc	Quasar 670
nos-2	ZK1127.1	WBGene 00003784	gtgattcatttcaccgcgag	Quasar 670
nos-2	ZK1127.1	WBGene 00003784	tatttcaactcacgtctcgg	Quasar 670
nos-2	ZK1127.1	WBGene 00003784	agtacctgaaatgctcacgt	Quasar 670
nos-2	ZK1127.1	WBGene 00003784	aacaactggctcgacggctt	Quasar 670
nos-2	ZK1127.1	WBGene 00003784	cggctgaaatcctcattgaa	Quasar 670
nos-2	ZK1127.1	WBGene 00003784	aatcgtcggttttcgaagtc	Quasar 670

Table A.1: smFISH and smiFISH probe sets used in this thesis

Transcript_name	Sequence_ID	Wormbase_ID	Probe_sequence	Fluorophore
nos-2	ZK1127.1	WBGene 00003784	aattgataacgactgcgctg	Quasar 670
nos-2	ZK1127.1	WBGene 00003784	cggatgatgcgtagatcttc	Quasar 670
nos-2	ZK1127.1	WBGene 00003784	aaataaacgggttggacccg	Quasar 670
nos-2	ZK1127.1	WBGene 00003784	atctgtttgtgaaagcttgt	Quasar 670
nos-2	ZK1127.1	WBGene 00003784	ggctatgaacgggtaactca	Quasar 670
nos-2	ZK1127.1	WBGene 00003784	gtgtgagatgggaaatttgg	Quasar 670
nos-2	ZK1127.1	WBGene 00003784	gaggaccattatacggtatt	Quasar 670
nos-2	ZK1127.1	WBGene 00003784	cttctacaactattcctttc	Quasar 670
B0495.7	B0495.7	WBGene 00015206	atcatcttctggttggtttt	Quasar 670
B0495.7	B0495.7	WBGene 00015206	gtctgaatccaatcgactct	Quasar 670
B0495.7	B0495.7	WBGene 00015206	ggcatctttctgtgtaaagc	Quasar 670
B0495.7	B0495.7	WBGene 00015206	aagatgttccatctcgtact	Quasar 670

Table A.1: smFISH and smiFISH probe sets used in this thesis

Transcript_name	Sequence_ID	Wormbase_ID	Probe_sequence	Fluorophore
B0495.7	B0495.7	WBGene 00015206	tacacgagctctttgttcac	Quasar 670
B0495.7	B0495.7	WBGene 00015206	ggatcattccaaaggctttt	Quasar 670
B0495.7	B0495.7	WBGene 00015206	cgagacgattcacaccaact	Quasar 670
B0495.7	B0495.7	WBGene 00015206	cttcggaccaattctcacaa	Quasar 670
B0495.7	B0495.7	WBGene 00015206	gtatctggcatcgtatcgaa	Quasar 670
B0495.7	B0495.7	WBGene 00015206	caagcaactgcatcatcagt	Quasar 670
B0495.7	B0495.7	WBGene 00015206	acttcgagtacatccatcat	Quasar 670
B0495.7	B0495.7	WBGene 00015206	ttcagttttggaatgagcca	Quasar 670
B0495.7	B0495.7	WBGene 00015206	aaagttctcttcagcaccat	Quasar 670
B0495.7	B0495.7	WBGene 00015206	atgaatccatgagcagcttg	Quasar 670
B0495.7	B0495.7	WBGene 00015206	atgacgccaaggatgttgat	Quasar 670
B0495.7	B0495.7	WBGene 00015206	tcttgagcaagaacggagca	Quasar 670

Table A.1: smFISH and smiFISH probe sets used in this thesis

Transcript_name	Sequence_ID	Wormbase_ID	Probe_sequence	Fluorophore
B0495.7	B0495.7	WBGene 00015206	gggattattccggattggaa	Quasar 670
B0495.7	B0495.7	WBGene 00015206	cccggaaaatacggaagtct	Quasar 670
B0495.7	B0495.7	WBGene 00015206	gtatatgcgatatcgagtcc	Quasar 670
B0495.7	B0495.7	WBGene 00015206	tctgtgtgatagaaccatcc	Quasar 670
B0495.7	B0495.7	WBGene 00015206	agaacattttcaccagctct	Quasar 670
B0495.7	B0495.7	WBGene 00015206	aaacccatctgttttcttca	Quasar 670
B0495.7	B0495.7	WBGene 00015206	aatgcgatagccaaatctcc	Quasar 670
B0495.7	B0495.7	WBGene 00015206	gatttcaggcattttgtacc	Quasar 670
B0495.7	B0495.7	WBGene 00015206	gaatgaacgattgctccagc	Quasar 670
B0495.7	B0495.7	WBGene 00015206	ccgaatacgattgttgtcgg	Quasar 670
B0495.7	B0495.7	WBGene 00015206	ggatcaggttattgagcaca	Quasar 670
B0495.7	B0495.7	WBGene 00015206	taacaccaaacagtccgagc	Quasar 670

Table A.1: smFISH and smiFISH probe sets used in this thesis

Transcript_name	Sequence_ID	Wormbase_ID	Probe_sequence	Fluorophore
B0495.7	B0495.7	WBGene 00015206	aggcaggaagcagaagagtt	Quasar 670
B0495.7	B0495.7	WBGene 00015206	gtcaacacattggctgatgg	Quasar 670
B0495.7	B0495.7	WBGene 00015206	tcttcccattactggaacaa	Quasar 670
B0495.7	B0495.7	WBGene 00015206	ggcccataataaactcagga	Quasar 670
B0495.7	B0495.7	WBGene 00015206	gagtactcgtatggatttcc	Quasar 670
B0495.7	B0495.7	WBGene 00015206	gtagatcgtacgattggcat	Quasar 670
B0495.7	B0495.7	WBGene 00015206	gcattgtccttttgtgttaa	Quasar 670
B0495.7	B0495.7	WBGene 00015206	cctctgtagtcgagtgaatg	Quasar 670
B0495.7	B0495.7	WBGene 00015206	acaactcctgtgcaatttgg	Quasar 670
B0495.7	B0495.7	WBGene 00015206	atggcatacgacagtactca	Quasar 670
B0495.7	B0495.7	WBGene 00015206	cagctcgtgaatagctgtat	Quasar 670
B0495.7	B0495.7	WBGene 00015206	gatgggacaggaacccaaag	Quasar 670

Table A.1: smFISH and smiFISH probe sets used in this thesis

Transcript_name	Sequence_ID	Wormbase_ID	Probe_sequence	Fluorophore
B0495.7	B0495.7	WBGene 00015206	atcatatccaccacgaatct	Quasar 670
B0495.7	B0495.7	WBGene 00015206	atctacgaacttctggagct	Quasar 670
B0495.7	B0495.7	WBGene 00015206	agccactccatttttatttt	Quasar 670
B0495.7	B0495.7	WBGene 00015206	ggatagctctatgttctcat	Quasar 670
B0495.7	B0495.7	WBGene 00015206	tatcctgatagattccgtga	Quasar 670
B0495.7	B0495.7	WBGene 00015206	ctctcaattgcctcaatgtt	Quasar 670
B0495.7	B0495.7	WBGene 00015206	taacaacgatctcggagcgt	Quasar 670
B0495.7	B0495.7	WBGene 00015206	aaatgctacacccatagtca	Quasar 670
mNeonGreen	N/A	N/A	agagaagccatgttgtcttc	Quasar 670
mNeonGreen	N/A	N/A	gtgaagctcgtgagttgctg	Quasar 670
mNeonGreen	N/A	N/A	ctccgttgatggatccgaaa	Quasar 670
mNeonGreen	N/A	N/A	ctgtccaaccatatcgaaat	Quasar 670
mNeonGreen	N/A	N/A	cgtcatttggatttccagtt	Quasar 670
mNeonGreen	N/A	N/A	ttttaagttgagctcttcgt	Quasar 670
mNeonGreen	N/A	N/A	agaattgaaggtctcccttc	Quasar 670
mNeonGreen	N/A	N/A	gtggggcactaaaatccatg	Quasar 670

Table A.1: smFISH and smiFISH probe sets used in this thesis

Transcript_name	Sequence_ID	Wormbase_ID	Probe_sequence	Fluorophore
mNeonGreen	N/A	N/A	attgatgaaatccgtatcca	Quasar 670
mNeonGreen	N/A	N/A	tcattccatctggatatgga	Quasar 670
mNeonGreen	N/A	N/A	accatagcggcttgaaaagg	Quasar 670
mNeonGreen	N/A	N/A	aacttggtatccggatccat	Quasar 670
mNeonGreen	N/A	N/A	cttcgaattgcattgttcga	Quasar 670
mNeonGreen	N/A	N/A	tttacagtaagggaagctcc	Quasar 670
mNeonGreen	N/A	N/A	cccctcataggtatatcgat	Quasar 670
mNeonGreen	N/A	N/A	aatccagttcccttgacttg	Quasar 670
mNeonGreen	N/A	N/A	gactgttggtcataactggt	Quasar 670
mNeonGreen	N/A	N/A	ttggataggtcttcttggag	Quasar 670
mNeonGreen	N/A	N/A	gttgaaatgatggtcttgtc	Quasar 670
mNeonGreen	N/A	N/A	ccagttgtgtaagaccattt	Quasar 670
mNeonGreen	N/A	N/A	ctgtcgatcggtatcttttt	Quasar 670
mNeonGreen	N/A	N/A	tttggcgaacgtgtacgttg	Quasar 670
mNeonGreen	N/A	N/A	tcaaatagttggcagccatt	Quasar 670
mNeonGreen	N/A	N/A	tacggaacacgtacattggc	Quasar 670
mNeonGreen	N/A	N/A	tttagagtgcttaagctcgg	Quasar 670
mNeonGreen	N/A	N/A	gccactccttgaagtttaat	Quasar 670
mNeonGreen	N/A	N/A	cattcccataacatcagtga	Quasar 670
mNeonGreen	N/A	N/A	agagaagccatgttgtcttc	Cal Fluor 610
mNeonGreen	N/A	N/A	gtgaagctcgtgagttgctg	Cal Fluor 610
mNeonGreen	N/A	N/A	ctccgttgatggatccgaaa	Cal Fluor 610
mNeonGreen	N/A	N/A	ctgtccaaccatatcgaaat	Cal Fluor 610
mNeonGreen	N/A	N/A	cgtcatttggatttccagtt	Cal Fluor 610

Table A.1: smFISH and smiFISH probe sets used in this thesis

Transcript_name	Sequence_ID	Wormbase_ID	Probe_sequence	Fluorophore
mNeonGreen	N/A	N/A	ttttaagttgagctcttcgt	Cal Fluor 610
mNeonGreen	N/A	N/A	agaattgaaggtctcccttc	Cal Fluor 610
mNeonGreen	N/A	N/A	gtggggcactaaaatccatg	Cal Fluor 610
mNeonGreen	N/A	N/A	attgatgaaatccgtatcca	Cal Fluor 610
mNeonGreen	N/A	N/A	tcattccatctggatatgga	Cal Fluor 610
mNeonGreen	N/A	N/A	accatagcggcttgaaaagg	Cal Fluor 610
mNeonGreen	N/A	N/A	aacttggtatccggatccat	Cal Fluor 610
mNeonGreen	N/A	N/A	cttcgaattgcattgttcga	Cal Fluor 610
mNeonGreen	N/A	N/A	tttacagtaagggaagctcc	Cal Fluor 610
mNeonGreen	N/A	N/A	cccctcataggtatatcgat	Cal Fluor 610
mNeonGreen	N/A	N/A	aatccagttcccttgacttg	Cal Fluor 610
mNeonGreen	N/A	N/A	gactgttggtcataactggt	Cal Fluor 610
mNeonGreen	N/A	N/A	ttggataggtcttcttggag	Cal Fluor 610
mNeonGreen	N/A	N/A	gttgaaatgatggtcttgtc	Cal Fluor 610
mNeonGreen	N/A	N/A	ccagttgtgtaagaccattt	Cal Fluor 610
mNeonGreen	N/A	N/A	ctgtcgatcggtatcttttt	Cal Fluor 610
mNeonGreen	N/A	N/A	tttggcgaacgtgtacgttg	Cal Fluor 610
mNeonGreen	N/A	N/A	tcaaatagttggcagccatt	Cal Fluor 610
mNeonGreen	N/A	N/A	tacggaacacgtacattggc	Cal Fluor 610
mNeonGreen	N/A	N/A	tttagagtgcttaagctcgg	Cal Fluor 610
mNeonGreen	N/A	N/A	gccactccttgaagtttaat	Cal Fluor 610
mNeonGreen	N/A	N/A	cattcccataacatcagtga	Cal Fluor 610
tes-1	B0496.8	WBGene 00015217	agacgtgacgtcggtcatta	Cal Fluor 610

Table A.1: smFISH and smiFISH probe sets used in this thesis

Transcript_name	Sequence_ID	Wormbase_ID	Probe_sequence	Fluorophore
tes-1	B0496.8	WBGene 00015217	cgagtcccagcttgaaaatt	Cal Fluor 610
tes-1	B0496.8	WBGene 00015217	cgtgtgcaagaatgtgttgc	Cal Fluor 610
tes-1	B0496.8	WBGene 00015217	aaatttctgcattgtgagcc	Cal Fluor 610
tes-1	B0496.8	WBGene 00015217	aagtccttcgcatctacaag	Cal Fluor 610
tes-1	B0496.8	WBGene 00015217	ttgcacattttcctccaaaa	Cal Fluor 610
tes-1	B0496.8	WBGene 00015217	atccattcgacatccacaat	Cal Fluor 610
tes-1	B0496.8	WBGene 00015217	tcggcaaaacgacatcatgc	Cal Fluor 610
tes-1	B0496.8	WBGene 00015217	tccaattacaatttgtgcgt	Cal Fluor 610
tes-1	B0496.8	WBGene 00015217	gttctcgtgctccaaataac	Cal Fluor 610
tes-1	B0496.8	WBGene 00015217	tttcgtgagcacttttcga	Cal Fluor 610
tes-1	B0496.8	WBGene 00015217	catttggtttatacattccc	Cal Fluor 610
tes-1	B0496.8	WBGene 00015217	gttttctttcgtttcatttt	Cal Fluor 610

Table A.1: smFISH and smiFISH probe sets used in this thesis

Transcript_name	Sequence_ID	Wormbase_ID	Probe_sequence	Fluorophore
tes-1	B0496.8	WBGene 00015217	tgttggctgagatcttgttg	Cal Fluor 610
tes-1	B0496.8	WBGene 00015217	ttctgaatcacttgatgcca	Cal Fluor 610
tes-1	B0496.8	WBGene 00015217	attgttagaacctcctcttt	Cal Fluor 610
tes-1	B0496.8	WBGene 00015217	cacgcatactggacgttttc	Cal Fluor 610
tes-1	B0496.8	WBGene 00015217	aggtttttgtctggaagtgg	Cal Fluor 610
tes-1	B0496.8	WBGene 00015217	gggctttcatgtatcgagaa	Cal Fluor 610
tes-1	B0496.8	WBGene 00015217	tctccttttgagccaacaag	Cal Fluor 610
tes-1	B0496.8	WBGene 00015217	gtagtcttgactttctgttc	Cal Fluor 610
tes-1	B0496.8	WBGene 00015217	tcataaagcgggagctggaa	Cal Fluor 610
tes-1	B0496.8	WBGene 00015217	tcgcgcatcttcaacattac	Cal Fluor 610
tes-1	B0496.8	WBGene 00015217	tcacatctttttcttccaca	Cal Fluor 610
tes-1	B0496.8	WBGene 00015217	cttccaactccaatcacatt	Cal Fluor 610

Table A.1: smFISH and smiFISH probe sets used in this thesis

Transcript_name	Sequence_ID	Wormbase_ID	Probe_sequence	Fluorophore
tes-1	B0496.8	WBGene 00015217	atcttttccgatttctacga	Cal Fluor 610
tes-1	B0496.8	WBGene 00015217	tgtattctcattgtctccat	Cal Fluor 610
tes-1	B0496.8	WBGene 00015217	taatcctttcaatgcggcag	Cal Fluor 610
tes-1	B0496.8	WBGene 00015217	cttgcaatctgtttctccaa	Cal Fluor 610
tes-1	B0496.8	WBGene 00015217	ccagtttccatcatttcatt	Cal Fluor 610
tes-1	B0496.8	WBGene 00015217	gatgacattctaccccaata	Cal Fluor 610
tes-1	B0496.8	WBGene 00015217	acgacatgtttcacaacgga	Cal Fluor 610
tes-1	B0496.8	WBGene 00015217	agcataatgtctaccacagt	Cal Fluor 610
tes-1	B0496.8	WBGene 00015217	ccgcacatcttggataaagt	Cal Fluor 610
tes-1	B0496.8	WBGene 00015217	ttggcgaagatgagctcatc	Cal Fluor 610
tes-1	B0496.8	WBGene 00015217	ctcttcggcaaatgtgtact	Cal Fluor 610
tes-1	B0496.8	WBGene 00015217	cctcgatcctcctaatttaa	Cal Fluor 610

Table A.1: smFISH and smiFISH probe sets used in this thesis

Transcript_name	Sequence_ID	Wormbase_ID	Probe_sequence	Fluorophore
tes-1	B0496.8	WBGene 00015217	tggattttcatctcttgtca	Cal Fluor 610
tes-1	B0496.8	WBGene 00015217	tcgcaggtctttgcgaaatg	Cal Fluor 610
tes-1	B0496.8	WBGene 00015217	ggtccgatttttgattgaca	Cal Fluor 610
tes-1	B0496.8	WBGene 00015217	tgtagtttagacgcttctcg	Cal Fluor 610
tes-1	B0496.8	WBGene 00015217	tgaaaacatcgttcctcggc	Cal Fluor 610
tes-1	B0496.8	WBGene 00015217	gagcatgaatttctttccga	Cal Fluor 610
tes-1	B0496.8	WBGene 00015217	ctttacactgggatgagcac	Cal Fluor 610
tes-1	B0496.8	WBGene 00015217	atccggattcgctgaattat	Cal Fluor 610
tes-1	B0496.8	WBGene 00015217	gtcccgcacaaaacagagaa	Cal Fluor 610
tes-1	B0496.8	WBGene 00015217	atcaacaggaagcgcatgaa	Cal Fluor 610
tes-1	B0496.8	WBGene 00015217	atgcttcgtctgcgcaaaaa	Cal Fluor 610
bpl-1	F13H8.10	WBGene 00000259	ggtacttgacgaactgtgga	Cal Fluor 610

Table A.1: smFISH and smiFISH probe sets used in this thesis

Transcript_name	Sequence_ID	Wormbase_ID	Probe_sequence	Fluorophore
bpl-1	F13H8.10	WBGene 00000259	tcttgatgtcaggaactggt	Cal Fluor 610
bpl-1	F13H8.10	WBGene 00000259	ggtttacacattgccttgaa	Cal Fluor 610
bpl-1	F13H8.10	WBGene 00000259	cctccggtatatacgagaac	Cal Fluor 610
bpl-1	F13H8.10	WBGene 00000259	gtgatctcatctggaggtaa	Cal Fluor 610
bpl-1	F13H8.10	WBGene 00000259	aaaccgttgatttttctgcc	Cal Fluor 610
bpl-1	F13H8.10	WBGene 00000259	ttcatcgtccaaatcgttcg	Cal Fluor 610
bpl-1	F13H8.10	WBGene 00000259	tatgcttgaattttctccca	Cal Fluor 610
bpl-1	F13H8.10	WBGene 00000259	atagcttattctggcagaca	Cal Fluor 610
bpl-1	F13H8.10	WBGene 00000259	tcacaacctgtgatacttgc	Cal Fluor 610
bpl-1	F13H8.10	WBGene 00000259	tagaagcgttcgctttactc	Cal Fluor 610
bpl-1	F13H8.10	WBGene 00000259	ctgtcgatttcggaagcttt	Cal Fluor 610
bpl-1	F13H8.10	WBGene 00000259	atttgctccaacactgacat	Cal Fluor 610

Table A.1: smFISH and smiFISH probe sets used in this thesis

Transcript_name	Sequence_ID	Wormbase_ID	Probe_sequence	Fluorophore
bpl-1	F13H8.10	WBGene 00000259	catctggttctttcttgagt	Cal Fluor 610
bpl-1	F13H8.10	WBGene 00000259	acaatgctgaagcatgcagg	Cal Fluor 610
bpl-1	F13H8.10	WBGene 00000259	tgttgagttgttgcatcaga	Cal Fluor 610
bpl-1	F13H8.10	WBGene 00000259	tcacagacgtttactcctac	Cal Fluor 610
bpl-1	F13H8.10	WBGene 00000259	tggttaatggaggcattgtc	Cal Fluor 610
bpl-1	F13H8.10	WBGene 00000259	ccagcgatgctttctataat	Cal Fluor 610
bpl-1	F13H8.10	WBGene 00000259	aatttcttcgcccaatcgaa	Cal Fluor 610
bpl-1	F13H8.10	WBGene 00000259	aacatcacttttcctgagca	Cal Fluor 610
bpl-1	F13H8.10	WBGene 00000259	gcttcaggaagtcctaattc	Cal Fluor 610
bpl-1	F13H8.10	WBGene 00000259	cctcgattggaagaagcttc	Cal Fluor 610
bpl-1	F13H8.10	WBGene 00000259	atttttactggttccagcat	Cal Fluor 610
bpl-1	F13H8.10	WBGene 00000259	acaagcagtacgacttgacc	Cal Fluor 610

Table A.1: smFISH and smiFISH probe sets used in this thesis

Transcript_name	Sequence_ID	Wormbase_ID	Probe_sequence	Fluorophore
bpl-1	F13H8.10	WBGene 00000259	atccattgtagttgttgcta	Cal Fluor 610
bpl-1	F13H8.10	WBGene 00000259	ttcgagtgatggaattccgg	Cal Fluor 610
bpl-1	F13H8.10	WBGene 00000259	tccgctgatttgacgatttg	Cal Fluor 610
bpl-1	F13H8.10	WBGene 00000259	ccacgtggacaaaggaactc	Cal Fluor 610
bpl-1	F13H8.10	WBGene 00000259	tgcgattctgctcttttttg	Cal Fluor 610
bpl-1	F13H8.10	WBGene 00000259	gtgccacacagaaaatgtgc	Cal Fluor 610
bpl-1	F13H8.10	WBGene 00000259	ggatatccagatagattccg	Cal Fluor 610
bpl-1	F13H8.10	WBGene 00000259	cagatcatttggccatttga	Cal Fluor 610
bpl-1	F13H8.10	WBGene 00000259	agcattccaccaactttatg	Cal Fluor 610
bpl-1	F13H8.10	WBGene 00000259	cggaatgaatcatccctagt	Cal Fluor 610
bpl-1	F13H8.10	WBGene 00000259	attcattccacatccgatac	Cal Fluor 610
bpl-1	F13H8.10	WBGene 00000259	aagcacatcgtcggtttatc	Cal Fluor 610

Table A.1: smFISH and smiFISH probe sets used in this thesis

Transcript_name	Sequence_ID	Wormbase_ID	Probe_sequence	Fluorophore
bpl-1	F13H8.10	WBGene 00000259	cttctttaggcagcatatca	Cal Fluor 610
bpl-1	F13H8.10	WBGene 00000259	gttcttttgtaatccgtgtt	Cal Fluor 610
bpl-1	F13H8.10	WBGene 00000259	gtttattgtttccgcaatca	Cal Fluor 610
bpl-1	F13H8.10	WBGene 00000259	tatcctcatagtccttcatg	Cal Fluor 610
bpl-1	F13H8.10	WBGene 00000259	ttctttttgaaggtttccgg	Cal Fluor 610
bpl-1	F13H8.10	WBGene 00000259	cttcttgttgtgaatgcagc	Cal Fluor 610
bpl-1	F13H8.10	WBGene 00000259	attcctcgaatcgttactcg	Cal Fluor 610
bpl-1	F13H8.10	WBGene 00000259	atattttatccgggttggac	Cal Fluor 610
bpl-1	F13H8.10	WBGene 00000259	aaggtatttccatcatcacc	Cal Fluor 610
bpl-1	F13H8.10	WBGene 00000259	acgaattagacccttcatca	Cal Fluor 610
bpl-1	F13H8.10	WBGene 00000259	gtatccgctacaatcctaat	Cal Fluor 610
imb-2	R06A4.4	WBGene 00002076	taattcgtgttggtctggtt	Quasar 670

Table A.1: smFISH and smiFISH probe sets used in this thesis

Transcript_name	Sequence_ID	Wormbase_ID	Probe_sequence	Fluorophore
imb-2	R06A4.4	WBGene 00002076	tgaacatctctgtctgtgga	Quasar 670
imb-2	R06A4.4	WBGene 00002076	attgagctgtaccaattgca	Quasar 670
imb-2	R06A4.4	WBGene 00002076	tcaatcatctccttcatgtc	Quasar 670
imb-2	R06A4.4	WBGene 00002076	tttttaagcaacaagccggc	Quasar 670
imb-2	R06A4.4	WBGene 00002076	acttattccattttgctcga	Quasar 670
imb-2	R06A4.4	WBGene 00002076	aaaaacttcacgtcctgcgg	Quasar 670
imb-2	R06A4.4	WBGene 00002076	caatgatacctactgtcgca	Quasar 670
imb-2	R06A4.4	WBGene 00002076	cttctgaagtgctccaagag	Quasar 670
imb-2	R06A4.4	WBGene 00002076	attggccgaagaaattccga	Quasar 670
imb-2	R06A4.4	WBGene 00002076	gcagcatgatgctcatagaa	Quasar 670
imb-2	R06A4.4	WBGene 00002076	gtcattgtggcgagcgaaaa	Quasar 670
imb-2	R06A4.4	WBGene 00002076	agcgtcagcgatctacataa	Quasar 670

Table A.1: smFISH and smiFISH probe sets used in this thesis

Transcript_name	Sequence_ID	Wormbase_ID	Probe_sequence	Fluorophore
imb-2	R06A4.4	WBGene 00002076	attcggcaaatgaggcatca	Quasar 670
imb-2	R06A4.4	WBGene 00002076	actcgttgtgatcttgagtc	Quasar 670
imb-2	R06A4.4	WBGene 00002076	aaaactcgcaggcctctaag	Quasar 670
imb-2	R06A4.4	WBGene 00002076	gagatgtggaagcaccattg	Quasar 670
imb-2	R06A4.4	WBGene 00002076	agcagaactggtatgagctt	Quasar 670
imb-2	R06A4.4	WBGene 00002076	ctcagaatatcgcatggagc	Quasar 670
imb-2	R06A4.4	WBGene 00002076	cattagctttcaacgcagga	Quasar 670
imb-2	R06A4.4	WBGene 00002076	aaacctaggcttgatatcct	Quasar 670
imb-2	R06A4.4	WBGene 00002076	gaacaccttctgatattcca	Quasar 670
imb-2	R06A4.4	WBGene 00002076	tccaacagatcctttccaaa	Quasar 670
imb-2	R06A4.4	WBGene 00002076	tcatcaatgtgtccttgagg	Quasar 670
imb-2	R06A4.4	WBGene 00002076	gcaagtattccagactcttt	Quasar 670

Table A.1: smFISH and smiFISH probe sets used in this thesis

Transcript_name	Sequence_ID	Wormbase_ID	Probe_sequence	Fluorophore
imb-2	R06A4.4	WBGene 00002076	catgaatggtatgagctcgc	Quasar 670
imb-2	R06A4.4	WBGene 00002076	gtggcttcttgtcaaacatc	Quasar 670
imb-2	R06A4.4	WBGene 00002076	cagcacgtgatcgatcgaac	Quasar 670
imb-2	R06A4.4	WBGene 00002076	cgtcggatgcaatatgcgaa	Quasar 670
imb-2	R06A4.4	WBGene 00002076	aacagcggagaagattggcg	Quasar 670
imb-2	R06A4.4	WBGene 00002076	tgaactttcttgtttccgtc	Quasar 670
imb-2	R06A4.4	WBGene 00002076	tcttcttcgagagttgcgaa	Quasar 670
imb-2	R06A4.4	WBGene 00002076	ttgaccagttgatcgaggat	Quasar 670
imb-2	R06A4.4	WBGene 00002076	gactacagcaccttgtgaat	Quasar 670
imb-2	R06A4.4	WBGene 00002076	gagccataatgtgttgttgg	Quasar 670
imb-2	R06A4.4	WBGene 00002076	tgataaagtccgtttcggga	Quasar 670
imb-2	R06A4.4	WBGene 00002076	catatgttccggtaacgact	Quasar 670

Table A.1: smFISH and smiFISH probe sets used in this thesis

Transcript_name	Sequence_ID	Wormbase_ID	Probe_sequence	Fluorophore
imb-2	R06A4.4	WBGene 00002076	cgtcacatctaacgagcaga	Quasar 670
imb-2	R06A4.4	WBGene 00002076	gtaacgcgaagcacgattgt	Quasar 670
imb-2	R06A4.4	WBGene 00002076	ggacacgctttcgtcaaatc	Quasar 670
imb-2	R06A4.4	WBGene 00002076	aatcgcattgttgcacacac	Quasar 670
imb-2	R06A4.4	WBGene 00002076	cccgatgaactgtttcattg	Quasar 670
imb-2	R06A4.4	WBGene 00002076	attctgctggctattgatga	Quasar 670
imb-2	R06A4.4	WBGene 00002076	tccgcgttatccttaatatt	Quasar 670
imb-2	R06A4.4	WBGene 00002076	cgacgggattcatgttgatc	Quasar 670
imb-2	R06A4.4	WBGene 00002076	tactgtccacgaagcgatag	Quasar 670
imb-2	R06A4.4	WBGene 00002076	gccgacttgttgtttgaatg	Quasar 670
imb-2	R06A4.4	WBGene 00002076	agagagacgttcacgcaacg	Quasar 670
gpd-2	K10B3.8	WBGene 00001684	gaatccgttgattccgacac	Quasar 670

Table A.1: smFISH and smiFISH probe sets used in this thesis

Transcript_name	Sequence_ID	Wormbase_ID	Probe_sequence	Fluorophore
gpd-2	K10B3.8	WBGene 00001684	gaggacaagacgtccgattc	Quasar 670
gpd-2	K10B3.8	WBGene 00001684	ttgacactgtccttctcgac	Quasar 670
gpd-2	K10B3.8	WBGene 00001684	tggatcgttgacggcaacaa	Quasar 670
gpd-2	K10B3.8	WBGene 00001684	ccatgtagtcgatggagatg	Quasar 670
gpd-2	K10B3.8	WBGene 00001684	gtggagtcgtactggaacaa	Quasar 670
gpd-2	K10B3.8	WBGene 00001684	gagcaacggttcccttgaag	Quasar 670
gpd-2	K10B3.8	WBGene 00001684	tggcgacaagaaggtagtct	Quasar 670
gpd-2	K10B3.8	WBGene 00001684	ttgatcttgtgctgcgactt	Quasar 670
gpd-2	K10B3.8	WBGene 00001684	tgggtctcttgagttgtaga	Quasar 670
gpd-2	K10B3.8	WBGene 00001684	ggtggactcaacgacatagt	Quasar 670
gpd-2	K10B3.8	WBGene 00001684	ttctcgatggtggtgaagac	Quasar 670
gpd-2	K10B3.8	WBGene 00001684	gagatgatgaccttcttggc	Quasar 670

Table A.1: smFISH and smiFISH probe sets used in this thesis

Transcript_name	Sequence_ID	Wormbase_ID	Probe_sequence	Fluorophore
gpd-2	K10B3.8	WBGene 00001684	tggagcatcagcagatggag	Quasar 670
gpd-2	K10B3.8	WBGene 00001684	ggttgactccgacgacgaac	Quasar 670
gpd-2	K10B3.8	WBGene 00001684	ttggcatgatcgtacttctc	Quasar 670
gpd-2	K10B3.8	WBGene 00001684	agcattggagatgatgtggt	Quasar 670
gpd-2	K10B3.8	WBGene 00001684	caaggcagttagtggtgcag	Quasar 670
gpd-2	K10B3.8	WBGene 00001684	attgatgaccttggcaagtg	Quasar 670
gpd-2	K10B3.8	WBGene 00001684	ccctcaataattccgaagtt	Quasar 670
gpd-2	K10B3.8	WBGene 00001684	ggcgtggacagtggtcataa	Quasar 670
gpd-2	K10B3.8	WBGene 00001684	cgtcaacagtcttttgggtg	Quasar 670
gpd-2	K10B3.8	WBGene 00001684	tctccagagctttcctgatg	Quasar 670
gpd-2	K10B3.8	WBGene 00001684	tagaggctgggatgatgttc	Quasar 670
gpd-2	K10B3.8	WBGene 00001684	gagctttccattgagctctg	Quasar 670

Table A.1: smFISH and smiFISH probe sets used in this thesis

Transcript_name	Sequence_ID	Wormbase_ID	Probe_sequence	Fluorophore
gpd-2	K10B3.8	WBGene 00001684	tgggacacggaaagccattc	Quasar 670
gpd-2	K10B3.8	WBGene 00001684	caacaacagacacatctggg	Quasar 670
gpd-2	K10B3.8	WBGene 00001684	ttctcaagacgagcagtgag	Quasar 670
gpd-2	K10B3.8	WBGene 00001684	gatgtcatcgagggaagctg	Quasar 670
gpd-2	K10B3.8	WBGene 00001684	cggcagccttgataactttc	Quasar 670
gpd-2	K10B3.8	WBGene 00001684	gagaattcccttcattggtc	Quasar 670
gpd-2	K10B3.8	WBGene 00001684	acaacttgatcctcagtgta	Quasar 670
gpd-2	K10B3.8	WBGene 00001684	atcggagacaaagtcggtgg	Quasar 670
gpd-2	K10B3.8	WBGene 00001684	gcatcgaagatggaagagtt	Quasar 670
gpd-2	K10B3.8	WBGene 00001684	gttgagtgagatggatgctc	Quasar 670
gpd-2	K10B3.8	WBGene 00001684	agacgagcttgacgaagtgt	Quasar 670
gpd-2	K10B3.8	WBGene 00001684	ccgaactcgttatcgtacca	Quasar 670

Table A.1: smFISH and smiFISH probe sets used in this thesis

Transcript_name	Sequence_ID	Wormbase_ID	Probe_sequence	Fluorophore
gpd-2	K10B3.8	WBGene 00001684	atcaacaactctgttggagt	Quasar 670
gpd-2	K10B3.8	WBGene 00001684	tggtggcgatgtacgagatg	Quasar 670
gpd-2	K10B3.8	WBGene 00001684	taggatgagacagcttaggc	Quasar 670
gpd-2	K10B3.8	WBGene 00001684	acaagcagttaactaggtga	Quasar 670
gpd-2	K10B3.8	WBGene 00001684	atacttgtaagcttctagga	Quasar 670
gpd-2	K10B3.8	WBGene 00001684	cctttattgagaagagacca	Quasar 670
clu-1	F55H2.6	WBGene 00000550	ctgatgagtctggagtgttt	Quasar 670
clu-1	F55H2.6	WBGene 00000550	tcctcttgaggaatttcgtg	Quasar 670
clu-1	F55H2.6	WBGene 00000550	cttgtcgacttgcttatctg	Quasar 670
clu-1	F55H2.6	WBGene 00000550	cgaaagcgtctccacaagat	Quasar 670
clu-1	F55H2.6	WBGene 00000550	atgacaagtagcttcacggt	Quasar 670
clu-1	F55H2.6	WBGene 00000550	ggaatagcacggacttcaga	Quasar 670

Table A.1: smFISH and smiFISH probe sets used in this thesis

Transcript_name	Sequence_ID	Wormbase_ID	Probe_sequence	Fluorophore
clu-1	F55H2.6	WBGene 00000550	agacgagcatcacgaatggt	Quasar 670
clu-1	F55H2.6	WBGene 00000550	gagtaattcacggacttggc	Quasar 670
clu-1	F55H2.6	WBGene 00000550	tcggaaggttttggttcttt	Quasar 670
clu-1	F55H2.6	WBGene 00000550	ctttaagggcaatgagctct	Quasar 670
clu-1	F55H2.6	WBGene 00000550	aaacctctagtgcaacaggt	Quasar 670
clu-1	F55H2.6	WBGene 00000550	gccgcttcaaaatttgagga	Quasar 670
clu-1	F55H2.6	WBGene 00000550	tctgaagctcttcattccaa	Quasar 670
clu-1	F55H2.6	WBGene 00000550	gcagcatttacgtaatcagc	Quasar 670
clu-1	F55H2.6	WBGene 00000550	tatgagttttcttgtcctct	Quasar 670
clu-1	F55H2.6	WBGene 00000550	cctagagtgttgagttttgg	Quasar 670
clu-1	F55H2.6	WBGene 00000550	gcagttcgtgatactttca	Quasar 670
clu-1	F55H2.6	WBGene 00000550	ttcaactcttccttaactcc	Quasar 670

Table A.1: smFISH and smiFISH probe sets used in this thesis

Transcript_name	Sequence_ID	Wormbase_ID	Probe_sequence	Fluorophore
clu-1	F55H2.6	WBGene 00000550	caattattcccttagcttcg	Quasar 670
clu-1	F55H2.6	WBGene 00000550	tggatatcccagtgttttag	Quasar 670
clu-1	F55H2.6	WBGene 00000550	cgaaagcttgtgcgggaatt	Quasar 670
clu-1	F55H2.6	WBGene 00000550	cggctgcttgcttaatcaaa	Quasar 670
clu-1	F55H2.6	WBGene 00000550	acgactttgtttttggcttc	Quasar 670
clu-1	F55H2.6	WBGene 00000550	tgttggtgcatgtttgacat	Quasar 670
clu-1	F55H2.6	WBGene 00000550	agacgctgttttcaagacgt	Quasar 670
clu-1	F55H2.6	WBGene 00000550	tgctttgcagatctagcaac	Quasar 670
clu-1	F55H2.6	WBGene 00000550	atgtacttgcggagagttga	Quasar 670
clu-1	F55H2.6	WBGene 00000550	cttcttattggctttcttcg	Quasar 670
clu-1	F55H2.6	WBGene 00000550	gttaacgaagaccaggcaga	Quasar 670
clu-1	F55H2.6	WBGene 00000550	tcttcacggatactattcca	Quasar 670

Table A.1: smFISH and smiFISH probe sets used in this thesis

Transcript_name	Sequence_ID	Wormbase_ID	Probe_sequence	Fluorophore
clu-1	F55H2.6	WBGene 00000550	tcgggtatccataatagctg	Quasar 670
clu-1	F55H2.6	WBGene 00000550	ctttgcaaatgcggcggaaa	Quasar 670
clu-1	F55H2.6	WBGene 00000550	ccaattggtaatctcttgct	Quasar 670
clu-1	F55H2.6	WBGene 00000550	catcagcagtgaatggttca	Quasar 670
clu-1	F55H2.6	WBGene 00000550	agtgattcgccaatacactc	Quasar 670
clu-1	F55H2.6	WBGene 00000550	ggcatatctggatgcattac	Quasar 670
clu-1	F55H2.6	WBGene 00000550	cgtgggacaatcttgcaaga	Quasar 670
clu-1	F55H2.6	WBGene 00000550	ccttatgctggttgttcaaa	Quasar 670
clu-1	F55H2.6	WBGene 00000550	tccaggaatgagaagtgctc	Quasar 670
clu-1	F55H2.6	WBGene 00000550	atgagatatctcgcacggta	Quasar 670
clu-1	F55H2.6	WBGene 00000550	attacaggatgtttctctcc	Quasar 670
clu-1	F55H2.6	WBGene 00000550	agtccaatgttggcatcaat	Quasar 670

Table A.1: smFISH and smiFISH probe sets used in this thesis

Transcript_name	Sequence_ID	Wormbase_ID	Probe_sequence	Fluorophore
clu-1	F55H2.6	WBGene 00000550	atgtttccttttcagcaact	Quasar 670
clu-1	F55H2.6	WBGene 00000550	gtgatttggtccatagagtt	Quasar 670
clu-1	F55H2.6	WBGene 00000550	tgagcctggaacaattcagt	Quasar 670
clu-1	F55H2.6	WBGene 00000550	tccaggaacaccaatgatca	Quasar 670
clu-1	F55H2.6	WBGene 00000550	aacatctgtagtcttgctct	Quasar 670
clu-1	F55H2.6	WBGene 00000550	cgagagtctcattgtcaagc	Quasar 670